Time-Dependent Quantum Many-Body Systems: Linear Response, Electronic Transport, and Reduced Density Matrices

Dissertation

zur Erlangung des akademischen Grades
Doctor rerum naturalium

vorgelegt von

Heiko Appel

Institut für Theoretische Physik
Freie Universität Berlin

Mai 2007

Diese Arbeit wurde im Zeitraum von Oktober 2003 bis Mai 2007 in der Arbeitsgruppe von Prof. E. K. U. Gross am Fachbereich Physik der Freien Universität Berlin erstellt.

Die Arbeit ist in elektronischer Form unter folgender URL verfügbar

http://www.physik.fu-berlin.de/~appel/PhDThesis/

Eingereicht am: 21. Mai 2007

1. Gutachter: Prof. Dr. E. K. U. Gross
2. Gutachter: Prof. Dr. K. D. Schotte

Tag der mündlichen Prüfung: 12. Juli 2007

Abstract

Time-dependent density functional theory (TDDFT) provides a successful approach to calculate excitation energies of atomic and molecular systems. In part I of this work we present a double-pole approximation (DPA) to the response equations of TDDFT. The double-pole approximation provides an exact description of systems with two strongly coupled excitations which are isolated from the rest of the spectrum. In contrast to the traditional single-pole approximation of TDDFT the DPA also yields corrections to the Kohn-Sham oscillator strengths. Several critical pole separations can be identified, e.g. we find that the pole coupling can cause transitions to vanish entirely from the optical spectrum. We also demonstrate how to invert the double-pole solution which allows us to predict matrix elements of the exchange-correlation kernel f_{xc} from experimental input. This can serve as benchmark for the construction of future approximations for the kernel f_{xc}.
Reduced density matrix functional theory (RDMFT) has emerged recently as promising candidate to treat strongly correlated electronic many-body systems beyond traditional density functional theory (DFT). The research within RDMFT was so far focussed on the static theory. In this work we attempt some first steps towards a time-dependent generalization of RDMFT. In part II we derive equations of motion for natural orbitals and occupation numbers. Using the equation of motion for the occupation numbers we show that an adiabatic extension of presently known ground-state functionals of static RDMFT always leads to occupation numbers which are constant in time. From the stationary conditions of the equations of motion for the N-body correlations (correlated parts of the N-body matrices) we derive a new class of ground-state functionals which can be used in static RDMFT. Applications are presented for a one-dimensional model system where the time-dependent many-body Schrödinger equation can be propagated numerically. We use optimal control theory to find optimized laser pulses for transitions in a model for atomic Helium. From the numerically exact correlated wavefunction we extract the exact time evolution of natural orbitals and occupation numbers for (i) laser-driven Helium and (ii) electron-ion scattering.
Part III of this work considers time-dependent quantum transport within TDDFT. We present an algorithm for the calculation of extended eigenstates of single-particle Hamiltonians which is especially tailored to a finite-difference discretization of the Schrödinger equation. We consider the propagation of finite mesoscopic systems and demonstrate the limitations of such an approach. To overcome the shortcomings of a description of quantum transport in terms of finite systems we develop a time-propagation scheme for extended states which utilizes a mixed basis representation. Our discretization scheme allows to treat central device and lead regions on the same footing thus preventing artificial reflections at grid boundaries.

Contents

List of Figures

List of Tables

Abbreviations

AFM	Atomic-force microscope
ALDA	Adiabatic local density approximation (see TDLDA)
ATI	Above-threshold ionization
BBGKY	Bogoliubov, Born, Green, Kirkwood, and Yvon
CMOS	Complementary metal oxide semiconductor
CN	Crank and Nicholson
CSE	Contracted Schrödinger equation
DFT	Density-functional theory
DNA	Deoxyribonucleic acid
DPA	Double-pole approximation
ETRS	Enforced time-reversal symmetry
ETDHF	Extended time-dependent Hartree-Fock
EUV	Extreme ultra violet
FCC	Face centered cubic
GGA	Generalized-gradient approximation
HF	Hartree-Fock
HHG	High-harmonic generation
HOMO	Highest occupied molecular orbital
HPC	High-performance computing
ITRS	International Technology Roadmap for Semiconductors
KLI	Krieger, Li, and Iafrate
KS	Kohn-Sham
LDA	Local-density approximation
MPI	Message Passing Interface
MPI	Multi-photon ionization
NEGF	Nonequilibrium Green's function

OCT	Optimal control theory
ODE	Ordinary differential equation
OEP	Optimized effective potential
OpenMP	Open Multi-Processing
PDE	Partial differential equation
PGG	Petersilka, Gossmann, and Gross
RC	Resistor-capacitor
RDMFT	Reduced density matrix functional theory
RG	Runge and Gross
RPA	Random-phase approximation
SCF	Self-consistent field
SIC	Self-interaction correction
SO	Split-operator
STM	Scanning tunneling microscope
SPA	Single-pole approximation
TBC	Transparent boundary condition
TDDFT	Time-dependent density functional theory
TDCDFT	Time-dependent current density functional theory
TDDMT	Time-dependent density matrix theory
TDHF	Time-dependent Hartree-Fock
TDLDA	Time-dependent local density approximation (see ALDA)
TDRDMFT	Time-dependent reduced density matrix functional theory
TDSE	Time-dependent Schrödinger equation
TDKS	Time-dependent Kohn-Sham
TRK	Thomas, Reiche, and Kuhn
XC	Exchange-correlation

Notation

Symbol	Description
$\mathbf{r}$	Position in space
j	Combined space, spin coordinate, $j \equiv (\mathbf{r}_j, \sigma_j)$
t	A point in time
ω	Frequency
$f(j)$	f is a *function* of the variable j
$f[\gamma]$	f is a *functional* of the function γ
$\hat{H}$	Interacting Hamiltonian
$\hat{H}_{\mathrm{KS}}$	Kohn-Sham Hamiltonian
$\hat{h}$	Bare single-particle Hamiltonian ($\hat{h} = -\frac{1}{2}\nabla^2 + \hat{v}_{\mathrm{ext}}$)
$\hat{T}$	Kinetic energy operator
$\hat{V}_{\mathrm{ext}}$	Operator for the (local) external potential
$\hat{V}_{\mathrm{ee}}$	Operator representing the Coulomb interaction
$\hat{U}(t, t')$	Time-evolution operator
E	Ground-state total energy
E_{H}	Ground-state Hartree energy
E_{x}	Ground-state exchange energy
E_{c}	Ground-state correlation energy
E_{xc}	Ground-state exchange-correlation energy ($E_{\mathrm{xc}} = E_{\mathrm{x}} + E_{\mathrm{c}}$)
$\Psi(1, 2, \ldots, N)$	Interacting many-body ground-state wavefunction
$\Psi_k(1, 2, \ldots, N)$	Eigenstate k of the interacting many-body Hamiltonian
$\Phi(1, 2, \ldots, N)$	Ground-state Kohn-Sham Slater determinant
$\rho(1)$	Ground-state electronic spin density
$\gamma_1(1, 1')$	Ground-state reduced one-body density matrix
$\gamma_2(12, 1'2')$	Ground-state reduced two-body density matrix
$\lambda_2(12, 1'2')$	Ground-state reduced two-body correlations
$\gamma_N(12..N, 1'2'..N')$	Ground-state reduced N-body density matrix
$\lambda_N(12..N, 1'2'..N')$	Ground-state reduced N-body correlations
$\gamma_N^{(k)}(12..N, 1'2'..N')$	N-body density matrix contracted from many-body eigenstate Ψ_k
$\lambda_N^{(k)}(12..N, 1'2'..N')$	N-body correlations contracted from many-body eigenstate Ψ_k
s	Ground-state correlation entropy
$s(1)$	Spatially resolved ground-state correlation entropy
n_j	Natural occupation number
$\varphi_j(1)$	Ground-state natural spin orbital
$\psi_j(1)$	Ground-state Kohn-Sham spin-orbital

Symbol	Description
E_j	Eigenvalues of the interacting Hamiltonian $\hat{H}$
ε_j	Kohn-Sham eigenvalues
$\mathcal{E}(k)$	Kohn-Sham bandstructure
q	Cumulative index for electronic transition ($q \equiv k \rightarrow j$)
Ω_q	Interacting excitation energy $\Omega_q = E_k - E_j$
ω_q	Kohn-Sham excitation energy $\omega_q = \varepsilon_k - \varepsilon_j$
$\Psi(1, 2, \ldots, N; t)$	Time-dependent many-body wavefunction
$\Phi(1, 2, \ldots, N; t)$	Time-dependent Kohn-Sham Slater determinant
$\rho(1; t)$	Time-dependent electronic spin density
$\gamma_1(1, 1'; t)$	Time-dependent reduced one-body density matrix
$\gamma_2(12, 1'2'; t)$	Time-dependent reduced two-body density matrix
$\lambda_2(12, 1'2'; t)$	Time-dependent reduced two-body correlations
$\gamma_N(12 \ldots N, 1'2' \ldots N'; t)$	Time-dependent reduced N-body density matrix
$\lambda_N(12 \ldots N, 1'2' \ldots N'; t)$	Time-dependent reduced N-body correlations
$\gamma_{N;abc\ldots;a'b'c'\ldots}(t)$	Expansion coefficients of the N-body matrices in the basis of the natural orbitals
$\lambda_{N;abc\ldots;a'b'c'\ldots}(t)$	Expansion coefficients of the N-body correlations in the basis of the natural orbitals
$s(t)$	Time-dependent correlation entropy
$s(1; t)$	Spatially resolved time-dependent correlation entropy
$n_j(t)$	Time-dependent natural occupation number
$\varphi_j(1; t)$	Time-dependent natural spin orbital
$\psi_j(1; t)$	Time-dependent Kohn-Sham spin-orbital
$\rho(\mathbf{r}, t)$	Time-dependent electronic particle density
$\boldsymbol{j}(\mathbf{r}, t)$	Time-dependent electronic current density
$v_{\mathrm{KS}}(\mathbf{r}, t)$	Time-dependent Kohn-Sham potential
$v_{\mathrm{ext}}(\mathbf{r}, t)$	Time-dependent external potential
$v_{\mathrm{H}}(\mathbf{r}, t)$	Time-dependent Hartree potential
$v_{\mathrm{xc}}(\mathbf{r}, t)$	Time-dependent exchange-correlation potential
$G(\mathbf{r}, \mathbf{r}', \omega)$	Green's function
$v_{\mathrm{ee}}(\mathbf{r}, \mathbf{r}')$	Bare Coulomb interaction ($1/\lvert\mathbf{r} - \mathbf{r}'\rvert$)
$\chi(\mathbf{r}, \mathbf{r}', \omega)$	Density-density response function
$\chi_{\mathrm{KS}}(\mathbf{r}, \mathbf{r}', \omega)$	Kohn-Sham density-density response function
$f_{\mathrm{xc}}(\mathbf{r}, \mathbf{r}', \omega)$	Exchange-correlation kernel
β	Inverse temperature
μ	Chemical potential
$\Re$	Real part
$\Im$	Imaginary part

1 Introduction

More than eight decades have passed, since E. Schrödinger published in 1926 his seminal paper which marked the beginning of wave mechanics [Sch26]. It was only shortly after Schrödinger's equation for the electronic wavefunction Ψ had been spectacularly validated for small systems like He and H_2 when Dirac remarked

> *The underlying physical laws necessary for the mathematical theory of a large part of physics and the whole of chemistry are thus completely known, and the difficulty is only that the exact application of these laws leads to equations much too complicated to be soluble. It therefore becomes desirable that approximate practical methods of applying quantum mechanics should be developed, which can lead to an explanation of the main features of complex atomic systems without too much computation.*
>
> — P. A. M. Dirac [Dir29].

Despite the tremendous progress which has been made since the discovery of Schrödingers equation, the theoretical description of many-particle systems is still a vivid and broad field of research in modern physics and chemistry. Present day computing facilities alleviate the calculation of properties of many-particle systems, but even with the fastest computers available today an *exact* numerical treatment of the basic laws of quantum mechanics is only feasible for very small atomic and molecular systems. If chemical accuracy is required, wavefunction methods face an exponential wall in computational effort when an increasing number of atoms is considered.
An alternative to the description of many-particle systems in terms of the wavefunction is provided by density-functional theory (DFT). DFT aims at describing an interacting many-electron system exclusively in terms of the electronic particle density. The theory relies on two basic theorems: (i) In principle, every quantum mechanical observable can be calculated solely from the knowledge of the electronic density. In other words, every observable can be written as *functional* of the density. (ii) The electronic density of a given interacting system can be calculated from the density of an auxiliary system of non-interacting electrons moving in an effective local potential, the so-called Kohn-Sham potential. Rather soon after the proof of the basic theorems by Hohenberg and Kohn [HK64] and Kohn and Sham [KS65], the method gained widespread use within solid-state physics. With the advent of more accurate functionals, in particular the so-called generalized gradient approximations (GGAs), DFT also started to conquer quantum chemistry which culminated 1998 in the award of the Nobel price to Walter Kohn *"for his development of the density-functional theory"* [KP98]. The original Hohenberg-Kohn-Sham formulation of DFT covers ground-state densities. An extension of DFT to the treatment of time-dependent quantum systems was established in 1984 when Runge and Gross proved a Hohenberg-Kohn-type theorem for time-dependent densities and potentials [RG84]. This opened the possibility

to treat electronic systems out of equilibrium, e.g., as encountered for atoms and molecules in strong laser fields, or for electronic transport.
Along these lines we devote the present work to the description of time-dependent quantum many-particle systems in terms of time-dependent DFT (TDDFT) and time-dependent reduced density matrix functional theory (TDRDMFT). We investigate the linear response regime of atomic and molecular systems, atoms in strong laser fields, electron-ion scattering, and electronic transport. By their very nature the different topics of the present work deserve their own introduction which we provide at the beginning of the respective chapters. We therefore restrict ourselves here to a brief overview of the structure of the thesis. We have divided the thesis into three parts:
In **Part I** we consider the calculation of excitation energies and oscillator strengths of atomic and molecular systems within TDDFT. This part contains a general introduction to time-dependent DFT and reviews the TDDFT linear-response formalism which became very popular for the calculation of excitation energies. Although the calculation of response properties within TDDFT is in widespread use, the development of new functionals and the understanding for the reliability and the accuracy of employed approximations is still limited. To gain more understanding for the TDDFT response formalism we develop in Chapter 3 a double-pole approximation to the TDDFT response equations. In contrast to the traditional single-pole approximation of TDDFT the double-pole approximation provides corrections to the Kohn-Sham oscillator strengths and gives insight in the corrections to the Kohn-Sham excitation energies when strong coupling between poles is present. The inversion of the double-pole solution allows us to compute matrix elements of the exchange-correlation kernel f_{xc} from experimental input which serves as benchmark for the future development of exchange-correlation kernels.
Part II is concerned with time-dependent reduced density matrices and their eigenvectors and eigenvalues which are termed natural orbitals and occupation numbers, respectively. We begin, in Chapter 4, with a brief review of static reduced density matrix functional theory (RDMFT) to introduce basic concepts and the used nomenclature. Due to the recent success of ground-state RDMFT it is desirable to extend the theory to the time-dependent domain. However, at the present stage not much is known about the time-dependence of natural orbitals and occupation numbers. We therefore attempt in the present work some preliminary steps towards a time-dependent extension of RDMFT. In Chapter 5 we introduce the BBGKY (Bogoliubov, Born, Green, Kirkwood, and Yvon) hierarchy of reduced density matrices which provides a set of coupled first order partial differential equations in time for the evolution of the reduced density matrices. Using this hierarchy we derive equations of motion for the natural orbitals and occupation numbers. We discuss some properties of these equations and show that an adiabatic extension of presently known ground-state functionals in RDMFT always leads to occupation numbers which are independent of time. By imposing stationary conditions on the equations of motion for the N-body correlations (correlated parts of the N-body matrices) we derive a new class of functionals which can be used for ground-state calculations in static RDMFT. The remainder of Chapter 5 is devoted to applications. We introduce the notion of a time-dependent correlation entropy and discuss briefly optimal control theory which we use to determine optimal pulse shapes for atomic transitions. From the fully correlated time-dependent many-body wavefunction of a one-dimensional model system we extract the exact time-dependence of natural orbitals and occupation numbers. This serves as exact reference for the construction of functionals in TDRDMFT.

In **Part III** we turn our attention to a description of molecular electronics within TDDFT. The basic difficulty of treating electronic transport within TDDFT lies in the fact that the time-dependent Kohn-Sham equations have to be solved, in principle, on an *infinite domain*. This raises several technical issues which have to be addressed before molecular electronics calculations can be performed in practice. The focus of part III lies therefore on the development of algorithms tailored to a real-space representation of the time-dependent Kohn-Sham equations. In Chapter 6 we present a numerical scheme to calculate extended eigenstates of single-particle Hamiltonians. To assess the possibility of using finite systems for a description of electronic transport we perform in Chapter 7 time propagations of finite model systems. This reveals several shortcomings which are due to the finite size of the employed charge reservoirs and artificial reflections at the boundaries of the finite simulation area. To overcome these limitations we develop a numerical scheme for the propagation of extended states. We perform first numerical tests and show that transparent boundary conditions can be achieved with the proposed method.

If not specified otherwise, atomic units ($e = m = \hbar = 1$) are used throughout this work.

Part I

Double-Pole Approximation in Time-Dependent Density Functional Theory

2 Foundations of Time-Dependent Density Functional Theory

I learned very early the difference between knowing the name of something and knowing something.

— R. P. Feynman, (1918-1988).

The basic idea of time-dependent density functional theory (TDDFT) is to describe the time evolution of an electronic quantum many-particle system solely in terms of the time-dependent particle density. The theory is founded on two basic theorems: (i) for a given and fixed initial state there exists a one-to-one mapping between time-dependent densities and local potentials. Every quantum mechanical observable can therefore be written as functional of the time-dependent density and the chosen initial state. (ii) the time-dependent density of a system of interacting electrons can be obtained from an auxiliary system of non-interacting electrons which move in an effective local multiplicative single-particle potential. In analogy to ground-state DFT this potential is termed time-dependent Kohn-Sham potential.

Historically, the first applications of time-dependent DFT were performed by Ando [And77a, And77b], who considered the optical absorption of semiconductor surfaces and Zangwill and Soven [ZS80], who investigated the photoabsorption in rare gases. The first steps towards a rigorous foundation of TDDFT were taken by Deb and Ghosh [DG82, GD82, GD83a, GD83b], who explored potentials that are periodic in time and by Bartolotti [Bar81], who investigated adiabatic processes. The breakthrough for modern TDDFT was achieved in 1984 when Runge and Gross [RG84] proved the uniqueness of the mapping between time-dependent densities and potentials. However, to establish a time-dependent Kohn-Sham scheme they had to postulate non-interacting v-representability[1]. It was shown later by van Leeuwen [vL99] that under mild restrictions on the initial states and boundary conditions it is always possible to find an effective single-particle potential which yields a given density of an *interacting* many-particle system. This solved the long standing v-representability problem of TDDFT and provided the full legitimation for the TDDFT approach.

In this chapter we give a short outline of the basic foundations of time-dependent DFT. This serves as base for all following chapters in this work and allows us to compare the results and extensions of this thesis to the traditional formulation and previous results in TDDFT. We begin in section 2.1 with a summary of the Runge-Gross theorem which provides a rigorous legitimation for a description of a time-dependent many-electron system in terms of the time-dependent electron density. We focus on the prerequisites for the validity of the theorem which are of special interest for the treatment of electronic transport considered in part III of this work. We continue in section 2.2 by introducing the time-dependent

[1] A given electronic density is termed non-interacting v-representable, if there exists a single-particle potential v which yields this density.

Kohn-Sham (TDKS) equations. They provide a practical scheme for the calculation of time-dependent densities and currents of an electronic many-body system. The linearization of the time-dependent Kohn-Sham equations is briefly reviewed in 2.3, where we discuss the linear-response formulation of TDDFT. The central result of the linear-response theory is a Dyson-type equation which connects the Kohn-Sham density-density response function to the response function of the corresponding interacting system.

2.1 Runge-Gross Theorem

The time-dependent extension of the Hohenberg-Kohn theorem of static DFT is directly based on the many-body Schrödinger equation

$$i\frac{\partial}{\partial t}\Psi(t) = \hat{H}(t)\Psi(t) \tag{2.1}$$

with arbitrary but *fixed* initial condition $\Psi(t_0) = \Psi_0$. The many-body Hamiltonian has the form

$$\hat{H}(t) = \hat{T} + \hat{W}_{\mathrm{ee}} + \hat{V}(t), \tag{2.2}$$

where

$$\hat{T} = \sum_{j=1}^{N}\left(-\frac{\nabla_j^2}{2}\right), \tag{2.3}$$

describes the kinetic energy of the electrons and $\hat{W}_{\mathrm{ee}}$ denotes their mutual Coulomb repulsion

$$\hat{W}_{\mathrm{ee}} = \frac{1}{2}\sum_{\substack{i,j=1\\ i\neq j}}^{N}\frac{1}{|\mathbf{r}_i - \mathbf{r}_j|}\,. \tag{2.4}$$

In the following we consider time-dependent potentials of the form

$$\hat{V}(t) = \sum_{i=1}^{N} v(\mathbf{r}_i, t)\,, \tag{2.5}$$

which are assumed to be Taylor expandable around the initial time t_0. Under these rather general prerequisites the following Hohenberg-Kohn-type theorem can be proven [RG84]:

Two solutions $\Psi(t)$ and $\Psi'(t)$ of the Schrödinger equation (2.1) which evolve from a fixed common initial state Ψ_0 under the influence of the potentials $v(\mathbf{r},t)$ and $v'(\mathbf{r},t)$, respectively, always lead to different electron densities $\rho(\mathbf{r},t)$ and $\rho'(\mathbf{r},t)$, provided the two potentials $v(\mathbf{r},t)$ and $v'(\mathbf{r},t)$ differ by more than a purely time-dependent function

$$v'(\mathbf{r},t) \neq v(\mathbf{r},t) + c(t). \tag{2.6}$$

The condition (2.6) assures that there exists an integer $k \geq 0$, such that the Taylor coefficients $v_k(\mathbf{r},t_0) = \partial^k v(\mathbf{r},t)/\partial t^k|_{t_0}$ and $v'_k(\mathbf{r},t_0) = \partial^k v'(\mathbf{r},t)/\partial t^k|_{t_0}$ differ by more than a constant, or equivalently, that the wavefunctions $\Psi(t)$ and $\Psi'(t)$ differ by more than just a purely time-dependent phase factor. The proof of the theorem employs the continuity

equation and the equation of motion for the paramagnetic current density to establish the following relation between the densities and the Taylor coefficients of the potentials [RG84]

$$\left(\frac{\partial}{\partial t}\right)^{k+2}\left(\rho(\mathbf{r},t)-\rho'(\mathbf{r},t)\right)\Big|_{t=t_0}=\nabla\cdot\left(\rho(\mathbf{r},t_0)\nabla(v_k(\mathbf{r},t_0)-v'_k(\mathbf{r},t_0))\right). \tag{2.7}$$

Assuming that the quantity $\rho(\mathbf{r},t)|\nabla v^2(\mathbf{r},t)|$ decays faster than $1/r^2$ for large r for both the primed and unprimed system it can be shown that the right hand side of Eq. (2.7) cannot vanish identically. Consequently, the densities $\rho(\mathbf{r},t)$ and $\rho'(\mathbf{r},t)$ become different infinitesimally later than t_0. In other words, the time-dependent density $\rho(\mathbf{r},t)$ uniquely determines the time-dependent potential $v(\mathbf{r},t)$ up to a purely time-dependent function $c(t)$. Once the potential is obtained, the Schrödinger equation can be solved and the wavefunction is known (up to a purely time-dependent phase $\alpha(t)$). In this sense, the wavefunction can be regarded as *functional* of the time-dependent density

$$\Psi(t)=e^{-i\alpha(t)}\tilde{\Psi}[\rho](t). \tag{2.8}$$

When constructing expectation values

$$O[\rho](t)=\langle\tilde{\Psi}[\rho](t)|\hat{O}(t)|\tilde{\Psi}[\rho](t)\rangle \tag{2.9}$$

the ambiguity in the phase cancels so that the expectation value of any quantum mechanical operator[2] $\hat{O}(t)$ is a *unique* functional of the density.
It is important to notice, that the right hand side of Eq. (2.7) is linear in the difference of the potentials $v_k(\mathbf{r},t_0)-v'_k(\mathbf{r},t_0)$. This implies that the difference between the two densities $\rho(\mathbf{r},t)$ and $\rho'(\mathbf{r},t)$ is non-vanishing already *in first order* of $v_k(\mathbf{r},t_0)-v'_k(\mathbf{r},t_0)$, which ensures the invertibility of linear-response operators.
From the above discussion we can infer that the Runge-Gross theorem does *not* hold for extended systems for which the quantity $\rho(\mathbf{r},t)|\nabla v^2(\mathbf{r},t)|$ is not decaying. The original proof of Runge and Gross therefore provides no legitimation for the treatment of time-dependent electronic transport in extended systems within TDDFT. To cover such systems we have to resort to time-dependent current density functional theory (TDCDFT), where the time-dependent current density is regarded as basic variable. A Hohenberg-Kohn-type theorem for TDCDFT has originally been proven by Ghosh and Dhara [GD88] and more recently a generalization has been been reported by Vignale [Vig04]. Under the assumption that the vector potential can be analytically continued along the real time-axis a proof for the one-to-one correspondence of current densities and vector potentials can be given (up to gauge transformations). Vignale's proof has the distinct advantage that no assumptions have to be made for the decay of charge and current densities at infinity. The proof also covers the Runge-Gross scenario, since any scalar potential can be gauge transformed to a longitudinal vector potential. Since no surface condition needs to be imposed on the charge densities, Vignale's proof can be regarded as an extension of the result of Runge and Gross. Therefore the proof provides a solid legitimation for the treatment of electronic transport within both TDDFT and TDCDFT.

[2] We emphasize that time-derivatives are not considered as being quantum-mechanical operators. Unlike operators which provide mappings between state vectors in Hilbert spaces, time-derivatives provide mappings of complete *paths*.

2.2 Time-Dependent Kohn-Sham Scheme

By virtue of the Runge-Gross theorem the one-to-one correspondence between time-dependent potentials and time-dependent densities can be established for an arbitrary particle interaction $\hat{W}$. In particular, we are free to choose a vanishing interaction $\hat{W} \equiv 0$, which corresponds to non-interacting particles. This fact allows us to relate interacting and non-interacting systems with equal time-dependent densities. Suppose we are interested in an *interacting* system with a given time-dependent density $\rho(\mathbf{r}, t)$. The one-to-one mapping between densities and potentials then guarantees the *uniqueness* of a (local) effective potential $v_{\mathrm{KS}}[\rho](\mathbf{r}, t)$ for *non-interacting* particles which reproduces the density $\rho(\mathbf{r}, t)$ of the *interacting* system. In the original work of Runge and Gross non-interacting v-representability was postulated, i.e. the *existence* of such a potential was assumed. Van Leeuwen [vL99] demonstrated later, by explicit construction, that under mild restrictions on the initial states and boundary conditions such a potential $v_{\mathrm{KS}}[\rho](\mathbf{r}, t)$ can always be found. Since uniqueness and existence of an effective single-particle potential $v_{\mathrm{KS}}[\rho](\mathbf{r}, t)$ are guaranteed we can therefore introduce an auxiliary system of *non-interacting* Kohn-Sham particles which move in the external potential $v_{\mathrm{KS}}(\mathbf{r}, t)$

$$i\frac{\partial}{\partial t}\psi_j(\mathbf{r}, t) = \left(-\frac{\nabla^2}{2} + v_{\mathrm{KS}}[\rho](\mathbf{r}, t)\right)\psi_j(\mathbf{r}, t), \qquad j = 1 \ldots N. \tag{2.10}$$

By construction, the density

$$\rho(\mathbf{r}, t) = \sum_{j=1}^{N} |\psi_j(\mathbf{r}, t)|^2 \tag{2.11}$$

of the non-interacting Kohn-Sham system corresponds to the interacting density $\rho(\mathbf{r}, t)$. In analogy to ground-state DFT, the effective single-particle potential $v_{\mathrm{KS}}(\mathbf{r}, t)$ is written according to

$$v_{\mathrm{KS}}[\rho](\mathbf{r}, t) = v_{\mathrm{ext}}[\rho](\mathbf{r}, t) + v_{\mathrm{H}}[\rho](\mathbf{r}, t) + v_{xc}[\rho](\mathbf{r}, t), \tag{2.12}$$

where

$$v_{\mathrm{H}}[\rho](\mathbf{r}, t) = \int \frac{\rho(\mathbf{r}', t)}{|\mathbf{r} - \mathbf{r}'|}\, d^3r' \tag{2.13}$$

denotes the time-dependent Hartree potential. The only unknown piece is the exchange-correlation potential $v_{xc}[\rho](\mathbf{r}, t)$ which has to be approximated in practice. We emphasize that (2.12) is the defining equation for the time-dependent exchange-correlation potential. The effective single-particle potential $v_{\mathrm{KS}}[\rho](\mathbf{r}, t)$ in the Kohn-Sham equations (2.10) is a local multiplicative operator in real-space which is a major computational advantage over approaches like time-dependent Hartree-Fock or time-dependent configuration interaction. To conclude the section we list some properties of the time-dependent Kohn-Sham scheme:

- It is important to recall that the one-to-one mapping between densities and potentials can only be established for fixed initial states. Therefore, the effective Kohn-Sham potential $v_{\mathrm{KS}}[\rho, \Psi_0, \Phi_0](\mathbf{r}, t)$ also carries a dependence on the initial many-body wavefunction Ψ_0 and the initial Kohn-Sham Slater determinant Φ_0. Compared to ground-state DFT, this is a serious complication, since a new density functional $v_{\mathrm{KS}}[\rho](\mathbf{r}, t)$ is required for every possible initial wavefunction. Fortunately, the initial-state dependence of the time-dependent Kohn-Sham potential drops out if we start from a non-degenerate ground state. In this case the initial wavefunction is a functional of the

ground-state density according to the Hohenberg-Kohn theorem of static DFT [HK64] and hence the time-dependent Kohn-Sham potential becomes a functional of the time-dependent density alone. Most practical calculations are covered by this case but the initial-state dependence has to be faced when time propagations are not started from the ground state. To date, only very little is known about the initial-state dependence of the time-dependent Kohn-Sham potential [MB01].

- The time-dependent Kohn-Sham scheme does not follow from a variational principle. Instead, only the one-to-one mapping provided by the Runge-Gross theorem and van Leeuwen's theorem for the non-interacting v-representability are required as ingredients.

- In perturbation theory one frequently utilizes an adiabatic switching procedure. We emphasize that time-dependent potentials which contain an adiabatic switching of the form $\exp(-\epsilon|t|)$ with $\epsilon \to 0^+$ for $t \to \pm\infty$ are not covered by the Kohn-Sham scheme. Such potentials possess an essential singularity at the initial time and hence violate the prerequisite of Taylor expandability in the Runge-Gross theorem.

- The traditional Kohn-Sham scheme does not allow for magnetic fields or vector potentials. Only time-dependent external fields that can be transformed to a pure scalar potential, using a gauge transformation, are considered. Under these restrictions it is currently not clear if the paramagnetic current densities of the auxiliary Kohn-Sham system and the interacting system are identical. Relating the interacting current and the current of the Kohn-Sham system with $\mathbf{j}(\mathbf{r},t) = \mathbf{j}_{\mathrm{KS}}(\mathbf{r},t) + \mathbf{j}_{\mathrm{xc}}(\mathbf{r},t)$ and using the continuity equation one arrives at

$$\nabla \cdot \mathbf{j}_{\mathrm{xc}}(\mathbf{r},t) = \nabla \cdot \mathbf{j}(\mathbf{r},t) - \nabla \cdot \mathbf{j}_{\mathrm{KS}}(\mathbf{r},t) = 0. \tag{2.14}$$

  In other words, the exchange-correlation current density $\mathbf{j}_{\mathrm{xc}}(\mathbf{r},t)$ is a purely transversal vector field which can be written as $\mathbf{j}_{\mathrm{xc}}(\mathbf{r},t) = \nabla \times \mathbf{K}(\mathbf{r},t)$ with some $\mathbf{K}(\mathbf{r},t)$. Therefore, an equivalence can only be drawn between the longitudinal parts of the interacting current density and the Kohn-Sham current density. It seems unlikely, from the present point of view, that the transversal parts of the two currents densities are in general identical when only scalar external potentials are allowed [MBA+02]. This circumstance has to be taken into account for the description of electronic transport within TDDFT and is considered more in detail in part III of this work.
  If we relax the possible set of external potentials and allow for vector potentials with transverse components then a time-dependent current density functional theory (TDCDFT) can be established, where the electronic current density becomes the basic variable. In this theory the Kohn-Sham system recovers by construction the full many-body current [GD88, Vig04].

2.3 Linear-Response Formulation of TDDFT

Despite the local nature of the effective single-particle potential v_{KS}, the full solution of the time-dependent Kohn-Sham equations can be quite demanding for very large systems. On the other hand, the calculation of physical observables like excitation energies or polarizabilities of atomic and molecular systems requires only the knowledge of the linear density response of the system. A much simpler perturbative solution of the TDKS equations therefore seems desirable.
Following Ref. [GDM96], let us consider a small perturbation $v_1(\mathbf{r},t)$ which is applied at time t_0 to a many-electron system in its ground state

$$v_{\mathrm{ext}}(\mathbf{r},t) = \begin{cases} v_0(\mathbf{r}) & t \le t_0, \\ v_0(\mathbf{r}) + v_1(\mathbf{r},t) & t > t_0. \end{cases} \tag{2.15}$$

The system reacts to this perturbation with a time-dependent density response which can be written as a functional Taylor series

$$\rho(\mathbf{r},t) - \rho_0(\mathbf{r}) = \rho_1(\mathbf{r},t) + \rho_2(\mathbf{r},t) + \rho_3(\mathbf{r},t) + \dots . \tag{2.16}$$

Here, $\rho_0(\mathbf{r})$ denotes the ground-state density of the unperturbed system at $t \le t_0$ and we use a lower index to indicate the order in the external perturbation v_1. The *exact* first oder density response $\rho_1(\mathbf{r},t)$ can be expressed according to

$$\rho_1(\mathbf{r},t) = \int\int \chi(\mathbf{r},t,\mathbf{r}',t')\, v_1(\mathbf{r}',t')\; d^3r'\, dt', \tag{2.17}$$

where χ denotes the density-density response function of the interacting system

$$\chi(\mathbf{r},t,\mathbf{r}',t') = \left.\frac{\delta\rho[v_{\mathrm{ext}}](\mathbf{r},t)}{\delta v_{\mathrm{ext}}(\mathbf{r}',t')}\right|_{v_0} . \tag{2.18}$$

Making use of the functional chain rule the interacting response function can also be written as

$$\chi(\mathbf{r},t,\mathbf{r}',t') = \int\int \left.\frac{\delta\rho(\mathbf{r},t)}{\delta v_{\mathrm{KS}}(\mathbf{y},\tau)}\frac{\delta v_{\mathrm{KS}}(\mathbf{y},\tau)}{\delta v_{\mathrm{ext}}(\mathbf{r}',t')}\right|_{v_0} d^3y\, d\tau. \tag{2.19}$$

Next, we take the functional derivative of Eq. (2.12) with respect to the external potential

$$\begin{aligned} \frac{\delta v_{\mathrm{KS}}(\mathbf{r},t)}{\delta v_{\mathrm{ext}}(\mathbf{r}',t')} &= \delta(\mathbf{r}-\mathbf{r}')\,\delta(t-t') \\ &\quad + \int\int \left(\frac{\delta(t-\tau)}{|\mathbf{r}-\mathbf{y}|} + \frac{\delta v_{\mathrm{xc}}(\mathbf{r},t)}{\delta\rho(\mathbf{y},\tau)}\right)\frac{\delta\rho(\mathbf{y},\tau)}{\delta v_{\mathrm{ext}}(\mathbf{r}',t')}\; d^3y\, d\tau. \end{aligned} \tag{2.20}$$

Inserting Eq. (2.20) into Eq. (2.19) we arrive at

$$\begin{aligned} \chi(\mathbf{r},t,\mathbf{r}',t') &= \chi_{\mathrm{KS}}(\mathbf{r},t,\mathbf{r}',t') + \int d^3y \int d\tau \int d^3y' \int d\tau'\, \chi_{\mathrm{KS}}(\mathbf{r},t,\mathbf{y},\tau) \\ &\quad \times \left(\frac{\delta(\tau-\tau')}{|\mathbf{y}-\mathbf{y}'|} + f_{\mathrm{xc}}[\rho_0](\mathbf{y},\tau,\mathbf{y}',\tau')\right)\chi(\mathbf{y}',\tau',\mathbf{r}',t')\,, \end{aligned} \tag{2.21}$$

where we have introduced the Kohn-Sham response function

$$\chi_{\mathrm{KS}}(\mathbf{r},t,\mathbf{r}',t') := \left.\frac{\delta\rho[v_{\mathrm{KS}}](\mathbf{r},t)}{\delta v_{\mathrm{KS}}(\mathbf{r}',t')}\right|_{v_{\mathrm{KS}}[\rho_0]} \tag{2.22}$$

and the so-called exchange-correlation kernel

$$f_{\mathrm{xc}}[\rho_0](\mathbf{r},t,\mathbf{r}',t') := \left.\frac{\delta v_{\mathrm{xc}}[\rho](\mathbf{r},t)}{\delta\rho(\mathbf{r}',t')}\right|_{\rho_0} . \tag{2.23}$$

Equation (2.21) is the central result of the TDDFT response formalism. It is a Dyson-type equation which relates the interacting and the Kohn-Sham response functions. Inserting the response equation (2.21) back into (2.17) leads to the time-dependent Kohn-Sham equation for the linear density response

$$\rho_1(\mathbf{r},t) = \int\!\!\int \chi_{\mathrm{KS}}(\mathbf{r},t,\mathbf{r}',t')\, v_{\mathrm{KS},1}(\mathbf{r}',t')\; d^3r'\, dt' . \tag{2.24}$$

The effective potential

$$v_{\mathrm{KS},1}(\mathbf{r},t) = v_1(\mathbf{r},t) + \int \frac{\rho_1(\mathbf{r}',t)}{|\mathbf{r}-\mathbf{r}'|}\, d^3r' + \int\!\!\int f_{\mathrm{xc}}[\rho_0](\mathbf{r},t,\mathbf{r}',t')\, \rho_1(\mathbf{r}',t')\; d^3r'\, dt' \tag{2.25}$$

contains the external perturbation v_1, as well as the Hartree- and exchange-correlation contributions up to first order in the perturbing potential v_1. The result in Eqs. (2.24), (2.25) shows, that the *exact* linear density response $\rho_1(\mathbf{r},t)$ of an interacting system can be written as the linear density response of a *non-interacting* system to the effective perturbation $v_{\mathrm{KS},1}(\mathbf{r},t)$.
For the treatment of excitation energies and polarizabilities it is useful to consider the linearized Kohn-Sham equation (2.24) in frequency space. Inserting Eq. (2.25) in Eq. (2.24) and performing a Fourier transform, the frequency-dependent linear density response can be written as

$$\begin{aligned}\rho_1(\mathbf{r},\omega) \;=\; & \int \chi_{\mathrm{KS}}(\mathbf{r},\mathbf{y};\omega) v_1(\mathbf{y},\omega)\, d^3y \\ & + \int\!\!\int \chi_{\mathrm{KS}}(\mathbf{r},\mathbf{y};\omega)\left(\frac{1}{|\mathbf{y}-\mathbf{y}'|} + f_{\mathrm{xc}}[\rho_0](\mathbf{y},\mathbf{y}';\omega)\right)\rho_1(\mathbf{y}',\omega)\, d^3y\, d^3y' .\end{aligned} \tag{2.26}$$

The Kohn-Sham response function χ_{KS} can be directly expressed in terms of the static unperturbed Kohn-Sham orbitals $\psi_k(\mathbf{r}) = \psi_k(\mathbf{r},t_0)$, their occupation numbers f_k (with values 0 or 1), and their orbital energies ϵ_k

$$\chi_{\mathrm{KS}}(\mathbf{r},\mathbf{r}';\omega) = \sum_{j,k}(f_k - f_j)\frac{\psi_j(\mathbf{r})\psi_k^*(\mathbf{r})\psi_j^*(\mathbf{r}')\psi_k(\mathbf{r}')}{\omega - (\epsilon_j - \epsilon_k) + i\eta} . \tag{2.27}$$

The summation extends over both occupied and unoccupied orbitals and includes also the continuum states. We emphasize that some functional derivatives that have been considered in the present section rely on the inverse mappings

$$v_{\mathrm{ext}}(\mathbf{r},t) = v_{\mathrm{ext}}[\rho](\mathbf{r},t), \qquad v_{\mathrm{KS}}(\mathbf{r},t) = v_{\mathrm{KS}}[\rho](\mathbf{r},t) . \tag{2.28}$$

The existence and uniqueness of these mappings are guaranteed by the Runge-Gross proof and van Leeuwen's theorem so that all functional derivatives are well defined (up to purely time-dependent functions in the potentials which cause non-vanishing null-spaces for the response operators).
From the defining relation (2.23) it can be seen that approximations for the exchange-correlation kernel f_{xc} can be obtained by evaluating the functional derivative of approximate time-dependent Kohn-Sham potentials with respect to the density. The most commonly used approximations for the kernel f_{xc} include the adiabatic LDA (ALDA) and the so-called PGG (Petersilka, Gossmann, Gross) kernel. The ALDA is based on the functional form of the static LDA and given by

$$f_{\mathrm{xc}}^{\mathrm{ALDA}}[\rho_0](\mathbf{r},\mathbf{r}';\omega) = \delta(\mathbf{r}-\mathbf{r}')\frac{d^2}{d\rho^2}\left(\rho\epsilon_{\mathrm{xc}}^{\mathrm{hom}}(\rho)\right)\Big|_{\rho=\rho_0(\mathbf{r})}, \tag{2.29}$$

where $\epsilon_{\mathrm{xc}}^{\mathrm{hom}}(\rho)$ is the energy density of the homogeneous electron gas with density ρ. The PGG kernel reads

$$f_{\mathrm{xc}}^{\mathrm{PGG}}[\rho_0](\mathbf{r},\mathbf{r}';\omega) = -\frac{2\left|\sum_k f_k\psi_k(\mathbf{r})\psi_k^*(\mathbf{r}')\right|^2}{|\mathbf{r}-\mathbf{r}'|\,\rho_0(\mathbf{r})\,\rho_0(\mathbf{r}')} \tag{2.30}$$

and is derived from the x-only limit of the time-dependent Kohn-Sham potential within the optimized effective potential (OEP) theory of TDDFT [GDM96]. Both approximations are frequency independent which has implications for the calculation of excitation energies within TDDFT (cf. chapter 3 and appendix A).
Important applications of the TDDFT response formalism include

- The calculation of excitation energies, as detailed in the next chapter.
- Optical absorption spectra of atoms and molecules which are accessible from the frequency-dependent polarizability

$$\alpha_{ij}(\omega) = -\frac{2}{E}\int \rho_1^{(i)}(\mathbf{r},\omega)\, r_j\, d^3r, \qquad i,j = x,y,z \tag{2.31}$$

  that emerges as response to a monochromatic perturbing potential $v_1^{(i)} = E\, r_i \cos(\omega t)$. In general, the photoabsorption cross section tensor $\sigma_{ij}(\omega)$ is related to the tensor of the frequency-dependent polarizability according to

$$\sigma_{ij}(\omega) = \frac{4\pi\omega}{c}\,\Im\,\alpha_{ij}(\omega). \tag{2.32}$$

- The calculation of van der Waals C_6 dispersion coefficients between two linear molecules A and B, which can be computed using the Casimir-Polder formula

$$C_6(A,B) = \frac{3}{\pi}\int_0^\infty \alpha_A(i\omega)\alpha_B(i\omega)\, d\omega. \tag{2.33}$$

To conclude, we stress that all response properties of a system can also be calculated from a direct propagation of the full TDKS equations in real-time with a weak perturbing potential. A key property of the present TDDFT response formalism is that all involved quantities are solely functionals of the ground-state density so that only a much cheaper KS ground-state calculation has to be performed to compute the density response $\rho_1(\mathbf{r},\omega)$.

3 Excitation Energies in Time-Dependent Density Functional Theory

It is a capital mistake to theorise before one has data.
Insensibly one begins to twist facts to suit theories
instead of theories to suit facts.

– Sherlock Holmes, the fictional creation
of Arthur Conan Doyle, (1859-1930).

The treatment of excited-state energies within *static* DFT is a notoriously difficult subject. Several attempts appeared in the literature to tackle the calculation of excitation energies. The perhaps oldest approach, known as ΔSCF, is based on the Rayleigh-Ritz principle for the lowest eigenstate of each symmetry class [GL76, ZRB77, vB79]. Excited-state energies can formally also be expressed exactly in terms of ensemble density functional theory [The79, Koh86, GOK88a, GOK88b, OGK88]. However, both approaches share the problem that very little is known about the specialized energy functionals which have to be employed for the respective technique. Due to lack of approximations, in practice these functionals are often simply replaced by LDA, GGA or other commonly used ground-state energy functionals [BPL95]. Another frequently utilized approach, e.g., as employed for the band structure of solids, is to consider the Kohn-Sham eigenvalues as excited-state energies [AM76]. However, this has no formal justification since the Kohn-Sham eigenvalues are merely a mathematical construct and cannot simply be interpreted as excited-state energies.

A breakthrough for the treatment of excited-state energies was achieved by employing time-dependent DFT. The basic idea of this approach relies on the fact that the frequency-dependent linear density response of a finite system has discrete poles at the true excitation energies of the unperturbed system. The Dyson-type equation (2.21) can be used to relate the poles of the Kohn-Sham response function (located at the Kohn-Sham excitation energies, cf. (2.27)) to the poles of the interacting response function. The perhaps simplest approximation along these lines is the single-pole approximation (SPA) [PGG96] which we briefly review in the next section. In the remainder of this chapter we introduce a double-pole approximation (DPA) to the TDDFT response equations which allows to treat strongly coupled poles and provides, in contrast to the SPA, corrections to the Kohn-Sham oscillator strengths. In other words the DPA accounts for changes in the position *and* the intensity of a transition.

3.1 Single-Pole Approximation

In order to relate the poles of the interacting response function to the poles of the Kohn-Sham response function we rewrite Eq. (2.26) in the form

$$\int \left(\delta(\mathbf{r}-\mathbf{y}') - \int \chi_{\mathrm{KS}}(\mathbf{r},\mathbf{y};\omega)\left(\frac{1}{|\mathbf{y}-\mathbf{y}'|} + f_{\mathrm{xc}}(\mathbf{y},\mathbf{y}';\omega)\right) d^3y\right)\rho_1(\mathbf{y}',\omega)\, d^3y' = \int \chi_{\mathrm{KS}}(\mathbf{r},\mathbf{y};\omega) v_1(\mathbf{y},\omega)\, d^3y\,. \tag{3.1}$$

We can now make use of the fact that in general the Kohn-Sham excitation energies $\omega_p = \epsilon_j - \epsilon_k$ are not identical with the interacting excitation energies Ω_q. Hence, if the frequency ω on the right hand side of Eq. (3.1) approaches one of the true excitation energies, i.e. $\omega \to \Omega_q$, the integral remains finite. On the other hand, the *exact* density response $\rho_1(\mathbf{r},\omega)$ on the left hand side has poles at the true excitation energies Ω_q. In order to preserve equality of both sides the integral operator acting on $\rho_1(\mathbf{r},\omega)$ on the left-hand side of Eq. (3.1) cannot be invertible for $\omega \to \Omega_q$, which leads to the condition

$$\int\int \chi_{\mathrm{KS}}(\mathbf{r},\mathbf{y};\omega)\left(\frac{1}{|\mathbf{y}-\mathbf{y}'|} + f_{\mathrm{xc}}(\mathbf{y},\mathbf{y}';\omega)\right) d^3y\, \zeta(\mathbf{y}',\omega)\, d^3y' = \lambda(\omega)\zeta(\mathbf{r},\omega). \tag{3.2}$$

At the *exact* excitation energies Ω_q the function $\lambda(\omega)$ satisfies

$$\lambda(\Omega_q) = 1\,. \tag{3.3}$$

So far no approximations have been made. For the exact Kohn-Sham response function and the exact exchange-correlation kernel, the relations (3.2) and (3.3) determine the *exact* excitation spectrum of the *interacting* system. To investigate the pole structure of the eigenvalue problem (3.2) more closely we perform a Laurent expansion around a given Kohn-Sham excitation energy ω_p

$$\zeta_p(\mathbf{r},\omega) = \zeta_p(\mathbf{r},\omega_p) + \left.\frac{d\zeta_p(\mathbf{r},\omega)}{d\omega}\right|_{\omega_p}(\omega-\omega_p) + \ldots, \tag{3.4}$$

$$\lambda(\omega) = \frac{A(\omega_p)}{\omega-\omega_p} + B(\omega_p), + \ldots\,. \tag{3.5}$$

Next, let us consider a scenario where a single pole ω_p of the excitation spectrum is well separated from the remaining poles of the response function. In addition we can expect that the corresponding interacting excitation energy Ω_q is located in the vicinity of the Kohn-Sham excitation ω_p. In this limit only the leading term of the Laurent series (3.5) is dominating and we can truncate the expansion according to

$$\lambda(\omega) \approx \frac{A(\omega_p)}{\omega-\omega_p}\,. \tag{3.6}$$

Using the the condition (3.3) and its complex conjugate $\lambda^*(\Omega_q) = 1$ together with Eq. (3.6) we arrive at the so-called single-pole approximation (SPA)

$$\Omega_q = \omega_p + \Re A(\omega_p), \tag{3.7}$$

where the Laurent coefficient $A(\omega_p)$ is found to be [PGG96]

$$A(\omega_p) = 2 \int\int \psi_k^*(\mathbf{r})\psi_j(\mathbf{r}) \left(\frac{1}{|\mathbf{r}-\mathbf{r}'|} + f_{\mathrm{xc}}(\mathbf{r},\mathbf{r}';\omega_p) \right) \psi_k(\mathbf{r}')\psi_j^*(\mathbf{r}') \; d^3r \, d^3r'. \tag{3.8}$$

The result in Eq. (3.7) shows that in the SPA the true excitation energies Ω_q are obtained from the Kohn-Sham excitations ω_p by simple additive shifts. In general, the Laurent coefficients $A(\omega_p)$ carry a dependence on the index p, so that a single Kohn-Sham excitation can lead to several interacting excitation energies. Of course, the above assumption of well separated poles is not always justified, e.g. for the dense excitation spectrum of Rydberg states. However, the simple additive structure of Eq. (3.7) allows to separately investigate the effects that are caused by approximate ground-state potentials and exchange-correlation kernels, i.e. the quality of the bare Kohn-Sham excitations versus the quality of the additive shifts. The SPA therefore became a useful tool for the analysis of excitation spectra in the TDDFT response formalism.

3.2 Double-Pole Approximation

The solution to the TDDFT response equations has been implemented in several quantum chemical software packages. Nowadays excitation spectra of molecules are calculated routinely and have been reported in numerous papers (see e.g. the references in [MBA+02, FR05]). Provided accurate Kohn-Sham ground-state potentials are used, the obtained transition frequencies are typically within about 0.2 eV of experiment. Due to the combination of accuracy with low computational cost TDDFT has seen its greatest use in the calculation of low-lying photo-excitations of molecules. Configuration interaction singles is the only alternative which is comparable in numerical effort for this purpose. Methods, such as more complete configuration-interaction, Bethe-Salpeter, or quantum Monte Carlo calculations, are more accurate, but also more expensive in practice which limits their usage to much smaller systems.
Although the TDDFT response methodology is in widespread use, the reliability and the accuracy of the underlying approximations in TDDFT are much less well understood than they are in ground-state DFT. Performing systematic calculations for many systems with various approximations for the involved functionals (i.e. v_{xc} and f_{xc}) is merely empirical and does not give much insight why the approximations are not reliable in some cases. Also, these calculations help little to improve existing functionals. It can be much more effective to develop simple approximations to the response equations to gain understanding for the reliability of the TDDFT response formalism [AGB03].
Along these lines we introduce a double-pole approximation (DPA) to the TDDFT response equation in this section. This extends the previously discussed single-pole approximation to the case of two strongly interacting poles. In contrast to the SPA the DPA provides a correction of the Kohn-Sham oscillator strengths and gives insight in the XC corrections to the Kohn-Sham excitations when strong coupling between poles is present. Inverting the DPA solution allows us to compute matrix elements of the exchange-correlation kernel f_{xc} from experimental input. This serves as benchmark for the future development of XC kernels.

3.2.1 Exact Solution of Casida's Equations

In the following we consider a three level system with energies E_j, states $|\,j\,\rangle$, $(j = 1, 2, 3)$, excitations $\Omega_1 = E_3 - E_2$, $\Omega_2 = E_3 - E_1$, and oscillator strengths f_1, f_2, as illustrated in Fig. 3.1. The transition $2 \to 1$ is assumed to be dipole forbidden. Furthermore, we denote with ϵ_j, $|\,j\,\rangle^{KS}$, $(j = 1, 2, 3)$, $\omega_1 = \epsilon_3 - \epsilon_2$, $\omega_2 = \epsilon_3 - \epsilon_1$ and f_1^{KS}, f_2^{KS} the corresponding Kohn-Sham energies, states, excitations, and oscillator strengths. With $x_1 = {}^{KS}\langle\,3\,|\,x\,|\,2\,\rangle^{KS}$ and $x_2 = {}^{KS}\langle\,3\,|\,x\,|\,1\,\rangle^{KS}$ we abbreviate the Kohn-Sham dipole matrix elements. In the matrix formulation of the TDDFT response equation for the spin-singlet case the exact eigenvalues and oscillator strengths of an interacting many-particle system can be obtained from the solution of the following eigenvalue problem [Cas95], (a derivation is given in appendix A):

$$\sum_{q'} W_{qq'}(\Omega_j)\; F_{q',j} = \Omega_j^2\; F_{q,j}, \tag{3.9}$$

where the matrix $W_{qq'}$ is given by

$$W_{qq'}(\Omega) = \omega_q^2\,\delta_{qq'} + 4\sqrt{\omega_q\,\omega_{q'}}\,M_{qq'}(\Omega) \tag{3.10}$$

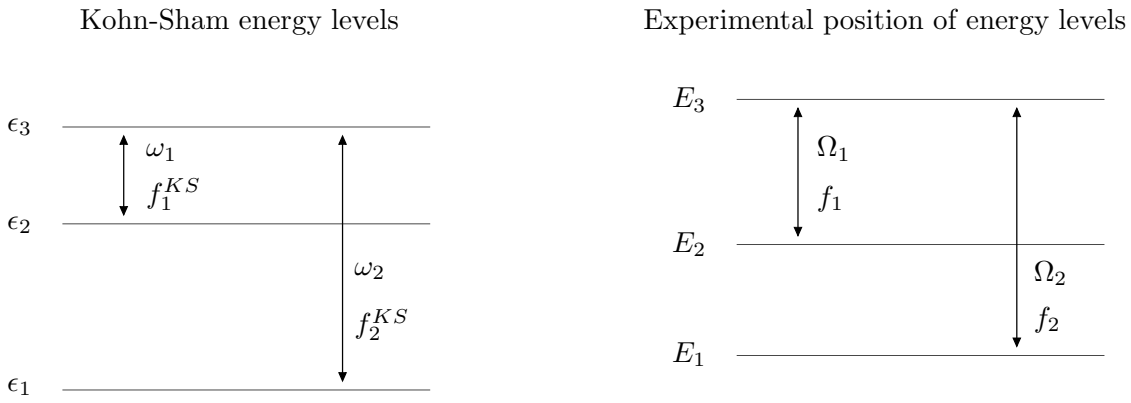

Figure 3.1: Schematic illustration of a 3-level model as considered in the double-pole approximation. Left panel: Level positions ϵ_j, excitation energies ω_j, and oscillator strengths f_j^{KS} of the Kohn-Sham system. Right panel: Level positions E_j, excitation energies Ω_j, and oscillator strengths f_j of the corresponding interacting system.

with

$$M_{qq'}(\Omega) := \langle q|K(\Omega)|q'\rangle = \int\int \Phi_q^*(\mathbf{r})K(\mathbf{r},\mathbf{r}',\Omega)\,\Phi_{q'}(\mathbf{r}')\;d^3r\,d^3r'. \tag{3.11}$$

The kernel $K(\mathbf{r},\mathbf{r}',\omega)$ consists of the bare Coulomb interaction and some approximate XC kernel $f_{xc}(\mathbf{r},\mathbf{r}',\omega)$

$$K(\mathbf{r},\mathbf{r}',\omega) = \frac{e^2}{|\mathbf{r}-\mathbf{r}'|} + f_{xc}(\mathbf{r},\mathbf{r}',\omega). \tag{3.12}$$

With q we denote a single-particle transition, $q \equiv k \to j$, and we have introduced the shorthand $\Phi_q(\mathbf{r}) := \psi_k(\mathbf{r})\psi_j^*(\mathbf{r})$ to abbreviate the product of Kohn-Sham orbitals which are involved in the transition. In the case of a three level system the eigenvalue problem (3.9) reduces to the following 2×2-system

$$\begin{pmatrix} \omega_1^2 + 4\omega_1^2\,M_{11} & 4\sqrt{\omega_1}\,M_{12}\sqrt{\omega_2} \\ 4\sqrt{\omega_2}\,M_{21}\sqrt{\omega_1} & \omega_2^2 + 4\omega_2^2\,M_{22} \end{pmatrix} \mathbf{F}_j = \Omega_j^2\,\mathbf{F}_j \qquad j = 1,2. \tag{3.13}$$

To simplify the discussion, we assume real orbitals and a real, frequency-independent kernel K, i.e. $M_{qq'} = M_{q'q}$. Casida's matrix elements $W_{qq'}$ are then related to the matrix elements $M_{qq'}$ of the kernel according to

$$\begin{gathered} W_{11} := \omega_1^2 + 4\omega_1\,M_{11}, \qquad W_{22} := \omega_2^2 + 4\omega_2\,M_{22}, \\ W_{12} = W_{21} := 4\,\sqrt{\omega_1\omega_2}\,M_{12}. \end{gathered} \tag{3.14}$$

For the further discussion we introduce the average and the difference of the diagonal elements

$$\Delta := \frac{1}{2}(W_{11} + W_{22}), \quad \delta := W_{22} - W_{11}, \tag{3.15}$$

and define a mixing angle θ by

$$\tan\theta = \frac{2\,W_{12}}{W_{22} - W_{11}}. \tag{3.16}$$

With these shorthands we obtain for the eigenvalues of Eq. (3.13)

$$\begin{aligned}\Omega_1^2 &= \Delta - \frac{1}{2}\frac{\delta}{\cos\theta} = \frac{1}{2}(W_{11}+W_{22}) - \frac{1}{2}\sqrt{(W_{22}-W_{11})^2 + 4\,W_{12}^2},\\ \Omega_2^2 &= \Delta + \frac{1}{2}\frac{\delta}{\cos\theta} = \frac{1}{2}(W_{11}+W_{22}) + \frac{1}{2}\sqrt{(W_{22}-W_{11})^2 + 4\,W_{12}^2},\end{aligned} \tag{3.17}$$

which allows to express the excitation energies Ω_j directly in terms of Kohn-Sham excitation energies and matrix elements of the kernel f_{xc}. Besides the excitation energies also the *normalized* eigenvectors of the matrix $W_{qq'}$ can be expressed in closed form as

$$\mathbf{F}_1 = \begin{pmatrix} -\cos\frac{\theta}{2} \\ \sin\frac{\theta}{2} \end{pmatrix}, \qquad \mathbf{F}_2 = \begin{pmatrix} \sin\frac{\theta}{2} \\ \cos\frac{\theta}{2} \end{pmatrix}. \tag{3.18}$$

The eigenvectors carry information about the physical oscillator strengths which can be obtained from [Cas95]

$$f_j = \frac{2}{3}\,|\mathbf{x}^T\, S^{-\frac{1}{2}}\,\mathbf{F}_j|^2, \tag{3.19}$$

where

$$S^{-\frac{1}{2}} := \begin{pmatrix} \sqrt{\omega_1} & 0 \\ 0 & \sqrt{\omega_2} \end{pmatrix}, \qquad \mathbf{x} := \begin{pmatrix} x_1 \\ x_2 \end{pmatrix} = \begin{pmatrix} {}^{KS}\langle\, 3\,|\,x\,|\,2\,\rangle^{KS} \\ {}^{KS}\langle\, 3\,|\,x\,|\,1\,\rangle^{KS} \end{pmatrix}. \tag{3.20}$$

Evaluating Eq. (3.19) with our result (3.18), we find for the oscillator strengths

$$\begin{aligned} f_1 &= \frac{2}{3}\left(\omega_1\,x_1^2\cos^2\frac{\theta}{2} + \omega_2\,x_2^2\sin^2\frac{\theta}{2} - \sqrt{\omega_1\omega_2}\,x_1\,x_2\sin\theta\right)\\ &= \left(\sqrt{f_1^{KS}}\cos\frac{\theta}{2} - \sqrt{f_2^{KS}}\sin\frac{\theta}{2}\right)^2, \end{aligned} \tag{3.21}$$

$$\begin{aligned} f_2 &= \frac{2}{3}\left(\omega_1\,x_1^2\sin^2\frac{\theta}{2} + \omega_2\,x_2^2\cos^2\frac{\theta}{2} + \sqrt{\omega_1\omega_2}\,x_1\,x_2\sin\theta\right)\\ &= \left(\sqrt{f_1^{KS}}\sin\frac{\theta}{2} + \sqrt{f_2^{KS}}\cos\frac{\theta}{2}\right)^2. \end{aligned} \tag{3.22}$$

Obviously, this solution to the TDDFT response equation obeys the Thomas-Reiche-Kuhn sum rule

$$\sum_{j=1}^{2} f_j = f_1 + f_2 = \frac{2}{3}(\omega_1\,x_1^2 + \omega_2\,x_2^2) = f_1^{KS} + f_2^{KS} = 1, \tag{3.23}$$

where we have normalized the sum without loss of generality. Since we have by definition $f_j \geq 0$, we can introduce two angles α^{KS} and α by

$$f_1^{\mathrm{KS}} = \sin^2\alpha^{\mathrm{KS}}, \qquad f_2^{\mathrm{KS}} = \cos^2\alpha^{\mathrm{KS}}, \tag{3.24}$$

and

$$f_1 = \sin^2\alpha, \qquad f_2 = \cos^2\alpha, \tag{3.25}$$

which gives the oscillator strengths a geometrical meaning. Using trigonometric identities, we find from Eqs. (3.21), (3.22)

$$\begin{aligned} f_1 \;=\; \sin^2\alpha \;&=\; \Big\{ \frac{1}{2}\left(\sin(\alpha^{\mathrm{KS}} - \theta/2) + \sin(\alpha^{\mathrm{KS}} + \theta/2)\right) \\ &\quad -\frac{1}{2}\left(\sin(\theta/2 - \alpha^{\mathrm{KS}}) + \sin(\theta/2 + \alpha^{\mathrm{KS}})\right)\Big\}^2 \\ &=\; \sin^2(\alpha^{\mathrm{KS}} - \theta/2) \end{aligned} \tag{3.26}$$

$$\begin{aligned} f_2 \;=\; \cos^2\alpha \;&=\; \Big\{ \frac{1}{2}\left(\cos(\alpha^{\mathrm{KS}} - \theta/2) - \cos(\alpha^{\mathrm{KS}} + \theta/2)\right) \\ &\quad -\frac{1}{2}\left(\cos(\alpha^{\mathrm{KS}} - \theta/2) + \cos(\alpha^{\mathrm{KS}} + \theta/2)\right)\Big\}^2 \\ &=\; \cos^2(\alpha^{\mathrm{KS}} - \theta/2), \end{aligned} \tag{3.27}$$

or, equivalently,

$$\alpha = \alpha^{\mathrm{KS}} - \theta/2. \tag{3.28}$$

Together with Eq. (3.17) this is the central result of the present section. The expression shows that the oscillator strengths are represented by a unit vector in 2D space. The coupling merely *rotates* this vector. We note in passing that the single-pole approximation of TDDFT can be recovered from these results by setting $\theta = 0$. From this point of view it is also obvious that the SPA predicts no variation in the interacting oscillator strengths.

3.2.2 Model Illustrations

To illustrate the DPA solution of the previous section, consider a weak lower-frequency transition ($\omega_1 = 9$ eV, $f_1^{KS} = 1/10$) and a strong higher-frequency transition ($\omega_2 = 12$ eV, $f_2^{KS} = 9/10$). Imagine both transitions have significant diagonal kernel matrix elements $M_{11} = 3$ eV, $M_{22} = 2$ eV, but are not strongly coupled to one another, $M_{12} = 0.2$ eV. We model the corresponding spectra in the following illustrations by using Lorentzians of width 0.2.

The left panel of Fig. 3.2 shows the interacting and Kohn-Sham spectra for this model. Due to the weak coupling, the single-pole approximation is excellent, and accurately predicts the large shifts in positions. However, SPA wrongly predicts no variation in oscillator strength. On the other hand, one can see from the DPA solution in the figure that the first peak has actually *lost* intensity relative to its Kohn-Sham value, whereas the second peak has *gained* intensity. Note that the total intensity of the spectrum is preserved, since the DPA solution obeys the TRK sum rule (cf. Eq. (3.23)). Next, we consider the same parameters as before, but imagine increasing ω_1. In the right panel of Fig. 3.2 we display the mixing angle θ as function of ω_1. For an excitation energy $\omega_c = 2\,(-3 + \sqrt{69}) \approx 10.61$ eV the matrix elements W_{11} and W_{22} become identical and ΔW vanishes. In this case the angle θ takes a value of $\theta = \pi/2$ and the excitations of the interacting system are a 50:50 mixture of the two Kohn-Sham excitations.

In the left panel of Fig. 3.3 we plot Kohn-Sham and interacting excitation energies as

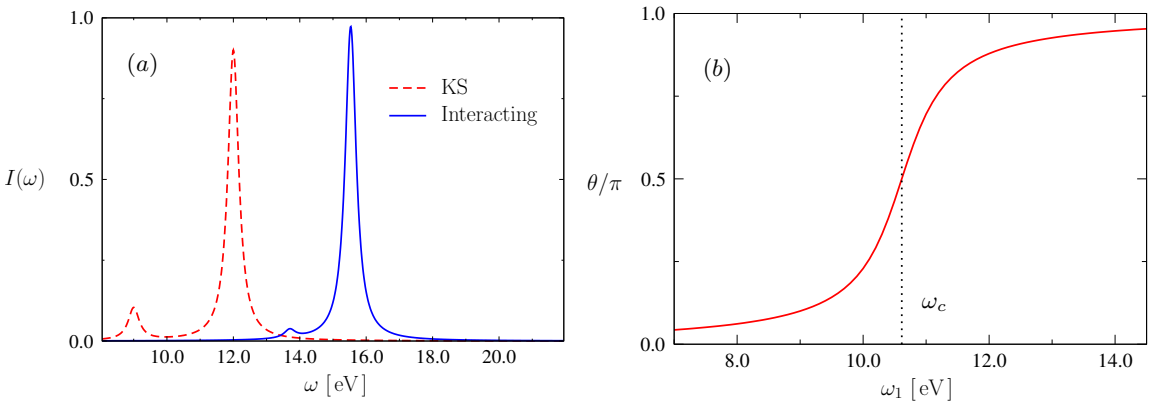

Figure 3.2: (a) Interacting and Kohn-Sham spectra as function of frequency ($\omega_1 = 9$ eV, $M_{12} = 0.2$ eV). (b) The scaled coupling angle θ/π as function of the position of the lower transition.

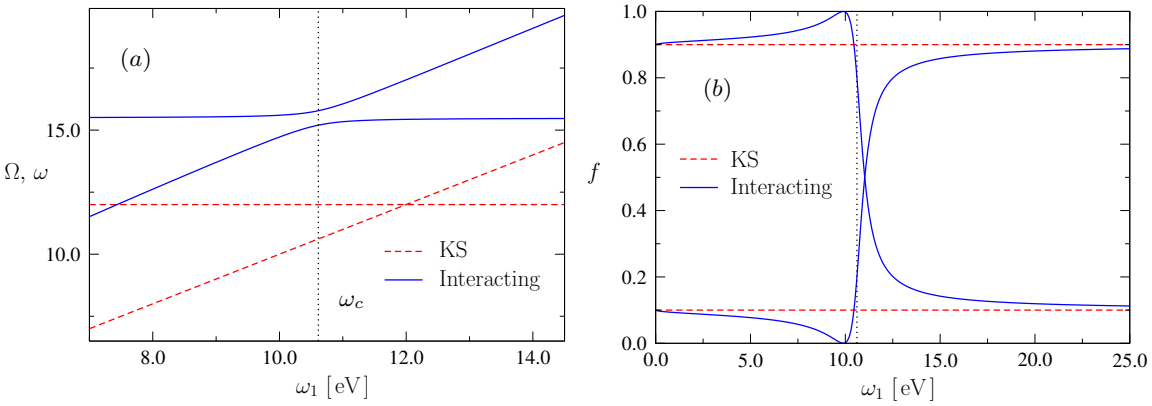

Figure 3.3: (a) Interacting and Kohn-Sham excitation energies as function of ω_1. (b) Oscillator strengths as function of ω_1.

functions of ω_1. The two poles undergo an avoided crossing at ω_c (c for *crossing*). Note that straight lines, extrapolated from the limits $\omega_1 \ll \omega_c$ and $\omega_1 \gg \omega_c$, yield extremely accurate results almost everywhere which corresponds to the SPA result.

In the right panel of Fig. 3.3 we display the associated oscillator strengths. The effect of the coupling is dramatic. Note first that, for ω_1 below the strong coupling region, the bigger peak is *enhanced* above its Kohn-Sham value, and the smaller one reduced. This is pole repulsion, and it is felt even very far from the strong coupling region. This effect is entirely missing in the SPA (recall, that the oscillator strengths in the SPA correspond merely to the unaltered Kohn-Sham oscillator strengths which are indicated with dashed lines). Increasing ω_1 further, we see that there is a critical value ω_d (d for *dark*) at which the smaller oscillator strength vanishes exactly, i.e. $f_1 = 0$. This illustrates that the interaction can cause a peak to vanish entirely from the optical spectrum of the system. If we rise ω_1 further, the intensities of the two excitations cross at ω_e (e for *equal*) and finally reverse in magnitude.

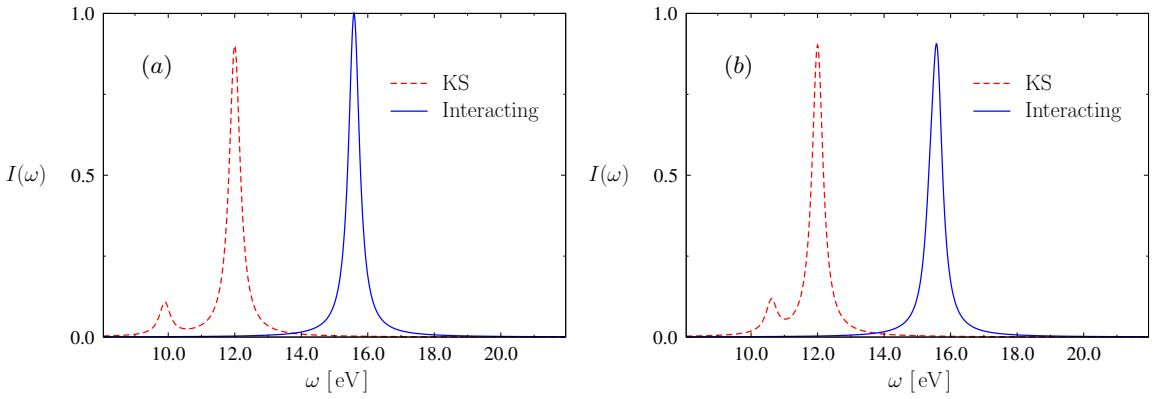

Figure 3.4: (a) Interacting and Kohn-Sham spectra at the critical value $\omega_1 = \omega_d \approx 9.90$ eV. All intensity is in the upper transition. (b) Interacting and Kohn-Sham spectra for $\omega_1 = \omega_c \approx 10.61$ eV.

3.2.3 Magic Positions in the Spectra

We have seen so far that the oscillator strengths exhibit several special features as function of the pole separation. Three critical pole separations have been identified. These magic positions are present in every interacting spectrum when two poles are coupled and separated from the rest of the spectrum. In this section we summarize the relations which can be used to calculate these magic pole separations.

ω_d - Dark point

The first interesting separation of excitation energies causes one of the peaks to vanish. As observed above, there exists a critical value ω_d for the first Kohn-Sham excitation energy ω_1 for which we have exactly

$$f_1 = \left(\sqrt{f_1^{KS}}\cos\frac{\theta}{2} - \sqrt{f_2^{KS}}\sin\frac{\theta}{2}\right)^2 = 0, \tag{3.29}$$

i.e.

$$\tan\frac{\theta}{2} = \frac{\sqrt{f_1^{KS}}}{\sqrt{f_2^{KS}}}. \tag{3.30}$$

Inserting Eq. (3.30) in Eq. (3.16) it is straight forward to see, that this position can be obtained from the roots of the following equation in ω_d

$$\tan\left(2\arctan\frac{\sqrt{f_1^{KS}}}{\sqrt{1-f_1^{KS}}}\right) - \frac{2W_{12}(\omega_d)}{\Delta W(\omega_d)} = 0. \tag{3.31}$$

The spectrum for this case is displayed in Fig. 3.4 (a), which shows clearly that the smaller peak has vanished and all intensity has been shifted to the larger peak.

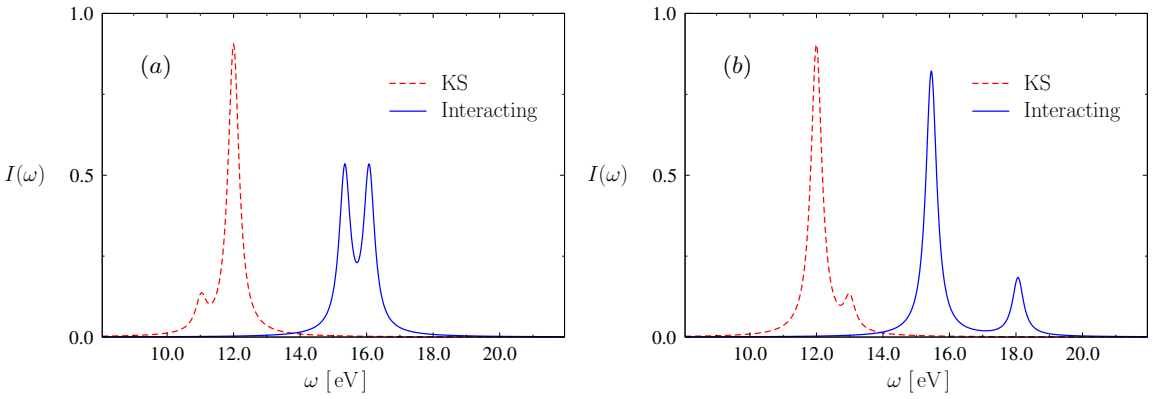

Figure 3.5: (a) Interacting and Kohn-Sham spectra for $\omega_1 = \omega_e \approx 11.02$ eV, producing equal interacting oscillator strengths. (b) Interacting and Kohn-Sham spectra for $\omega_1 = 13$ eV.

ω_c - Position of the Avoided Crossing

The avoided crossing of the interacting excitation energies appears exactly at $\theta = \pi/2$, i.e. for

$$\Delta W(\omega_c) = 0 \quad \Rightarrow \quad \omega_c^2 + 4\,M_{11}\,\omega_c - (\omega_2^2 + 4\,\omega_2\,M_{22}) = 0, \tag{3.32}$$

with solutions

$$\omega_c^{\pm} = -2\,M_{11} \pm \sqrt{4\,M_{11}^2 + \omega_2^2 + 4\,\omega_2\,M_{22}}. \tag{3.33}$$

For the parameters of the model $\omega_c^+ = -6+2\sqrt{9+36+24}$ eV $= 2\,(-3+\sqrt{69}) \approx 10.61$ eV. For the oscillator strengths Eqs. (3.21), (3.22) yield in this case

$$f_{1,2} = \frac{1}{2} \pm \sqrt{f_1^{\mathrm{KS}}\,f_2^{\mathrm{KS}}}. \tag{3.34}$$

In our case, this results in $f_1 = 0.2$ and $f_2 = 0.8$, respectively, giving the lower peak *double* its Kohn-Sham weight. In Fig. 3.4 (b), we show the spectrum for $\omega_1 = \omega_c$, and observe how much it differs from the Kohn-Sham spectrum. There appears to be only one peak, but in fact there are still two, although the broadening obscures the second peak.

ω_e - Equal Interacting Oscillator Strengths

The final interesting point is ω_e (e for *equal*), where the interacting oscillator strengths equal, i.e., both are 1/2. At the equality point, $\alpha = \pi/4$, and hence $\theta = \pi/2 - 2\alpha^{\mathrm{KS}}$.
By equating Eqs. (3.21) and (3.22), the position of ω_e can be obtained from the roots of the following equation

$$\tan\left(2\,\arctan\frac{\sqrt{f_1^{KS}} - \sqrt{1-f_1^{KS}}}{\sqrt{f_1^{KS}} + \sqrt{1-f_1^{KS}}}\right) - \frac{2W_{12}(\omega_e)}{\Delta W(\omega_e)} = 0. \tag{3.35}$$

This situation is shown in Fig. 3.5 (a) where we illustrate the corresponding Kohn-Sham

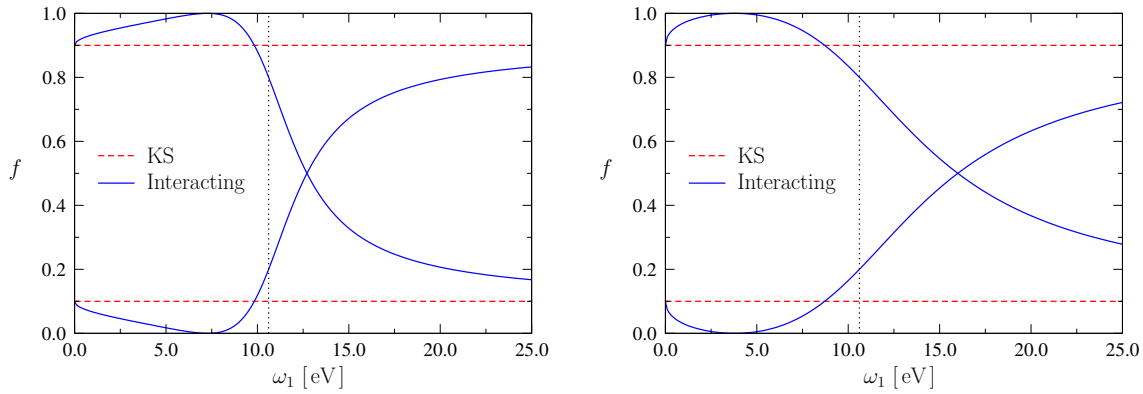

Figure 3.6: Same as Fig. 3.3, but for the case $M_{12} = 1.0$ eV (left panel) and for the case $M_{12} = 2.5$ eV (right panel).

and interacting spectra.

To conclude this section we display in Fig. 3.5 (b) a frequency of $\omega_1 = 13$ eV for the first Kohn-Sham excitation energy, so that $\omega_1 > \omega_2$. For this value of ω_1 the oscillator strengths have returned (almost) to their Kohn-Sham values, cf. Fig. 3.3. However, the interacting intensities are reversed in magnitude compared to Fig. 3.2, where $\omega_1 < \omega_2$.

3.2.4 Strength of the Interaction

In Fig. 3.7, we demonstrate the dependence of the coupling angle θ on the strength of the coupling M_{12} relative to the diagonal elements. So far we have presented only the case $M_{12} << M_{ii}$. Increasing M_{12} does not change the shape of the curves (around the turnover point), but only changes the scale on which the action takes place. Therefore, the scale to compare the off-diagonal matrix element to is not the absolute magnitude of the diagonal matrix elements but the splitting of the excitation energies. The corresponding oscillator strengths as functions of pole separation are illustrated in Fig. 3.6. Compared to Fig. 3.3 the overall shape stays the same for stronger pole coupling, only a broader interaction area is observed which is expected from the spreading of the mixing angle in Fig. 3.7.

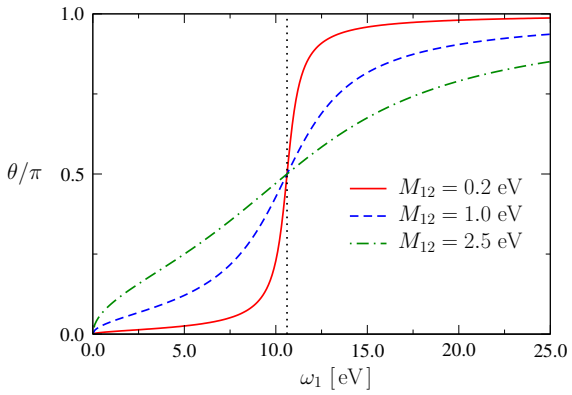

Figure 3.7: The scaled coupling angle θ/π as function of ω_1. The plot compares three different regimes for the off-diagonal matrix element M_{12}.

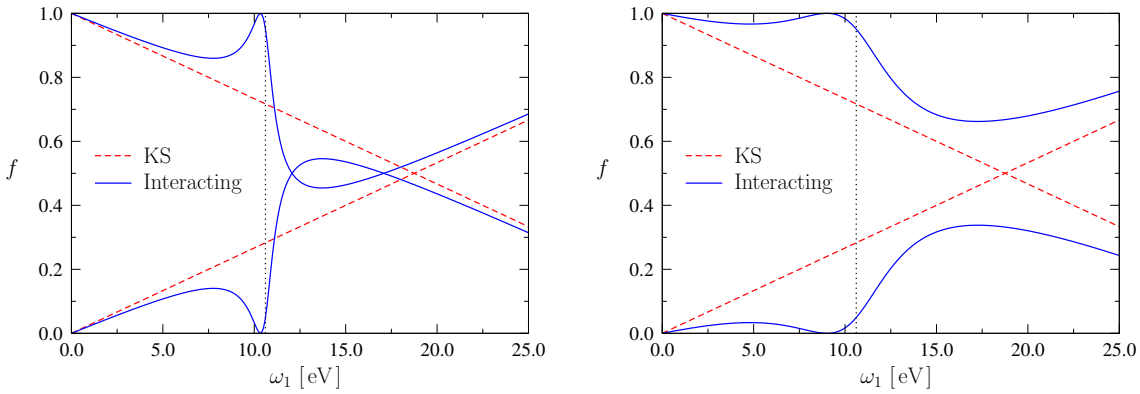

Figure 3.8: Left panel: Linear frequency dependence of Kohn-Sham oscillator strengths for the case $M_{12} = 0.2$ eV. Right panel: Same as the left panel, but for a stronger coupling of the poles with $M_{12} = 1.0$ eV.

3.2.5 Frequency-Dependent Kohn-Sham Oscillator Strengths

So far, we have only considered frequency-independent Kohn-Sham oscillator strengths. However, already from their definition

$$f_q^{\mathrm{KS}} = \frac{2}{3}\,\omega_q\,|\langle\, x_q \,\rangle_{\mathrm{KS}}|^2, \tag{3.36}$$

we observe an inherent frequency dependence - even for frequency-independent dipole matrix elements. We therefore investigate a linear frequency dependence for f_1^{KS} in Fig. 3.8. The second oscillator strength is adjusted such as to satisfy the TRK sum rule. From the figures it is apparent that the interacting oscillator strengths asymptotically follow their Kohn-Sham counterparts. Deviations occur only in the interaction region around the position of the avoided crossing and around the crossing of the Kohn-Sham oscillator strengths. This feature remains even for frequency-dependent dipole matrix elements $\langle\, x_q \,\rangle_{\mathrm{KS}}$, i.e. no matter how strong the frequency dependence of the Kohn-Sham oscillator strengths will be, the interacting oscillator strengths will follow their Kohn-Sham counterparts far away from the crossing points. Depending on the magnitude of M_{12} there can be two intersection points (left panel of Fig. 3.8), or no intersection point (right panel of Fig. 3.8). The order in the asymptotic region is not reversed in both cases.

3.2.6 Inversion of the Double-Pole Solution

The above sections present the TDDFT response equations in the usual manner. First one solves the ground-state Kohn-Sham problem, finding occupied and unoccupied levels, then one calculates the matrix elements of the kernel (with some functional approximation), and calculates the true transitions and oscillator strengths of the system. However, we are motivated to gain insight into the excitations, and so we ask the reverse question [SGA+05]: Given the experimental spectrum, what can we learn about the kernel? Inverting Eq. (3.28) to solve for θ yields

$$\theta = 2\,(\alpha - \alpha^{\mathrm{KS}}). \tag{3.37}$$

Thus, knowledge of the Kohn-Sham oscillator strengths, combined only with the experimental oscillator strengths, yields the angle θ, which measures how strongly the transitions are mixed. No knowledge of the *positions* of the transitions is needed.
Solving for the diagonal matrix elements we arrive at

$$\begin{aligned} W_{11} &= \overline{\Omega^2} - \Delta\Omega^2 \cos\theta/2, \\ W_{22} &= \overline{\Omega^2} + \Delta\Omega^2 \cos\theta/2, \end{aligned} \tag{3.38}$$

where $\overline{\Omega^2}$ is the average and $\Delta\Omega^2$ is the difference of the squared excitation energies, while the off-diagonal matrix element is

$$W_{12} = \Delta\Omega^2 \ \sin\theta/2. \tag{3.39}$$

Again, the experimental positions combined with the mixing angle are sufficient to determine the elements of the matrix $W_{qq'}$. The kernel matrix elements themselves are then found simply, by using the Kohn-Sham transition frequencies, i.e.

$$M_{qq} = \frac{W_{qq}}{4\,\omega_q} - \frac{\omega_q}{4}, \qquad q = 1, 2 \tag{3.40}$$

and

$$M_{12} = \frac{\Delta\Omega^2 \ \sin\theta}{8\sqrt{\omega_1\omega_2}}. \tag{3.41}$$

These equations provide an exact way to recover the matrix elements $W_{qq'}$ of the Casida matrix and therefore the matrix elements $M_{qq'}$ of the kernel $K(\mathbf{r}, \mathbf{r}', \omega)$ solely from the knowledge of the Kohn-Sham eigenvalues and the angle θ.

3.3 Summary and Outlook

Time-dependent density functional theory has become a popular method to calculate the neutral photo-excitations of atomic and molecular systems. Especially the low computational cost is an attractive feature which has established the TDDFT approach as method of choice for many applications in physics and quantum chemistry. Although the TDDFT methodology is in widespread use, there is still a lack of understanding in the approximations which are involved in the calculations. Simple approximations of the response equations, like the SPA, turn out to be useful in practice to gain insight into the effects which are caused by different approximate functionals.
In this work we have presented a double-pole approximation to the TDDFT response equations. The DPA extends the treatment of the traditional SPA to the case of two strongly coupled poles. In contrast to the SPA, the DPA yields a correction of the Kohn-Sham oscillator strengths. Our analysis reveals that interacting oscillator strengths can deviate significantly from their Kohn-Sham values, even when the coupling between poles is very weak. With help of the DPA we have shown that interacting spectra exhibit several critical pole separations. As example, the coupling of two excitations can cause a dark point where the weaker pole completely vanishes in the interacting spectrum. Also, the corrections to the Kohn-Sham excitations can be studied. We found that the positions of the interacting excitation energies undergo an avoided crossing as a function of the pole separation. In

the present analysis we have also shown how to construct an inversion of the DPA solution to predict matrix elements of the exchange-correlation kernel f_{xc} from experimental input. This can be utilized in the future as reference for the construction of functionals for the kernel f_{xc}. Besides providing such a reference, the exact analytical solution of the DPA can also serve as a useful tool for the investigation of scenarios where strongly coupled poles are present. A prominent example are conical intersections of molecular potential energy surfaces. Since the DPA stays valid for arbitrary coupling strength the change of oscillator strengths and excitation energies in the vicinity of a conical intersection can be explored in that case and the effect of different approximations for v_{xc} and f_{xc} can be studied.

Part II

Time-Dependent Natural Orbitals and Reduced Density Matrices

4 Static Reduced Density Matrix Functional Theory

It doesn't matter how beautiful your theory is,
it doesn't matter how smart you are.
If it doesn't agree with experiment, it's wrong.

— R. P. Feynman, (1918-1988).

Consider a non-relativistic quantum many-body system with N electrons. The stationary properties of such a system are described by the many-body wavefunction $|\,\Psi\,\rangle$ which obeys the time-independent many-body Schrödinger equation

$$\left(\hat{H} - E\right) \,|\,\Psi(1,...,N)\,\rangle = 0. \tag{4.1}$$

Although the ground-state properties of such a system are completely determined by Eq. (4.1), the solution of the Schrödinger equation is not desirable in practice. Even if it were possible to solve for the wavefunction of a large system which is of chemical, biological or technological interest, the result is usually too complicated to provide an intuitive physical picture of the system. Instead, it is physically more appealing to work with integrated quantities like currents or densities which provide direct insight into the properties of the system. One approach along these lines is density-functional theory (DFT). Although DFT has been very successful in the last decades, the theory fails to describe strongly correlated systems. Another shortcoming lies in the development of functionals. Despite the fact, that in DFT every observable is guaranteed to be a functional of the electron density, the theory provides no guidance on how to construct the functional for a given observable of interest. For some system properties, like the ground-state energy, very good approximations are available, while for others, especially excited state properties, only little is known.

In recent years a renewed interest in reduced density matrices has emerged. Similar to DFT, reduced density matrix functional theory (RDMFT) aims at reformulating the many-body Schrödinger equation in terms of physically more intuitive quantities. The central variable in RDMFT is the reduced one-body density matrix, a density distribution derived directly from the many-body wavefunction. RDMFT is a promising candidate to treat correlated electronic systems beyond DFT. In this chapter we briefly review the basic ingredients of the static theory to introduce some nomenclature and to set the stage for an extension to the time-dependent case which we consider in the next chapter.

In the following we consider electronic many-body Hamiltonians for Eq. (4.1) with the form

$$\hat{H} = \hat{T} + \hat{V}_{\text{ext}} + \hat{W}_{\text{ee}}, \tag{4.2}$$

where the operators for the kinetic energy and the external potential are given by

$$\hat{T} = \sum_{j=1}^{N} \left(-\frac{\nabla_j^2}{2} \right), \quad \hat{V}_{\text{ext}} = \sum_{j=1}^{N} \hat{v}_{\text{ext}}(j), \tag{4.3}$$

and the particle-particle interaction has the form

$$\hat{W}_{\text{ee}} = \frac{1}{2} \sum_{\substack{i,j=1 \\ i \neq j}}^{N} \hat{v}_{\text{ee}}(i,j). \tag{4.4}$$

For notational convenience we frequently abbreviate spatial and spin coordinates with a common index $j \equiv (\mathbf{r}_j, \sigma_j)$. A combined summation over spin degrees of freedom and integration over spatial coordinates is abbreviated as

$$\int \ldots d1 := \sum_{\sigma_1 = \uparrow, \downarrow} \sigma_1 \int \ldots d^3 r_1. \tag{4.5}$$

In the case of Coulombic systems the particle-particle interaction in Eq. (4.4) is given by

$$v_{\text{ee}}(i,j) = \frac{1}{|\mathbf{r}_i - \mathbf{r}_j|} \tag{4.6}$$

and we allow, in general, for non-local external operators $\hat{v}_{\text{ext}}(j)$ whose action is defined by

$$\hat{v}_{\text{ext}}(j)\, \Psi(1..j..N) = \int v_{\text{ext}}(j, j') \Psi(1..j'..N)\, dj'. \tag{4.7}$$

For the particular case of spin independent local external potentials $v_{\text{ext}}(\mathbf{r})$ we have

$$v_{\text{ext}}(1, 1') = \delta(1 - 1') v_{\text{ext}}(\mathbf{r}_1), \tag{4.8}$$

so that Eq. (4.7) reduces again to the usual case of a local multiplicative potential.

4.1 Reduced Density Matrices

Suppose the solution of the many-body Schrödinger equation (4.1) is known for a given system of interest. In terms of the many-body eigenfunctions Ψ_k, the reduced density matrices of q-th order for pure states can then be introduced as

$$\gamma_q^{(k)}(1, ..., q; 1', ..., q') := \tag{4.9}$$
$$\begin{pmatrix} N \\ q \end{pmatrix} \int \Psi_k(1, ..., q, q+1, ..., N) \Psi_k^*(1', ..., q', (q+1), ..., N)\, d^3(q+1) ... d^3 N.$$

We use an upper index (k) to denote the eigenstate from which the reduced q-body density matrices have been contracted. If we omit the index, then the ground state is implied, i.e. $\gamma_q := \gamma_q^{(0)}$.
By further contracting the reduced density matrix of order q, a relation to the matrix of order $q-1$ can be established

$$\gamma_{q-1}^{(k)}(1,...,q-1;1',...,q'-1) = \frac{q}{N-q+1}\int \gamma_q^{(k)}(1,...,q;1',...,q')dq, \tag{4.10}$$

which can be directly seen from the definition of the matrices in Eq. (4.9). The contraction for $k=0$ establishes a map $\Psi^{(0)} \to \gamma_q \to \gamma_{q-1}$ and by recursively applying the contraction (4.10) the maps

$$G \quad : \qquad \Psi^{(0)} \to \gamma_1, \tag{4.11}$$
$$R \quad : \qquad \Psi^{(0)} \to \gamma_2 \tag{4.12}$$

can be obtained. It is interesting to observe that both maps can be inverted for systems with non-degenerate ground states[1]. This is ensured by the following two theorems:

Gilbert's theorem

The inverse of map G is guaranteed by Gilbert's theorem [Gil75] which states, that for systems with non-degenerate ground states and a Hamiltonian with fixed interaction and a possibly non-local external potential, the ground-state wavefunction is uniquely determined by the reduced one-body matrix.

Rosina's theorem

Similarly, it was shown in a theorem by Rosina [Ros68], that provided a q-th order reduced density matrix originates from a non-degenerate ground state of a Hamiltonian with q-particle interaction, the q-th order reduced density matrix is sufficient to determine the ground-state wavefunction uniquely. No reference to the particular form of the particle interaction enters in Rosina's case. Merely the order of the particle interaction needs to be known. For $q=2$, i.e. the case of binary interactions, this allows to invert the map R.

Due to Gilbert's and Rosina's theorems all ground-state expectation values $\langle A\rangle$ of an interacting many-particle system can be written as functionals of the ground-state reduced one-body matrix, or alternatively as functionals of the ground-state reduced two-body matrix

$$\langle A\rangle \quad \to \quad \langle A\rangle[\gamma_1], \tag{4.13}$$
$$\langle A\rangle \quad \to \quad \langle A\rangle[\gamma_2]. \tag{4.14}$$

From the above discussion it is evident that the most important matrices for binary particle interactions are the reduced one-body matrix γ_1 and the reduced two-body matrix γ_2. All

[1] Note that the restriction to non-degenerate ground states is rather severe. This excludes most atoms and all paramagnetic, ferromagnetic and anti-ferromagnetic materials.

properties of these matrices which directly follow from their definition can be summarized as follows

(a) Symmetry property of γ_2

$$\gamma_2(12;1'2') = \pm\gamma_2(21;1'2') = \pm\gamma_2(12;2'1'), \tag{4.15}$$

where + holds for bosons and − has to be used for fermions.

(b) Hermiticity

$$\gamma_q(1,\ldots,q;1',\ldots,q') = \gamma_q^*(1',\ldots,q';1,\ldots,q). \tag{4.16}$$

(c) Relation between γ_2 and γ_1 (cf. (4.10))

$$\gamma_1(1;1') = \frac{2}{N-1}\int \gamma_2(12;1'2)d2. \tag{4.17}$$

(d) Traces

$$\int \gamma_q(1,\ldots,q;1,\ldots,q)\,d1\ldots dq \;=\; \begin{pmatrix} N \\ q \end{pmatrix}$$

in particular

$$\begin{aligned} \int \gamma_1(1;1)\,d1 &= N, \\ \int \gamma_2(12;12)\,d1d2 &= \frac{N(N-1)}{2}. \end{aligned} \tag{4.18}$$

(e) Non-negativity

$$\int f^*(1,\ldots,q)\gamma_q(1,\ldots,q;1',\ldots,q')f(1',\ldots,q')\,d1\ldots dq\,d1'\ldots dq' \geq 0 \tag{4.19}$$

for any $f(1,\ldots,q)$.

Having defined the reduced density matrices it is useful for practical considerations to work with their eigenvalues and eigenvectors. The matrices can be viewed as kernels of linear integral operators. From properties (b), (d), (e) above it can be seen that for finite systems these integral operators are non-negative Hermitian operators with finite trace. Such operators have a purely discrete spectrum and the corresponding eigenfunctions form a complete set. In the case of the reduced one-body matrix the eigenvalue equation can be written as

$$\int \gamma_1(1;1')\,\varphi_j(1')\,d1' = n_j\,\varphi_j(1). \tag{4.20}$$

The eigenfunctions $\varphi_j(1)$ are called natural orbitals and the eigenvalues n_j are termed natural occupation numbers. Equivalently, the reduced two-body density matrix can be

used as kernel of an integral operator. The eigenvalue equation of the operator becomes

$$\int\int \gamma_2(12;1'2')\, g_j(1'2')\, d1'd2' = \eta_j\, g_j(12). \tag{4.21}$$

Here, the $g_j(12)$ are called natural geminals and the η_j are the occupation numbers of electron pairs in the natural state $g_j(12)$. Similar eigenvalue equations can be considered for density kernels of higher order. For N-particle systems it turns out that the eigenvalues of different matrices are related. As proven by Carlson and Keller [CK61], the non-zero eigenvalues of γ_q and γ_{N-q} are identical.

4.2 Direct Minimization of the Total Energy in Terms of γ_2

Already during the 1950s Löwdin [Löw55] and Mayer [May55] had independently noticed that the ground-state energy of a non-relativistic quantum many-body system, as described by the Hamiltonian (4.2), can be formulated without direct reference to the full many-body wavefunction. Since electrons interact only pairwise it turned out that the knowledge of the reduced two-body density matrix is sufficient for the calculation of the ground-state energy and many other observables of the system. In terms of the two-body matrix the *exact* ground-state energy of a many-electron system can be written as

$$\begin{aligned} E[\gamma_2] = &\int \lim_{1'\to 1}\left[-\frac{\nabla_1^2}{2}\right]\gamma_1(1;1')\, d1 \\ &+ \int\int v_{\text{ext}}(1,1')\gamma_1(1';1)\, d1d1' + \int\int \frac{\gamma_2(11';11')}{|\mathbf{r}_1 - \mathbf{r}_1'|}\, d1d1'. \end{aligned} \tag{4.22}$$

In other words, the ground-state energy is a *linear* functional of the reduced two-body density matrix γ_2. The fact, that the ground-state energy is exactly known in terms of the reduced two-body matrix seems to open the possibility to minimize the energy directly with respect to γ_2, rather than with respect to the wavefunction. However, early variational calculations demonstrated that a direct minimization of (4.22) with respect to γ_2 leads to energies which are substantially *below* the exact ground-state energy of the system [Tre57, Ayr58, MI57, Bop59]. The reason for this lies in the fact, that not all possible two-electron density distributions γ_2 which are encountered in a free variational minimization of the ground-state energy correspond to a possible many-body wavefunction. It was soon noticed, that two-body matrices need to be constrained non-trivially, in order to be representable by an anti-symmetric many-body wavefunction. These constraints are known as N-representability conditions and a reduced two-body matrix which originates from an anti-symmetric many-body wavefunction is termed N-representable [Col63, Erd78, Har78]. Although the N-representability conditions for the reduced two-body matrix had been found very soon [GP64, Kum67], their practical implementation turned out to be rather cumbersome. Besides this, the limitations in computer resources and the lack of software adapted to constrained optimization prevented the widespread use of a direct minimization of the total energy in terms of the reduced two-body matrix.

Interest in a direct minimization of the energy functional (4.22) emerged again in the 1990s in the context of contracted Schrödinger equations (CSE). The CSE were first introduced by Cohen and Frishberg [CF76] and Nakatsuji [Nak76]. Matrix formulations and a sec-

ond quantized form of the CSE have been presented by Harriman [Har79] and Valdemoro [Val85], respectively. The CSE, also termed density or hierarchy equations, provide direct Schrödinger like equations for the static reduced density matrices. In the particular case of the two-body matrix, the corresponding CSE depends also on the three- and four-body matrices. Therefore, the CSE converts the N-representability problem for the reduced two-body matrix into a problem involving the reconstruction of the tree-body matrix and the four-body matrix from the two-body matrix [Maz99].
Schemes based on the particle-hole duality [CPdVV93, CV93], or approaches based on the theory of cumulants and Grassmann algebras [Maz98b, Maz98a, Maz99] have been proposed to reconstruct the three and four-body matrices from the two-body matrix. The CSE are typically solved with a contracted power method. Also, an algorithm was introduced to purify the reduced two-body density matrix during the power iterations [Maz02a].
Another route towards minimizing the total energy with respect to the reduced two-body matrix makes use of positivity conditions which particle and hole matrices obey [Maz02c, Maz02b]. The technique of positive semidefinite programming [VB96] is used to take the positivity conditions during the minimization approximately into account. A popular software package for this purpose is SeDuMi [Stu99] which implements a primal-dual interior-point method for solving positive semidefinite programs. More recently, an algorithm for first order semidefinite programming has been introduced [Maz04] which cuts down the number of floating-point operations for the semidefinite program by more than an order of magnitude. Applications to the potential energy curves of H_6 and N_2 show that this approach yields very accurate energies at equilibrium distances, as well as at the molecular dissociation limit.
We conclude this section by emphasizing that in contrast to traditional variational wave-function methods which deliver upper bounds to the ground-state energy, the direct minimization of the total energy with respect to the two-body matrix under the consideration of approximate N-representability conditions yields a *lower* bound to the total energy. The combination of traditional approaches and such a two-body minimization is therefore suitable to narrow down the exact location of the ground-state energy.

4.3 Direct Minimization of the Total Energy in Terms of γ_1

An alternative to the minimization of the total energy with respect to the two-body matrix is established by Gilbert's theorem. As briefly mentioned in section 4.1, the theorem guarantees for non-degenerate ground states a one-to-one correspondence between the reduced one-body matrix and the ground-state wavefunction. Hence, the ground-state energy can also be viewed as a functional of the reduced one-body density matrix.
In contrast to the case of the two-body matrix it is trivial to ensure the N-representability conditions for reduced one-body matrices. As shown by Coleman [Col63], the necessary and sufficient conditions for a reduced one-body matrix to be ensemble N-representable can be summarized by the following conditions for the occupation numbers

$$\text{Normalization:} \qquad \sum_{j=1}^{\infty} n_j = N, \tag{4.23}$$

$$\text{Bounds:} \qquad 0 \leq n_j \leq 1, \qquad \forall j. \tag{4.24}$$

Since the N-representability conditions are trivial for the one-body matrix and can be easily imposed in practice it seems advantageous to work with the one-body matrix, or equivalently with natural orbitals and occupation numbers, instead of dealing with the two-body matrix. This approach has enjoyed renewed popularity in recent years and is termed reduced-density matrix functional theory (RDMFT)[2] in the literature [Mül84, GU98, BB02]. However, there is a price to pay when the one-body matrix is used as basic variable. Contrary to the case of γ_2 the energy is *not* known exactly in terms of the one-body matrix γ_1. In terms of γ_1 the total energy can merely be written in the form

$$E[\gamma_1] = E_{\text{kin}}[\gamma_1] + E_{\text{ext}}[\gamma_1] + E_{\text{H}}[\gamma_1] + E_{\text{x}}[\gamma_1] + E_{\text{c}}[\gamma_1], \tag{4.25}$$

where

$$E_{\text{kin}}[\gamma_1] = \int\int \delta(1-1') \left[-\frac{\nabla_1^2}{2}\right] \gamma_1(1;1')\, d1d1' \tag{4.26}$$

and

$$E_{\text{ext}}[\gamma_1] = \int\int v_{\text{ext}}(1,1')\gamma_1(1';1)\, d1d1' \tag{4.27}$$

denote the kinetic E_{kin} and external E_{ext} energies, respectively. Also, the Hartree E_{H} and the exchange E_{x} energies can be exactly expressed in terms of γ_1

$$E_{\text{H}}[\gamma_1] = \frac{1}{2}\int\int \frac{\gamma_1(1;1)\gamma_1(1';1')}{|\mathbf{r}_1 - \mathbf{r}_1'|}\, d1d1', \tag{4.28}$$

$$E_{\text{x}}[\gamma_1] = -\frac{1}{2}\int\int \frac{\gamma_1(1;1')\gamma_1(1';1)}{|\mathbf{r}_1 - \mathbf{r}_1'|}\, d1d1'. \tag{4.29}$$

The only unknown piece in Eq. (4.25) is the correlation energy E_{c}, which has to be approximated in practice. It is important to notice the difference compared to DFT. In DFT the kinetic energy is computed from the orbitals of the non-interacting Kohn-Sham system.

[2] The notion of the acronym RDMFT is a bit misleading at first sight. Due to Rosina's theorem it is perfectly eligible to denote also a treatment in terms of γ_2 as reduced-density matrix functional theory. We emphasize that RDMFT refers in the literature exclusively to a description with γ_1 as basic variable.

The difference between the exact kinetic energy of the interacting system, Eq. (4.26), and the kinetic energy of the Kohn-Sham system is part of the exchange-correlation functional of DFT. This is also the reason why the behavior of the exchange-correlation functional under uniform coordinate scaling is "polluted" in DFT. The situation in RDMFT is different. Here, the kinetic energy can be *exactly* expressed in terms of γ_1. No kinetic contributions are included in the correlation energy. Furthermore, we emphasize that the exchange energy in Eq. (4.29) corresponds only to the conventional definition of exchange in quantum chemistry, if the functional $E_\mathrm{x}[\gamma_1]$ is evaluated with the Hartree-Fock one-body density matrix γ_1^HF. If the expression (4.29) is evaluated with the one-body matrix that results from a direct minimization of Eq. (4.25) with some approximate E_c, then $E_\mathrm{x}[\gamma_1]$ already contains contributions, which are considered as part of the correlation energy in quantum chemistry.
In analogy to the second part of the Hohenberg-Kohn theorem a variational principle can be established in RDMFT. It can be shown that the ground-state energy E_GS of a system is a lower bound of the energy functional $E[\gamma_1]$ for all N-representable reduced one-body density matrices γ_1

$$E_\mathrm{GS} \leq E[\gamma_1]. \tag{4.30}$$

The equality only holds for the ground-state one-body matrix $\gamma_1 = \gamma_1^{(0)}$. Hence, given an approximate functional for the correlation-energy E_c in terms of the one-body matrix, a direct minimization of Eq. (4.25) under the N-representability constraints (4.23), (4.24) can be performed. In practice, variational calculations are carried out in terms of natural orbitals and occupation numbers. There are mainly two reasons for this approach:

(i) The N-representability conditions for the one-body matrix affect only the occupation numbers. To impose N-representability it is advantageous to access the occupation numbers directly.

(ii) Dealing directly with orbitals and occupation numbers provides much more flexibility for the construction of functionals. If the one-body matrix is taken as basic variable for the variational calculation, only functionals with an *explicit* dependence on γ_1 can be utilized. Instead, if natural orbitals and occupation numbers are used as basic variables, then also *implicit* functionals

$$E[\{n_j\}, \{\varphi_j\}] = E[\gamma_1] \tag{4.31}$$

of the one-body matrix can be used.

We emphasize that the last item above relies on the functional dependence

$$\begin{aligned} n_j &= n_j[\gamma_1], \qquad \forall j, \\ \varphi_j(1) &= \varphi_j[\gamma_1](1) \qquad \forall j. \end{aligned} \tag{4.32}$$

These relations only hold true if the one-body matrix does not have degenerate eigenvalues. Once degenerate eigenvalues are present it is possible to perform unitary transformations in the respective subspaces that are spanned by all natural orbitals with equivalent occupation numbers. Such a transformation leaves the density matrix invariant and consequently also the total energy. The relation for the orbitals in (4.32) is then not unique anymore. In practice, this only poses a problem for approximate functionals which are not *explicit* functionals of γ_1.

Practical Minimization Scheme

In the following we briefly sketch how the minimization of the functional (4.25) is performed in practice. To impose the normalization condition for the occupation numbers, Eq. (4.23), a Lagrange multiplier μ is introduced and the direct minimization is performed for the following functional

$$F[\{n_j\},\{\varphi_j\}] = E[\{n_j\},\{\varphi_j\}] + \mu\left(\sum_{j=1}^{q} n_j - N\right). \tag{4.33}$$

The second N-representability condition, Eq. (4.24), is usually taken into account by writing $n_j = \sin^2\theta_j$ and minimizing with respect to θ_j instead of n_j. The minimization is started with an initial guess for natural orbitals and occupation numbers. In principle, randomized input data can be used as starting point. However, to achieve faster convergence it is advantageous to start from reasonable initial values. Typically, the orbitals and occupation numbers (0 or 1) of a Hartree-Fock calculation are used as input for a RDMFT minimization. The initial chemical potential μ is set to the HF energy eigenvalue of the HOMO. The minimization then proceeds by freezing the values of the orbitals in the current iteration step. With frozen orbitals a minimization with respect to the occupation numbers is performed taking the constraint of a given particle number N into account. Typically Brent's root finding algorithm [Bre73] or a simple bisection method are used to find the chemical potential μ for which $M(\mu) - N = 0$. The occupation numbers are considered as converged, if the Euclidean norm of the occupation vectors of two successive iterations $k-1$, k falls below a given threshold $\delta^{(n)}$

$$\sum_{j=1}^{q} \left|n_j^{(k)} - n_j^{(k-1)}\right|^2 < \delta^{(n)}. \tag{4.34}$$

Once optimal occupation numbers have been found for the current iteration step they are held fixed and the orbitals are released in the next step. The gradients $\delta F/\delta\varphi_j$ are computed and the orbitals are updated according to

$$\varphi_j = \varphi_j + s_j\,\delta F/\delta\varphi_j \qquad \forall j, \tag{4.35}$$

where s_j denotes an orbital resolved step size that is automatically adjusted during the minimization in order to lower the energy. This procedure is iterated until the change in the orbitals lies below a given threshold $\delta^{(\varphi)}$. As stopping criteria, e.g. $\max|s_j| < \delta^{(\varphi)}$ can be used. The overall minimization of orbitals and occupation numbers is iterated until the change in total energy in two successive iterations is smaller than a prescribed threshold $\delta^{(E)}$. Practical calculations show that for small molecules typically $q = 10 - 40$ natural orbitals need to be taken into account to achieve sufficient convergence with the above scheme.

Applications of RDMFT

A variety of functionals for the application of RDMFT has been proposed in recent years [Mül84, GU98, CA00, BB02, CGA02, GPB05, LHG07] and the theory has been especially applied to observables which pose difficulties for DFT based methods. Prominent examples

include the dissociation limit of diatomic molecules [GPB05] or the calculation of the fundamental gap of extended systems [HLAG07]. Also, van der Waals interactions have been investigated recently [GB06].
Finally, we remark that RDMFT has only been used for fermionic systems so far. An extension of the theory to bosonic systems might prove useful. For bosonic systems there is no N-representability condition (4.24) and one finds that the formation of a Bose condensate in an extended system of bosons leaves a direct signature in the reduced one-body density matrix: In that case one of the occupation numbers tends to infinity.

5 Time-Dependent Reduced Density Matrix Functional Theory

Insofern sich die Sätze der Mathematik auf die Wirklichkeit beziehen sind sie nicht sicher, und insofern sie sicher sind, beziehen sie sich nicht auf die Wirklichkeit.

— Albert Einstein, (1879-1955).

Due to the success of ground-state RDMFT in areas where the traditional DFT approach is facing limitations it seems desirable to consider density matrices also in a time-dependent context in order to go beyond TDDFT. At the present stage such an extension to time-dependent RDMFT (TDRDMFT) is still in its infancy. Not much has been explored for the case of time-dependent non-local external potentials. Especially, it is still an open question whether an extension of Gilbert's theorem to the case of time-dependent systems can be achieved. In this chapter we attempt some preliminary steps towards a description of many-body systems in terms of time-dependent reduced one-body density matrices.
This chapter is organized as follows: In section 5.1 we introduce the BBGKY (Bogoliubov, Born, Green, Kirkwood, and Yvon) hierarchy of reduced density matrices. This hierarchy provides a set of coupled first order partial differential equations in time for the evolution of the reduced density matrices. In its original form, the hierarchy is not well suited for truncation since mean-field and correlated parts of the matrices enter on the same footing. We therefore discuss, in section 5.1.2, a cluster expansion which allows us to reformulate the hierarchy in terms of so-called N-body correlations λ_n. Since the N-body correlations are expected to decrease in magnitude for higher orders of n, a truncation of the corresponding hierarchy is less severe than in the case of the original reduced N-body matrices. Starting with section 5.2 we present our own work. Using the BBGKY hierarchy we derived equations of motion for the natural orbitals and occupation numbers which we present in 5.2.1. We discuss some properties of the equations of motion and show that an adiabatic extension of present ground-state functionals in RDMFT always leads to occupation numbers which are *constant in time*. In section 5.3 we use the stationary limit of the equations of motion for the N-body correlations to derive a new class of functionals which can be used for ground-state calculations in static RDMFT. Section 5.4 is devoted to applications. First, we introduce some tools that we use to investigate the time-dependence of natural orbitals and occupation numbers. We present in section 5.4.1 a time-dependent correlation entropy to measure the degree of correlation in the many-body wavefunction. Section 5.4.2 briefly reviews optimal control theory which we use as technique to find optimal pulse shapes for laser-induced transitions in atomic Helium. Having introduced all ingredients for the numerical treatment we turn our attention in section 5.4.3 to the description of a model system which we employ for the time propagations in this chapter. We characterize the ground-state properties of the model with special emphasis on one-body density matrices,

natural orbitals and occupation numbers. In sections 5.4.4 and 5.4.5 we perform numerical propagations of the full many-body wavefunction for a one-dimensional model system. The full solution of the TDSE for interacting particles is used to extract the exact time evolution of the natural orbitals and occupation numbers during (i) laser excitation and (ii) for the case of electron-ion scattering.

5.1 The BBGKY Hierarchy of Reduced Density Matrices

Due to rapid experimental and technological progress, the description of electronic quantum many-body systems out of equilibrium has become an important research topic in recent years. Prominent examples for the need of a non-equilibrium description are atoms and molecules exposed to ultrashort intense laser fields or the microscopic description of quantum transport as discussed in part III of this work. All applications share common interest in how many-body systems evolve on transient or non-adiabatic time-scales, how they thermalize or which kind of behavior under external drivings is to be expected. The strong nonlinearities, present in many situations, are not accessible by approaches based on perturbation theory, resulting in a need for non-perturbative methods. A consistent non-perturbative description of many-body systems is provided by the equations of motion for the Green's functions. The non-equilibrium Green's function equations of motion were first obtained by Kadanoff and Baym [KB76, Dan84] and have been derived independently by Keldysh [Kel65] and by Fujita [Fuj64]. Although these equations provide a rigorous ground to investigate the dynamics of many-body systems out of equilibrium, so far only *ab-initio* solutions for the time evolution of very small atomic or molecular systems under special assumptions have been achieved [DLS06]. A more comprehensive *ab-initio* treatment of non-equilibrium systems with many degrees of freedom is still beyond the scope of current computing facilities.

An alternative for the study of non-equilibrium processes in many-body systems is provided by time-dependent density functional theory (TDDFT) [MUN$^+$06]. TDDFT is currently the method of choice for electronic systems out of equilibrium because of its combination of accuracy combined with low computational cost. The theory is in principle exact, in the sense that the exact time-dependent exchange-correlation functional ensures that the evolution of the single-particle time-dependent Kohn-Sham equations yields the exact time-dependent particle density of the many-body system [RG84]. All physical observables are functionals of the time-dependent density. However, it is sometimes rather cumbersome to find approximate expressions for observables of interest. Not to mention the exact expression. A prominent example is above-threshold ionization of atoms and molecules in strong laser fields, where no density functional for the observables (in that case the ionization yields) is known. Although the time-dependent Kohn-Sham orbitals have in principle no direct physical meaning and are only a means to construct the time-dependent density, they are often (ab)used to compute physical quantities directly.

Time-dependent reduced density matrices bridge the gap between the single determinant picture of TDDFT and a full-fledged propagation of the Kadanoff-Baym equations for the Green's function. The BBGKY hierarchy can be viewed as the equal-time limit of the Martin-Schwinger hierarchy [MS59] for the Green's functions. In this sense the double-time structure which is present in the Green's functions is avoided in the case of the density matrices, although some information is lost in this way. Historically, the prop-

agation of reduced density matrices was pioneered in nuclear physics. Early work along these lines appeared under the term extended time-dependent Hartree-Fock (ETDHF) theory [WT78, WT79]. In this approach a modified TDHF equation is propagated in combination with time-dependent occupation numbers. The time dependence of the occupation numbers is determined from a collision integral which is based on the equal-time limit of the two-body Green's function. Several other approaches for the collision integral have been proposed, ranging from statistical considerations [Ayi80, Ayi84] to a description within a random-matrix model [GWW81]. More recently, the inclusion of memory terms has been considered in the treatment of one-dimensional model systems [LCA99]. The second generation of approaches in nuclear physics is directly based on the BBGKY hierarchy for the density matrices and is termed time-dependent density matrix theory (TDDMT) [SJC85, Toh85, Toh87, CNW88]. In this approach a cluster expansion for the reduced density matrices is utilized to separate mean-field and correlated contributions (N-body correlations) of the reduced density matrices. In practice, the reduced density matrices and N-body correlations are expanded in a set of single-particle TDHF-like orbitals. The expansion matrices are then propagated in combination with a mean-field single-particle equation for the TDHF-like orbitals.
Quantum kinetic equations which are related to the BBGKY hierarchy are also popular in plasma physics and semiconductor physics where Wigner and Bloch representations of the hierarchy are frequently in use [Bon98].
In the following sections we base our own discussion of time-dependent reduced density matrices on the hierarchy of N-body correlations of Ref. [SJC85]. However, contrary to the TDDMT approach we represent the reduced density matrices and N-body correlations directly in terms of natural orbitals and occupation numbers. This results in equations of motion for the natural orbitals and occupation numbers which we discuss in section 5.2.1. Before we turn our attention to natural orbitals and occupation numbers, we briefly recall the BBGKY hierarchy of reduced density matrices and the hierarchy of equations of motion for the N-body correlations.

5.1.1 Formulation in Terms of N-Body Matrices

The basis for the following discussion is the time-dependent many-body Schrödinger equation

$$i\partial_t \Psi(t) = \hat{H}(t)\Psi(t), \tag{5.1}$$

where $\hat{H}(t) = \hat{H}_0(t) + \hat{W}_{\mathrm{ee}}$. Like in the static case we consider binary interactions among the particles

$$\hat{W}_{\mathrm{ee}} = \frac{1}{2}\sum_{\substack{i,j=1 \\ i\neq j}}^{N} v_{\mathrm{ee}}(i,j) \tag{5.2}$$

but we allow for an explicitely *time-dependent* (local) external potential

$$\hat{H}_0(t) = \sum_{j=1}^{N} \hat{h}(j;t), \qquad \hat{h}(j;t) = -\frac{\nabla^2_{\mathbf{r}_j}}{2} + v_{\mathrm{ext}}(\mathbf{r}_j;t), \tag{5.3}$$

where $\hat{h}(j;t)$ denotes just a bare single-particle Hamiltonian. In the same way as in the static case, one can introduce time-dependent reduced density matrices in terms of the

time-evolved many-body state $\Psi(t)$

$$\gamma_q(1,...,q,1',...,q';t) := \binom{N}{q} \int \Psi(1,...,q,q+1,...,N;t)\Psi^*(1',...,q',(q+1),...,N;t)\, d^3(q+1)...d^3N. \tag{5.4}$$

Furthermore, we use the following notation

$$[f(1), g(11')] \equiv f(1)g(11') - f(1')g(11') \tag{5.5}$$

and

$$\operatorname*{Tr}_{(j)} \Big\{ \dots \Big\} \equiv \sum_{\sigma_j} \int \dots d^3\mathbf{r}_j. \tag{5.6}$$

The BBGKY hierarchy of equations of motion for the reduced density matrices provides a reformulation of the many-body TDSE (5.1) and can be written in the following compact form [SJC85]

$$\begin{aligned}
i\partial_t\gamma_1 &= \Big[\hat{h}, \gamma_1\Big] + \operatorname*{Tr}_{(2)}\Big([v_{\mathrm{ee}}, \gamma_2]\Big), \\
i\partial_t\gamma_2 &= \left[\sum_{i=1}^{2}\hat{h}(i), \gamma_2\right] + [v_{\mathrm{ee}}, \gamma_2] + \operatorname*{Tr}_{(3)}\left(\left[\sum_{i=1}^{2} v_{\mathrm{ee}}(i,3), \gamma_3\right]\right), \\
&\vdots \quad\quad \vdots \\
i\partial_t\gamma_n &= \left[\sum_{i=1}^{n}\hat{h}(i), \gamma_n\right] + \left[\sum_{j>i=1}^{n-1} v_{\mathrm{ee}}(i,j), \gamma_n\right] + \operatorname*{Tr}_{(n+1)}\left(\left[\sum_{i=1}^{n} v_{\mathrm{ee}}(i,n+1), \gamma_{n+1}\right]\right).
\end{aligned} \tag{5.7}$$

As in the case of the Martin-Schwinger hierarchy for the Green's functions, the BBGKY hierarchy couples reduced density matrices of order n to the respective matrix of next higher order. Solving these equations in principle amounts to including all N levels of the hierarchy. Due to the coupling of the different levels and the fact that at level n the equations of the hierarchy depend on $2n$ spatial coordinates this is even more involved than a direct solution of the many-body TDSE. Therefore, any application in practice aims at truncating the hierarchy at some level $n \ll N$. The most obvious truncation is to consider only equations of the hierarchy up to level n and to set γ_q with $q \geq n+1$ equal to zero. Although straightforward, this provides only a very crude approximation. This can be attributed to the fact that correlated and uncorrelated terms are mixed in (5.7). In addition the density matrices γ_n do not decrease in magnitude with increasing order n, so that terms of non-negligible size would always be neglected. In the next section we show that a reformulation of the hierarchy in terms of so-called N-body correlations is more suitable for truncations.

5.1.2 Formulation in Terms of N-Body Correlations

As preliminary step we introduce operators $\hat{A}$ and $\hat{S}$ which are defined by

$\hat{S}_{(n)}$: symmetrizes with respect to all pair indices (i,i') and (j,j')

$\hat{A}_{(n)}$: antisymmetrizes with respect to all exchanges between indices i', j'

The lower index (n) indicates that the symmetrization or anti-symmetrization is carried out among n particles.
With the help of the operators $\hat{A}, \hat{S}$ it is then possible to introduce a very compact form of the antisymmetrized cluster expansion for reduced density matrices [SJC85, Bon98]

$$\gamma_n = \underset{(n)}{\hat{A}\hat{S}} \sum_{p=1}^{n} \gamma_{n-p}\lambda_p = \underset{(n)}{\hat{A}\hat{S}} \sum_{p=1}^{n-1} \gamma_{n-p}\lambda_p + \lambda_n, \tag{5.8}$$

where $\gamma_0 = 1$ and $\lambda_1 = \gamma_1$. For reasons that become evident later, the λ_n are called N-body correlations. In the literature this expansion is also referred to as Ursell-Mayer expansion [Bon98][1].
To illustrate the effect of the operators $\hat{A}, \hat{S}$ and to introduce the concept of *linked* and *unlinked* terms consider the following example

$$\begin{aligned}
&v_{\mathrm{ee}}(12)\, \underset{(3)}{\hat{A}\hat{S}} \Big[\gamma_1(11')\lambda_2(23,2'3')\Big] \\
&\quad = v_{\mathrm{ee}}(12)\, \underset{(3)}{\hat{A}} \Big[\gamma_1(11')\lambda_2(23,2'3') + \gamma_1(22')\lambda_2(13,1'3') + \gamma_1(33')\lambda_2(21,2'1')\Big] \\
&\quad = v_{\mathrm{ee}}(12)\Big[\gamma_1(11')\lambda_2(23,2'3') + \gamma_1(22')\lambda_2(13,1'3') \\
&\qquad + \underline{\gamma_1(33')\lambda_2(12,1'2')} - \gamma_1(12')\lambda_2(23,1'3') \\
&\qquad - \gamma_1(21')\lambda_2(13,2'3') - \underline{\gamma_1(31')\lambda_2(12,3'2')} \\
&\qquad - \gamma_1(13')\lambda_2(23,2'1') - \gamma_1(23')\lambda_2(13,1'2') \\
&\qquad - \underline{\gamma_1(32')\lambda_2(12,1'3')}\Big].
\end{aligned} \tag{5.9}$$

The underlined terms in (5.9) are separable with respect to the two-body interaction $v_{\mathrm{ee}}(12)$ and are termed *unlinked*. All other terms cannot be factorized and are called *linked*.
The properties of γ_n and λ_n can be summarized as follows:

a) γ_n contains all possible correlations among n particles.

b) γ_n is symmetric with respect to any exchange of pairs (ii') and (jj') and antisymmetric with respect to any exchange of i and j, i.e.

$$\underset{(n)}{\hat{A}}\, \gamma_n = \underset{(n)}{\hat{S}}\, \gamma_n = \underset{(n)}{\hat{A}\hat{S}}\, \gamma_n = \gamma_n. \tag{5.10}$$

c) the N-body correlation λ_n has the same symmetry as γ_n as well as all terms $\hat{A}\hat{S}_{(n)}\, \gamma_{n-p}\lambda_p$.

[1] The classical cluster or Ursell-Mayer expansion corresponds to the expansion of the pressure ρ and the density ρ of a classical gas in the grand-canonical ensemble in terms of the fugacity $z = e^{\beta\mu}$, where μ is the chemical potential and $\beta = 1/k_B T$ denotes the inverse temperature.

As explicit example of (5.8) we have for the one-, two- and three-body correlations

$$\begin{aligned}
\gamma_1(11';t) &= \gamma_1(11';t), \\
\gamma_2(12,1'2';t) &= \gamma_1(11';t)\gamma_1(22';t) - \gamma_1(12';t)\gamma_1(21';t) + \lambda_2(12,1'2';t), \\
\gamma_3(123,1'2'3';t) &= \gamma_1(11';t)\gamma_1(22';t)\gamma_1(33';t) - \gamma_1(12';t)\gamma_1(21';t')\gamma_1(33';t) \\
&\quad - \gamma_1(22';t)\gamma_1(31';t)\gamma_1(13';t) + \gamma_1(13';t)\gamma_1(21';t')\gamma_1(32';t) \\
&\quad - \gamma_1(11';t)\gamma_1(32';t)\gamma_1(23';t) + \gamma_1(12';t)\gamma_1(31';t')\gamma_1(23';t) \\
&\quad + \gamma_1(11';t)\lambda_2(23,2'3';t) - \gamma_1(12';t)\lambda_2(23,1'3';t) \\
&\quad - \gamma_1(13';t)\lambda_2(23,2'1';t) + \gamma_1(22';t)\lambda_2(13,1'3';t) \\
&\quad - \gamma_1(21';t)\lambda_2(13,2'3';t) - \gamma_1(23';t)\lambda_2(13,1'2';t) \\
&\quad + \gamma_1(33';t)\lambda_2(12,1'2';t) - \gamma_1(31';t)\lambda_2(12,3'2';t) \\
&\quad - \gamma_1(32';t)\lambda_2(12,1'3';t) + \lambda_3(123,1'2'3',;t).
\end{aligned} \tag{5.11}$$

Anti-symmetrized products in Eq. (5.11), which contain only one-body matrices γ_1, correspond to the uncorrelated superposition of particles. Hence, the N-body correlations λ_n contain only true correlations among n particles, which cannot be factorized into lower order contributions, and are therefore expected to decrease in magnitude with increasing order. This is in contrast to the reduced N-body matrices γ_n which contain simultaneously uncorrelated superpositions and correlated terms and do not show a decrease in magnitude with increasing order. Having defined the N-body correlations it is desirable to transform the original equations of motion for the reduced density matrices into equations of motion for the N-body correlations. This transformation is rather technical and we refer to Ref. [SJC85] for further details. Here, we only state the final form for the equations of motion for the N-body correlations

$$\begin{aligned}
i\partial_t \lambda_n &= \left[\left(\sum_{i=1}^{n} \hat{h}(i) + \sum_{j>i=1}^{n-1} v_{\mathrm{ee}}(i,j) \right), \lambda_n \right] + \operatorname*{Tr}_{(n+1)} \left[\sum_{i=1}^{n} v_{\mathrm{ee}}(i,n+1), \lambda_{n+1} \right] \\
&\quad + \hat{A}\hat{S} \sum_{p=1}^{n-1} \left[\sum_{j>i=1}^{n-1} v_{\mathrm{ee}}(i,j), \gamma_{n-p}\gamma_p \right]_{\mathrm{linked}} \\
&\quad + \sum_{p=1}^{n} \operatorname*{Tr}_{(n+1)} \left[\sum_{i=1}^{n} v_{\mathrm{ee}}(i,n+1), \hat{A}\hat{S}\, \gamma_{n-p+1}\gamma_p \right]_{\mathrm{linked}}.
\end{aligned} \tag{5.12}$$

The set of equations for the N-body correlations still constitutes a coupled hierarchy. However, since uncorrelated and correlated terms have been separated, this hierarchy is better suited for truncations with respect to the order of correlations. For $n = 1, 2$ Eq. (5.12) reads more explicitly

$$i\partial_t \gamma_1 = \left[\hat{h}, \gamma_1 \right] + \operatorname*{Tr}_{(2)} \left(\left[v_{\mathrm{ee}}(1,2), \hat{A}\, \gamma_1\gamma_1 + \lambda_2 \right] \right), \tag{5.13}$$

$$
\begin{aligned}
i\partial_t\,\lambda_2 \;=\; & \Big[\,\hat{h}(1)+\hat{h}(2)+v_{\mathrm{ee}}(1,2),\lambda_2\,\Big]+\operatorname*{Tr}_{(3)}\left[v_{\mathrm{ee}}(1,3)+v_{\mathrm{ee}}(2,3),\lambda_3\right] \\
& +\left[v_{\mathrm{ee}}(12),\operatorname*{\hat{A}}_{(2)}\gamma_1\gamma_1\right]+\operatorname*{Tr}_{(3)}\left[v_{\mathrm{ee}}(1,3)+v_{\mathrm{ee}}(2,3),\operatorname*{\hat{A}\hat{S}}_{(2)}(\gamma_1\gamma_1\gamma_1+\gamma_1\lambda_2)\right]_{\mathrm{linked}}.
\end{aligned}
\tag{5.14}
$$

Setting three body correlations to zero, i.e. $\lambda_3 = 0$, the explicit form of the second equation reads

$$
\begin{aligned}
& i\partial_t\,\lambda_2(12,1'2';t) \\
& \quad = \Big[\hat{h}(1;t)+\hat{h}(2;t)+v_{\mathrm{ee}}(12),\lambda_2(12,1'2';t)\Big] \\
& \quad + \Big[v_{\mathrm{ee}}(12),\gamma_1(11';t)\gamma_1(22';t)-\gamma_1(12';t)\gamma_1(21';t)\Big] \\
& \quad - \operatorname*{Tr}_{(3)}\Big\{(v_{\mathrm{ee}}(13)-v_{\mathrm{ee}}(13'))\gamma_1(11';t)\gamma_1(23';t)\gamma_1(32';t) \\
& \qquad -(v_{\mathrm{ee}}(23)-v_{\mathrm{ee}}(2'3))\gamma_1(13';t)\gamma_1(22';t)\gamma_1(13';t) \\
& \qquad -(v_{\mathrm{ee}}(23)-v_{\mathrm{ee}}(1'3))\gamma_1(13';t)\gamma_1(21';t)\gamma_1(32';t) \\
& \qquad -(v_{\mathrm{ee}}(13)-v_{\mathrm{ee}}(2'3))\gamma_1(12';t)\gamma_1(23';t)\gamma_1(31';t) \\
& \qquad -(v_{\mathrm{ee}}(13)-v_{\mathrm{ee}}(1'3))\Big[\\
& \qquad\quad \gamma_1(33';t)\lambda_2(12,1'2';t)-\gamma_1(31';t)\lambda_2(12,3'2';t) \\
& \qquad -\gamma_1(32';t)\lambda_2(12,1'3';t)+\gamma_1(11';t)\lambda_2(23,2'3';t) \\
& \qquad -\gamma_1(13';t)\lambda_2(23,2'1';t)-\gamma_1(23';t)\lambda_2(13,1'2';t)\Big] \\
& \qquad -(v_{\mathrm{ee}}(23)-v_{\mathrm{ee}}(2'3))\Big[\\
& \qquad\quad \gamma_1(33';t)\lambda_2(12,1'2';t)-\gamma_1(31';t)\lambda_2(12,3'2';t) \\
& \qquad -\gamma_1(32';t)\lambda_2(12,1'3';t)+\gamma_1(22';t)\lambda_2(13,1'3';t) \\
& \qquad -\gamma_1(23';t)\lambda_2(13,1'2';t)-\gamma_1(13';t)\lambda_2(23,2'1';t)\Big]\Big\}.
\end{aligned}
\tag{5.15}
$$

In the above expression the terms proportional to $\gamma_1\lambda_2$ are called polarization terms and terms proportional to $v_{\mathrm{ee}}\lambda_2$ denote two-particle ladder terms.
It can be shown that the stationary limit $i\partial_t\,\lambda_2(12,1'2';t)=0$ of (5.15) leads to the Bethe-Goldstone equation, if all terms proportional to $v_{\mathrm{ee}}\lambda_2$ are neglected. If all possible types of four body correlations (terms proportional to λ_4, $v_{\mathrm{ee}}\gamma_1\gamma_1\lambda_2$, $v_{\mathrm{ee}}\gamma_1\lambda_3$, and $v_{\mathrm{ee}}\lambda_2\lambda_2$) are neglected then the Fadeev equations can be recovered from the stationary limit of the lowest three equations, $n<3$, of the hierarchy [SJC85]. In general, four different variants of approximations are common in the literature [Bon98]:

(i) The second Born approximation consists of neglecting ladder and polarization terms in (5.15). In this limit the Landau kinetic equation [BBK97] can be derived.

(ii) The ladder approximation also consists of neglecting all polarization terms but keeping terms proportional to $\gamma_1\lambda_2$. This approximation can be used as a starting point to derive the non-Markovian Boltzmann equation [KBKS97]. Also, the equivalence to the T-matrix approximation for the self-energy in Green's function theory can be drawn [KKER86].

(iii) The polarization approximation neglects all ladder terms. This approximation yields the Balescu-Lenard equation [Bal60, Len60], and an equivalence to the random phase approximation (RPA) for the self-energy in Green's function theory can be established [KB76].

(iv) Finally, the screened-ladder approximation [KKER86] retains all terms of (5.15).

5.1.3 Orbital Representation

We define the time-dependent natural orbitals and occupation numbers as the instantaneous eigenvalues and eigenvectors of the reduced one-body matrix γ_1 at each given point in time. Hence, the time-dependent reduced one-body density matrix has the following spectral representation

$$\gamma_1(11';t) = \sum_k n_k(t)\varphi_k(1;t)\varphi_k^*(1';t). \tag{5.16}$$

Since the eigenvectors $\varphi_j(1;t)$ form a complete set at each instant in time, we can express the reduced two-body matrix in the basis of natural orbitals of the reduced one-body matrix

$$\gamma_2(12,1'2';t) = \sum_{ijkl} \gamma_{2,ijkl}(t)\varphi_i(1;t)\varphi_j(2;t)\varphi_k^*(1';t)\varphi_l^*(2';t). \tag{5.17}$$

In a similar way we expand higher order reduced density-matrices and N-body correlations and introduce coefficient matrices $\gamma_{n;i_1\ldots i_N;j_1\ldots j_N}(t)$ and $\lambda_{n;i_1\ldots i_N;j_1\ldots j_N}(t)$ according to

$$\begin{aligned}
&\gamma_n(1,\ldots,N,1',\ldots,N';t) = \\
&\quad \sum_{i_1\ldots i_N;j_1\ldots j_N} \gamma_{n;i_1\ldots i_N;j_1\ldots j_N}(t)\,\varphi_{i_1}(1;t)\ldots\varphi_{i_N}(N;t)\varphi_{j_1}^*(1';t)\ldots\varphi_{j_N}^*(N';t), \\
&\lambda_n(1,\ldots,N,1',\ldots,N';t) = \\
&\quad \sum_{i_1\ldots i_N;j_1\ldots j_N} \lambda_{n;i_1\ldots i_N;j_1\ldots j_N}(t)\,\varphi_{i_1}(1;t)\ldots\varphi_{i_N}(N;t)\varphi_{j_1}^*(1';t)\ldots\varphi_{j_N}^*(N';t).
\end{aligned} \tag{5.18}$$

5.2 Time-Dependent Natural Spin Orbitals and Occupation Numbers

The time-dependent reduced one-body matrix is a rather complicated object. It depends on six spatial coordinates and on one time coordinate. The full-scale propagation of Eq. (5.13) for realistic systems in three spatial dimensions is beyond the capacity of current computing facilities. Fortunately, the full treatment of the matrix can be simplified. Instead of considering the time evolution of the reduced one-body matrix, it is sufficient to consider only the evolution of its eigenvalues and eigenvectors.

In the present section we show how to achieve this simplification and introduce equations of motion for the natural spin orbitals and occupation numbers. We also investigate some properties of the new equations and show that an adiabatic extension of existing ground-state functionals in RDMFT leads to occupation numbers which are independent of time.

5.2.1 Equations of Motion

For the following discussion it will be useful to introduce matrix elements containing the time-derivative of natural orbitals. Since the natural spin orbitals form a complete set we can expand the time derivative of a given orbital in the following form

$$i\partial_t \varphi_j(1;t) = \sum_k \alpha_{jk}(t)\varphi_k(1;t), \tag{5.19}$$

where the $\alpha_{jk}(t)$ denote complex valued coefficients. Due to the orthonormality of the eigenvectors of γ_1 this leads to the matrix elements

$$\int \varphi_l^*(1;t)\, i\,\partial_t\, \varphi_j(1;t)\, d1 = \sum_k \alpha_{jk}(t)\delta_{lk} =: \alpha_{jl}(t). \tag{5.20}$$

By taking the time-derivative of the orthonormality relation

$$0 = i\partial_t \delta_{lj} = i\partial_t \int \varphi_l^*(1;t)\varphi_j(1;t)\, d1 \tag{5.21}$$

it follows that $\alpha_{jl}(t)$ is a Hermitian matrix

$$-\alpha_{lj}^*(t) + \alpha_{jl}(t) = 0 \quad \Leftrightarrow \quad \alpha_{jl}(t) = \alpha_{lj}^*(t). \tag{5.22}$$

Having collected these ingredients we can state the following result:

The time evolution of natural spin orbitals and occupation numbers is governed by the following coupled set of equations

$$i\partial_t n_a(t) = \sum_{ijl} \gamma_{2,ijal}(t)\langle\, ij \,|\, v_{\mathrm{ee}} \,|\, al \,\rangle(t) - c.c. \tag{5.23}$$

and

$$\left(i\,n_a(t)\partial_t - n_a(t)\hat{h}(1;t)\right)\varphi_a(1;t) - \sum_{ijl}\gamma_{2,ijal}(t)\int v_{\mathrm{ee}}(12)\varphi_j(2;t)\varphi_l^*(2;t)\,d2\,\varphi_i(1;t)$$
$$+\sum_j\left(n_a(t)(\alpha_{aj}(t) - \langle\, j\,|\,\hat{h}\,|\,a\,\rangle(t)) - \sum_{ikl}\gamma_{2,ikal}(t)\langle\, ik\,|\,v_{\mathrm{ee}}\,|\,jl\,\rangle(t)\right)\varphi_j(1;t) = 0. \tag{5.24}$$

The set of equations comprises ordinary differential equations for the occupation numbers (5.23) and partial differential equations for the natural orbitals (5.24). It has to be accompanied by suitable initial conditions $n_a(t = t_0)$, $\forall a$ for the occupation numbers and $\varphi_a(1; t = t_0)$, $\forall a$ for the natural orbitals. The most commonly used initial state in applications is the ground state, e.g., as computed with static RDMFT, but also excited configurations can be chosen as initial datum. Especially for scattering calculations the latter choice is more natural.

Note that contrary to the TDHF or TDKS equations not only the lowest N orbitals have to be propagated. Instead, *all* occupation numbers and orbitals are included in the propagation. In practice, it is a priori not obvious how to truncate the infinite set for a given dynamical situation of interest. Including only orbitals whose ground-state occupation numbers have a significant magnitude will not always be sufficient because some of the occupation numbers that were initially, at $t = t_0$, very small might gain relevance at later points in time[2]. However, if these orbitals and occupation numbers have not been included from the start, the truncated propagation will not even approximately resemble the full solution.

To prove that Eqs. (5.23) and (5.24) are equivalent to the first equation of the BBGKY hierarchy we have to show

(i) $\quad (5.13) \implies (5.23), (5.24)$

(ii) $\quad (5.13) \impliedby (5.23), (5.24)$

for a given choice of initial conditions. Both directions can be obtained by explicit construction. We start with assertion (i).

Proof of part (i)

Starting point is the equation of motion for the reduced one-body density matrix, cf. (5.13)

$$i\partial_t\gamma_1(11';t) = \left(\hat{h}(1;t) - \hat{h}(1';t)\right)\gamma_1(11';t) + \int\left(v_{\mathrm{ee}}(12) - v_{\mathrm{ee}}(1'2)\right)\gamma_2(12,1'2';t)|_{2'=2}\,d2. \tag{5.25}$$

Multiplying Eq. (5.25) with $\varphi_a(1';t)\varphi_b^*(1;t)$ and integrating over coordinates 1 and $1'$ we

[2] This circumstance is illustrated in section 5.4 where we show how initially small occupation numbers can grow over time.

arrive at

$$\begin{aligned} i\,\partial_t\, n_a(t)\delta_{ab} + \Big(\alpha_{ab}(t) - \langle\, b \,|\, \hat{h}(t) \,|\, a \,\rangle(t)\Big)\,(n_a(t) - n_b(t)) \\ = \sum_{ijl} \gamma_{2,ijal}(t) \langle\, ij \,|\, v_{\mathrm{ee}} \,|\, bl \,\rangle(t) - \sum_{jkl} \gamma_{2,bjkl}(t) \langle\, aj \,|\, v_{\mathrm{ee}} \,|\, kl \,\rangle(t), \end{aligned} \tag{5.26}$$

where (5.22) and the representations (5.16), (5.17) have been used. Exploiting the symmetry properties of the expansion coefficients

$$\gamma_{2,ijkl}(t) = \gamma^*_{2,klij}(t) \tag{5.27}$$

and matrix elements

$$\langle\, ij \,|\, v_{\mathrm{ee}} \,|\, kl \,\rangle(t) = \langle\, ji \,|\, v_{\mathrm{ee}} \,|\, lk \,\rangle(t), \qquad \langle\, ij \,|\, v_{\mathrm{ee}} \,|\, kl \,\rangle^*(t) = \langle\, kl \,|\, v_{\mathrm{ee}} \,|\, ij \,\rangle(t) \tag{5.28}$$

the diagonal of Eq. (5.26) can be written in the form

$$i\partial_t n_a(t) = \sum_{ijl} \gamma_{2,ijal}(t) \langle\, ij \,|\, v_{\mathrm{ee}} \,|\, al \,\rangle(t) - c.c. \tag{5.29}$$

which constitutes the equation of motion for the occupation numbers.
Next, we turn our attention to the natural orbitals. Multiplying Eq. (5.25) with $\varphi_a(1';t)(t)$ and integrating over 1' we find

$$\begin{aligned} &\varphi_a(1;t)\, i\,\partial_t n_a(t) + i\, n_a(t) \partial_t \varphi_a(1;t) - \sum_j n_j(t) \alpha_{aj}(t) \varphi_j(1;t) \\ &\quad = n_a(t)\, \hat{h}(1;t)\, \varphi_a(1;t) - \sum_j n_j(t) \langle\, j \,|\, \hat{h}(t) \,|\, a \,\rangle\, \varphi_j(1;t) \\ &\qquad + \sum_{ijl} \gamma_{2,ijal}(t) \int v_{\mathrm{ee}}(12) \varphi_i(1;t) \varphi_j(2;t) \varphi^*_l(2;t)\, d2 \\ &\qquad - \sum_{ijkl} \gamma_{2,ijkl}(t) \langle\, aj \,|\, v_{\mathrm{ee}} \,|\, kl \,\rangle \varphi_i(1;t). \end{aligned} \tag{5.30}$$

Rewriting Eq. (5.26) as

$$\begin{aligned} n_b(t)\, \alpha_{ab}(t) = n_a(t)\, \alpha_{ab}(t) + \langle\, b \,|\, \hat{h}(t) \,|\, a \,\rangle (n_a(t) - n_b(t)) + \delta_{ab}\, i\, \partial_t n_a(t) \\ + \sum_{ijl} \gamma_{2,ijal}(t) \langle\, ij \,|\, v_{\mathrm{ee}} \,|\, bl \,\rangle(t) - \sum_{jkl} \gamma_{2,bjkl}(t) \langle\, aj \,|\, v_{\mathrm{ee}} \,|\, kl \,\rangle(t) \end{aligned} \tag{5.31}$$

and inserting it into Eq. (5.30), we arrive at

$$\begin{aligned} &\Big(i\, n_a(t) \partial_t - n_a(t) \hat{h}(1;t)\Big)\, \varphi_a(1;t) - \sum_{ijl} \gamma_{2,ijal}(t) \int v_{\mathrm{ee}}(12) \varphi_j(2;t) \varphi^*_l(2;t)\, d2\, \varphi_i(1;t) \\ &+ \sum_j \left(n_a(t)(\alpha_{aj}(t) - \langle\, j \,|\, \hat{h} \,|\, a \,\rangle(t)) - \sum_{ikl} \gamma_{2,ikal}(t) \langle\, ik \,|\, v_{\mathrm{ee}} \,|\, jl \,\rangle(t) \right) \varphi_j(1;t) = 0. \end{aligned} \tag{5.32}$$

This is the desired equation of motion for the natural orbitals and completes together with (5.29) part (i) of the proof. ■

Proof of part (ii)

Having the equations for natural orbitals and occupation numbers at hand it is straightforward to show that a solution of these equations is also a solution of the first equation of the BBGKY hierarchy. Provided the initial values for occupation numbers and orbitals are compatible with the initial one-body matrix, part (ii) can be verified by direct construction of the equation of motion for γ_1. To that end we introduce an *assembly* operator $\hat{C}$ by the prescription

$$g(1,1';t) = \hat{C} f_a(1;t) := \sum_a \varphi_a^*(1';t) f_a(1;t) - \sum_a \varphi_a(1;t) f_a^*(1';t). \tag{5.33}$$

Acting with $\hat{C}$ on the equation of motion for the natural spin orbitals, substituting equation (5.29) and using the representations in Eqs. (5.16) and (5.17) recovers the first equation of the BBGKY hierarchy. ■

At this point it is important to observe that the equations of motion for the natural orbitals are not unique. Choosing an arbitrary Hermitian matrix $\beta_{aj}(t)$ and adding terms of the form

$$p_a(1;t) = \sum_j \beta_{aj}(t) \varphi_j(1;t) \tag{5.34}$$

to the right hand side of (5.24), does not alter the first equation of the BBGKY hierarchy while following the steps of proof (ii). This can be attributed to the differences which are taken in the application of the *assembly* operator. Acting with $\hat{C}$ on (5.34) shows

$$\hat{C} p_a(1;t) = \sum_{aj} \beta_{aj}(t) \varphi_j(1;t) \varphi_a^*(1';t) - \sum_{aj} \beta_{aj}^*(t) \varphi_a(1;t) \varphi_j^*(1';t) = 0. \tag{5.35}$$

The ambiguity arising from terms like (5.34) is reminiscent of the static case at zero temperature, where the effective non-local Hamiltonian for the natural orbitals is determined only up to the entries on the diagonal [Per05]. Similarly here, the time-dependent phases of the orbitals are not determined uniquely since the choice of $\beta_{aj}(t)$ is arbitrary. Looking at the spectral representation of the reduced one-body matrix

$$\gamma_1(11';t) = \sum_k n_k(t) \varphi_k(1;t) e^{-i\, s_k(t)} \varphi_k^*(1';t) e^{i\, s_k(t)}. \tag{5.36}$$

this was expected, since already phases of the general form $\exp(-i\, s_k(t))$ with real valued $s_k(t)$ cancel and leave the density matrix unchanged.

We emphasize that the equations of motion for the natural orbitals in Eq. (5.24) already have a single-particle form. Given the exact coefficients $\gamma_{2,ijkl}(t)$ the coupled equations for occupation numbers and natural orbitals yield the exact reduced one-body matrix of the *interacting* system. Contrary to time-dependent DFT it is therefore *not* necessary to introduce an auxiliary system of non-interacting particles whose (non-local) external

potential is designed to recover the one-body matrix of the interacting system.
As illustrated in chapter 2.3, the consideration of neutral excitations in the framework of linear response in TDDFT allows to correct the Kohn-Sham energy spectrum towards the excitation energies of the interacting system. Due to the undetermined diagonal elements of the auxiliary non-local Hamiltonian of static RDMFT and because of the ambiguity which arises due to terms like (5.34) in the equation of motion for the natural orbitals, a response formalism in analogy to TDDFT is not possible in TDRDMFT at zero temperature. At the current stage this seems to require a treatment of TDRDMFT at non-zero temperature.

5.2.2 Cluster Expansion

So far we have written the equations of motion for the occupation numbers in terms of the expansion coefficients $\gamma_{2,abcd}(t)$ for the reduced two-body density matrix. In the present section we show that only the correlated part of the two-body matrix determines the time evolution of the occupation numbers. Mean-field contributions in form of Hartree or Fock terms cancel and do not contribute.
For the matrix elements $\gamma_{2,abcd}(t)$ of the reduced two-body matrix the cluster expansion introduced in Eq. (5.8) can be written in the following form

$$\gamma_{2,abcd}(t) = n_a(t)n_b(t)(\delta_{ac}\delta_{bd} - \delta_{ad}\delta_{bc}) + \lambda_{2,abcd}(t). \tag{5.37}$$

In the literature the contribution $\lambda_{2,abcd}$ beyond the mean-field is also referred to as cumulant of the reduced two-body density matrix [KF98, KM99]. Here, we use the terms N-body correlation and cumulant interchangeably. Note that $\lambda_{2,abcd}(t) = 0$ for non-interacting particles as well as in Hartree-Fock.
Inserting (5.37) into Eq. (5.23) leads to

$$\begin{aligned} i\partial_t n_k(t) = &\sum_m n_k(t)n_m(t)\langle\, km \,|\, v_{\mathrm{ee}} \,|\, km \,\rangle(t) - n_m(t)n_k(t)\langle\, mk \,|\, v_{\mathrm{ee}} \,|\, km \,\rangle(t) \\ &+ \sum_m n_k(t)n_m(t)\langle\, km \,|\, v_{\mathrm{ee}} \,|\, mk \,\rangle(t) - n_k(t)n_m(t)\langle\, km \,|\, v_{\mathrm{ee}} \,|\, km \,\rangle(t) \\ &+ \sum_{ijl} \lambda_{2,ijkl}(t)\langle\, ij \,|\, v_{\mathrm{ee}} \,|\, kl \,\rangle(t) - \sum_{ijl} \lambda_{2,klij}(t)\langle\, kl \,|\, v_{\mathrm{ee}} \,|\, ij \,\rangle(t). \end{aligned} \tag{5.38}$$

The first two sums cancel due to (5.28) so that only the cumulant coefficients of the reduced two-body density matrix remain and the time evolution of the occupation numbers is given by

$$i\partial_t n_k(t) = \sum_{ijl} \lambda_{2,ijkl}(t)\langle\, ij \,|\, v_{\mathrm{ee}} \,|\, kl \,\rangle(t) - c.c. \tag{5.39}$$

Using this result, the equations of motion for the natural spin orbitals can be written in a more compact form as

$$\begin{aligned} \Big[i\, n_j(t)\partial_t - n_j(t)\hat{h}(1;t) + \sum_{abc} \lambda_{2,abjc}(t)\langle\, ab \,|\, v_{\mathrm{ee}} \,|\, jc \,\rangle(t) \Big] \varphi_j(1;t) \\ - \sum_{abd} \gamma_{2,abjd}(t) \int v_{\mathrm{ee}}(12)\varphi_b(2;t)\varphi_d^*(2;t)\, d2\, \varphi_a(1;t) = 0. \end{aligned} \tag{5.40}$$

Similar to Eq. (5.24) the equations in (5.40) together with (5.39) lead directly to the first equation of the BBGKY hierarchy. Due to the compact form we use (5.40) for further considerations in the following sections.

5.2.3 Phase Transformations

The third term in the bracket of Eq. (5.40) is a purely time-dependent function. If we define

$$g_j(t) := \sum_{abc} \lambda_{2,abjc}(t) \langle\, ab \,|\, v_{\mathrm{ee}} \,|\, jc \,\rangle(t) \tag{5.41}$$

we can write

$$\begin{aligned} i\, n_j(t)\, \partial_t \varphi_j(1;t) &= \Big[n_j(t) \hat{h}(1;t) - g_j(t) \Big]\, \varphi_j(1;t) \\ &\quad + \sum_{abd} \gamma_{2,abjd}(t) \int v_{\mathrm{ee}}(12) \varphi_b(2;t) \varphi_d^*(2;t)\, d2\, \varphi_a(1;t). \end{aligned} \tag{5.42}$$

At first sight it appears that the purely time-dependent term can be absorbed in the phase of the natural orbitals. However, this is only the case for special approximate forms of $\gamma_{2,abcd}(t)$. To show this, we consider a phase transformation of the following form

$$\begin{aligned} \varphi_j(1;t) \quad \longrightarrow \quad & \tilde{\varphi}_j(1;t) = \exp\left(-i \int^t f_j(\tau) d\tau \right) \varphi_j(1;t), \\ & f_j(t) = \frac{1}{n_j(t)} g_j(t), \quad n_j(t) \neq 0. \end{aligned} \tag{5.43}$$

Taking the time-derivative of $\tilde{\varphi}_j(1;t)$ and multiplying with $n_j(t) \exp\left(+i \int^t f_j(\tau) d\tau \right)$ we find

$$n_j(t) \exp\left(+i \int^t f_j(\tau) d\tau \right) i \partial_t \tilde{\varphi}_j(1;t) = i\, n_j(t)\, \partial_t \varphi_j(1;t) + g_j(t) \varphi_j(1;t). \tag{5.44}$$

Hence, if we multiply Eq. (5.42) with $\exp\left(-i \int^t f_j(\tau) d\tau \right)$ and use Eq. (5.43) to replace φ_j by $\tilde{\varphi}_j$ we arrive at

$$\begin{aligned} i\, n_j(t)\, \partial_t \tilde{\varphi}_j(1;t) &= n_j(t) \hat{h}(1;t) \tilde{\varphi}_j(1;t) \\ &\quad + \sum_{abd} \gamma_{2,abjd}(t) \int v_{\mathrm{ee}}(12) \tilde{\varphi}_b(2;t) \tilde{\varphi}_d^*(2;t)\, d2\, \tilde{\varphi}_a(1;t) \\ &\quad \times \exp\left(-i \int^t f_j(\tau) - f_a(\tau) - f_b(\tau) + f_d(\tau) d\tau \right). \end{aligned} \tag{5.45}$$

Note that the phase factor in the last term of Eq. (5.45) does not vanish in general. Only for particular choices of γ_2 this phase reduces to $\exp(0) = 1$. One possible form for $\gamma_{2,ijkl}(t)$ is suggested by the structure of many functionals in ground-state RDMFT where $\gamma_{2,ijkl}$ is approximated by

$$\gamma_{2,ijkl} = z_{ij} \left(\delta_{ik} \delta_{jl} - \delta_{il} \delta_{jk} \right) \tag{5.46}$$

with some matrix z_{ij}. Allowing in Eq. (5.46) for time-dependent matrices $z_{ij}(t)$ and inserting this into Eq. (5.45) we find

$$\begin{aligned} i\,n_j(t)\,\partial_t\tilde{\varphi}_j(1;t) &= n_j(t)\hat{h}(1;t)\tilde{\varphi}_j(1;t) \\ &\quad + \sum_d z_{jd}(t)\int v_{\mathrm{ee}}(12)\tilde{\varphi}_d(2;t)\tilde{\varphi}_d^*(2;t)\,d2\,\tilde{\varphi}_j(1;t) \\ &\quad \times \exp\left(-i\int^t f_j(\tau) - f_j(\tau) - f_d(\tau) + f_d(\tau)d\tau\right) \\ &\quad - \sum_d z_{dj}(t)\int v_{\mathrm{ee}}(12)\tilde{\varphi}_j(2;t)\tilde{\varphi}_d^*(2;t)\,d2\,\tilde{\varphi}_d(1;t) \\ &\quad \times \exp\left(-i\int^t f_j(\tau) - f_d(\tau) - f_j(\tau) + f_d(\tau)d\tau\right). \end{aligned} \tag{5.47}$$

For this special choice of γ_2 the phases cancel and the final equation has a TDHF-like form with generalized Hartree and exchange terms

$$\begin{aligned} i\,n_j(t)\,\partial_t\tilde{\varphi}_j(1;t) &= n_j(t)\hat{h}(1;t)\tilde{\varphi}_j(1;t) \\ &\quad + \sum_d z_{jd}(t)\int v_{\mathrm{ee}}(12)\tilde{\varphi}_d(2;t)\tilde{\varphi}_d^*(2;t)\,d2\,\tilde{\varphi}_j(1;t) \\ &\quad - \sum_d z_{dj}(t)\int v_{\mathrm{ee}}(12)\tilde{\varphi}_j(2;t)\tilde{\varphi}_d^*(2;t)\,d2\,\tilde{\varphi}_d(1;t). \end{aligned} \tag{5.48}$$

5.2.4 Time-Dependent Hartree-Fock Limit

The equations of motion for the natural orbitals and occupation numbers reduce as special case to the TDHF equations, if we consider the following limit

$$n_j(t) \equiv 1, \quad j = 1,\ldots,N, \qquad n_j(t) \equiv 0, \quad \forall j > N, \tag{5.49}$$

$$\begin{aligned} \gamma_{2,ijkl}(t) &= n_i(t)n_j(t)(\delta_{ik}\delta_{jl} - \delta_{il}\delta_{jk}) \\ &= \begin{cases} \delta_{ik}\delta_{jl} - \delta_{il}\delta_{jk}, & i,j \le N \\ 0, & \text{else} \end{cases} \\ \lambda_{2,ijkl}(t) &= 0. \end{aligned} \tag{5.50}$$

The equations of motion for the natural spin orbitals then reduce to

$$\begin{aligned} i\,n_j(t)\,\partial_t\varphi_j(1;t) &= n_j(t)\hat{h}(1;t)\varphi_j(1;t) \\ &\quad - \sum_{d=1}^{N} n_j(t)n_d(t)\int v_{\mathrm{ee}}(12)\varphi_d(2;t)\varphi_d^*(2;t)\,d2\,\varphi_j(1;t) \\ &\quad + \sum_{d=1}^{N} n_d(t)n_j(t)\int v_{\mathrm{ee}}(12)\varphi_j(2;t)\varphi_d^*(2;t)\,d2\,\varphi_d(1;t). \end{aligned} \tag{5.51}$$

Using Eq. (5.49) and

$$\rho(1;t) = \gamma_1(11;t) = \sum_{j=1}^{N} n_j(t)\varphi_j(1;t)\varphi_j^*(1;t) = \sum_{j=1}^{N} |\varphi_j(1;t)|^2 \tag{5.52}$$

we can write

$$\begin{aligned} i\,\partial_t\varphi_j(1;t) &= \hat{h}(1;t)\varphi_j(1;t) + \int v_{\mathrm{ee}}(12)\,\rho(2;t)\,d2\,\varphi_j(1;t) \\ &\quad - \sum_{d=1}^{N} \int v_{\mathrm{ee}}(12)\varphi_j(2;t)\varphi_d^*(2;t)\,d2\,\varphi_d(1;t), \end{aligned} \tag{5.53}$$

which is the single-particle form of the TDHF equation. Note that because of $\lambda_2(t) \equiv 0$ we have $i\partial_t n_j(t) = 0$ in Eq. (5.49), so that the occupation numbers are independent of time, as expected for TDHF.

5.2.5 Adiabatic Extension of Ground-State Functionals

As in DFT one could think of extending existing ground-state functionals adiabatically to the time-dependent domain. In TDRDMFT this amounts to replacing static occupation numbers and natural orbitals with their time-dependent counterparts. Like for the adiabatic LDA such a replacement is expected to be accurate, if the temporal change in the system is small. The hope is then that the adiabatic functional also performs well, if larger temporal changes arise during the evolution of the system. In this section we demonstrate that this adiabatic procedure applied to presently known functionals in RDMFT always leads to occupation numbers which are *independent* of time. In other words, such adiabatic extensions are not capable to reproduce the time-dependence of the occupation numbers at all.

The functional form of most commonly used ground-state functionals in RDMFT, written in the basis of the natural orbitals, can be summarized with the following expression

$$\gamma_{2,ijkl} = f_{ijkl}\delta_{ik}\delta_{jl} - g_{ijkl}\delta_{il}\delta_{jk} \tag{5.54}$$

which contains Hartree ($\delta_{ik}\delta_{jl}$) and exchange-like ($\delta_{il}\delta_{jk}$) terms. As example, for the Müller functional [Mül84] we have

$$f_{ijkl} = \frac{1}{2}\,n_i\,n_j, \qquad g_{ijkl} = \frac{1}{2}\,\sqrt{n_i\,n_j}, \tag{5.55}$$

the self-interaction corrected functional of Goedecker and Umrigar [GU98] reads

$$\begin{aligned} f_{ijkl} &= \frac{1}{2}\,\left(n_i\,n_j - n_i^2\delta_{ij}\delta_{ik}\delta_{il}\right), \\ g_{ijkl} &= \frac{1}{2}\,\left(\sqrt{n_i\,n_j} - n_i\delta_{ij}\delta_{ik}\delta_{il}\right), \end{aligned} \tag{5.56}$$

and the BBC1 functional of Baerends et al. [GPB05] has the form

$$\begin{aligned} f_{ijkl} &= \frac{1}{2}\, n_i\, n_j, \\ g_{ijkl} &= \sqrt{n_i\, n_j}\left(\frac{1}{2} - \delta_{il}\delta_{jk}(1-\delta_{ij})\Theta(i-N-\epsilon)\Theta(j-N-\epsilon)\right), \end{aligned} \tag{5.57}$$

where Θ denotes the usual Heaviside step function and $0 < \epsilon < 1$. In a similar fashion the BBC2/BBC3 functionals and the tensor product expansion of Csány and Arias [CA00] can be written in the form of Eq. (5.54). Note that all functionals have the symmetry $g_{ijkl} = g_{jilk}$ and all matrices f_{ijkl}, g_{ijkl} are real valued.
By replacing the static occupation numbers which appear in Eq. (5.54) with their time-dependent counterparts and inserting this approximation for the two-body matrix into the equation of motion for the occupation numbers (5.23) we arrive at

$$\begin{aligned} i\,\partial_t n_k(t) = &\sum_j (f_{kjjk}(t) - f^*_{kjjk}(t))\langle\, kj \,|\, v_{\mathrm{ee}} \,|\, kj \,\rangle(t) \\ &+ \sum_j (g^*_{jkkj}(t) - g_{jkkj}(t))\langle\, jk \,|\, v_{\mathrm{ee}} \,|\, kj \,\rangle(t), \end{aligned} \tag{5.58}$$

which shows that all functionals of the form (5.54) with real valued matrices f_{ijkl}, g_{ijkl} cause a zero right-hand-side in (5.58). Hence, if this class of approximations is used for the time evolution of the one-body matrix γ_1, *the occupation numbers stay constant in time*. This is a severe shortcoming of an adiabatic extension of present functionals of static RDMFT which needs to be addressed in the development of future functionals for time-dependent RDMFT. Possible functional forms that lead to a non-vanishing right hand side in (5.58) would be

$$\gamma_{2,ijkl}(t) = h(\sigma_{ik}(t)\,\sigma_{jl}(t) - \sigma_{il}(t)\,\sigma_{jk}(t)) \tag{5.59}$$

or

$$\gamma_{2,ijkl}(t) = h((\sigma_{ij}(t) - \sigma_{ji}(t))(\sigma_{kl}(t) - \sigma_{lk}(t))), \tag{5.60}$$

where σ_{ij} is a non-diagonal real-valued matrix and h some Taylor-expandable function. Alternatively, functionals with complex valued matrices could be employed.

5.3 Obtaining Static Functionals from TDRDMFT

In static DFT an alternative route to express the ground-state energy of a many-particle system is provided by the zero-temperature fluctuation-dissipation theorem [PN66]. Combining the fluctuation-dissipation theorem with the linear response equation of TDDFT [LP75, GL76, LG06] and utilizing a coupling constant integration allows one to express the ground-state energy in terms of the exchange-correlation kernel f_{xc}. In that way the ground-state exchange-correlation functional can be expressed in terms of a functional which has its origin solely in time-dependent DFT. In a similar spirit we use in the following the time-dependent variant of RDMFT to construct a new class of functionals that can be employed for ground-state calculations.
The new class of ground-state functionals is based on the stationary limit

$$i\partial_t \lambda_n = 0, \qquad n = 1, \ldots, N \tag{5.61}$$

of the equations of motion for the N-body correlations, Eq. (5.12). At this point we emphasize that stationary N-body correlations do not necessarily imply that the ground state of the system has been reached. The N-body correlations are stationary for an arbitrary eigenstate of the many-body Hamiltonian that evolves freely in time. Inserting the time evolution $\Psi_j(t) = \Psi_j(0)\exp(-iE_j t)$ of such a state into the definition of the q-th order reduced density matrix

$$\gamma_q(1,...,q;1',...,q';t) := \binom{N}{q} \int \Psi(1,...,q,q+1,...,N;t)\Psi^*(1',...,q',(q+1),...,N;t)\, d^3(q+1)...d^3N \tag{5.62}$$

shows that the energy phases cancel. Hence, all γ_q are independent of time in that particular case. The same holds for the N-body correlations which can be seen directly from the cluster expansion (5.8). Take as example $n = 2$. Then λ_2 has the form

$$\lambda_2(12,1'2';t) = \gamma_2(12,1'2';t) - \gamma_1(11';t)\gamma_1(22';t) + \gamma_1(12';t)\gamma_1(21';t). \tag{5.63}$$

Since the right hand side consists only of reduced density matrices which are constant in time, λ_2 is independent of time as well. The argument can be continued recursively for higher order correlations if the cluster expansion in Eq. (5.8) is written in the form

$$\lambda_n = \gamma_n - \underset{(n)}{\hat{A}\hat{S}} \sum_{p=1}^{n-1} \gamma_{n-p}\lambda_p. \tag{5.64}$$

Although the stationary condition in Eq. (5.61) does not guarantee that the ground state has been reached, it provides nevertheless a useful condition. To explore this, let us consider in the following the case $n = 2$. We truncate the hierarchy for the N-body correlations by neglecting all terms that contain λ_n with $n \geq 3$. If we furthermore express all remaining terms of Eq. (5.12) in the basis of the natural orbitals, then the stationary limit in Eq. (5.61) leads to a linear system of equations for the expansion coefficients λ_{ijkl} (cf. Eq. (5.18)) of

the two-body correlations. If we define

$$\Lambda_{ij} := \langle\, i \,|\, \hat{h} \,|\, j \,\rangle + \sum_k n_k \left(\langle\, jk \,|\, v_{\mathrm{ee}} \,|\, ik \,\rangle - \langle\, kj \,|\, v_{\mathrm{ee}} \,|\, ik \,\rangle \right), \tag{5.65}$$

this linear system can be written as

$$\sum_{ijkl} \theta_{abcd;ijkl}\ \lambda_{ijkl} = \zeta_{abcd}, \tag{5.66}$$

where the system matrix $\theta_{abcd;ijkl}$ has the following sparse form

$$\begin{aligned}
\theta_{abcd;ijkl} \;:=\; & \Lambda_{ai}\delta_{bj}\delta_{ck}\delta_{dl} + \delta_{ai}\,\Lambda_{bj}\delta_{ck}\delta_{dl} - \delta_{ai}\delta_{bj}\,\Lambda^*_{ck}\delta_{dl} - \delta_{ai}\delta_{bj}\delta_{ck}\,\Lambda^*_{dl} \\
& + \delta_{ck}\delta_{dl}\,\langle\, ij \,|\, v_{\mathrm{ee}} \,|\, ab \,\rangle - \delta_{ai}\delta_{bj}\,\langle\, cd \,|\, v_{\mathrm{ee}} \,|\, kl \,\rangle \\
& + n_a \Big[\delta_{bi}\delta_{cl}\,\langle\, dj \,|\, v_{\mathrm{ee}} \,|\, ka \,\rangle - \delta_{dk}\delta_{cl}\,\langle\, ij \,|\, v_{\mathrm{ee}} \,|\, ba \,\rangle \\
& \qquad + \delta_{bi}\delta_{dk} \Big(\langle\, cj \,|\, v_{\mathrm{ee}} \,|\, la \,\rangle - \langle\, cj \,|\, v_{\mathrm{ee}} \,|\, al \,\rangle \Big) \Big] \\
& + n_b \Big[\delta_{ai}\delta_{dl}\,\langle\, cj \,|\, v_{\mathrm{ee}} \,|\, kb \,\rangle - \delta_{dk}\delta_{cl}\,\langle\, ij \,|\, v_{\mathrm{ee}} \,|\, ba \,\rangle \\
& \qquad + \delta_{ai}\delta_{ck} \Big(\langle\, dj \,|\, v_{\mathrm{ee}} \,|\, lb \,\rangle - \langle\, dj \,|\, v_{\mathrm{ee}} \,|\, bl \,\rangle \Big) \Big] \\
& + n_c \Big[\delta_{ai}\delta_{bj}\,\langle\, dc \,|\, v_{\mathrm{ee}} \,|\, lk \,\rangle - \delta_{ai}\delta_{dl}\,\langle\, jc \,|\, v_{\mathrm{ee}} \,|\, bk \,\rangle \\
& \qquad + \delta_{bi}\delta_{dk} \Big(\langle\, cj \,|\, v_{\mathrm{ee}} \,|\, al \,\rangle - \langle\, jc \,|\, v_{\mathrm{ee}} \,|\, al \,\rangle \Big) \Big] \\
& + n_d \Big[\delta_{ai}\delta_{bj}\,\langle\, cd \,|\, v_{\mathrm{ee}} \,|\, kl \,\rangle - \delta_{bi}\delta_{cl}\,\langle\, jd \,|\, v_{\mathrm{ee}} \,|\, ak \,\rangle \\
& \qquad + \delta_{ai}\delta_{ck} \Big(\langle\, dj \,|\, v_{\mathrm{ee}} \,|\, bl \,\rangle - \langle\, jd \,|\, v_{\mathrm{ee}} \,|\, bl \,\rangle \Big) \Big],
\end{aligned} \tag{5.67}$$

and the right-hand side is given by

$$\begin{aligned}
\zeta_{abcd} :=& \Big(n_a\, n_b - n_c\, n_d + n_a\, n_c\, n_d + n_b\, n_c\, n_d \\
& - n_a\, n_b\, n_c - n_a\, n_b\, n_d \Big) \Big(\langle\, cd \,|\, v_{\mathrm{ee}} \,|\, ab \,\rangle - \langle\, cd \,|\, v_{\mathrm{ee}} \,|\, ba \,\rangle \Big).
\end{aligned} \tag{5.68}$$

Given a set of natural orbitals and occupation numbers, the system matrix $\theta_{abcd;ijkl}$ and the right hand side ζ_{abcd} can be constructed. The solution of the linear system then yields coefficients λ_{ijkl} for the two-body correlations which correspond to the input orbitals and occupations. By virtue of condition (5.61) these coefficients correspond only to a stationary many-body state, not necessarily to the ground state. However, from the coefficients λ_{ijkl} the reduced two-body matrix can be constructed and hence the expression for the ground-state energy can be evaluated. If solving Eq. (5.66) is combined with the direct minimization of the energy functional, then the stationary two-body correlation with the *lowest* total energy can be found. In other words, for the evaluation of the functional one performs a minimization of the total energy under the subsidiary condition of Eq. (5.66). Alternatively, this minimization can be formulated in terms of Lagrange multipliers. The

complete functional for the minimization can then be written in the form

$$G[\{n_j\},\{\varphi_j\}] = E[\{n_j\},\{\varphi_j\}] + S_1[\{n_j\},\{\varphi_j\}] + S_2[\{n_j\},\{\varphi_j\}], \tag{5.69}$$

which includes the N-representability condition of Eq. (4.23)

$$S_1[\{n_j\},\{\varphi_j\}] = \mu\left(\sum_j n_j - N\right) \tag{5.70}$$

and the stationary conditions for the two-body correlations

$$S_2[\{n_j\},\{\varphi_j\}] = \sum_{abcd} \sigma_{abcd}\left(\sum_{ijkl} \theta_{abcd;ijkl}\ \lambda_{ijkl} - \zeta_{abcd}\right), \tag{5.71}$$

where μ and σ_{abcd} denote Lagrange multipliers.
So far we have restricted ourselves to $n = 2$. The above prescription can be extended to include higher order stationary conditions. In general, the truncation of the hierarchy for the N-body correlations at order n neglects all terms that contain λ_p with $p \geq n+1$. Expressing the remaining terms again in the basis of the natural orbitals and using the stationary conditions (5.61) leads to a set of coupled equations for higher order N-body correlations which have to be solved concurrently. As in the case $n = 2$ above, the solution then leads to stationary coefficients $\lambda_{ijk..xyz}$ which can be used in combination with a direct minimization of the energy functional to find the lowest energy state of the system.
We note in passing that the size of the system matrices scales as $q^{2n} \times q^{2n}$, where q is the number of natural orbitals that are used in the direct minimization and n is the order of the N-body correlations which are used for the functional. For small to medium size molecules typically $q = 10$ to $q = 40$ natural orbitals are sufficient to converge the ground-state energy of the system in the direct minimization process. Considering the lowest stationary order, i.e. $n = 2$, the matrix in (5.67) has a size of 10.000×10.000 to $2.560.000 \times 2.560.000$. Due to the large size and the sparse form of the system matrix $\theta_{abcd;ijkl}$ it is advantageous in practice to use iterative schemes to solve Eq. (5.66). This also has the benefit that the solution from the previous minimization step can be used as starting value for the next step in the minimization process.
Since all possible index combinations for the Coulomb matrix elements $\langle\, ij \,|\, v_{\mathrm{ee}} \,|\, kl \,\rangle$ enter the description, we expect the presented class of functionals to behave differently compared to existing functionals in RDMFT which only utilize Hartree or exchange-like combinations for the indices. On the other hand this feature also increases the computational cost since more matrix elements need to be evaluated.
As noted in section 5.1.2, if all λ_n with $n \geq 3$ are neglected, the remaining terms in the equation of motion for the two-body correlations correspond to a screened-ladder approximation. In a diagrammatic language the approximation contains an infinite ladder summation (summation of the complete Born series) and in addition considers an infinite bubble summation over all polarization contributions. This level of approximation is therefore able to describe strongly coupled polarizable systems.

5.4 Applications

Theory without practice cannot survive
and dies as quickly as it lives.

— Leonardo da Vinci, (1452-1519), cited from [Mor72].

In the following sections we investigate the time-dependence of natural orbitals and occupation numbers for two prototypes of dynamical systems: (i) atoms in strong laser fields and (ii) electron-ion scattering. Unfortunately, as shown in section 5.2.5, currently all functionals that are available in TDRDMFT cause time-independent occupation numbers. For this class of approximations the solution of the equations of motion of TDRDMFT therefore gives no insight in the temporal evolution of the occupation numbers. We therefore take a different route here. To assess the time evolution of both, the natural orbitals *and* the occupation numbers we restrict ourselves to one spatial dimension where the full many-body Schrödinger equation can be solved numerically for small atomic systems. Having the full time-dependent many-body wavefunction at hand we then compute the reduced one-body density matrix via Eq. (5.62). The natural orbitals and occupation numbers are subsequently found at every instant in time by direct diagonalization of the one-body matrix. This procedure allows us to extract - at least numerically - the *exact* time-dependence of the occupation numbers and natural orbitals and establishes an exact reference which can be used in the future for the development of new functionals in TDRDMFT.
This section is organized as follows: First, we introduce in section 5.4.1 the notion of a time-dependent correlation entropy which is used later in the applications to monitor the particle correlations during the time evolution of the system. Section 5.4.2 briefly introduces optimal control theory which is utilized to find optimal laser pulses for the atomic transitions that are considered in section 5.4.4. In section 5.4.3 we introduce the one-dimensional model system which serves as an exact reference for the calculation of the time-dependent natural orbitals and occupation numbers. We investigate some ground-state properties of the model before we turn our attention in sections 5.4.4 and 5.4.5 to our actual objective, the time evolution of natural orbitals and occupation numbers.

5.4.1 Correlation Entropy

Terms like *weak correlation* or *strong correlation* are used frequently in many-body theory. In this section we review a quantitative measure to determine the degree of correlation in many-body states. We extend this correlation measure to the time-dependent case and also show how a spatially resolved correlation measure can be defined in a time-dependent context.

If a many-body state is described by a single Slater determinant then the corresponding reduced one-body density matrix is idempotent

$$Tr(\gamma_1 - \gamma_1^2) = 0. \tag{5.72}$$

If many Slater determinants contribute significantly to the state, then the reduced one-body matrix is not idempotent anymore and the trace in (5.72) starts to differ from zero. The deviation from exact idempotency can be used to introduce a possible measure of correlation. However, it seems arbitrary to use the second power of γ_1 in Eq. (5.72). Any

higher power of γ_1 would yield a viable measure for the deviation from exact idempotency as well. In general, one can introduce a q-th order non-idempotency per particle [Zie95, Zie00] with the following expression

$$c(q) = 1 - \frac{1}{N}\mathrm{Tr}\,\gamma_1^q = 1 - \frac{1}{N}\sum_k (n_k)^q, \quad q \geq 0. \tag{5.73}$$

This function starts at $q = 1$ with $c(1) = 0$ and saturates for $q \to \infty$ with $c(\infty) = 1$. The ascent at $q = 1$ is increasingly steep with enhanced correlation. This fact allows to define a q-independent correlation measure by considering the derivative of $c(q)$ at $q = 1$

$$s := \frac{d}{dq}\, c(q)\Big|_{q=1} = -\frac{1}{N}\mathrm{Tr}\,\gamma_1 \ln \gamma_1 = -\frac{1}{N}\sum_k n_k \ln n_k. \tag{5.74}$$

The expression in Eq. (5.74) has the form of an entropy and is therefore called *correlation entropy* [Col93, Zie95]. Defined in this way, the correlation entropy is a global scalar quantity that summarizes the overall correlation of the wavefunction. In some applications it might be of interest in which regions of space the correlations in the system are most pronounced. Using the natural orbitals $\varphi_k(\mathbf{r})$, one can define for such purposes a spatially resolved correlation entropy

$$s(\mathbf{r}) := -\frac{1}{N}\sum_k n_k \ln n_k |\varphi_k(\mathbf{r})|^2. \tag{5.75}$$

The correlation entropy of Eq. (5.74) was so far only considered for static systems [Col93, Zie95, GJPZ97, Zie00]. For the applications that we present in the following sections we extend this correlation measure to the realm of time-dependent many-body states. To that end we replace the ground-state occupation numbers in Eq. (5.74) by their time-dependent counterparts and define a *time-dependent correlation entropy*

$$s(t) := -\frac{1}{N}\mathrm{Tr}\,\gamma_1(t) \ln \gamma_1(t) = -\frac{1}{N}\sum_k n_k(t) \ln n_k(t). \tag{5.76}$$

For time-dependent processes in many-body systems, like scattering events, chemical reactions, or also for systems under the influence of external drivings, this function allows to monitor the increase or decrease of correlations during the temporal evolution of the system. Similar to the static case a spatially resolved correlation entropy $s(\mathbf{r};t)$ can be introduced with help of the time-dependent natural orbitals

$$s(\mathbf{r};t) := -\frac{1}{N}\sum_k n_k(t) \ln n_k(t) |\varphi_k(\mathbf{r};t)|^2. \tag{5.77}$$

5.4.2 Optimal Control Theory

In this section we give a very brief overview of optimal control theory (OCT), which we use in section 5.4.4 to study the time-dependence of natural orbitals and occupation numbers during laser excitation.

The objective of optimal control theory is to find an optimal laser pulse $\epsilon(t)$ which drives the quantum state $|\,\Psi(t)\,\rangle$ of the system in a *finite* time interval T from a given initial state

$|\,\Phi_i\,\rangle$ to a prescribed target state $|\,\Phi_f\,\rangle$. We remark that the pulse shape $\epsilon(t)$ corresponds to a simple CW laser with frequency $\omega = (E_f - E_i)/\hbar$ if we consider the linear response regime and take the limit $T \to \infty$. However, it differs quite substantially from a CW pulse if T is finite and of the order of a few femto- or picoseconds ($\omega T \approx \mathcal{O}(1)$). Thinking of an atomic or molecular system, one typically selects the ground state as initial state and some excited state of the system as target state. Mathematically, the optimum that can be achieved within a finite time T corresponds to the maximum of the following overlap functional

$$J_1[\Psi] = |\,\langle\,\Psi(T)\,|\,\Phi_f\,\rangle\,|^2. \tag{5.78}$$

To adjust the significance of the laser intensity, the total fluence of the pulse is weighted with a penalty factor $\alpha_0 \geq 0$

$$J_2[\epsilon] = -\alpha_0 \int_0^T \epsilon^2(t)\,dt. \tag{5.79}$$

The larger the intensity of the pulse, the smaller is the sum $J_1 + J_2$. Finally, we require that the system obeys the time-dependent Schrödinger equation, i.e. that the state $|\,\Psi(t)\,\rangle$ actually represents a time-evolved quantum state. This can be written as

$$J_3[\Psi, \chi, \epsilon] = -2\,\mathrm{Im} \int_0^T \left\langle \chi(t) \,\middle|\, \left(\mathrm{i}\partial_t - \hat{H}(t)\right) \middle|\, \Psi(t) \right\rangle dt, \tag{5.80}$$

where $\chi(t)$ plays the role of a Lagrange multiplier. The dependence of J_3 on the laser field $\epsilon(t)$ enters through the Hamiltonian $\hat{H}$ of the system.
In summary, the optimal laser pulse $\epsilon(t)$ for the transition $i \to f$ maximizes the functional

$$J[\chi, \Psi, \epsilon] = J_1[\Psi] + J_2[\epsilon] + J_3[\chi, \Psi, \epsilon]. \tag{5.81}$$

The extrema of J can be found by setting the total variation of the functional to zero

$$\delta J = \delta_\Psi J + \delta_\chi J + \delta_\epsilon J = 0, \tag{5.82}$$

which is, in this case, equivalent to

$$\delta_\Psi J = 0, \qquad \delta_\chi J = 0, \qquad \delta_\epsilon J = 0, \tag{5.83}$$

since the variables χ, Ψ, ϵ can be considered as independent. Evaluating Eq. (5.83) leads to the following set of coupled differential equations

$$\begin{aligned}
\delta_\Psi J = 0 \quad &: \quad \left(i\partial_t - \hat{H}(t)\right) |\,\chi(t)\,\rangle = i\,(|\,\chi(t)\,\rangle - |\,\Phi_f\,\rangle\,\langle\,\Phi_f\,|\,\Psi(t)\,\rangle)\,\delta(t-T), \\
\delta_\chi J = 0 \quad &: \quad \left(i\partial_t - \hat{H}(t)\right) |\,\Psi(t)\,\rangle = 0, \qquad |\,\Psi(0)\,\rangle = |\,\Phi_i\,\rangle\,, \qquad (5.84) \\
\delta_\epsilon J = 0 \quad &: \quad \alpha_0\,\epsilon(t) = -\mathrm{Im}\,\langle\chi(t)|\hat{\mu}|\Psi(t)\rangle. \qquad (5.85)
\end{aligned}$$

For solutions $|\,\chi(t)\,\rangle$ which are continuous at $t = T$, the first equation is equivalent to

$$\left(i\partial_t - \hat{H}(t)\right) |\,\chi(t)\,\rangle = 0, \qquad |\,\chi(T)\,\rangle = |\,\Phi_f\,\rangle\,\langle\,\Phi_f\,|\,\Psi(T)\,\rangle\,, \tag{5.86}$$

which shows that the Lagrange multiplier satisfies the TDSE with an initial condition at the end of the time interval, i.e. at $t = T$.
The expressions in (5.84)-(5.86) together with the boundary conditions comprise the control equations. Their solution corresponds to a stationary point of the control functional J. At this point we emphasize that solutions of the control equations do not allow for a laser pulse which results in 100% overlap with a final state $|\,\Phi_f\,\rangle \neq |\,\Phi_i\,\rangle$. This can be proven by contradiction. Suppose a pulse $\epsilon(t)$ is known which yields perfect overlap, i.e. $\langle\,\Phi_f\,|\,\Psi(T)\,\rangle = 1$. Since we excluded the trivial case of no transition, i.e. $|\,\Phi_f\,\rangle = |\,\Phi_i\,\rangle$, this pulse must have a finite fluence

$$\int_0^T \epsilon^2(t)\,dt > 0. \tag{5.87}$$

For perfect overlap the initial state for the Lagrange multiplier in (5.86) becomes

$$|\,\chi(T)\,\rangle = |\,\Phi_f\,\rangle = |\,\Psi(T)\,\rangle\,. \tag{5.88}$$

In addition, the Hamiltonians in (5.84) and (5.86) are identical for the optimal pulse. Hence, the time-evolution operators for $|\,\chi(t)\,\rangle$ and $|\,\Psi(t)\,\rangle$ are the same and by acting with $\hat{U}(t,T)$ on (5.88) we arrive at

$$\hat{U}(t,T)\,|\,\chi(T)\,\rangle = \hat{U}(t,T)\,|\,\Psi(T)\,\rangle \Rightarrow |\,\chi(t)\,\rangle = |\,\Psi(t)\,\rangle \tag{5.89}$$

Inserting this in (5.85) yields

$$\alpha_0\,\epsilon(t) = -\mathrm{Im}\,\langle\Psi(t)|\hat{\mu}|\Psi(t)\rangle = 0, \tag{5.90}$$

which contradicts our initial assumption of $|\,\Phi_f\,\rangle \neq |\,\Phi_i\,\rangle$.

Experience shows that the overlap (5.78) often exceeds a value of 90%, which is sufficient for almost all practical applications[3].
In section 5.4.2 we solve these equations with an iterative scheme that was proposed in Ref. [ZBR98]. Using the control equations we compute optimal laser pulses which drive the system from the ground state to the first excited state. Along the path of this transition we compute the natural orbitals and the occupation numbers as functions of time.

[3] Provided the system is controllable, i.e. that the target state can actually be reached in finite time T with *some* time-evolution operator $\hat{U}(T,0)$ that originates from the system Hamiltonian. Not all systems share this property. For a more detailed discussion of controllability we refer the reader to Refs. [HTC83, PDR88, RSD+95, SFS01].

5.4.3 Model System

Time-dependent occupation numbers and natural orbitals are a largely unexplored domain. Not much is known about the quantitative behavior of the time evolution that occupation numbers and natural orbitals undergo in various physical processes. It is therefore desirable to study a reference system which allows - at least numerically - for an exact solution of the many-body TDSE. This reference can then be used in turn to construct approximate functionals for TDRDMFT. The aim of the present section is to provide and to characterize such a reference system. We utilize a model which has been used extensively for the theoretical description of atoms and molecules in intense laser fields [SE91]. Originally, the idea for the model was based on the observation that the motion of the electrons in strong laser fields is mainly directed along the polarization axis of the laser. It therefore seems appealing to reduce the complexity of a three dimensional treatment by restricting the motion of the electrons to one spatial dimension. In the model the 3D Coulomb interactions are replaced by soft Coulomb interactions in 1D according to

$$\frac{1}{\sqrt{x^2+y^2+z^2}} \quad \longrightarrow \quad \frac{1}{\sqrt{x^2+\zeta^2}}. \tag{5.91}$$

Here, ζ is a constant and plays the role of a softening parameter. It has been shown that this model reproduces qualitatively non-linear phenomena, such as multi-photon ionization (MPI) [ESJ89, PGB91] above-threshold ionization (ATI) [GE92, GE93, SF94], or high-harmonic generation (HHG) [LSW+96]. The model has also proven useful to study correlation effects of atomic systems in strong laser fields [Bau97, LvL98, LGE00]. Despite the appealing properties of the model, it is important to keep in mind that the reduction to one spatial dimension also introduces some shortcomings. For example, no angular distributions can be investigated, circular laser polarizations cannot be treated and the energy spectra of model potentials in 1D are lacking many of the level degeneracies which are present in three spatial dimensions.

For the time propagations that we present in the following sections we consider a two-electron system which is described by the Hamiltonian

$$\begin{aligned} \hat{H}_\lambda \;=\; & \frac{\hat{p}_1^2}{2}+\frac{\hat{p}_2^2}{2}-\frac{2}{\sqrt{\hat{x}_1^2+\zeta^2}}-\frac{2}{\sqrt{\hat{x}_2^2+\zeta^2}} \\ & +\frac{\lambda}{\sqrt{(\hat{x}_1-\hat{x}_2)^2+\zeta^2}}. \end{aligned} \tag{5.92}$$

A softening parameter of $\zeta = 1$ is employed. To vary the degree of correlation in the many-body wavefunction we introduce a coupling constant λ in the Hamiltonian which controls the strength of the electron-electron interaction.
Before we investigate the time evolution of the natural orbitals and occupation numbers for this model we first summarize some ground-state properties of the system. This summary places special emphasis on density matrices, natural orbitals and occupation numbers to set the stage for the following sections.

Ground-State Description of the Model System

We have calculated the exact ground state and several of the lowest excited states of the interacting Hamiltonian (5.92). To that end a nine-point finite-difference discretization of the kinetic energy has been performed and the real-space representation of the Hamiltonian has been diagonalized with a preconditioned Lanczos-scheme [SSC+96]. From the correlated eigenstates we have computed the reduced one-body density matrix and have extracted natural orbitals and occupation numbers.

In Table 5.1 we summarize the eigenenergies E_j, correlation entropies s_j, and occupation numbers n_k for two different values of the interaction strength λ. All occupation numbers are spin-degenerate and we only list the values for one of the spin channels. To compare to the interacting values in the table, let us first recall the non-interacting case, i.e. $\lambda = 0$. The two-electron wavefunction for the ground state and lowest singly-excited states of

Table 5.1: Eigenenergies E_j, correlation entropies s_j, and occupation numbers for the correlated eigenstates of Helium at coupling parameters $\lambda = 1.0$ (upper panel) and $\lambda = 1.5$ (lower panel of the table). The symmetry of the eigenstates of the 1D model is alternating with increasing j which we indicate with S (singlet) and T (triplet).

$\lambda = 1$		Eq. (5.74)		Occupation Numbers			
Eigenstate j		E_j	s_j	n_1	n_2	n_3	n_4
0	S	-2.238258	0.02717	0.99095	0.00830	0.00071	0.00003
1	T	-1.816070	0.35507	0.49880	0.49880	0.00118	0.00118
2	S	-1.704655	0.35493	0.49882	0.49882	0.00118	0.00118
3	T	-1.643550	0.35832	0.49825	0.49825	0.00174	0.00174
4	S	-1.628780	0.36570	0.56226	0.42873	0.00851	0.00045
5	T	-1.582463	0.35107	0.49943	0.49943	0.00056	0.00056
6	S	-1.566512	0.35037	0.49953	0.49953	0.00047	0.00047
7	T	-1.549178	0.34946	0.49966	0.49965	0.00034	0.00034
8	S	-1.545593	0.35535	0.53001	0.46685	0.00302	0.00009
$\lambda = 1.5$							
0	S	-1.905931	0.06459	0.97411	0.02319	0.00262	0.00006
1	T	-1.625570	0.36854	0.49632	0.49632	0.00365	0.00365
2	S	-1.545842	0.36457	0.49707	0.49707	0.00293	0.00293
3	T	-1.536331	0.35894	0.49813	0.49813	0.00185	0.00185
4	S	-1.528424	0.35300	0.56662	0.43000	0.00259	0.00074
5	T	-1.515078	0.35156	0.49935	0.49935	0.00064	0.00064
6	S	-1.505208	0.35128	0.49939	0.49939	0.00061	0.00061
7	T	-1.502949	0.34949	0.49965	0.49965	0.00035	0.00035
8	S	-1.501087	0.34881	0.53282	0.46634	0.00068	0.00015

Parahelium have the form[4]

$$\begin{aligned}
\Psi_0(1,2) &= \psi_0(\mathbf{r}_1)\psi_0(\mathbf{r}_2)\chi(1,2), \\
\Psi_j(1,2) &= \frac{1}{\sqrt{2}}\left(\psi_0(\mathbf{r}_1)\psi_j(\mathbf{r}_2) + \psi_j(\mathbf{r}_1)\psi_0(\mathbf{r}_2)\right)\chi(1,2), \quad j>0, \\
\chi(1,2) &= \frac{1}{\sqrt{2}}\left(\alpha(1)\beta(2) - \beta(1)\alpha(2)\right).
\end{aligned} \tag{5.93}$$

where $\alpha(j), \beta(j)$ denote the usual spin functions and we use as cumulative index $j \equiv (nml)$. With the wavefunctions in (5.93) the reduced one-body matrices for the ground state and the singly-excited states become simply

$$\begin{aligned}
\gamma_1^{(0)}(1,2) &= \psi_0(\mathbf{r}_1)\psi_0^*(\mathbf{r}_2)\,\eta(1,2), \\
\gamma_1^{(j)}(1,2) &= \frac{1}{2}\left(\psi_0(\mathbf{r}_1)\psi_0^*(\mathbf{r}_2) + \psi_j(\mathbf{r}_1)\psi_j^*(\mathbf{r}_2)\right)\eta(1,2), \quad j>0, \\
\eta(1,2) &= \alpha(1)\alpha(2) + \beta(1)\beta(2).
\end{aligned} \tag{5.94}$$

Here, and in the following, we use an upper label (j) to indicate the index of the eigenstate to which density matrices, occupation numbers and natural orbitals belong. As expected, the result in (5.94) shows that ground and excited states have the single-particle states $\psi_j(\mathbf{r}_1)\sigma(1), \sigma = \alpha, \beta$ as natural spin orbitals. In the ground state only the lowest occupation numbers $n_{1\alpha}^{(0)}, n_{1\alpha}^{(0)}$ are non-zero with $n_{1\alpha}^{(0)} = n_{1\beta}^{(0)} = 1$. For all singly-excited states the occupation numbers are $n_{1\alpha}^{(j)} = n_{1\beta}^{(j)} = 1/2$ and $n_{k\alpha}^{(j)} = n_{k\beta}^{(j)} = 1/2\,\delta_{jk}, \forall k > 1$. In other words, there are always four spin orbitals occupied by 1/2, all others have zero occupation. The same statements hold for singly-excited Orthohelium, where only the symmetries of spatial and spin wavefunction are reversed. Let us now consider the interacting case $\lambda = 1$. As can be seen in the table, in the ground state ($j = 0$) the lowest orbital ($k = 1$) has an occupation number of of $n_1^{(0)} = 0.99095$, i.e. this orbital is almost fully occupied. All other orbitals have only very small occupations which decrease rapidly with the order of the orbital k. This closely resembles the non-interacting picture where the $1s$ orbital is doubly occupied and all remaining orbitals have zero occupation. The electron-electron interaction causes only a slight deviation from this picture. In other words the system has to be considered as weakly correlated. This can also be seen from the small magnitude of the correlation entropy $s_0(\lambda = 1.0) = 0.02717$ which indicates only a slight deviation from exact idempotency for the reduced one-body matrix of the ground state. Next, consider the first excited triplet state ($j = 1$, Orthohelium) and the first excited singlet state ($j = 2$, Parahelium). As discussed above, in both cases the lowest two orbitals (1s, 2p) in each spin channel are half occupied in the non-interacting case. Only the spin symmetry changes from anti-symmetric (Parahelium) to symmetric (Orthohelium). Here, in the interacting case the deviation from the non-interacting picture is more pronounced than in the ground state with occupation numbers of 0.49880 for Orthohelium and 0.49882 for Parahelium. A similar picture is found for all other excited states with $j > 3$. Note that the occupation numbers have been ordered according to magnitude, so that the orbitals which correspond to $k = 1, 2$ are not always 1s or 2p orbitals, but can become other orbitals if excited

[4] States where both orbitals are excited (doubly-excited states), are located energetically above the He^+ threshold in the first continuum of Helium. For brevity these autoionizing levels are not considered for the present example.

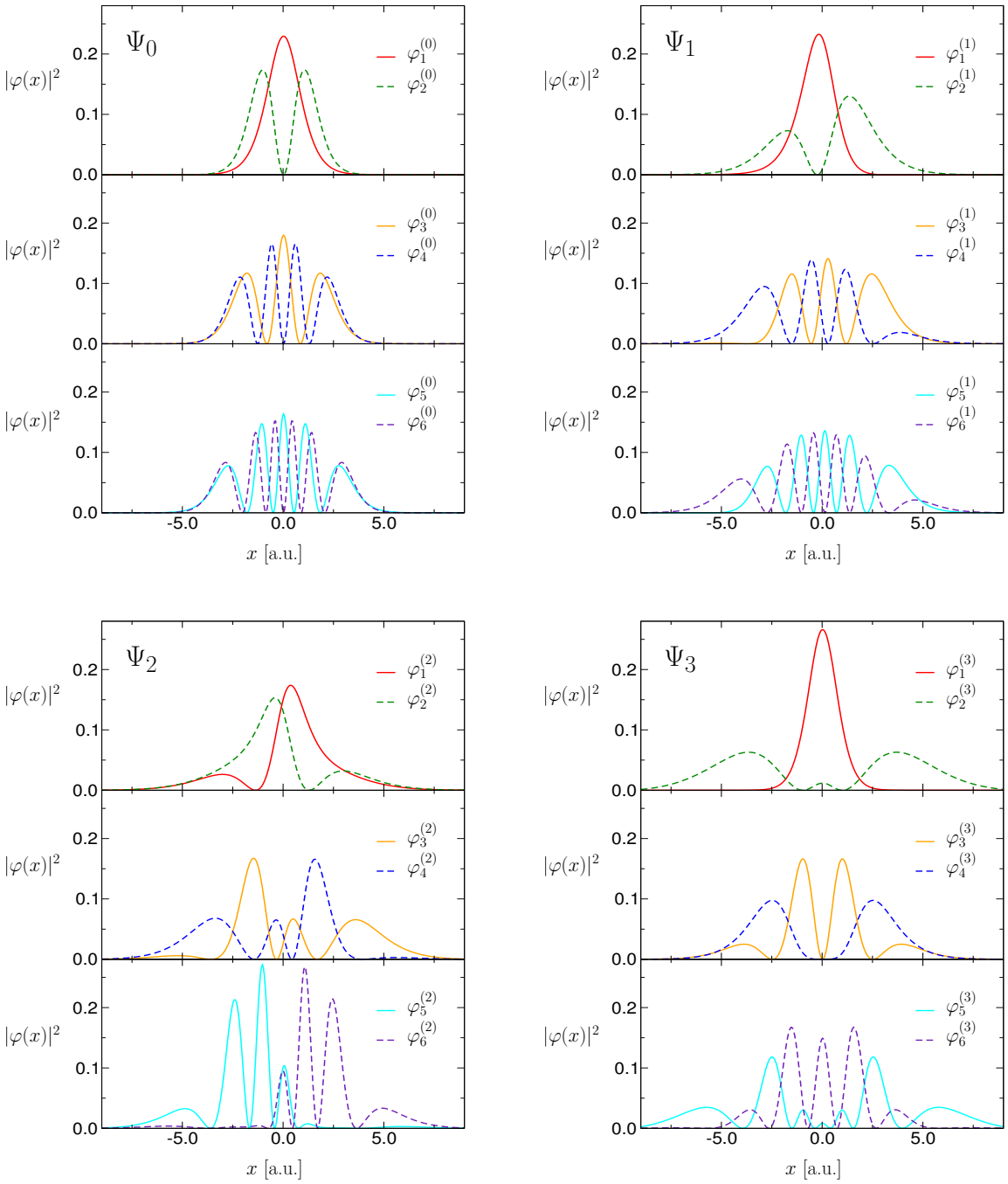

Figure 5.1: Lowest 6 natural orbitals which correspond to the reduced one-body density matrix of the ground state Ψ_0 and the three lowest excited states Ψ_j, $j = 1, 2, 3$ of Helium.

states with larger j are considered. As can be seen in the table, for the excited states there are some cases ($j = 4, j = 8$ and higher excited states), where the interaction causes the lowest occupation numbers to *exceed* the non-interacting value of $1/2$. In these cases the second lowest occupation numbers experience a stronger leakage and more weight is shifted into the third and higher order occupation numbers. We also emphasize that the correlation entropy for excited states is sizeable compared to the ground state which shows that all excited states have to be considered as more strongly correlated than the ground state. The whole picture remains similar for the case $\lambda = 1.5$. The eigenenergies E_j of the two-electron Hamiltonian are all shifted upwards due to the larger (positive) contribution of the electron-electron interaction. The stronger repulsion among the electrons causes the occupation numbers to deviate more strongly from the non-interacting case than for $\lambda = 1.0$. However, even for this interaction strength the system still has to be considered as weakly correlated.
In Fig. 5.1 we plot the natural orbitals for the ground state and a few excited states at different interaction strengths λ. It is interesting to observe that in the interacting case the natural orbitals $\varphi_k^{(j)}, j > 0$ of excited states differ quite substantially from the natural orbitals $\varphi_k^{(0)}$ of the ground state. Recall from our example above that they are identical for non-interacting particles. This shows, that excited states cannot be constructed simply by keeping the natural orbitals of the ground state and modifying the occupation numbers only. Hence, besides the modification of the occupation numbers, a change in the natural orbitals is also required to construct excited states in RDMFT. Already at this point we can therefore conclude that the transition from the ground state of Helium to one of the excited states involves a change in the occupation numbers as well as a change in the natural orbitals. From the above discussion, the largest modification is expected for

$$n_1^{(0)} \to n_1^{(j)}, n_2^{(j)} \qquad \varphi_1^{(0)} \to \varphi_1^{(j)}, \quad \varphi_2^{(0)} \to \varphi_2^{(j)} \qquad j > 0. \tag{5.95}$$

Transitions among excited states $i \to j$

$$n_1^{(i)}, n_2^{(i)} \to n_1^{(j)}, n_2^{(j)} \qquad \varphi_1^{(i)} \to \varphi_1^{(j)}, \quad \varphi_2^{(i)} \to \varphi_2^{(j)} \qquad i, j > 0 \tag{5.96}$$

have a smaller effect on the occupation numbers, while the modifications of the orbitals are comparable to (5.95). This will become more evident in section 5.4.4 where we follow the actual time evolution of the orbitals and occupation numbers during the transition.
In Fig. 5.2 we display the reduced one-body matrices for a few of the lowest eigenstates of our one-dimensional Helium at different interaction strengths λ. In all cases a stronger coupling of the electrons causes a larger spread of the density matrices. The reduced one-body matrices of higher excited states show an intriguing nodal structure as can be seen from the contour lines in the last two rows of the figure.

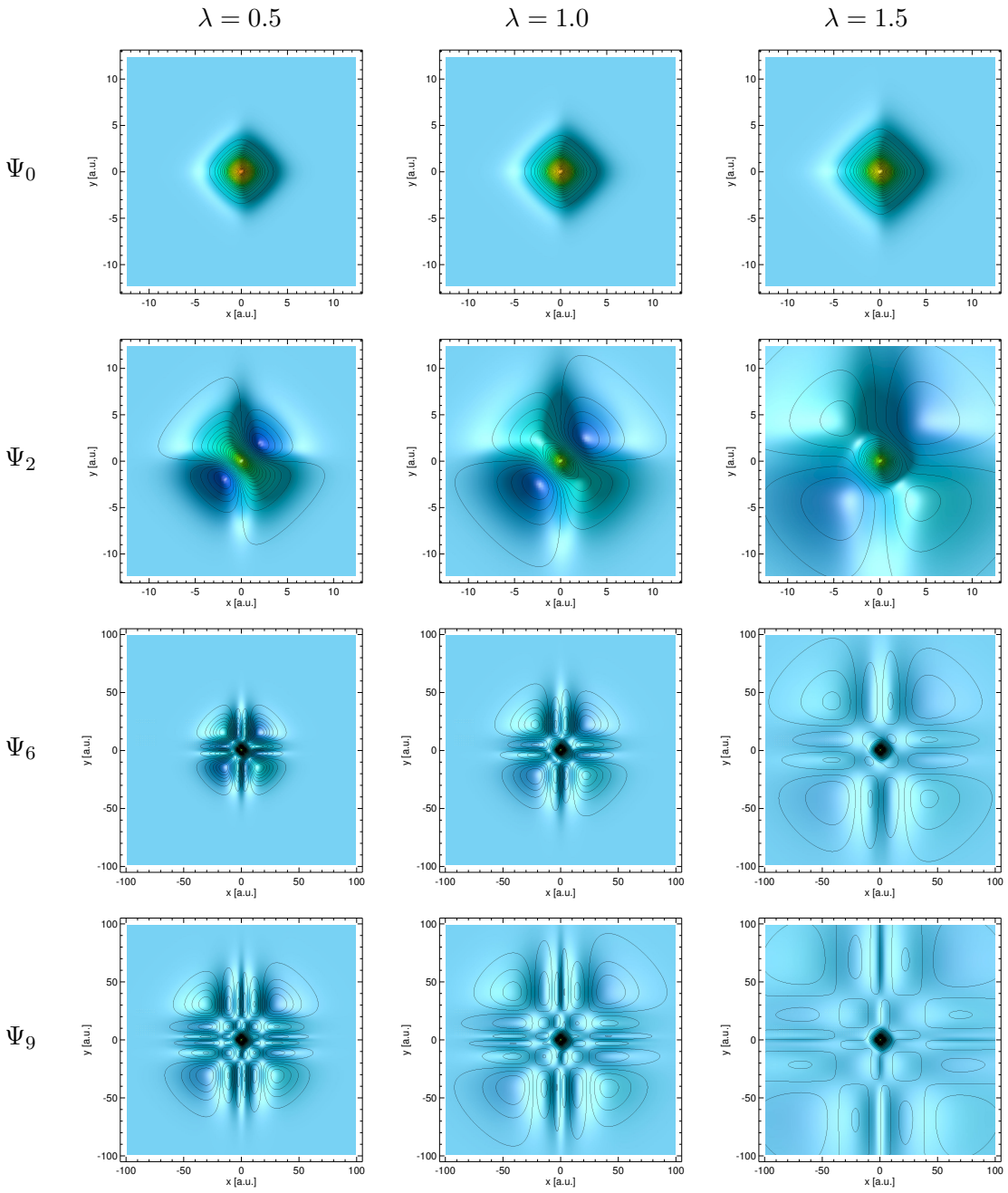

Figure 5.2: Real-space representations of reduced one-body density matrices $\gamma_1^{(j)}(x, y)$ for a few of the lowest singlet eigenstates Ψ_j of correlated Helium at different interaction strengths λ. The left, center and right column contain the matrices which correspond to $\lambda = 0.5$, $\lambda = 1.0$ and $\lambda = 1.5$. In each row we indicate at the left border which eigenstate Ψ_j has been used to compute the one-body matrices in the respective row. The density matrices of the ground state Ψ_0 and the second excited state Ψ_2 in the first two rows are shown on a scale from -12.5 a.u. to +12.5 a.u. The reduced one-body matrices of the 6th and 9th excited state are spatially more extended and are shown in a range from -100 a.u. to +100 a.u.

5.4.4 Atoms in Strong Laser Fields

To study laser induced transitions in the Helium atom we add an external dipole laser field of the form

$$\hat{V}(\hat{x}_1, \hat{x}_2; t) = (\hat{x}_1 + \hat{x}_2)\ \epsilon(t) \tag{5.97}$$

to the Hamiltonian $\hat{H}_\lambda$ in Eq. (5.92). We use standard optimal control theory as introduced in section 5.4.2 to find the optimal laser pulse $\epsilon(t)$ which drives the atom in a finite time-interval $[0, T]$ from some initial state $\Psi_i(1, 2)$ to a final state $\Psi_f(1, 2)$. With this approach we have the correlated wavefunction for the full temporal path of the atomic transitions at hand. For a given instant in time we then construct the reduced one-body density matrix from the wavefunction and diagonalize the matrix to find natural orbitals and occupation numbers.

As first example we consider the transition from the ground state $\Psi_0(1, 2)$ of Helium to the first excited singlet state $\Psi_2(1, 2)$ at an interaction strength $\lambda = 1$. In table 5.2 we summarize the parameters that we employed for the laser pulse optimization with OCT. We have chosen a time-interval $[0, T]$, with $T = 250$ a.u., which corresponds to a propagation time of 6.025 fs. As initial laser pulse for the OCT iteration we use a CW pulse with an intensity $I_0 = \epsilon(0)^2$ of 1.4×10^{13} W/cm^2. To constrain the optimization of the laser we employ an additional time-dependent penalty factor in Eq. (5.84) with the form

$$\alpha(t) = \alpha_0\, e^{-(t-T/2)^2/\sigma^2}. \tag{5.98}$$

This Gaussian is centered at the middle of the optimization interval and ensures that the laser pulses turn on and off smoothly in time. For all pulse optimizations we have performed 12 OCT iterations which have been sufficient to achieve saturation for the absolute value of the control functional J in Eq. (5.81).

In Fig. 5.3, we display the optimal laser pulse, occupation numbers, and the correlation entropy for the transition to the first excited singlet state as function of time for the two different interaction strengths $\lambda = 1.0$ and $\lambda = 1.4$. For $\lambda = 1.0$, the optimal pulse contains three trains which also become visible in the occupation numbers. The smaller occupation number (green line) increases every time a pulse train decays from the maximum of its envelope till the end of the corresponding pulse segment. In other words, there is a small delay after each pulse surge until internal rearrangements in the wavefunction start to appear. The largest occupation number (red line) behaves inversely, i.e. the spectral weight that the second largest occupation number gains during the transition is mainly taken away from the largest occupation number. At the end of the optimization interval,

Table 5.2: Parameters for the time propagations in the iterative OCT scheme. For all pulse optimizations a total of 12 OCT iterations have been performed.

$x_{\min} \ldots x_{\max}$	Δx	T	Δt	I_0	α_0	σ
(a.u.)	(a.u.)	(a.u.)	(a.u.)	W/cm^2	(a.u.)	(a.u.)
-20 ... 20	0.2	250	0.025	1.4×10^{13}	2.5	60

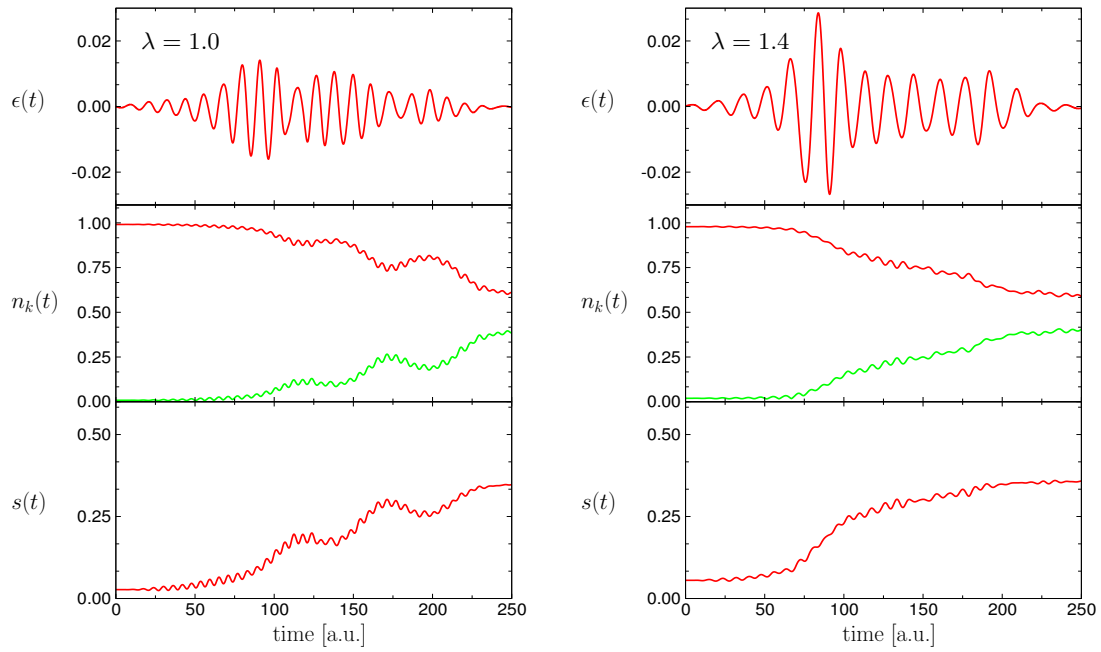

Figure 5.3: Optimal laser pulse $\epsilon(t)$, correlation entropy $s(t)$, and the two largest occupation numbers $n_k(t)$ as function of time during the transition from the ground state to the first excited state of Helium. In the left panel an interaction strength of $\lambda = 1.0$ has been employed and in the right panel we used $\lambda = 1.4$.

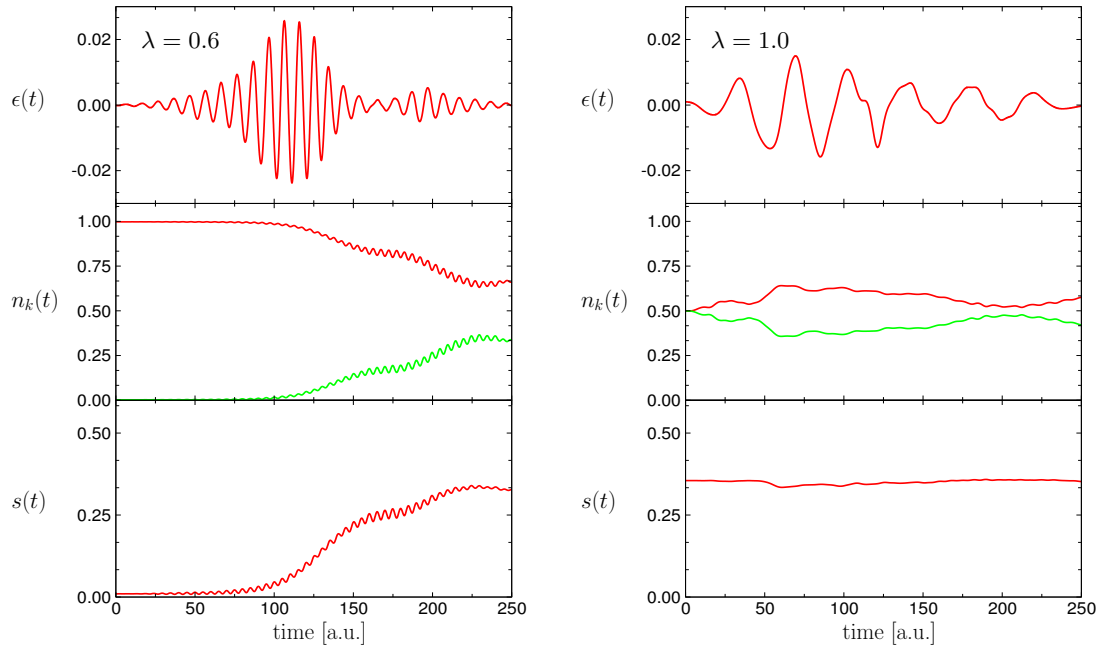

Figure 5.4: Left panel: Same as Fig. 5.3, but here we consider an interaction strength of $\lambda = 0.6$. Right panel: Shown are optimal laser pulse, occupation numbers and correlation entropy for the transition from the first to the second excited triplet state.

the exact occupation numbers of the first excited state (cf. table 5.2) have not been reached completely. This can be attributed to the fact that not 100% overlap with the target state has been achieved during the pulse optimization. In table 5.3 we summarize the achieved wavefunction overlaps for the lowest singlet and triplet transitions at various interaction strengths λ. We also indicate with the ratio $n_k(T)/n_k^{(f)}$ how close the occupation numbers of the optimized state resemble the occupations of the target state. The sensitive behavior of the occupation numbers is surprising. From the first row of the table we infer that there are cases in which the wavefunction overlap exceeds 99%, but the occupation numbers still differ by more than 16% from the target occupations. From this very susceptible behavior we conclude that occupation numbers provide a very characteristic fingerprint of a many-body state. This suggests their use as a complement or even as an alternative to the wavefunction overlap in the OCT functional J of (5.81) to measure the quality of the optimized state $|\,\Psi(T)\,\rangle$. This would also provide a starting point for combining TDRDMFT and OCT.

Next, consider the correlation entropy $s(t)$. As in the ground state at $t = 0$, the correlation entropy is mainly dominated by the second largest occupation number $n_2(t)$ during the whole laser excitation. The shape of the entropy closely follows the temporal evolution of $n_2(t)$. During the transition the entropy rises considerably in magnitude which shows that the reduced one-body matrix of the system is departing more and more from exact idempotency while the excited state is approached.
The optimal pulses behave qualitatively quite differently for the cases $\lambda = 1.4$ and $\lambda = 0.6$ which we show in the right panel of Fig. 5.3 and in the left panel of Fig. 5.4, respectively. In the case $\lambda = 0.6$ only two smoothly connected pulse trains are visible while the pulse for $\lambda = 1.4$ shows mainly a single train with a long plateau on the backside. Again, the pulse structure is directly visible in the occupation numbers. For $\lambda = 0.6$ the lower occupation number rises in two successive steps after about $t = 130$ a.u. and $t = 200$ a.u., which corresponds to the onset of the two trailing edges of the optimal pulse. Likewise, in

Table 5.3: The table summarizes the reached overlaps of the optimized wavefunctions with the target state after 12 OCT iterations. We also indicate how much the occupation numbers deviate from the target occupations at the end of the optimization interval.

λ (a.u.)	Transition $(i \to f)$	$\lvert\langle\,\Psi(T)\,\rvert\,\Phi_f\,\rangle\rvert^2$ %	$n_1(T)/n_1^{(f)}$ %	$n_2(T)/n_2^{(f)}$ %
0.5	$0 \to 2$	99.18	116.29	83.53
	$1 \to 3$	98.21	108.11	91.56
1.0	$0 \to 2$	98.59	122.58	77.04
	$1 \to 3$	97.93	115.52	84.47
1.5	$0 \to 2$	94.30	131.72	68.21
	$1 \to 3$	86.67	115.14	84.85

the case of $\lambda = 1.4$, the first larger increment in the second occupation number starts to appear when the first pulse train decays. Due to the consecutive plateau in the laser pulse the occupation number continues to increase smoothly. In all cases the largest occupation number evolves inversely to the second largest occupation number. Other occupation numbers do not come into play for the present two-electron model. This is expected to be different when more electrons are involved.
Finally, in the right panel of Fig. 5.4, we consider the transition from the first to the second excited triplet state. Contrary to the transitions from the ground state, here the largest occupation number initially gains spectral weight but then returns close to its original value at the end of the time-interval. This gain is mostly at the expense of the second largest occupation number which behaves inversely to the first, as in the cases above. From the correlation entropy $s(t)$, it can be seen that the level of non-idempotency of the one-body matrix remains approximately the same during the whole transition. This is already suggested by table 5.2, where all excited states are shown to have a correlation entropy of similar magnitude. For the transition among excited states of Helium the correlation entropy is no longer dominated by only a single occupation number. Here the two largest occupation numbers contribute on an equal footing.
The qualitatively quite different pictures of time-dependent occupation numbers at different coupling strengths λ show how dominantly the electron-electron interaction influences the transition to the first excited state. At this point we emphasize that time-dependent approaches like TDHF, or TDDFT which are based on a single-determinant picture do not capture the time-dependence of the occupation numbers at all, since by construction the occupation numbers stay in both theories frozen at their initial values of 0 or 1. It will be a challenging task in TDRDMFT to develop new functionals which recover the time-dependence of the occupation numbers at least qualitatively.
To conclude this section, we consider the time evolution of the natural orbitals. In Fig. 5.5 we plot, (a) the diagonal of the reduced one-body matrix $\rho(x;t) = \gamma_1(x,x;t)$ and (b), (c) the orbital density $|\varphi_j(x;t)|^2$ for the natural orbitals with the two largest occupation numbers for two different interaction strengths $\lambda = 1.0$ and $\lambda = 1.5$. Both natural orbitals show nicely the electronic quiver motion in the laser field. For $\lambda = 1.0$ the quiver amplitude of the second orbital, Fig. 5.5 (c) is almost twice as large compared to the first orbital, Fig. 5.5 (b). During the laser cycles charge is shuffled from the left side to the right side of the atom and vice versa, which can be seen in the alternating maxima that appear left and right from the nucleus. Initially it is evident that the natural orbital with the largest occupation number contributes almost exclusively to the total density. But during the course of time the second occupation number starts to increase (cf. Fig. 5.3) so that the second natural orbital also starts to contribute to the density. Similar behavior can be observed for an interaction strength of $\lambda = 1.5$ for which we depict the density and the partial orbital densities in Figs. 5.5 (d)-(f) respectively. In the case of stronger electron-electron interaction the quiver motion is more enhanced. Since the electrons repel each other more strongly it is easier for the laser to distribute the charge across the system.

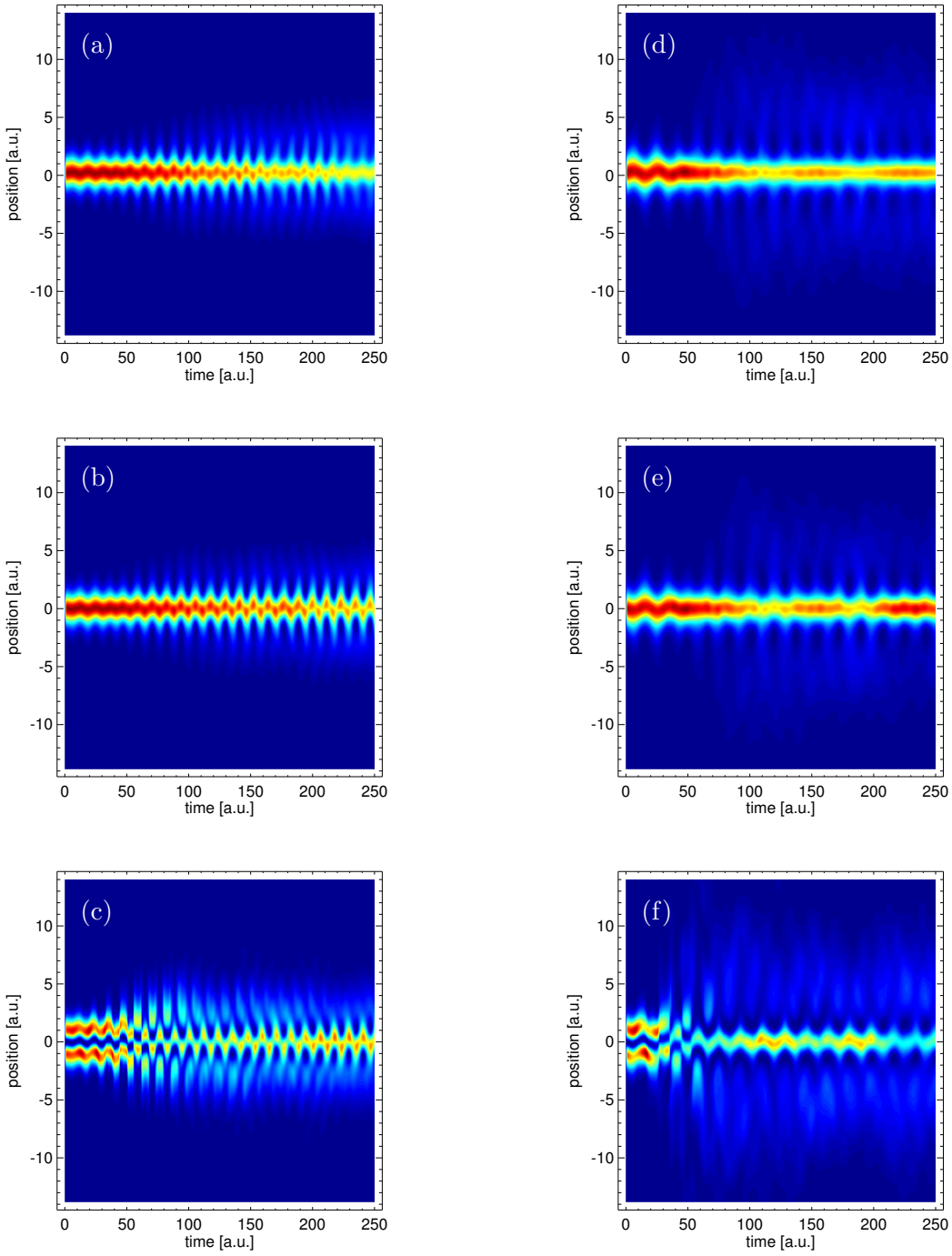

Figure 5.5: Left column: (a) time evolution of the electron density $\gamma_1(x, x; t)$ and (b), (c) the orbital density $|\varphi_j(x; t)|^2$ for the two natural orbitals with the largest occupation numbers for the case $\lambda = 1.0$. Right column: same as the left column, but for $\lambda = 1.5$. The natural orbitals show nicely the quiver motion of the electrons in the strong laser field. A larger quiver amplitude is observed for the interaction strength $\lambda = 1.5$.

5.4.5 Electron-Ion Scattering

As a second prototypical situation for time propagations, we consider e^- – He^+ scattering. In table 5.4 we list the numerical parameters that have been employed for the time propagations. We investigate two different parameter sets which are indicated in the table with case (i) and (ii), respectively. For the initial state of the propagation we use an antisymmetric spin-singlet product wavefunction formed from a Gaussian wave packet

$$\psi(x) = \exp(-(x - x_0)^2/\sigma^2)\exp(-k_0 x) \tag{5.99}$$

which represents the incoming electron and the ground state $\phi_0(x)$ of the He^+-ion. In case (i) the incoming electron is located closer to the ionic core, has a smaller momentum k_0 and is spatially more delocalized compared to case (ii). Note that we start with an uncorrelated state (Slater determinant), but evolve this initial state under the *interacting* Hamiltonian (5.92). The reduced one-body matrix of the system is therefore idempotent at $t = 0$, but becomes non-idempotent during the evolution in time. This is nicely reflected in the correlation entropy in Fig. 5.6 (a), where we consider case (i). The correlation entropy starts with $s = 0$ at $t = 0$ and increases during time. From Fig. 5.7 we infer that at approximately $t = 30$ a.u. the wave packet of the incoming electron has arrived at the ionic core. While the electron approaches the ion, the occupation numbers start to deviate from their determinantal values. After the collision transmitted and reflected waves leave the ionic core (cf. 5.7 (a)) and the occupation numbers return to their original values. At the same time the correlation entropy drops again to zero. This indicates that in this case the many-body state after the collision is again well represented by a Slater determinant. Next, we consider the scattering process for different interaction strengths λ. As expected, Fig. 5.6 shows that for an interaction strength of $\lambda = 1.5$ (green lines) the correlations are enhanced compared to $\lambda = 1.0$ (red lines). However, this trend is not continued if the interaction is increased further to $\lambda = 2.0$. In that case the electron-electron repulsion is already so strong that the initial wave packet is mostly scattered back, as can be seen from Fig. 5.7 (b). The initial surge in the entropy and the occupation numbers is larger for $\lambda = 2.0$, but also decays faster due to the strong backscattering.
In Fig. 5.8 we consider the parameter set (ii) from table 5.4. The overall picture remains similar to the case (i). However, now the occupation numbers do not decay to zero right after the collision. Instead they saturate at non-zero values. The same behavior is found

Table 5.4: Numerical parameters used in the time propagation of e^- – He^+ scattering for the two examples (i) and (ii) as considered in the text. A total of 2,560,000 grid points have been used for the representation of the wavefunction.

Case	x_0 (a.u.)	k_0 (a.u.)	σ (a.u.)	$x_{\min}...x_{\max}$ (a.u.)	Δx (a.u.)	T (a.u.)	Δt (a.u.)
(i)	-15.0	0.3	5.0	-240 ... 240	0.3	300	0.01
(ii)	-25.0	0.5	2.0				

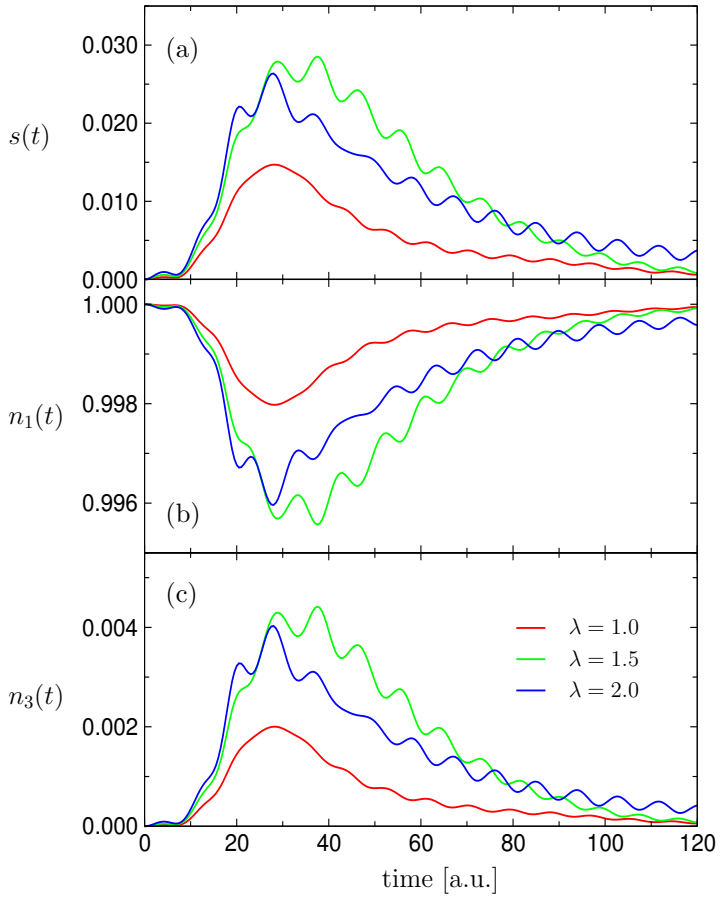

Figure 5.6: (a) Correlation entropy of e^- – He^+ scattering for different interaction strengths λ. (b), (c) Occupation numbers for the first and third natural orbital, respectively.

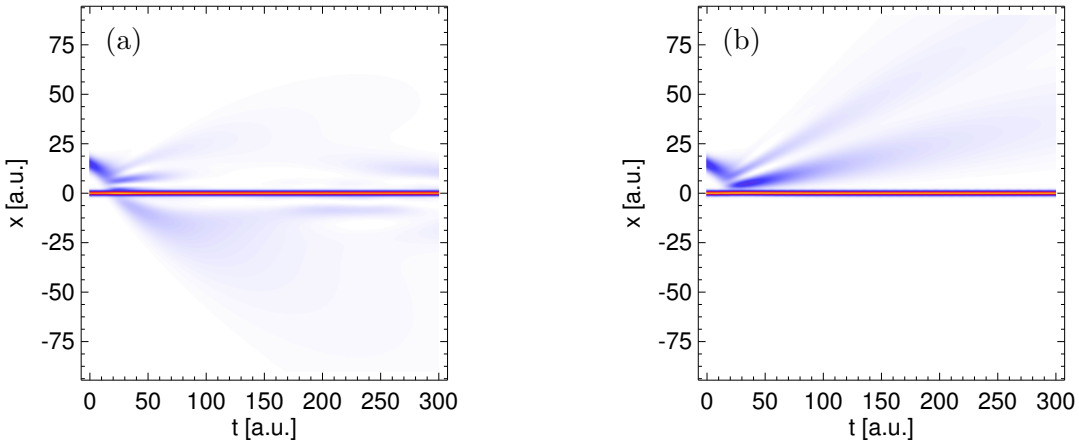

Figure 5.7: Space-time plot of the electron density for e^- – He^+ scattering. (a) $\lambda = 1.0$, (b) $\lambda = 2.0$. In both cases the parameter set of case (i) (cf. table 5.4) has been used.

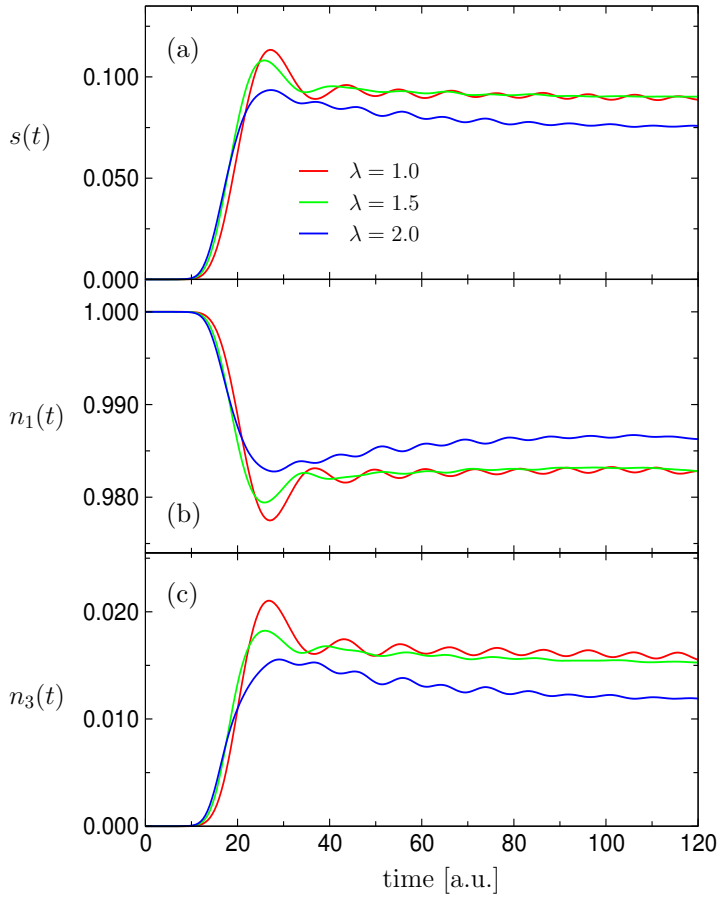

Figure 5.8: Correlation entropy and occupation numbers of e^- – He^+ scattering for different interaction strengths λ: Similar to Fig. 5.6, but for the parameters of case (ii).

in the correlation entropy, 5.8 (a). This shows that the many-body state does not return immediately after the scattering process to a product form, as observed for case (i).
To conclude this section, we show in Figs. 5.9 and 5.10 some snapshots of the time evolution of the reduced one-body density matrix which illustrate nicely the wave nature of the matrix. Note that the spatial extend of the matrix grows rapidly with time due to the wave packet dispersion. After $t = 300$ a.u. (≈ 7.26 fs) the matrix extends already over the whole computational grid which spans a spatial region of 12.7 nm $\times$ 12.7 nm. In Fig. 5.9 we consider an interaction strength of $\lambda = 1.0$. In this case wave amplitude is found both for transmitted waves ($x > 0$, $x' > 0$) and also for reflected waves ($x < 0$, $x' < 0$). Due to the strong electron-electron repulsion this picture changes in the case $\lambda = 2.0$ which we consider in Fig. 5.10. There, dominantly reflected amplitudes ($x < 0$, $x' < 0$) are visible in the reduced one-body matrix[5].

[5] Movies of all time propagations which have been presented in this chapter can be found on the homepage of the thesis [App07].

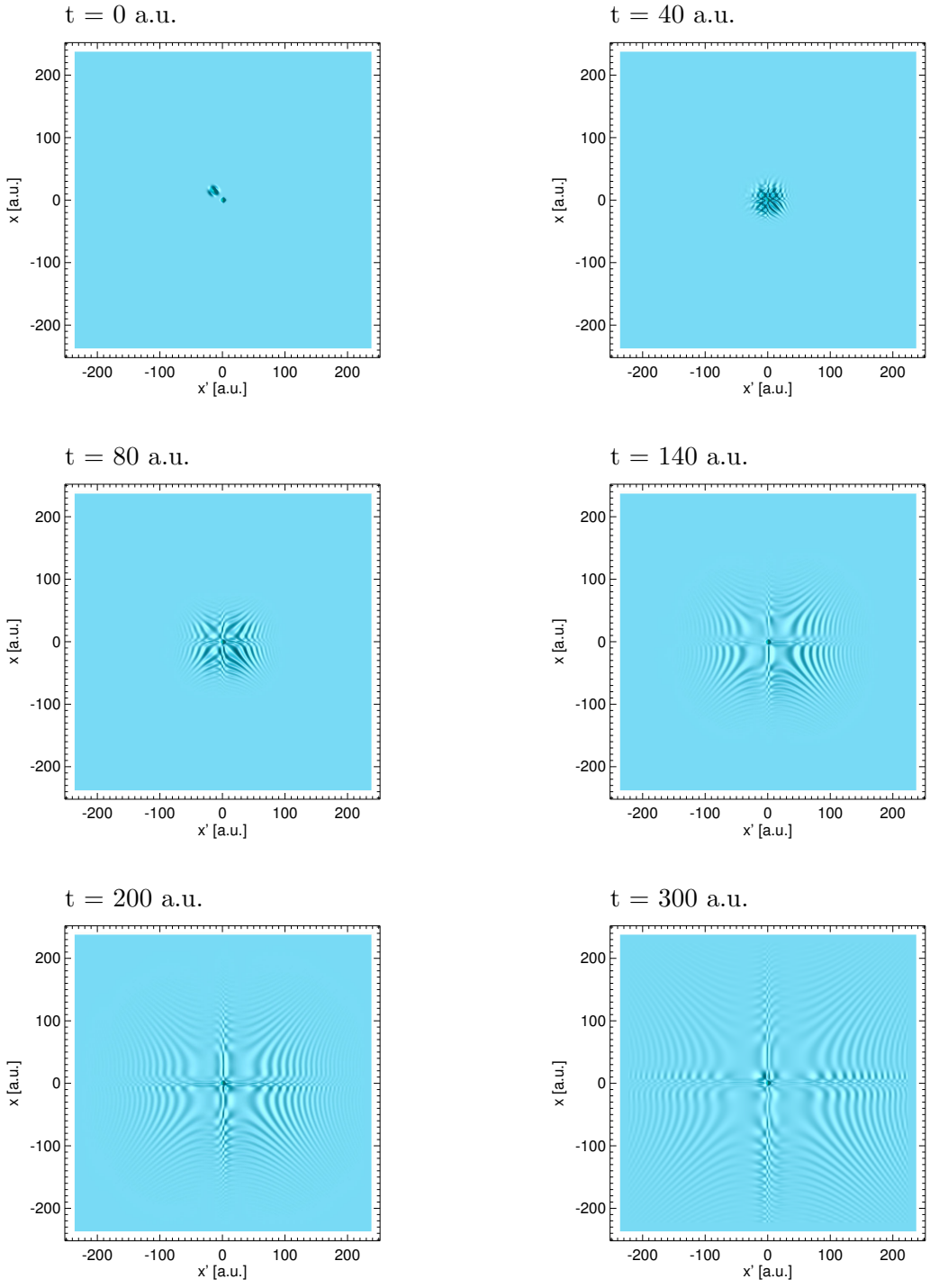

Figure 5.9: Real-part of the reduced one-body density matrix $\gamma_1(x, x'; t)$ for e^- – He^+ scattering at different points in time. Initially a Gaussian wave packet is placed at a distance of 15 a.u. away from the He^+ core at the origin. The packet has a momentum of 0.3 a.u. pointing towards the ion. Considered is an interaction strength of $\lambda = 1.0$.

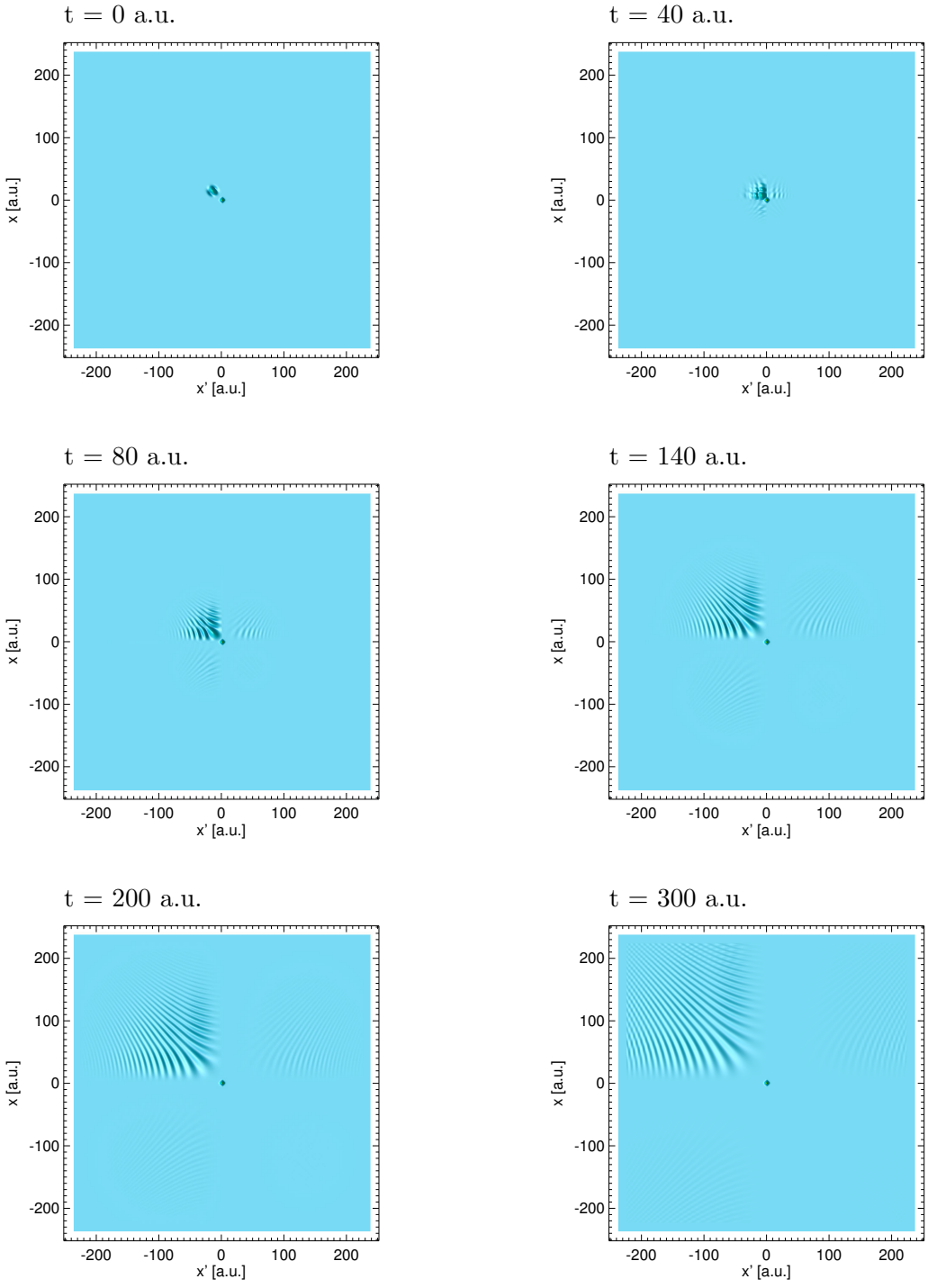

Figure 5.10: Same as Fig. 5.9, but for an interaction strength of $\lambda = 2.0$. Due to the strong interaction the incoming electron is mostly scattered back.

5.5 Summary and Outlook

Reduced density matrix functional theory has recently attracted renewed interest. The theory is a promising candidate to treat strongly correlated systems which are not easily accessible to approaches like DFT. Also other quantities like the fundamental gap are more readily accessible in RDMFT compared to DFT. A number of functionals have been developed in the last few years and their application to finite and extended systems are currently being explored.
In this work we have attempted the first steps towards a time-dependent extension of RDMFT. Using the well-known BBGKY hierarchy for reduced density matrices we have derived equations of motion for the natural spin-orbitals and occupation numbers. In the equation of motion for the natural orbitals we found an invariance which is reminiscent of the undetermined diagonal matrix elements of the effective non-local Hamiltonian of static RDMFT. Using our equation of motion for the occupation numbers, we have been able to show that present ground-state functionals of RDMFT, when extended adiabatically to the time-dependent domain, always yield occupation numbers which are independent of time. From the stationary limit of the equations of motion for the N-body correlations we have derived a new class of functionals which can be employed for ground-state calculations in RDMFT. To asses the exact time-dependence of natural orbitals and occupation numbers we have performed time propagations of a fully interacting model with reduced dimensionality. The exact time evolution of orbitals and occupation numbers has been explored for atomic systems exposed to strong laser pulses and for electron-ion scattering. To our surprise we found that the occupation numbers provide a very sensitive fingerprint of a correlated many-body state. This qualifies them as suitable targets for a combination of optimal control theory and time-dependent RDMFT. Our analysis also revealed that occupation numbers show a time lag when the system is irradiated with a laser pulse. We found that an increase or decrease of occupation took primarily place during the decay of the laser amplitude.
Open questions in TDRDMFT include an extension of Gilbert's theorem to the case of time-dependent reduced one-body density matrices. At present it is still not clear if such an extension can be achieved. This extension is necessary to base the theory on solid ground. Another challenging and still open issue is the development of new functionals for TDRDMFT which are able to capture the time-dependence of the occupation numbers - at least qualitatively - correctly. To study the nuclear motion in molecules also the inclusion of the nuclear degrees of freedom in the time-dependent density matrices needs to be investigated. So far the linear-response regime of TDRDMFT has not been explored. At present it appears that treatment at zero temperature is not sufficient for the description of optical excitations. Here, the extension of the present formalism of TDRDMFT to the case of finite electronic temperatures might be the solution to this problem. Finally we remark that the presence of time-dependent occupation numbers, which deviate from the determinantal values of 0 or 1, corresponds to true correlations in the many-body wavefunction. TDRDMFT is therefore a promising candidate for long-standing problems like the "knee" in Helium double-ionization.

Part III

Electronic Transport within Time-Dependent Density Functional Theory

6 Ab-Initio Approaches to Electronic Transport

There is nothing new to be discovered in physics now;
All that remains is more and more precise measurement.

— Lord Kelvin, speaking to the British Association
for the Advancement of Science, 1900.

In his famous lecture *"There's Plenty of Room at the Bottom"* given in 1959 at the annual meeting of the American Physical Society at the California Institute of Technology, R. P. Feynman surveyed the general possibilities of manipulating matter on the atomic scale [Fey59]. In his talk he considered chemical synthesis by mechanical manipulation, denser computer circuitry, storing the "entire 24 volumes of the Encyclopedia Britannica on the head of a pin", electron microscopes with better resolution, or the possibility of nano-mechanical machines. Almost 50 years after his talk many of his visions for nanotechnology became reality, disproving Lord Kelvin's cheerless attitude concerning the advancement of science. Better microscopes have been realized with the development of the scanning tunneling microscope (STM) or the atomic force microscope (AFM). In 2005 the Millipede storage technology, developed by IBM, reached a data storage capacity of 800 GB/inch^2. This corresponds to pit sizes of approximately 10 nm, or more pictorially to a data volume of 25 DVDs on the area of a postage stamp[1]. Over the past decades the fabrication of computer circuits steadily followed Moore's Law which states that the number of transistors on a chip doubles about every two years [Moo65, Moo07b]. Keeping the overall chip size constant this corresponds to an exponential decrease of transistor size. In Fig. 6.1 we illustrate the average complementary metal oxide semiconductor (CMOS) structure size of modern microprocessors at their market launch as function of time. Starting with Intel's 80286, which was fabricated with a structure size of 1500 nm at market launch in 1982, we have seen a reduction of transistor size by more than a factor of 30 in the last 25 years. At present, 30 million transistors fit on the head of a pin [Moo07a], clearly impressive scientific and technological achievements when looking back to the days of Feynman.
Even beyond the present 45 nm technology, which Intel will introduce by the end of 2007 for the Penryn microarchitecture, there is *plenty of room at the bottom* for the fabrication of electronic circuits. Following naively the extrapolation of the data set in Fig. 6.1, the average CMOS structure size reaches one nanometer in 2034 and finally the Bohr radius of atomic hydrogen in 2054. Although Moore's law will not stay valid indefinitely the extrapolation in Fig. 6.1 shows that electronic circuits soon approach molecular length scales. Hence, provided the miniaturization of transistors continues in the near future with the same pace as in the last 25 years, the limits of the present silicon based technology will soon be reached. The industry leader Intel already switched for its current 45 nm Penryn

[1] As comparison, modern hard disk drives which employ perpendicular recording reach capacities of 230 GB/inch^2.

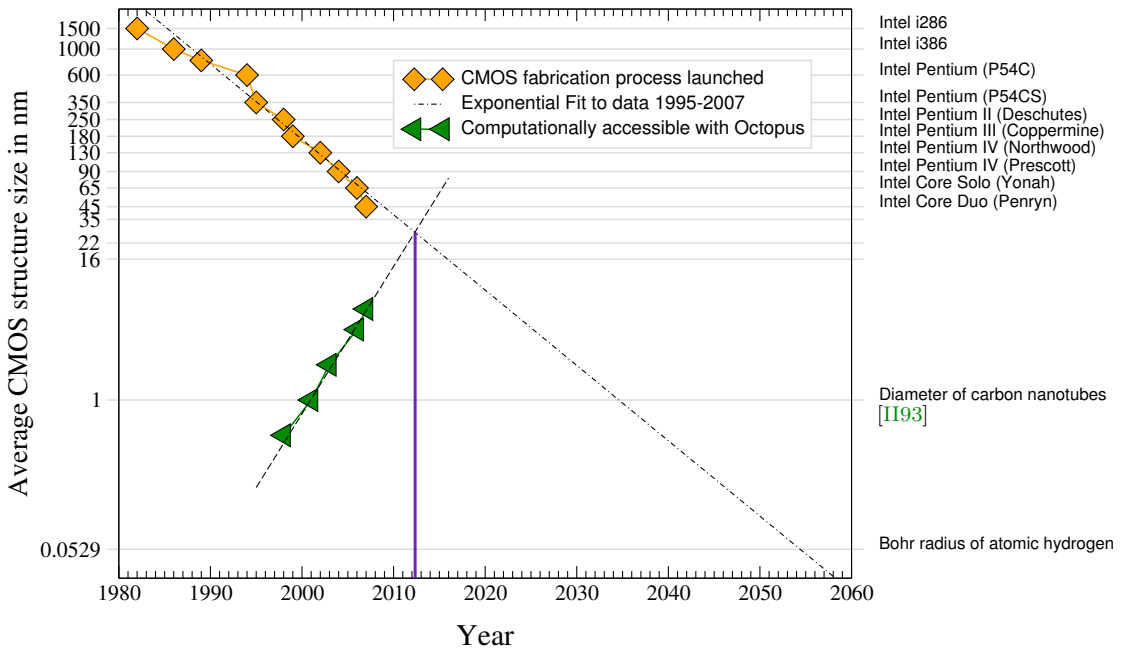

Figure 6.1: The graph displays the average CMOS structure size of commercially available microprocessors at their market launch (source: `wikipedia.org`). Also shown are the numerically reachable transversal grid sizes (in nm) for 2D simulations with OCTOPUS (based on simple commodity hardware accessible to the author in the past years. HPC clusters excluded.). The extrapolation of both data sets is crossing approximately in the first half of 2012.

microarchitecture to hafnium for metal gate electrodes and utilizes a high-k gate dielectric to reduce leakage currents which are a major obstacle in transistor miniaturization. According to Intel's co-founder Gordon Moore this is the *most significant* change in the materials used to manufacture silicon chips since the beginning of commercial semiconductor production four decades ago [Moo07a]. Within the next 25 years of microprocessor fabrication we can expect further drastic changes, both in the employed materials and in the used fabrication techniques. Several materials have been proposed to replace silicon as basic ingredient for the production of electronic transistors, ranging from carbon nanotubes [PTY+01, CAL+06] to graphene [NGM+04, GN07]. Also, the currently used fabrication techniques start to reach limits, e.g. the next generation in CMOS structure size already requires lithography in the extreme ultra violet. Several alternatives to the presently used lithography techniques are investigated, with nano-imprint lithography (NIL) among the most promising candidates for a replacement of optical lithography. The basic idea of NIL is to pattern a resist by deforming its shape through embossing (with a mold), rather than by altering the chemical structures of the resist through radiation [CKG02, CYW+02].
The ultimate limit of electronic circuits will be reached when single atoms and molecules are used as building blocks. In this regime laws from classical physics, e.g. Ohm's law, break down and the functional behavior of device components is dominated by their quantum mechanical nature. A thorough understanding of the underlying physics is therefore indispensable for the selection and design of new device materials for the future quest of transistor miniaturization.

Molecular Electronics

Molecular electronics is the name of a possible future technology which uses single molecules as basic elements of electronic circuits. The first theoretical considerations along these lines appeared in 1974 when Aviram and Ratner investigated a molecular rectifier [AR74]. The experimental realization of conductance through single molecules, however, is a demanding task. It took more than 20 years until Reed and coworkers were able to measure the electronic characteristics of individual molecules attached to gold electrodes [RZM+97]. Since then the preparation of molecular junctions has been improved dramatically. Nowadays, metallic point contacts, atomic wires, or single molecule devices are routinely fabricated with the help of mechanically controllable break junctions [RZM+97, CRRT99, XT03], electro-migration [PLA+99], or scanning tunneling microscopes [GBSN00, ROB+02]. Besides the expected break-down of Ohm's law for molecular devices several other effects have been found which directly originate from the quantum nature of the devices. Examples include the violation of Kirchhoff's law in RC circuits [GFB+06], hysteresis in junction charge transport [JR05], Coulomb blockade effects [Kor97, PPG+02], negative differential resistances [CRRT99], asymmetries in the differential conductance [ROB+02], or signatures of the Kondo effect [PPG+02, LSB+02].

Ab-initio description of Molecular Electronics

Despite the tremendous advances in molecular electronics in the last years, the correspondence between experimental and theoretical studies is currently still limited [NR03]. Theoretical *ab-initio* calculations deviate several orders of magnitude from the experimentally measured current-voltage characteristics in some cases [LA00]. Reasons for this discrepancy have to be attributed both to experiment and to theory. A major problem of experimental studies is reproducibility of results. A prominent example which shows the large uncertainties in experiments is the conductance of DNA. In independent studies DNA was either found to be an *insulator* [DGSB93], *semiconductor* [PBdVD00], or *conductor* [FS99]. Also, the *precise* geometry of the contacting region, and in turn the bonding structure between leads and molecules, is rather difficult to determine experimentally. Similar problems plague the theoretical side. Molecular junctions are usually prepared in experiments by depositing dilute solutions on the break-junctions. Due to the complexity of describing solvents, theoretical calculations are almost exclusively performed *without* the solvents. Because of the non-equilibrium character of electronic transport and the large system sizes very crude and often uncontrolled approximations are utilized and it is not uncommon that theoretical studies based on different approaches deviate from each other considerably [NR03]. At present, the most commonly employed theoretical *ab-initio* methods belong to one of the following two categories:

(i) Landauer formula combined with transmission functions obtained from the static Kohn-Sham potential

As noticed originally by Landauer [Lan57] in the context of metallic conduction, even elastic scattering from localized scattering centers can prevent electrons to traverse a scattering region. The corresponding conductance G can be expressed in terms of transmission and reflection coefficients T and R according to

$$G = G_0 \, T/R, \tag{6.1}$$

where $G_0 = 2e^2/h$ denotes the conductance quantum. Expressions similar to (6.1) can be derived for scattering centers which are connected to multiple channels [BILP85, Dat95, BF04].
To arrive at a practical scheme for the calculation of current-voltage characteristics Eq. (6.1) is combined with transmission functions for elastic scattering from the static Kohn-Sham potential, e.g., as computed with a Lippmann-Schwinger equation [Lan95, LA00, DVPL00].

(ii) Nonequilibrium Green's function (NEGF) theory combined with static Kohn-Sham Green's functions

In this approach the conductance of a molecular junction is expressed in terms of non-equilibrium (or Keldysh) Green's functions [MW92]. In practice, the non-equilibrium Green's functions in the appearing formulas are replaced by the Green's function of the static Kohn-Sham system to resolve the electronic structure of the contacts and the molecular device [BMO+02, XDR02].

Both approaches are by construction not rigorous in the sense that they cannot yield the exact current-voltage characteristics of a molecular junction even if the *exact* static exchange-correlation potential was available. This is basically due to the fact that they attempt to describe an inherent non-equilibrium problem, which involves particle and energy exchange with the reservoirs, in terms of the electronic structure of the *ground state*.
Several aspects are not accounted for in calculations of category (i). The Landauer formula is exclusively based on elastic scattering so that inelastic effects, e.g. due to the coupling to the nuclei, are not taken into account. If the static Kohn-Sham potential is used to compute transmission functions then the energies of resonant tunneling are located in the wrong places since the static Kohn-Sham potential is only designed to yield the correct ground-state density, but not the correct excitation energies of the interacting system (cf. chapter 3). Finally, Landauer's formula assumes non-interacting particles so that particle correlations which build up during the scattering processes in the molecular junction are completely neglected. Transport calculations of category (ii) are more general than Landauer-type approaches, e.g. current formulas in terms of Green's functions are valid also for interacting particles and inelastic effects due to nuclear coupling can be taken into account with appropriate self-energies, but also there resonances are located in energetically wrong positions.
So far, *ab-initio* calculations in quantum transport were mainly concerned with the computation of current-voltage characteristics for steady-state currents. However, to construct active electronic components (e.g. transistors) on the molecular scale also switching processes need to be considered. Such switching can either be achieved with mechanical forces or by using static or time-dependent electromagnetic fields to induce transitions or conformational changes in the molecular system. Since both, Landauer-type approaches and NEGF theory, rely on static DFT such dynamical situations are difficult to describe.
Many of the problems encountered in approaches based on ground-state DFT are naturally taken care of in a time-dependent description. In the present work we therefore aim at using TDDFT to describe time-dependent transport phenomena. Since TDDFT is designed to yield the exact time-dependent density of an interacting system, also the exact time-dependent longitudinal current density can be obtained using the continuity equation. In a transport calculation one is interested in the total current I through a molecular junction

which can be computed from a surface integral of the form

$$I(t) = e \int_S \mathbf{j}_{\mathrm{KS}}(t) \cdot \mathbf{n}\, dS. \tag{6.2}$$

Note that only the longitudinal current density contributes to the integral if we choose a plane perpendicular to the longitudinal geometry of the system for the surface S. Hence, TDDFT has no fundamental limitations and yields, in principle, the correct (time-dependent) total current in the system. As we have seen in chapter 3, time-dependent DFT is capable to recover the exact neutral excitation energies of an interacting system. In terms of molecular transport we can therefore expect that energies for resonant tunneling appear in the correct positions. Other benefits of a time-dependent approach to transport include the possibility to study transients in the current during switching processes, external electromagnetic fields can be incorporated in the description, and the nuclear motion, e.g. in terms of Ehrenfest dynamics, can be accounted for. Of course, there is a price to pay for this additional flexibility which materializes in a higher computational cost compared to existing approaches based on static DFT.

In the following sections we will see that the description of transport within TDDFT requires so-called transparent, or open boundary conditions: since the time propagation of the, in principle, infinite system can only be performed on a finite domain, the boundary conditions have to be chosen such that wave packets suffer no artificial reflections when they enter or leave the simulation area. To date the solution of the time-dependent Kohn-Sham equations for such *open* systems in three spatial dimensions has not been accomplished (normally only zero boundary conditions or periodic boundary conditions are used). There are many technical issues which still have to be resolved until full-scale time propagations of the TDKS equations for quantum transport geometries can be performed. The primary focus of the present work lies therefore on the development of algorithms to implement TDDFT with open boundary conditions. Since all time propagations start in the ground state of the unbiased system the need emerges to find the extended eigenstates of the ground-state Kohn-Sham potential. As first step we therefore introduce, in section 6.1, an algorithm which we have developed to calculate extended eigenstates of single-particle Hamiltonians. The scattering states, obtained from this algorithm, can be used to construct the ground state of the system which serves as initial state for time propagations within TDDFT. In chapter 7 we turn our attention to the description of time-dependent phenomena in quantum transport. In section 7.1 we compare the assets and drawbacks of presently employed approaches for the solution of the time-dependent Kohn-Sham equations. Section 7.2 explores the feasibility of a description of transport in terms of finite systems. Within certain limits the time propagations of our finite model gives useful insight into the transient dynamics of the system but also reveals the shortcomings of a treatment in terms of finite systems. To overcome these limitations we develop, in section 7.3, an algorithm for the propagation of extended states. We present first numerical tests of the method which show that transparent boundary conditions can be achieved within this approach.

To conclude, we emphasize that to date most of the theoretical descriptions consider leads with "infinite" extent in the transversal direction and "semi-infinite" leads in the longitudinal direction. In our opinion only the latter is justified in light of the steady miniaturization of electronic circuits. In Fig. 6.2 we display an atomic force microscope tomograph

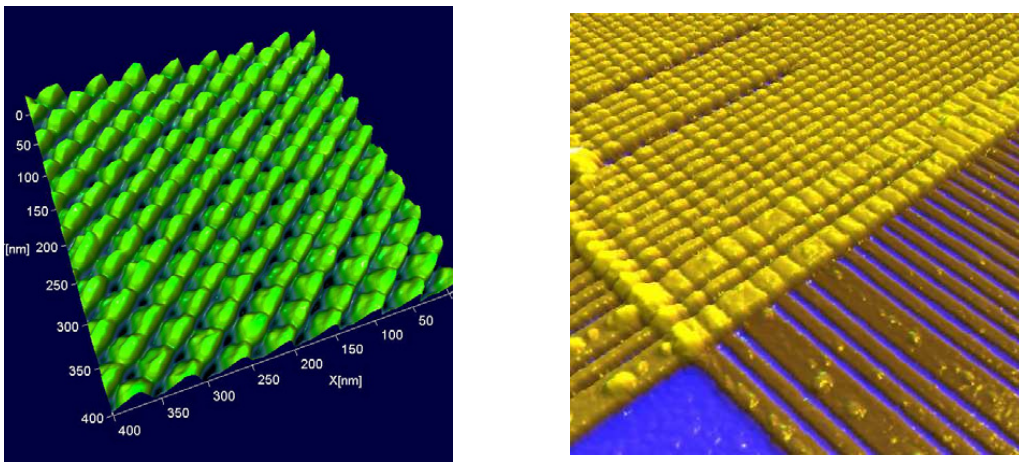

Figure 6.2: Atomic force microscope tomographs of 34 nm pitch field-programmable nanowire interconnects (images taken from Ref. [SW07]). Left panel: nearly defect free region. Right panel: highly defective region.

of a field-programmable nanowire interconnect. The wires in this device have an average transversal size of 34 nm which corresponds to about 90 metal atoms in a row only. To describe leakage currents between such wires the model of an infinite solid in transversal direction is clearly not adequate. We therefore adopt the view of finite transversal system geometries and regard only the infinite nature in the longitudinal direction as justified. In Fig. 6.1 we illustrate with green triangles the maximum transversal grid sizes which have been accessible with the TDDFT package OCTOPUS [MCBR03] for 2D model simulations in the past years. The extrapolation of both data sets in the graph shows that experimental miniaturization and the gain in computational power causes both curves to cross approximately in the year 2012. This example shows that a first-principles description of commercially fabricated devices is soon accessible.

6.1 Real-Space Algorithm for Scattering States

In this section we develop a numerical algorithm to calculate extended eigenstates of a single-particle Hamiltonian $\hat{H}$. The approach is tailored to a real-space finite-difference discretization of the Schrödinger equation for the scattering problem. To illustrate the method we compute scattering states as well as reflection and transmission coefficients for model potentials. The extended eigenstates, calculated with the present method, can be used as initial states for the time propagations considered in the next chapter.
The objective of scattering calculations is to find solutions ψ of the static Schrödinger equation

$$(\hat{H} - E)\,\psi = 0 \tag{6.3}$$

at given energy E accompanied with appropriate boundary conditions. In the following we are concerned with quantum transport calculations where the overall domain is partitioned into a central region and left and right leads, respectively. This is illustrated in Fig. 6.3, where we have schematically placed a benzene ring between two leads with FCC crystal structure. The central region is enclosed by green lines and contains, apart from the molecule, also several unit cells of the leads. The grid points of the underlying finite-difference discretization are indicated with a mesh of grey dots. Referring to Fig. 6.3 we define the computational domain Ω_C and its complement Ω_R by

$$\Omega_C := \{\mathbf{r} = (x, y, z) \,|\, \text{point } \mathbf{r} \text{ is enclosed by green lines in Fig. 6.3}\}, \tag{6.4}$$

$$\Omega_R := \mathbb{R}^3 \backslash \Omega_C. \tag{6.5}$$

In an ideal case the computational domain is chosen large enough so that all points inside Ω_R can be considered as asymptotic points. However, in practice, a compromise between computational cost and system size has to be found. In the asymptotic region (points in Ω_R and area close to the boundary of Ω_C but part of Ω_C) the scattering states with energy E are assumed to take the following form

$$\psi(E;\,\mathbf{r}) \;=\; \sum_{\substack{j=1 \\ \mathcal{E}(\mathbf{k}_j)=E}}^{N} R_j(E)\, u_j(\mathbf{r}) e^{i\mathbf{k}_j\mathbf{r}}. \tag{6.6}$$

Here, $\mathcal{E}(\mathbf{k})$ is the band structure in the respective asymptotic area, j denotes a combined index, $j = (\mathbf{k}, n)$, of $\mathbf{k}$-vector and band index n and we use $\mathbf{k}_j$ to refer to the $\mathbf{k}$-vector that is part of the tuple $j = (\mathbf{k}, n)$. Note that for fixed expansion coefficients $R_j(E)$ this form of the scattering state is valid for arbitrary points $\mathbf{r}$ in the asymptotic region.
In order to simplify the discussion we restrict ourselves in the following to the case of a simple cubic lattice for the lead materials. To evaluate the kinetic energy with a finite-difference stencil, points close to the boundary of Ω_C require the knowledge of the wavefunction *outside* of Ω_C. This is indicated with a star-like stencil in Fig. 6.3 which is centered inside Ω_C and leaks into domain Ω_R. Consider a point $\mathbf{r}_{\text{ref}}$ outside the computational domain for which the value $\psi(E;\mathbf{r}_{\text{ref}})$ is required to calculate the kinetic energy for an interior point (i.e. the point $\mathbf{r}_{\text{ref}}$ is not enclosed by the green lines in Fig. 6.3 but is part of the stencil). By translating the point $\mathbf{r}_{\text{ref}}$ by multiples of the bulk unit cell size a along a given Cartesian coordinate axis $\mathbf{e}_i$, we can construct a series of N points which are members of

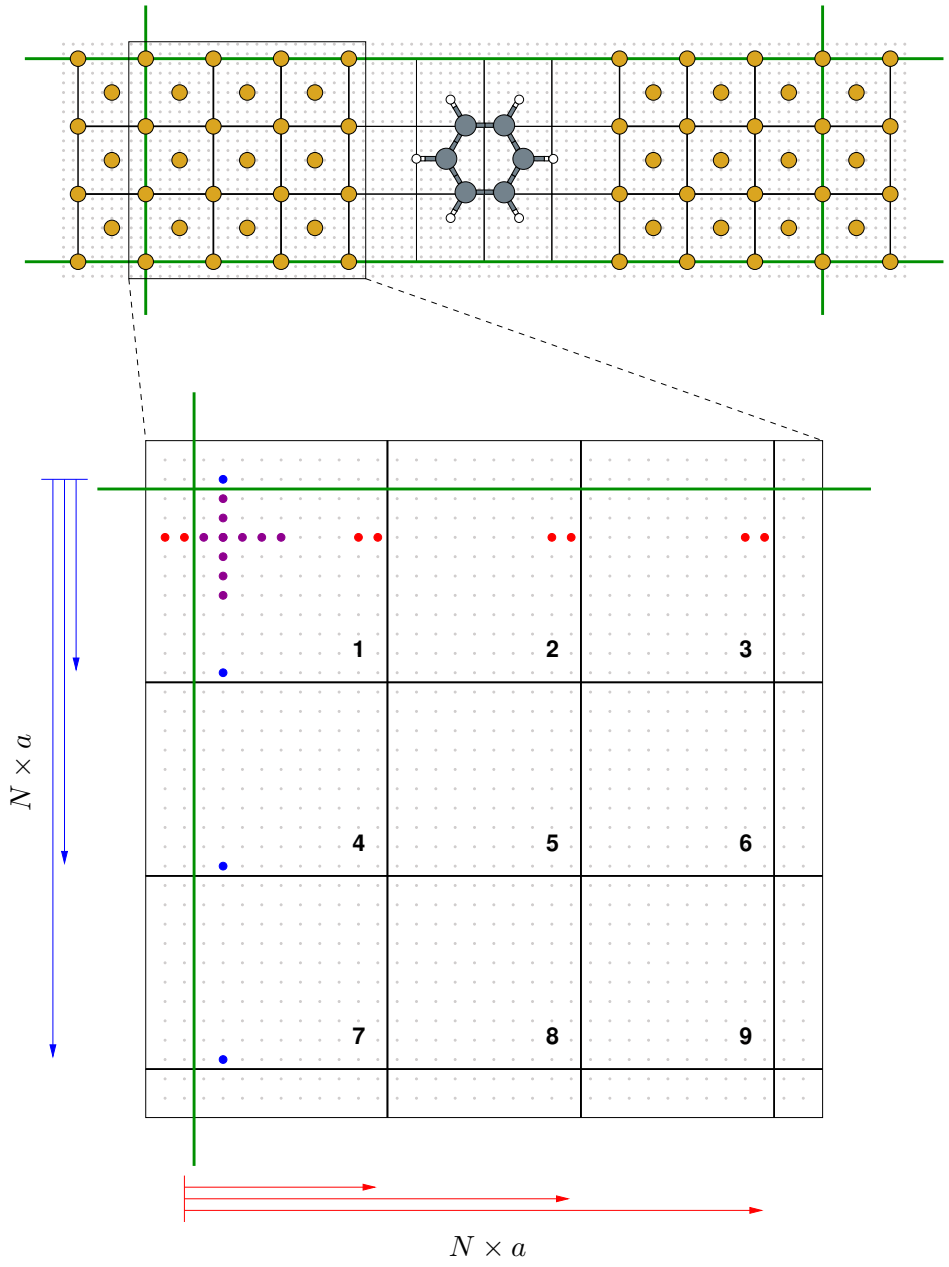

Figure 6.3: Upper panel: Uniform finite-difference mesh spanning a generic transport geometry with FCC unit cells for the lead materials. All points enclosed by green lines are part of the computational domain. Lower panel: Left asymptotic area magnified. The red and blue points left or above the green line (exterior boundary points) are required for the evaluation of a finite-difference stencil located close to the boundary. The red and blue arrows indicate a folding of exterior points into the interior according to the Bloch relation $u_{\mathbf{k},n}(\mathbf{r}) = u_{\mathbf{k},n}(\mathbf{r} + \mathbf{R})$, where $\mathbf{R}$ is a Bravais lattice vector.

the computational domain Ω_C

$$\mathbf{r}_q = \mathbf{r}_{\text{ref}} + \sigma\, q\, a\, \mathbf{e}_i, \qquad q = 1, \ldots, N, \quad \sigma = \pm 1, \tag{6.7}$$

where σ and i are chosen such that $\mathbf{r}_q \in \Omega_C$ (as indicated by the red and blue arrows in Fig. 6.3). Hence, we have

$$\mathbf{r}_{\text{ref}} \in \Omega_R, \tag{6.8}$$

$$\mathbf{r}_q \in \Omega_C \qquad \text{for} \quad q = 1, \ldots, N. \tag{6.9}$$

If the computational domain is chosen large enough then the points $\mathbf{r}_q$ can be considered to be still part of the asymptotic region so that Eq. (6.6) remains valid for all $\mathbf{r}_q$. Evaluating Eq. (6.6) at the N points $\mathbf{r}_q$ gives a set of N equations which relate the scattering coefficients $R_j(E)$ to the values $\psi(E;\mathbf{r}_q)$ of the wavefunction inside the computational domain

$$\begin{aligned} \psi(E;\mathbf{r}_1) &= \sum_{j=1}^{N} R_j(E)\, u_j(\mathbf{r}_1) e^{i\mathbf{k}_j \mathbf{r}_1}, \\ &\vdots \quad\quad \vdots \\ \psi(E;\mathbf{r}_N) &= \sum_{j=1}^{N} R_j(E)\, u_j(\mathbf{r}_N) e^{i\mathbf{k}_j \mathbf{r}_N}. \end{aligned} \tag{6.10}$$

By making use of the Bloch relation

$$u_j(\mathbf{r}_q) = u_j(\mathbf{r}_{\text{ref}} + \sigma\, q\, a\, \mathbf{e}_i) = u_j(\mathbf{r}_{\text{ref}}), \tag{6.11}$$

the right-hand side can be written in terms of the reference point $\mathbf{r}_{\text{ref}}$

$$\begin{aligned} \psi(E;\mathbf{r}_1) &= \sum_{j=1}^{N} R_j(E)\, u_j(\mathbf{r}_{\text{ref}})\, e^{i\mathbf{k}_j \mathbf{r}_{\text{ref}}} \left(e^{i\mathbf{k}_j\, \sigma\, a\, \mathbf{e}_i}\right)^1, \\ &\vdots \quad\quad \vdots \\ \psi(E;\mathbf{r}_N) &= \sum_{j=1}^{N} R_j(E)\, u_j(\mathbf{r}_{\text{ref}})\, e^{i\mathbf{k}_j \mathbf{r}_{\text{ref}}} \left(e^{i\mathbf{k}_j\, \sigma\, a\, \mathbf{e}_i}\right)^N. \end{aligned} \tag{6.12}$$

Provided the $\psi(E;\mathbf{r}_j)$ are known this can be viewed as a system of linear equations for the unknown scattering coefficients $R_j(E)$. A closer look reveals that the system can be written in column-scaled Vandermonde form

$$\begin{bmatrix} \alpha_1^1 & \alpha_2^1 & \cdots & \alpha_N^1 \\ \alpha_1^2 & \alpha_2^2 & \cdots & \alpha_N^2 \\ \vdots & \vdots & \ddots & \vdots \\ \alpha_1^N & \alpha_2^N & \cdots & \alpha_N^N \end{bmatrix} \begin{bmatrix} \nu_1 & 0 & \cdots & 0 \\ 0 & \nu_2 & 0 & \cdots \\ & \ddots & \ddots & \ddots \\ 0 & \cdots & 0 & \nu_N \end{bmatrix} \begin{bmatrix} R_1 \\ R_2 \\ \vdots \\ R_N \end{bmatrix} = \begin{bmatrix} \psi(\mathbf{r}_1) - u_0(\mathbf{r}_1)\, e^{i\mathbf{k}_0 \mathbf{r}_1} \\ \psi(\mathbf{r}_2) - u_0(\mathbf{r}_2)\, e^{i\mathbf{k}_0 \mathbf{r}_2} \\ \vdots \\ \psi(\mathbf{r}_N) - u_0(\mathbf{r}_N)\, e^{i\mathbf{k}_0 \mathbf{r}_N} \end{bmatrix}, \tag{6.13}$$

with $\alpha_j = e^{i\mathbf{k}_j\, a\mathbf{e}_i}$ and $\nu_j = u_j(\mathbf{r}_{\text{ref}})\, e^{i\mathbf{k}_j \mathbf{r}_{\text{ref}}}$. In short

$$\mathbf{AD}\,\{R_j(E)\} = \{\psi(E;\mathbf{r}_j)\} - \{\phi_0(E;\mathbf{r}_j)\}, \qquad \mathbf{r}_j \in \Omega_C, \tag{6.14}$$

where $\mathbf{A}$ abbreviates the Vandermonde matrix, $\mathbf{D}$ denotes the diagonal Bloch matrix, and $\{R_j(E)\}, \{\psi(E;\mathbf{r}_j)\}, \{\phi_0(E;\mathbf{r}_j)\}$ are shorthands for the column vectors in Eq. (6.13). Note that we have moved $\{\phi_0(E;\mathbf{r}_j)\}$ to the right-hand side of the equation since we assume a unit amplitude, $R_0 = 1$, for the incoming wave.
Initially, we started out to find solutions of the static Schrödinger equation

$$(\hat{H} - E)\psi = 0 \tag{6.15}$$

for scattering states with given energy E. Therefore, the values $\psi(E;\mathbf{r}_j)$ are unknown at this point. In fact, as we can see from (6.14), knowing them amounts to knowing the solution. Hence, Eq. (6.14) cannot be viewed as system of linear equations, but merely as a relation between the unknown right hand side and the unknown scattering amplitudes. However, we can invert the matrices[2] in Eq. (6.14) to express the scattering amplitudes in terms of the (still unknown) wavefunction values $\psi(E;\mathbf{r}_j)$

$$\{R_j(E)\} = \mathbf{D}^{-1}\mathbf{A}^{-1}\{\psi(E;\mathbf{r}_j)\} - \mathbf{D}^{-1}\mathbf{A}^{-1}\{\phi_0(E;\mathbf{r}_j)\}, \qquad \mathbf{r}_j \in \Omega_C. \tag{6.16}$$

Together with Eq. (6.6) this can be used to express *exterior* points by *interior* points. In that way the derivatives at the boundary can be calculated and the solution of the Schrödinger equation for a given energy E can be found. Note that the second term in Eq. (6.16) is independent of the solution of the Schrödinger equation and therefore introduces a constant right hand side in Eq. (6.15). In other words the relation in Eq. (6.16) leads together with the Schrödinger equation (6.15) to a system of inhomogeneous linear equations which *explicitly* includes the boundary condition (6.6).
An implementation of the above scheme requires the inversion of Vandermonde matrices (cf. Eq. (6.16)). Although the form of the inverse of Vandermonde matrices is known analytically this is not of much help in practice since a direct evaluation of the analytical expression is numerically not stable. This is related to the fact that Vandermonde systems are known to become *ill-conditioned* with increasing matrix size very quickly. Already for system sizes of $N = 40$, condition numbers[3] on the order of 10^{10} appear. This is basically due to the fact that the matrix has entries spanning several orders of magnitude. Suppose $\alpha = 2$ and $N = 40$, then the smallest entry is $\alpha^1 = 2$ but the largest entry already has a value of $2^{40} \approx 1.1 \times 10^{12}$. The eigenvalues of the matrix span a similar range and hence the condition number of the matrix is very large. To circumvent these problems we use the Parker-Traub algorithm for the inversion of the Vandermonde system which provides a numerically more stable scheme [Par64, Tra66, CH92, CR93, GO97]. In practice, care must be taken for the choice of reference points $\mathbf{r}_{\text{ref}}$. In two or three dimensions nodal lines of the wavefunction need to be avoided since they render the inverse of the diagonal Bloch matrix invalid.
To illustrate the scheme we construct the explicit form of the linear system for a one-dimensional three-point finite-difference discretization with incoming boundary condition

[2] Provided the entries of the diagonal matrix $\mathbf{D}$ are all non-zero it is always possible to invert the product $\mathbf{AD}$ since Vandermonde matrices always have non-vanishing determinants.
[3] The condition number of a matrix A which is normal is defined as ratio of largest to smallest eigenvalue.

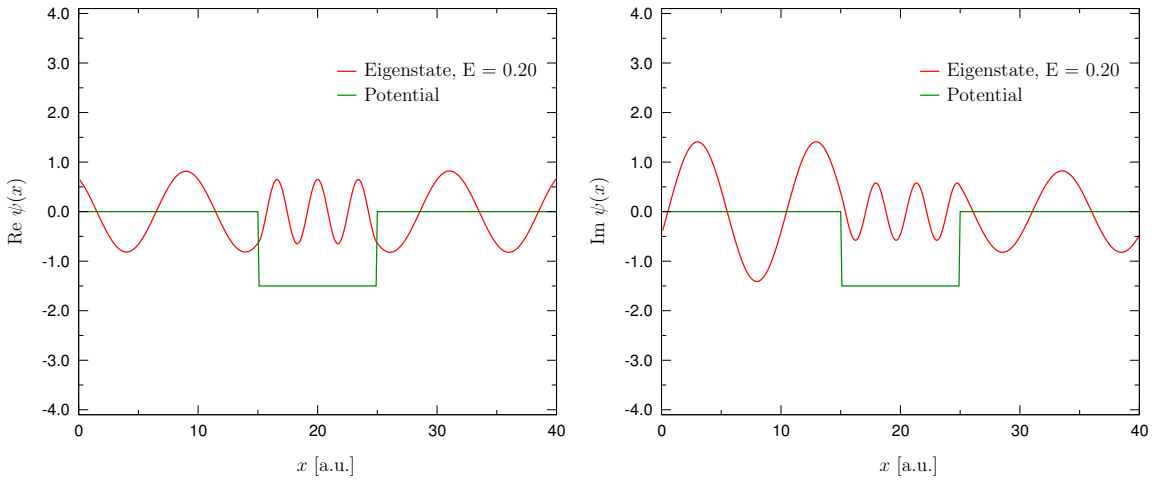

Figure 6.4: Left panel: Real part of a scattering state with energy $E = 0.2$ a.u. for an attractive potential well computed with the present algorithm. Right panel: Imaginary part.

from the left. Due to relation (6.16) the finite-difference representation of the kinetic energy is locally modified at the boundary points

$$\mathbf{T}(E) = -\frac{1}{2\Delta x^2}\begin{bmatrix} -2+\frac{\phi_0^{(-)}(E)}{\phi_1^{(-)}(E)} & 1 & 0 & 0 & 0 \\ 1 & -2 & 1 & 0 & 0 \\ & \ddots & \ddots & \ddots & \\ 0 & 0 & 1 & -2 & 1 \\ 0 & 0 & 0 & 1 & -2+\frac{\phi_{N+1}^{(+)}(E)}{\phi_N^{(+)}(E)} \end{bmatrix} \tag{6.17}$$

and a right-hand side of the form

$$\mathbf{b}(E) = \frac{1}{2\Delta x^2}\Big(\phi_0^{(+)}(E) - \frac{\phi_0^{(-)}(E)}{\phi_1^{(-)}(E)}\phi_1^{(+)}(E), 0, 0, \ldots, 0\Big). \tag{6.18}$$

is introduced in Eq. (6.15). Note that both, the kinetic energy $\mathbf{T}(E)$ and the right-hand side $\mathbf{b}(E)$ are energy dependent and in general complex valued. The potential part remains unchanged

$$\mathbf{V} = \mathrm{diag}\Big(V_1, V_2, \ldots, V_N\Big), \tag{6.19}$$

so that the Schrödinger equation can finally be written in the form

$$\Big(\mathbf{T}(E) + \mathbf{V} - E\Big)\psi(E) = \mathbf{b}(E). \tag{6.20}$$

In the above expressions we denote the grid spacing with Δx and V_j represents the external potential at grid point j. The $\phi_j^{(\pm)}(E)$ are numerical plane waves of the form

$$\phi_j^{(\pm)}(E) = \beta^{\pm j}(E), \tag{6.21}$$

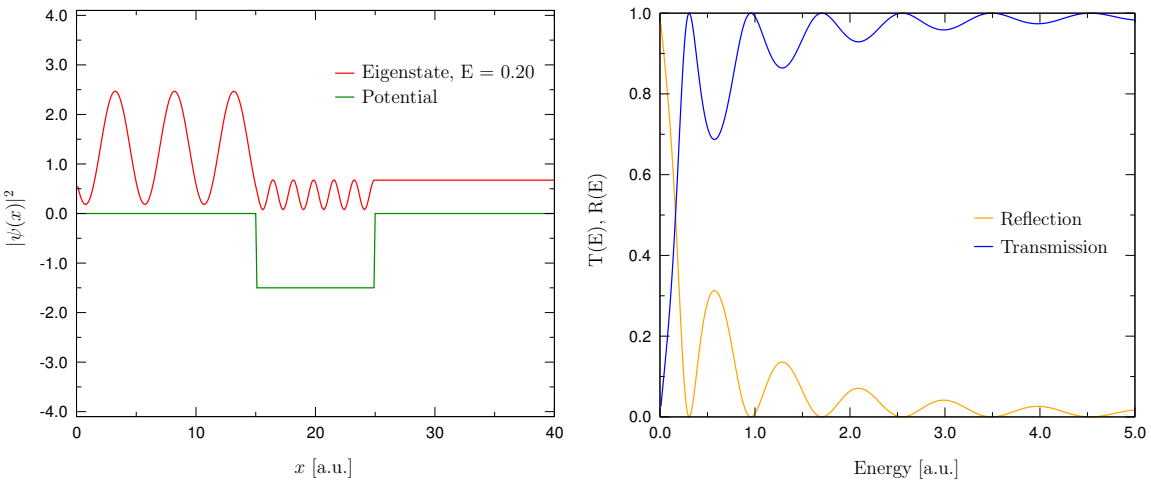

Figure 6.5: Left panel: Orbital density $|\psi(x)|^2$ of the scattering state with energy $E = 0.2$ a.u.. Right panel: Reflection and transmission coefficients as functions of energy.

which are solutions of the discretized free Schrödinger equation

$$-\frac{1}{2}\frac{\phi_{j-1}(E) - 2\phi_j(E) + \phi_{j+1}(E)}{\Delta x^2} = E\,\phi_j(E), \tag{6.22}$$

with

$$\beta_{1,2}(E) = 1 - E\Delta x^2 \pm i\sqrt{2E\Delta x^2 - E^2\Delta x^4}. \tag{6.23}$$

The central result in Eq. (6.20) is a linear system whose solution at a given energy E yields directly the scattering states with incoming boundary condition. A similar system of linear equations is obtained for an incoming boundary condition from the right and higher order finite-difference discretizations of the kinetic energy can be treated along the same lines. Once the scattering states have been found from the solution of Eq. (6.20) the reflection and transmission coefficients can be computed from

$$R(E) = \frac{\psi_1(E) - \phi_1^{(+)}(E)}{\phi_1^{(-)}(E)}, \qquad T(E) = \frac{\psi_N(E)}{\phi_N^{(+)}(E)}. \tag{6.24}$$

In Figs. 6.4 and 6.5 we display eigenstates and reflection and transmission coefficients for an attractive potential well as computed with the present method. The results match directly the textbook solutions for this case which demonstrates the validity of the present approach. We emphasize that our method allows one to compute scattering states *without* constructing the Green's function, or solving the Lippmann-Schwinger equation. Only the solution of a complex-valued and state-dependent linear system is required to find the scattering states. In practice, the limiting prerequisite is that all points $\mathbf{r}_q$ in Eq. (6.7) can be considered as asymptotic points. This of course matches the desire to include as much of the contacts in the computational domain Ω_C as is computationally feasible.

7 Ab-Initio Methods for Time-Dependent Electronic Transport

We can only see a short distance ahead, but
we can see plenty there that needs to be done.

— Alan Turing, (1912-1954), cited from his paper on the Turing test [Tur50].

In this chapter we discuss practical schemes aiming at an *ab-initio* description of time-dependent phenomena in quantum transport within TDDFT. We begin in section 7.1 by listing the assets and drawbacks of presently employed approaches for the solution of the TDKS equations. In section 7.2 we perform time propagations for finite models of two-dimensional mesoscopic systems in order to explore the feasibility of using finite systems for the description of electronic transport. Within certain limits our analysis provides useful insight into the transient dynamics of the model but in general also reveals several shortcomings of such an approach which are due to the finite nature of the reservoirs and the general limitations of absorbing boundary conditions. To overcome these shortcomings we develop a novel scheme for the time propagation of extended states in section 7.3. Our approach utilizes a hybrid basis to represent the extended states of the overall system. We present numerical applications of the method and conclude the chapter with an outlook.

7.1 Comparison of Approaches for the Solution of the TDKS Equations

The propagation of the time-dependent Kohn-Sham equations for electronic transport geometries is a rather demanding task. This is mainly due to the fact that the set of equations has to be solved, in principle, on an infinite domain in real-space. To arrive at computationally tractable implementations, practical applications have to introduce simplifications or special assumptions. The approaches generally fall into two distinct classes: the first class (A) contains methods which replace the initial physical problem, formulated on an infinite domain, by a simpler finite model problem. Methods which belong to the second class (B) retain the infinite domain and try to formulate (finite) effective equations for the central region. So called transparent boundary conditions (TBC's) have to be imposed to avoid artificial reflections of wave packets at the boundaries of the central region.
At present the following approaches can be found in the literature:

(i) Type A - Propagation of finite systems

The perhaps simplest *ab-initio* approach to time-dependent phenomena in quantum transport relies on a modelling in terms of finite-systems [VT04]. In this scheme the charge reservoirs, attached leads, and the central device are all contained in the *same*

finite simulation volume and Dirichlet boundary conditions are used for the Kohn-Sham orbitals of the system. As in a classical capacitor one of the reservoirs is charged and after contacting the central device to the "capacitor plates", i.e. the quantum charge reservoirs, electrons flow across the junction until equilibrium is reached. This form of modelling has the advantage that all subsystems can be propagated on equal footing and allows one to use the *same* time-dependent exchange-correlation potential for all components of the system. Another advantage lies in the fact that existing numerical packages for the solution of the TDKS equations are applicable immediately. As drawback, very large simulation areas need to be considered to encompass central device and reservoirs of reasonable size. Furthermore, due to the finite character of the reservoirs there will be only a small time span during which a steady current through the device can be sustained. Aspects like reservoir depletion, the geometrical shape of the finite reservoirs, or artificial backscattering from the non-thermalized finite reservoirs and the simulation boundaries influence the charge flow through the central device and have to be taken into account when a comparison to experiment is drawn.
We study these effects more in detail in section 7.2 of the present chapter.

(ii) Type A - Propagation of a closed loop

In this approach the central device together with parts of the lead is repeated periodically which corresponds to a ring geometry [GBC06]. The propagation of the TDKS equations with periodic boundary conditions is straightforward within present real-space TDDFT codes so that this method has similar benefits as approach (i). However, replacing the original infinite domain by a ring structure introduces infinitely many images of the central device. Large lead regions have to be employed to prevent image interaction and it is difficult to thermalize the electrons in the "reservoirs" of the ring. Another problem appears in the description of spatially constant electric fields $\mathbf{E}$ across the molecular junction. Since the position operator $\mathbf{r}$ is not periodic, a length gauge with scalar potentials of the form $v(\mathbf{r}) = \mathbf{E}\cdot\mathbf{r}$ cannot be used for the ring geometry. To induce charge flow in the ring typically a magnetic flux inside the ring is utilized. In velocity gauge this corresponds to a time-dependent vector potential of the form $\mathbf{A}(t) = \alpha\mathbf{E}\,t$, where α denotes a constant and $\mathbf{E}$ the electric field strength in the corresponding length gauge. Due to the linear dependence of the vector potential on time the Hamiltonian of the system carries an explicit time-dependence and is in addition not bounded anymore. The steady increase of the vector potential can be compensated with gauge transformations at regular time-intervals during the simulation [GBC06].

(iii) Type A - Propagation of quantum master equations

For electronic transport calculations several system-bath partitioning schemes are of interest, e.g. cases where the leads are treated as bath, or cases where the phonons are treated as bath. By tracing out the bath degrees of freedom in all cases an effective Liouville equation for the density matrix of the system, i.e. the central device, is obtained.
Recently, a Runge-Gross type-theorem was proven for quantum master equations [BCG05]. The theorem states that for fixed electron-electron interaction and super-

operator C, and for a given initial density matrix S_0, two one-body potentials which differ by more than a purely time-dependent function always lead to different particle densities. This opens the possibility to describe an interacting system with associated bath in terms of a Kohn-Sham system of non-interacting particles which evolves under an effective superoperator C_{KS}. The time-dependent Kohn-Sham potential is, in this case, a functional of the time-dependent density, the initial density matrix, and the superoperator C. Although the theorem of Ref. [BCG05] provides a formal ground for such an approach, currently no functional approximations for the involved Kohn-Sham potential $v_{\mathrm{KS}}[\rho, S_0, C]$ are available. Only the usual TDDFT approximations for v_{KS} could be employed which, of course, do not account for the dependence on the initial density matrix S_0 and the superoperator C. The application of quantum master equations is typically suited best for weak system-bath coupling since the derivation of the superoperator relies on Fermi's golden rule, i.e. only first-order time-dependent perturbation theory.

(iv) Type B - Dirichlet-to-Neumann maps

Dirichlet-to-Neumann maps are a means to transform Dirichlet boundary conditions which are imposed on the spatial part of a partial differential equation (PDE) at infinity into Neumann boundary conditions at the surface of a given *finite* domain. By construction, the solution of the PDE on the finite domain, as obtained with the mapped Neumann boundary conditions, exactly matches the solution on the infinite domain. In the context of parabolic partial differential equations such impedance boundary conditions were first employed for the wide-angle approximation to the Helmholtz equation in underwater acoustics [Pap81]. Later applications to the Fresnel equation in optics [SD95, YFS01] and the time-dependent Schrödinger equation in quantum mechanics [BP94, SY97] appeared. The analytic form of the impedance boundary conditions, which are also termed open, artificial, or transparent boundary conditions, is non-local in time and depends on the wavefunction values at the boundary of the finite domain at all past times. In one dimension the impedance boundary condition takes the explicit form [Arn01]

$$\left[\frac{\partial\psi(x,t)}{\partial x} - \frac{\partial\psi_{in}(x,t)}{\partial x}\right]_{x=x_b} = \sqrt{\frac{2}{\hbar\pi}}e^{-i\frac{\pi}{4}}\frac{d}{dt}\int_0^t \frac{\psi(x_b,\tau)-\psi_{in}(x_b,\tau)}{\sqrt{t-\tau}}d\tau, \tag{7.1}$$

where x_b denotes a boundary point and ψ_{in} an incoming wave. The convolution term in Eq. (7.1) can be written as fractional $\left(\frac{1}{2}\right)$ time derivative[1]

$$\frac{1}{\sqrt{\pi}}\frac{d}{dt}\int_0^t \frac{\psi(x,\tau)}{\sqrt{t-\tau}}\,d\tau =: \sqrt{\frac{d}{dt}}\,\psi(x,t), \tag{7.2}$$

which establishes a direct connection between the impedance boundary condition and a formal factorization of the Schrödinger equation into left and right travelling waves

$$\left(\frac{\partial}{\partial x} - \sqrt{\frac{2}{\hbar}}e^{-i\frac{\pi}{4}}\sqrt{\frac{\partial}{\partial t}}\right)\left(\frac{\partial}{\partial x} + \sqrt{\frac{2}{\hbar}}e^{-i\frac{\pi}{4}}\sqrt{\frac{\partial}{\partial t}}\right)\psi = 0. \tag{7.3}$$

[1] A comprehensive introduction to fractional derivatives and their discretization can be found in [Lub86].

At this point we emphasize that transparent boundary conditions for the Dirac equation involve no convolution terms in the form of Eq. (7.1) since this PDE is first order in space *and* time. Fractional derivatives and corresponding impedance terms appear only for the Schrödinger equation, or similar PDEs, containing space and time derivatives of different orders.
Early attempts to discretize the analytic expression (7.1) for the boundary conditions of the Schrödinger equation showed artificial reflections at the boundaries of the finite domain. It was noticed later that the discretization of both, the PDE *and* the Dirichlet-to-Neumann map, have to be carried out on equal footing to avoid artificial reflections [EA01]. To date applications of open-boundary conditions for the TDSE have been considered in one and two spatial dimensions [AES03, ABM04]. Calculations aiming at quantum transport [Arn01] or investigating transparent boundary conditions for nonlinear Schrödinger equations [ABD06] have been performed, so far, only for single particles in one dimension.

(v) Type B - Propagation of effective equations with source and memory terms

This approach is similar in spirit to the methods in (iv). It allows one to formulate an effective equation for a finite domain Ω_C whose solution is equivalent to the solution of the whole-space problem inside Ω_C. The technique was pioneered by Hellums et. al. [HF94] and later extended to explicitely time-dependent driving potentials by Kurth et. al. [KSA+05]. In the latter work, also a practical scheme for the efficient calculation of the involved source and memory terms was proposed. The basic idea of the approach is to partition space into three regions, i.e. the left lead Ω_L, the central device Ω_C, and the right lead Ω_R, so that the time-dependent Kohn-Sham equation takes the block form

$$i\frac{\partial}{\partial t}\begin{bmatrix}\psi_L(t)\\ \psi_C(t)\\ \psi_R(t)\end{bmatrix} = \begin{bmatrix}\boldsymbol{H}_{LL}(t) & \boldsymbol{H}_{LC} & 0\\ \boldsymbol{H}_{CL} & \boldsymbol{H}_{CC}(t) & \boldsymbol{H}_{CR}\\ 0 & \boldsymbol{H}_{RC} & \boldsymbol{H}_{RR}(t)\end{bmatrix}\begin{bmatrix}\psi_L(t)\\ \psi_C(t)\\ \psi_R(t)\end{bmatrix}. \tag{7.4}$$

In general, lead-lead interactions ($\boldsymbol{H}_{LR}, \boldsymbol{H}_{RL}$) are negligible and due to the local multiplicative nature of the Kohn-Sham potential the block Hamiltonian carries a time-dependence only on the diagonal. The partitioning of the infinite-dimensional matrix in Eq. (7.4) is chosen such that $\psi_C(t)$ covers the region of the molecular system, the contacts, and ideally also a few unit cells of the left and the right lead regions so that the separation between center and leads appears deep enough in the leads. This guarantees that all essential physical scattering processes are contained in region Ω_C and the remaining lead regions can be considered as bulk materials in equilibrium. The wavefunction $\psi_C(t)$ of the center and the corresponding Hamiltonian $\boldsymbol{H}_{CC}(t)$ are by construction finite in dimension, whereas all other quantities have a semi-infinite character.
Using the lead Green's function $\mathbf{G}_\alpha(t,t')$ which obeys

$$\left[i\frac{\partial}{\partial t} - \boldsymbol{H}_{\alpha\alpha}(t)\right]\mathbf{G}_\alpha(t,t') = \delta(t-t'), \qquad \alpha = L, R \tag{7.5}$$

with boundary conditions $\mathbf{G}_\alpha(t^+,t) = -i$ and $\mathbf{G}_\alpha(t,t^+) = 0$, the solution of Eq. (7.4) for the lead wavefunctions $\psi_\alpha(t)$ can be written according to

$$\psi_\alpha(t) = i\mathbf{G}_\alpha(t,0)\psi_\alpha(0) + \int_0^t \mathbf{H}_{C\alpha}\mathbf{G}_\alpha(t,\tau)\mathbf{H}_{\alpha C}\,\psi_C(\tau)\,d\tau, \qquad \alpha = L,R. \tag{7.6}$$

Inserting this result back into the equation for the component $\psi_C(t)$ of (7.4) one arrives at the effective equation for the domain Ω_C

$$i\partial_t\psi_C(t) = \mathbf{H}_{CC}\psi_C(t) + \psi^{(S)}(t) + \psi^{(M)}(t), \tag{7.7}$$

which contains a so-called source term

$$\psi^{(S)}(t) \;:=\; i\sum_{\alpha=L,R}\mathbf{H}_{C\alpha}\mathbf{G}_\alpha(t,0)\,\psi_\alpha(0) \tag{7.8}$$

and a memory term

$$\psi^{(M)}(t) := \sum_{\alpha=L,R}\int_0^t \mathbf{H}_{C\alpha}\mathbf{G}_\alpha(t,\tau)\mathbf{H}_{\alpha C}\,\psi_C(\tau)\,d\tau. \tag{7.9}$$

The charming feature of the present scheme is that the effective equation (7.7) can be solved on a finite domain in real-space and its solution exactly matches the solution of the whole space problem (7.4) in the central region Ω_C. In other words, the equation describes a quantum-mechanical system with open boundary conditions. In this way infinite reservoirs in thermal equilibrium can be attached to a finite molecular system and the coherent overall propagation of the system can be followed inside Ω_C.
Although the effective equation (7.7) appears appealing it has the drawback that the propagation in three spatial dimensions becomes prohibitive. This can be attributed to the memory term $\psi^{(M)}(t)$ which scales quadratically with the maximum propagation time. In addition, the wavefunction values at the surface of the central region have to be stored for the evaluation of the term over the *entire* history of the system. Experience shows that truncations of the memory integral, which aim at keeping only the recent past, introduce artificial reflections in practice.

(vi) Type B - Propagation of the overall system in a mixed basis

The time propagation in terms of a hybrid basis is a novel approach that we have developed in the present work. The motivation for the development was to find a way to circumvent the memory integral of approach (v) and to compute all required quantities on the fly. The basic idea of the method is to use a mixed representation of the overall wavefunction for different regions in space. While wavefunctions are delocalized in the region of the metallic leads, a more localized structure, especially in the transversal directions, is expected for atomic or molecular systems in the central device. The character of the transport problem therefore suggests an extended, i.e. delocalized, basis set for the description of the leads and a localized basis, or alternatively, a real-space grid for the representation of the wavefunction in the central device. The localized description in the center has the additional benefit of provid-

ing a larger degree of flexibility if additional external electric or magnetic fields are applied to the system, or if the motion of the ions is taken into account. The details of the method are introduced in section 7.3 of the present chapter.

In summary, a solution of the TDKS equations for electronic transport geometries in three spatial dimensions has been achieved so far only for the approaches (i) and (ii). All other methods have only been investigated for reduced dimensionality and the case of non-interacting electrons. In the next section, we will see that methods of type (A) are only of limited use so that approaches of type (B) are the preferred techniques for the solution of the TDKS equations in quantum transport.

7.2 Quantum Transport in Finite Systems

To explore the feasibility of a description of transport within finite systems we investigate the charge flow through mesoscopic systems in two spatial dimensions in this section. Using the real-space real-time software package OCTOPUS (cf. Ref. [MCBR03] and Appendix B) we solve the time-dependent Kohn-Sham equations within a finite rectangular simulation area in the x-y plane. To alleviate the effect of artificial reflections at the grid boundaries we utilize absorbing boundary conditions as e.g. common for the treatment of atomic or molecular systems in strong laser fields. In each time step the Kohn-Sham orbitals are multiplied with a spatial mask function

$$\phi_j(r_x, r_y, t) = m(r_x)\, m(r_y)\, \phi_j(r_x, r_y, t), \tag{7.10}$$

where

$$m(r_j) = \begin{cases} 1 - \sin^2 \frac{\pi}{2} \frac{(r_j - r_{j;\,w})}{r_{j;\,w}}, & r_{j;\,\max} - r_{j;\,w} < |r_j| \le r_{j;\,\max} \\ 1, & |r_j| \le r_{j;\,\max} - r_{j;\,w} \end{cases}, \quad j = x, y \tag{7.11}$$

and $r_{j;\,w}$, $r_{j;\,\max}$ denote the width of the absorbing region and the maximum grid size in the respective direction. In this way charge is discarded which leaves the simulation area. However, one has to keep in mind that such absorbing boundaries can never be made perfect. The different momentum contributions which are contained in the wavefunction are not absorbed on equal footing [BKV93].
For the external potential of the single-particle Kohn-Sham Hamiltonian we consider the following building blocks which were inspired by Ref. [IS06]

- Stadium (used as reservoir and as scattering center)

$$\begin{aligned} V_{\text{Stadium}}(x, y) = &- V_S\, \theta\left(x_s - |x - x_0|\right)\theta(y_s - |y|) \\ &- V_S\, \theta\left(x_s - \sqrt{(x - x_0)^2 + (y - y_s)^2}\right)\theta(y - y_s) \\ &- V_S\, \theta\left(x_s - \sqrt{(x - x_0)^2 + (y + y_s)^2}\right)\theta\Big(-y - y_s\Big), \end{aligned} \tag{7.12}$$

  where θ denotes the usual Heaviside step function.

Table 7.1: Parameters used for the numerical simulation of the 2D model. The time evolution was computed for $N_t = 10000$ time steps, leading to a total simulation time of $t_{\max} = 50$ a.u. The grid spacings Δx, Δy in the longitudinal and transversal directions have been set to 0.1 a.u. so that the simulation area covers a rectangle of 160 a.u. × 24 a.u. A total of 20,032,050 points have been used to represent the Kohn-Sham orbitals.

N_x	N_y	Δx, Δy (a.u.)	Δt (a.u.)	V_D, V_R, V_S (a.u.)	d_D, d_R, d_L (a.u.)	R_0 (a.u.)	x_s, y_s (a.u.)	x_0 (a.u.)
1600	240	0.1	0.005	50.0	4.0	4.0	4.0, 6.0	-70

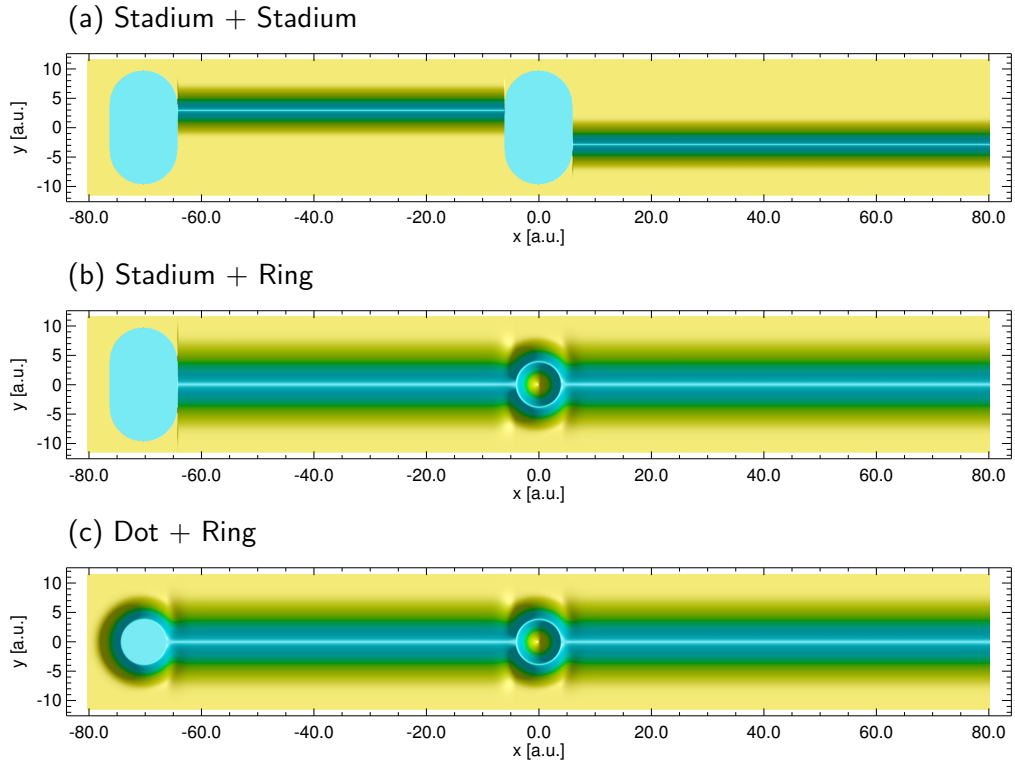

Figure 7.1: Top view on the external potentials in the x-y plane. For the ground state we consider only the reservoir (stadium or dot) centered at $x_0 = -70$ a.u. At times $t > 0$ we add conduction channels and a scattering center (stadium or ring located at $x_0 = 0$ a.u.) to the external potential and evolve the ground state of the reservoir on the shown potential landscapes.

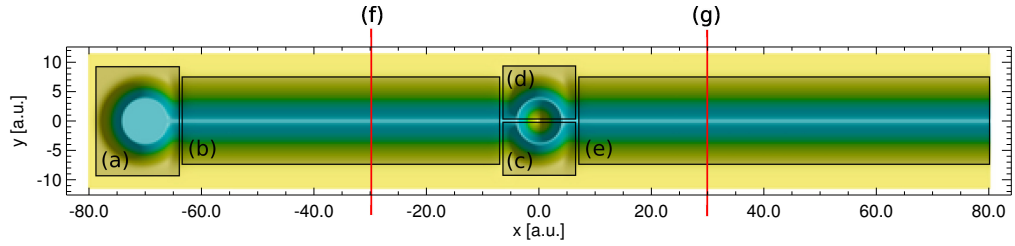

Figure 7.2: Example for the definition of integration areas: (a) dot reservoir, (b) left channel, (c) ring - lower branch, (d) ring - upper branch (e) right channel. Similar integration areas have been used for the external potentials in Fig. 7.1 (a) and (b). During the time evolution of the system we integrate the charge density in the shaded areas to determine the number of electrons in the respective region. Along the stripes (f) and (g) we integrate the longitudinal component of the paramagnetic current density to determine the charge flow through the channels.

- Dot (used as reservoir)

$$\begin{aligned} V_{\text{Dot}}(x,y) = &- V_D\,\theta(\sqrt{(x-x_0)^2+y^2} - R_0)\,e^{-(r-R_0)^2/d_D^2} \\ &- V_D\,\theta(R_0 - \sqrt{(x-x_0)^2+y^2}) \end{aligned} \tag{7.13}$$

  with $r^2 = (x-x_0)^2 + y^2$.

- Ring (used as scattering center)

$$V_{\text{Ring}}(r) = -V_R\,e^{-(r-R_0)^2/d_R^2}\,. \tag{7.14}$$

- Finally, the leads are constructed with a confinement of the form

$$V_{\text{Lead}}(x,y) = -V_L\,e^{-y^2/d_L^2}, \tag{7.15}$$

  where V_L and the longitudinal extent of $V_{\text{Lead}}(x,y)$ are adjusted such that the lead boundaries smoothly connect to the respective dot, ring or stadium.

In table 7.1 we summarize the corresponding parameters that have been used for the calculations of the present section.
For the simulations we perform the following steps: first we place either a quantum dot or a stadium at $x_0 = -70$ a.u. which serves as charge reservoir. We fill the reservoir with 100 spin-unpolarized electrons and solve the static Kohn-Sham equation to find the ground state. Next, we attach channels to the reservoir (cf. Fig. 7.2 (b), (e)) and place an obstacle in the center of the simulation area (cf. Fig. 7.2 (c), (d)) which serves as scattering center. As scattering centers we utilize quantum rings or stadiums. The ground state of the *unconnected* reservoir is then propagated on the *connected* potential landscapes of Figs. 7.1 (a)-(c). This strategy is equivalent to the following sudden switching in the external potential

$$V_{\text{Total}}(r,t) = V_{\text{Reservoir}}(r) + \theta(t)\,V_{\text{Channels+Obstacle}}(r). \tag{7.16}$$

Due to the channel which has been attached to the reservoir (cf. Fig. 7.2 (b)) the electrons can leave the reservoir at times $t > 0$ freely without overcoming potential barriers. At this point we emphasize that we are not applying an external bias to the system. The charge flow through the channels is entirely driven by the electron-electron repulsion and the wave-packet dispersion in the reservoir. To follow the electronic motion quantitatively we integrate the charge density in the shaded areas of Fig. 7.2. In addition, we monitor the current in the channels by integrating the longitudinal component of the paramagnetic current density along the stripes (f) and (g). We consider three levels of approximations for the single-particle potential v_{KS} in the Kohn-Sham equations: (i) non-interacting particles ($v_{\text{KS}} = v_{\text{ext}}$), (ii) time-dependent Hartree approximation ($v_{\text{KS}} = v_{\text{ext}} + v_{\text{H}}$) and (iii) adiabatic LDA ($v_{\text{KS}} = v_{\text{ext}} + v_{\text{H}} + v_{\text{ALDA}}$). We use a direct summation for the Hartree term and the two-dimensional LDA of Attaccalite et. al. [AMGGB02] for the exchange-correlation potential.

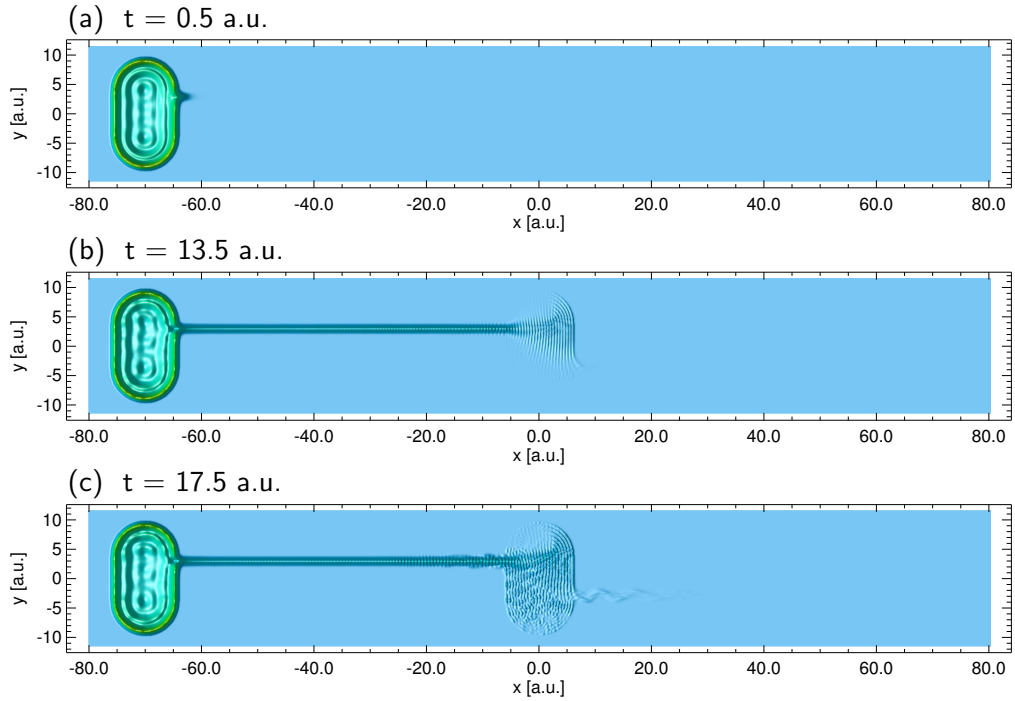

Figure 7.3: Electron density for transport through a quantum stadium computed with the adiabatic LDA. Initially 100 electrons have been placed in the left stadium. Inside the central stadium a standing wave pattern is formed, before the electrons start to leave to the right.

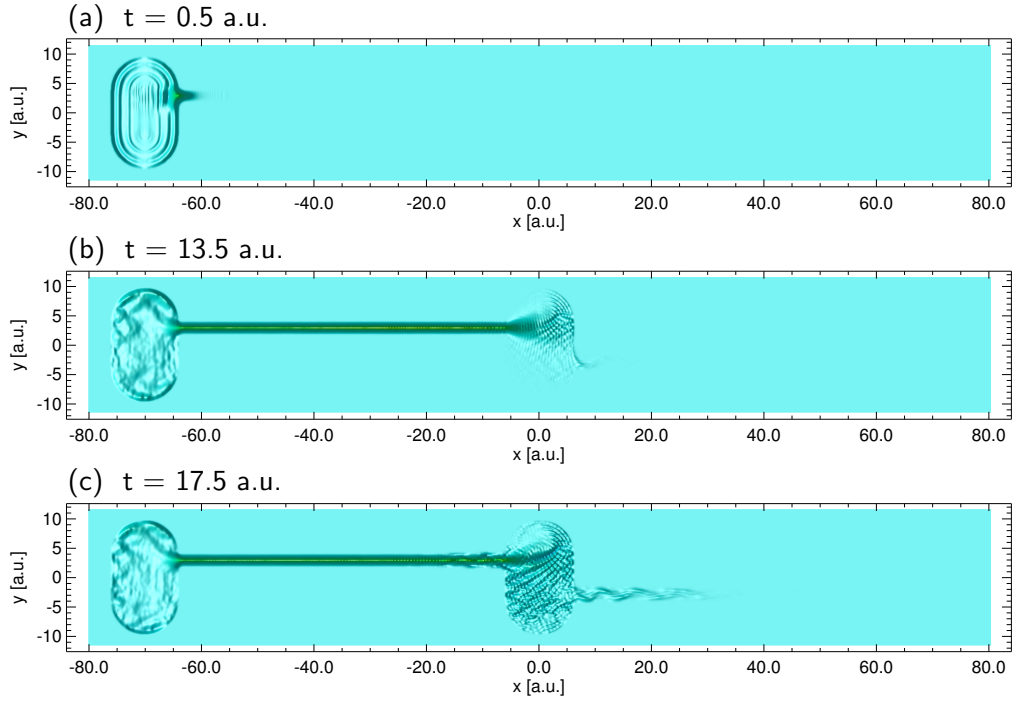

Figure 7.4: Same as Fig. 7.3, but shown is the longitudinal component of the Kohn-Sham current density.

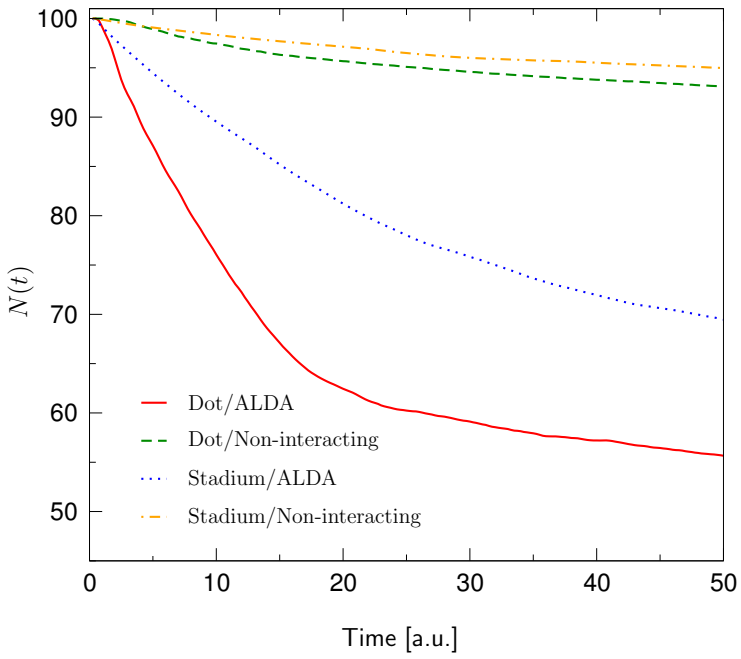

Figure 7.5: Shown is the reservoir depletion for dot and stadium reservoirs as function of time within the ALDA and for non-interacting particles.

In Figs. 7.3 and 7.4 we display snapshots of the time-dependent charge and longitudinal current densities for electron transport through a quantum stadium at different points in time. Initially, at $t = 0$, the reservoir exhibits a shell-like arrangement of the electrons, which becomes also visible shortly after $t = 0$ in the longitudinal component of the current density, cf. 7.4 (a). Due to the wave-packet dispersion and the electron-electron repulsion inside the stadium some charge starts to flow into the left channel. The first electrons reach the stadium in the center after about $t = 12$ a.u. and as time passes a standing-wave pattern is formed inside the stadium. In the same time-span the longitudinal current density in the left stadium, i.e. the "reservoir", shows characteristic maxima which are reminiscent of Heller's quantum scars [Hel07]. After about $t = 15$ a.u. some wave amplitude is leaving the central stadium to the right. Note that the electrons enter the right channel under an angle, so that scattering at the channel walls is taking place and an oscillatory motion inside the channel is observed.
In Fig. 7.5 we investigate the reservoir depletion of the employed finite dot and stadium reservoirs. The graph compares the integrated charge densities for the stadium and the dot reservoirs (i.e. integration areas of type (a) in Fig. 7.2) for ALDA propagations and for the case of non-interacting electrons. In general a rather rapid reservoir depletion is observed within the ALDA, while the charge leakage is less pronounced for non-interacting electrons due to lacking electron-electron repulsion in the reservoir. Within the ALDA, after $t = 50$ a.u., only about 69 electrons are left in the stadium and about 56 electrons in the dot, which compares to about 93 and 95 electrons, respectively for non-interacting particles.

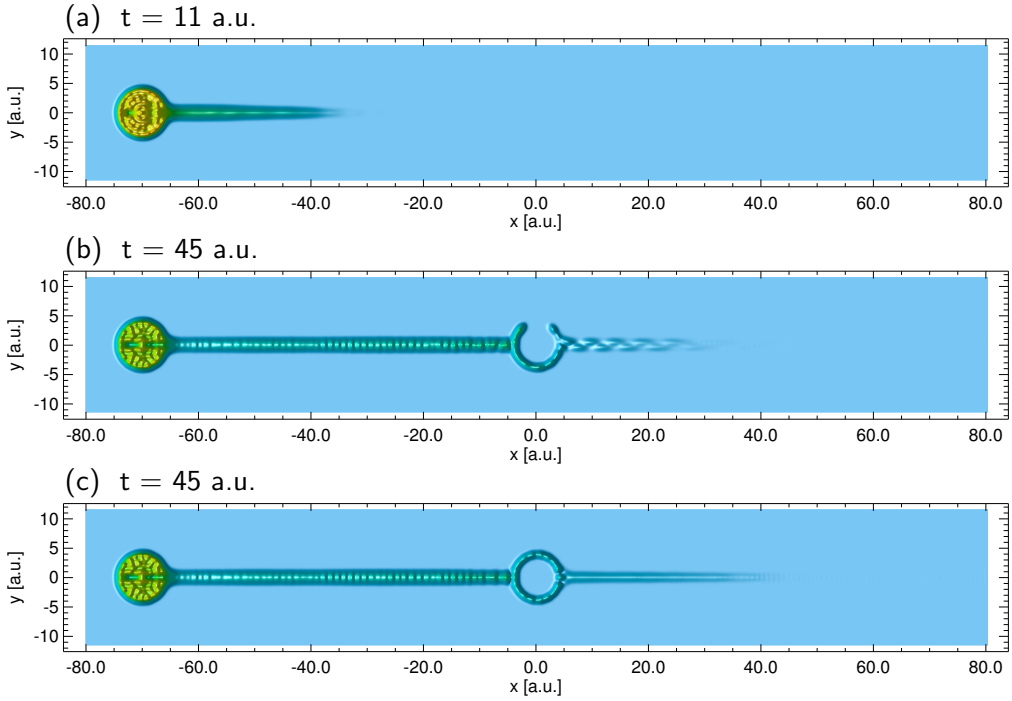

Figure 7.6: Impurity scattering with non-interacting electrons. (a) Electron density at $t = 11$ a.u. (b) Electron density at $t = 45$ a.u. for the ring potential with a small Gaussian impurity in the upper branch of the ring. (c) Same as (b), but for the ring potential without impurity.

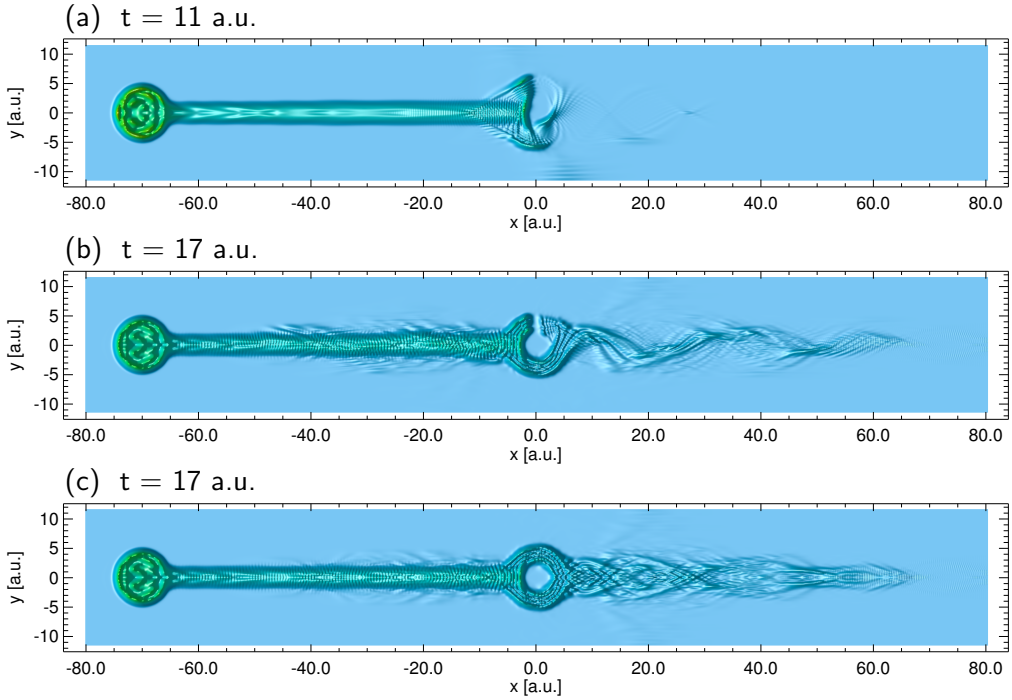

Figure 7.7: Similar to Fig. 7.6, but the electrons have been propagated using the TD-Hartree approximation. Note that compared to Fig. 7.6 the electrons have a much larger velocity.

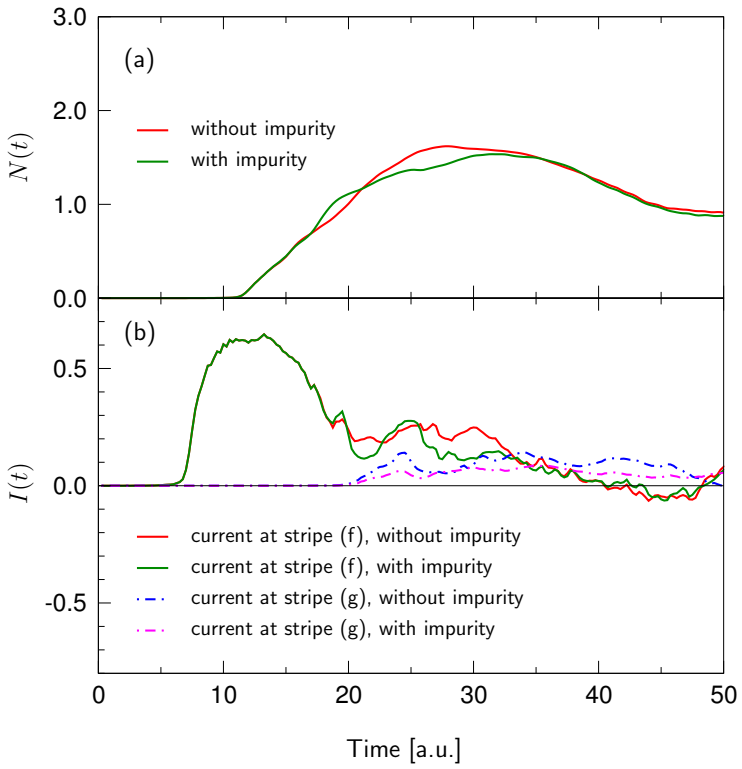

Figure 7.8: Panel (a): Integrated charge densities for impurity scattering within the ALDA. Shown is the charge in the lower branch of the ring which corresponds to integration area (c) in Fig. 7.2. Panel (b): corresponding longitudinal current densities which have been integrated along the stripes (f) and (g) of Fig. 7.2.

In Figs. 7.6 and 7.7 we employ a quantum dot as reservoir. We compute the reservoir ground state for non-interacting and Hartree-interacting electrons, respectively. In the following we propagate these ground states on potential landscapes which contain (a), (b) a quantum ring with a small Gaussian impurity in the upper branch and (c) a defect-free quantum ring. The corresponding snapshots in time are shown in Fig. 7.6 for non-interacting electrons and in Fig. 7.7 for Hartree-interacting electrons. In general, we observe in all simulations that the speed of the wave-packets in the time-dependent Hartree approximation is *considerably* higher than for non-interacting electrons which can be attributed to the electron-electron repulsion. Also the transversal extent of the charge distribution is larger in Fig. 7.7, which leads together with the large momenta of the Hartree electrons to a completely different wave pattern compared to Fig. 7.6.

Figure 7.8 shows integrated charge and current densities for impurity scattering within the ALDA. Here we employ a stadium as reservoir and propagate the ground state of the reservoir on the potential landscape of Fig. 7.1 (b). As before we consider a defect-free quantum ring and a quantum ring which contains a small Gaussian impurity in the upper branch. Panel (a) shows that in the time-span between $t = 25$ a.u. and $t = 35$ a.u. about 2 electrons are contained in the lower branch of the ring (integration area (c) in Fig. 7.2). In the presence of the impurity we observe initially, for $t < 20$ a.u., slightly more charge

in the lower branch, but due to backscattering less electrons pass the scattering region when the impurity is present. This can also be seen in panel (b), where we display the integrated current densities along the stripes (f) and (g) of Fig. 7.2. We emphasize that only a very small plateau in the time span $t = 10 - 14$ a.u. is visible in the current at stripe (f) and that no plateau can be observed in the current at (g). Furthermore, the integrated currents cannot be fully trusted for times $t > 25$ a.u., since wave packets arrive at the grid boundaries and suffer reflections which become visible in the current density. Although some quantitative information can be extracted from the present model for short time scales, this example illustrates the general limitation of determining steady-state current-voltage characteristics from finite models.

Finally, we demonstrate in Figs. 7.9 and 7.10 the artefacts which arise due to the finite simulation area. As before, the electrons leave the left dot reservoir for $t > 0$ and enter the ring in the center after some time (snapshots (a) and (b)). However, if we continue the time propagation, the wave packets eventually arrive at the right grid boundary at $x = +80$ a.u.. Although a considerable fraction of the total charge is removed due to the absorbing mask function (7.10), there are always wave-packets which are scattered back and start to travel again to the left towards the ring in the center. Since the ring is already filled with charge at this point in time, the ring potential cannot sufficiently bind the arriving wave packets in the transversal direction. As result, jets of charge are leaving the ring under an angle of about 45 degrees which is indicated in Figs. 7.9 (c) and 7.10 (c) with arrows[2].

To summarize this section, we have seen that the description of electronic transport in terms of mesoscopic models with finite extent gives some insight in the transient evolution of the system on short time scales. However, weak points of this approach include the finite reservoirs which cannot maintain a steady-state current over long time spans and the finite simulation area whose boundaries cause reflections. Such reflections are of course the correct solution for a zero boundary condition but are not adequate for the description of an infinite system in the longitudinal direction. In this sense we have to view e.g. the charge jets in Figs. 7.9 (c) and 7.10 (c) as artefacts which are not present when a system with infinite longitudinal extent is considered.

[2] Movies of all time propagations which have been presented in this chapter can be found on the homepage of the thesis [App07].

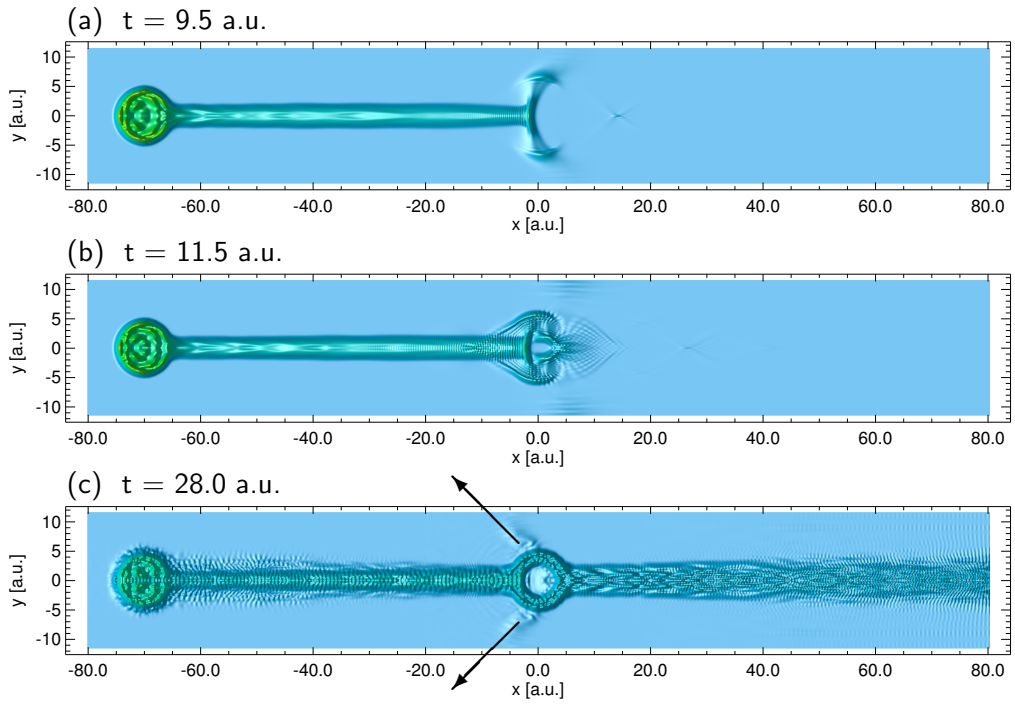

Figure 7.9: Electron density for charge flow through a quantum ring. Due to the finite grid size in the longitudinal direction, the electrons scatter back from the right border of the simulation box and enter the ring again from the right side. The large momentum of the electrons causes charge to leave the ring in jet-like fashion, as indicated with arrows.

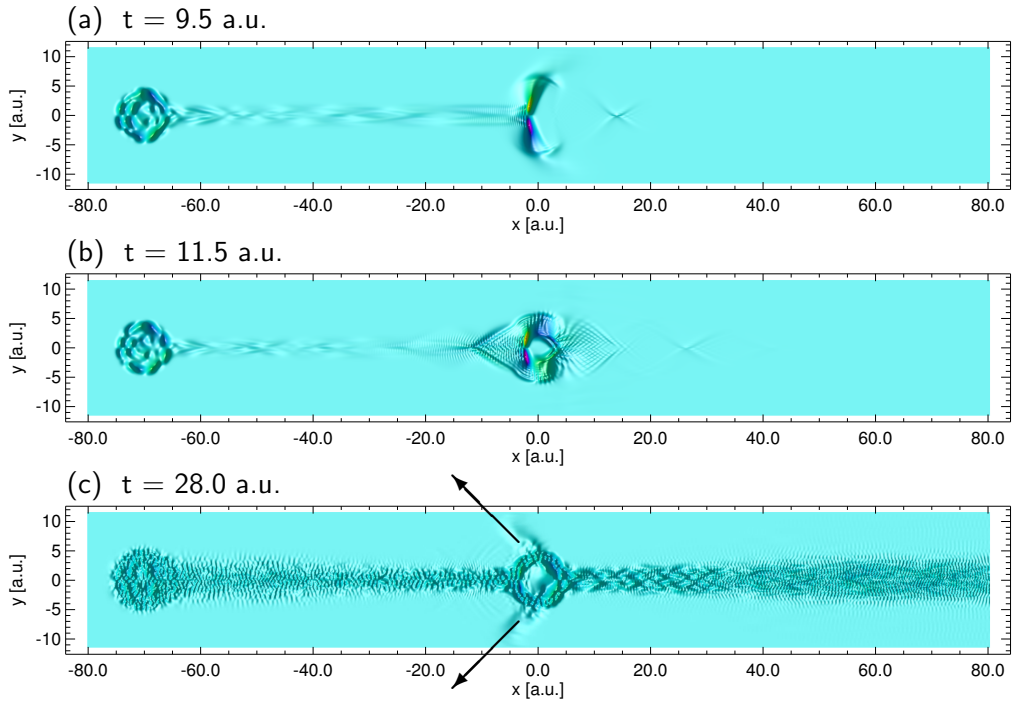

Figure 7.10: Same as Fig. 7.9, but shown is the transversal component of the Kohn-Sham current density.

7.3 Propagation with a Hybrid Basis

In the previous section we have demonstrated that time propagations for quantum transport suffer several limitations when they rely on a description in terms of finite systems. Although larger computational grids will be accessible with increasing computational power the basic shortcomings of such a description remain. In this section we develop an approach which tries to overcome these shortcomings and allows to propagate extended systems. The basic idea of our method rests on a mixed representation of the wavefunction in different spatial regions. The overall wavefunction is described in terms of delocalized states in the leads and in terms of a localized basis set, or alternatively in terms of a real-space grid, in the central device. In the following we show how to construct a propagation scheme for such a hybrid description.
Starting point is the Bloch representation of the lead orbitals. For the description of the leads it is natural to think in terms of Bloch orbitals and the corresponding band structure. In fact, this is the maximum one can get from a ground-state DFT calculation for periodic systems. The scattering wavefunction deep inside the leads will be a superposition of Bloch orbitals with certain (time-dependent) reflection and transmission coefficients

$$\psi^{\mathrm{KS}}(\mathbf{r},t) = \sum_{\mathbf{k},n} R_{\mathbf{k},n}(t) u_{\mathbf{k},n}(\mathbf{r}) e^{i\mathbf{k}\mathbf{r}}. \tag{7.17}$$

Therefore, it is appealing to work only with time-dependent expansion coefficients and to use the corresponding Bloch orbitals as (static) basis set.
As before, we divide space into three regions

$$\Omega_L := \{\mathbf{r} = (x,y,z) \,|\, x < -q\}, \tag{7.18}$$
$$\Omega_C := \{\mathbf{r} = (x,y,z) \,|\, -q \le x \le q\}, \tag{7.19}$$
$$\Omega_R := \{\mathbf{r} = (x,y,z) \,|\, q < x\}, \tag{7.20}$$

where q is assumed to be an integer multiple of the bulk lattice constant a, so that e.g. for a simple cubic crystal

$$u_{\mathbf{k},n}(\mathbf{r} + q\,\mathbf{e}_j) = u_{\mathbf{k},n}(\mathbf{r}). \tag{7.21}$$

Starting with a grid representation, the whole-space Schrödinger equation for a given single-particle orbital can then be written in partitioned form

$$i\frac{\partial}{\partial t}\begin{bmatrix} \psi_L(t) \\ \psi_C(t) \\ \psi_R(t) \end{bmatrix} = \begin{bmatrix} \boldsymbol{H}_{LL}(t) & \boldsymbol{H}_{LC} & 0 \\ \boldsymbol{H}_{CL} & \boldsymbol{H}_{CC}(t) & \boldsymbol{H}_{CR} \\ 0 & \boldsymbol{H}_{RC} & \boldsymbol{H}_{RR}(t) \end{bmatrix} \begin{bmatrix} \psi_L(t) \\ \psi_C(t) \\ \psi_R(t) \end{bmatrix}, \tag{7.22}$$

where lead-lead interactions ($\boldsymbol{H}_{LR}, \boldsymbol{H}_{RL}$) have been neglected and due to the grid representation only the diagonal elements are time-dependent (local time-dependent potentials). Without loss of generality, to keep the notation simple we illustrate the use of a mixed basis in terms of a Crank-Nicholson (CN) propagation scheme for the time-dependent Schrödinger equation. Any other propagation scheme that requires only powers of $\mathbf{H}$ can be used in exactly the same way as we will see in the following. For the whole-space problem the

Crank-Nicholson propagator reads

$$(\mathbf{1} + i\delta\mathbf{H}^{(n+1/2)})\psi^{(n+1)} = (\mathbf{1} - i\delta\mathbf{H}^{(n+1/2)})\psi^{(n)}, \tag{7.23}$$

where

$$\mathbf{H}^{(n+1/2)} = \frac{1}{2}\left(\mathbf{H}(t_n) + \mathbf{H}(t_{n+1})\right) \tag{7.24}$$

and

$$\psi^{(n)} \approx \psi(t_n), \quad t_n = n\Delta t, \quad \delta = \frac{\Delta t}{2}. \tag{7.25}$$

In the next step we construct eigenfunctions of the left and right ground-state lead Hamiltonians $\boldsymbol{H}_{LL}$, $\boldsymbol{H}_{RR}$. To that end consider shifted whole-space ($\pm$) functions of the form

$$\varphi_{\mathbf{k},n}^{(\pm),\pm q}(\mathbf{r}) = u_{\mathbf{k},n}(\mathbf{r})e^{ik_x(x\mp q)}e^{i\mathbf{k}_{yz}\mathbf{r}_{yz}} \pm u_{-\mathbf{k},n}(\mathbf{r})e^{-i\mathbf{k}(x\mp q)}e^{-i\mathbf{k}_{yz}\mathbf{r}_{yz}}, \tag{7.26}$$

where

$$\mathbf{k}_{yz} = (k_y, k_z)^T, \qquad \mathbf{r}_{yz} = (y, z)^T. \tag{7.27}$$

By restricting the (-) states to the respective real space regions, we define the following basis functions

$$\phi_{\mathbf{k},n}^{(-q)}(\mathbf{r}) := \begin{cases} \varphi_{\mathbf{k},n}^{(-),-q}(\mathbf{r}), & \mathbf{r} \in \Omega_L \\ 0, & \mathbf{r} \in \Omega_C \\ 0, & \mathbf{r} \in \Omega_R, \end{cases} \tag{7.28}$$

$$\phi_{\mathbf{k},n}^{(q)}(\mathbf{r}) := \begin{cases} 0, & \mathbf{r} \in \Omega_L \\ 0, & \mathbf{r} \in \Omega_C \\ \varphi_{\mathbf{k},n}^{(-),q}(\mathbf{r}), & \mathbf{r} \in \Omega_R. \end{cases} \tag{7.29}$$

Note that the $\phi_{\mathbf{k},n}^{(\pm q)}(\mathbf{r})$ functions defined in this way are continuous, since the $\varphi_{\mathbf{k},n}^{(-),\pm q}(\mathbf{r})$ have nodes at $\pm q$, respectively. The $\phi_{\mathbf{k},n}^{(\pm q)}(\mathbf{r})$ are eigenfunctions of the operators

$$\mathbf{H}_L = \mathrm{diag}(\mathbf{H}_{LL}, 0, 0), \tag{7.30}$$

$$\mathbf{H}_R = \mathrm{diag}(0, 0, \mathbf{H}_{RR}) \tag{7.31}$$

and, therefore, form complete sets in the subspaces Ω_L, Ω_R. Due to the completeness and orthonormality of the basis functions in Eqs. (7.28), (7.29) we can construct the following unitary transformation

$$\mathbf{U} := \begin{bmatrix} & & & 0 & & & \\ \cdots & \phi_3^{(-q)} & \phi_2^{(-q)} & \phi_1^{(-q)} & \mathbf{1_{CC}} & \phi_1^{(q)} & \phi_2^{(q)} & \phi_3^{(q)} & \cdots \\ & & & 0 & & & \end{bmatrix} \tag{7.32}$$

$$= \begin{bmatrix} \mathbf{U}_{LN} & 0 & 0 \\ 0 & \mathbf{1}_{CC} & 0 \\ 0 & 0 & \mathbf{U}_{RN} \end{bmatrix},$$

where the $\phi_j^{(\pm q)}$ appear as column vectors, the common index $j = (\mathbf{k}, n)$ has been introduced for brevity and N denotes the size of the basis[3].
Performing a unitary transformation (7.32) of the CN time stepping (7.23), we find

$$\mathbf{U}^{-1}(\mathbf{1} + i\delta\mathbf{H}^{(n+1/2)})\mathbf{U}\mathbf{U}^{-1}\psi^{(n+1)} = \mathbf{U}^{-1}(\mathbf{1} - i\delta\mathbf{H}^{(n+1/2)})\mathbf{U}\mathbf{U}^{-1}\psi^{(n)}, \tag{7.33}$$

or equivalently

$$(\mathbf{1} + i\delta\tilde{\mathbf{H}}^{(n+1/2)})\tilde{\psi}^{(n+1)} = (\mathbf{1} - i\delta\tilde{\mathbf{H}}^{(n+1/2)})\tilde{\psi}^{(n)}, \tag{7.34}$$

where

$$\tilde{\psi}^{(n)} = \mathbf{U}^{-1}\psi^{(n)} \tag{7.35}$$

and

$$\tilde{\mathbf{H}}^{(n+1/2)} = \mathbf{U}^{-1}\,\mathbf{H}^{(n+1/2)}\,\mathbf{U} \tag{7.36}$$

$$= \begin{bmatrix} \mathbf{U}_{LN}^{-1}\mathbf{H}_{LL}\mathbf{U}_{LN} & \mathbf{U}_{LN}^{-1}\mathbf{H}_{LC} & 0 \\ \mathbf{H}_{CL}\mathbf{U}_{LN} & \mathbf{H}_{CC} & \mathbf{H}_{CR}\mathbf{U}_{RN} \\ 0 & \mathbf{U}_{RN}^{-1}\mathbf{H}_{RC} & \mathbf{U}_{RN}^{-1}\mathbf{H}_{RR}\mathbf{U}_{RN} \end{bmatrix}. \tag{7.37}$$

For a three-point finite-difference discretization in one spatial dimension the transformed Hamiltonian matrix takes the explicit form

$$\tilde{\mathbf{H}}^{(n+1/2)} = \begin{bmatrix} \ddots & \vdots & \vdots & \vdots & 0 & \cdots & & & \\ \cdots & \mathcal{E}_1^L(\mathbf{k}_2) & 0 & \phi_2^{(-q)}(\mathbf{r}_L) & 0 & \cdots & & \mathbf{0} & \\ \cdots & 0 & \mathcal{E}_1^L(\mathbf{k}_1) & \phi_1^{(-q)}(\mathbf{r}_L) & 0 & \cdots & & & \\ \cdots & \phi_2^{*(-q)}(\mathbf{r}_L) & \phi_1^{*(-q)}(\mathbf{r}_L) & \mathbf{H}_{11,CC} & \mathbf{H}_{12,CC} & \mathbf{H}_{13,CC} & \vdots & \vdots & \\ & 0 & 0 & \mathbf{H}_{21,CC} & \mathbf{H}_{22,CC} & \mathbf{H}_{23,CC} & 0 & 0 & \\ & \vdots & \vdots & \mathbf{H}_{31,CC} & \mathbf{H}_{32,CC} & \mathbf{H}_{33,CC} & \phi_1^{(q)}(\mathbf{r}_R) & \phi_2^{(q)}(\mathbf{r}_R) & \cdots \\ & & & \cdots & 0 & \phi_1^{*(q)}(\mathbf{r}_R) & \mathcal{E}_1^R(\mathbf{k}_1) & 0 & \cdots \\ & \mathbf{0} & & \cdots & 0 & \phi_2^{*(q)}(\mathbf{r}_R) & 0 & \mathcal{E}_1^R(\mathbf{k}_2) & \cdots \\ & & & \cdots & 0 & \vdots & \vdots & \vdots & \ddots \end{bmatrix},$$

where $\mathbf{k}_j$ are the k-points of the discretization, $\mathcal{E}_n^{L/R}(\mathbf{k})$ is the bandstructure of the left and right lead, and $\mathbf{r}_L$, $\mathbf{r}_R$ denote the first grid point inside the left and right leads, respectively.

The purpose of the unitary transformation is twofold:

(i) to change the representation in the leads (from a real-space representation to the more natural Bloch basis). This introduces *half-infinite* basis functions that cover the *complete* lead regions.

(ii) to truncate the original Hilbert space. This can be achieved by keeping only a finite number of basis functions (7.28), (7.29) for the left and right lead.

Higher order propagation schemes can be treated in the same fashion, since only further

[3] An exact unitary transformation within the original Hilbert space of $\mathbf{H}$ is obtained for $N \to \infty$.

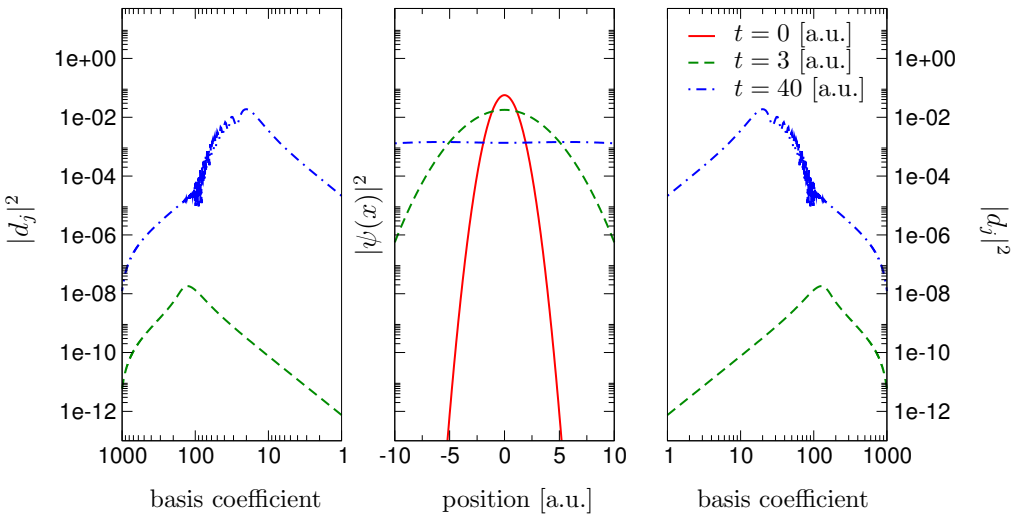

Figure 7.11: Snapshots of the time evolution in the mixed-basis representation. As initial state we place a Gaussian wave packet without initial momentum at the origin. In the left and right panels we display the time evolution of left- and right-lead basis coefficients in a double-logarithmic scale. The panel in the center shows the orbital density of the central device in a real-space representation. Due to the transparent boundary condition the Gaussian wave packet passes during the propagation the grid boundaries of the central region at ± 10 a.u. seamlessly. No interference or reflections are observed while the tails of the wave packet pass through the boundaries of the central device.

unit operators in the form $\mathbf{U}\mathbf{U}^{-1}$ have to be inserted in higher order products of $\mathbf{H}$. It is therefore possible to use the standard time-reversal algorithm [FKW78, MCBR03] employed in OCTOPUS, but also Magnus propagators [HL03] can be used. Only spectral methods, like the popular split-operator [FFS82] or Suzuki-Trotter [Suz93, SY92] splittings are excluded, since they rely on an explicit separation of the Hamiltonian into terms which are either diagonal in position space or diagonal in momentum space. Such a splitting is not available for the transformed Hamiltonian (7.37).

Numerical applications

To test our method we have implemented the propagation scheme (7.34) for a mixed representation in terms of grid points for the central device and a plane wave basis set for the lead regions. We use a constant potential for the overall space. In Figs. 7.11-7.13 we present the time evolution for some examples in one spatial dimension. The sequence of figures is organized as follows: In each figure the left and right panel show the squared absolute value $|d_j|^2$ of the coefficients of the left and right lead basis functions (numerical plane-waves for the potential free case considered here). The lowest frequency modes of the lead basis sets are always plotted starting inside, with growing frequencies pointing outwards. The panel in the center displays the orbital density $n(x) = |\psi(x)|^2$ as a function of position. Both, the density in the center and the basis coefficients on the left and right are shown in a logarithmic scale. For all calculations $N_C = 200$ grid points for the central device and $N_B = 1000$ basis functions for the left and right lead have been used, respectively.

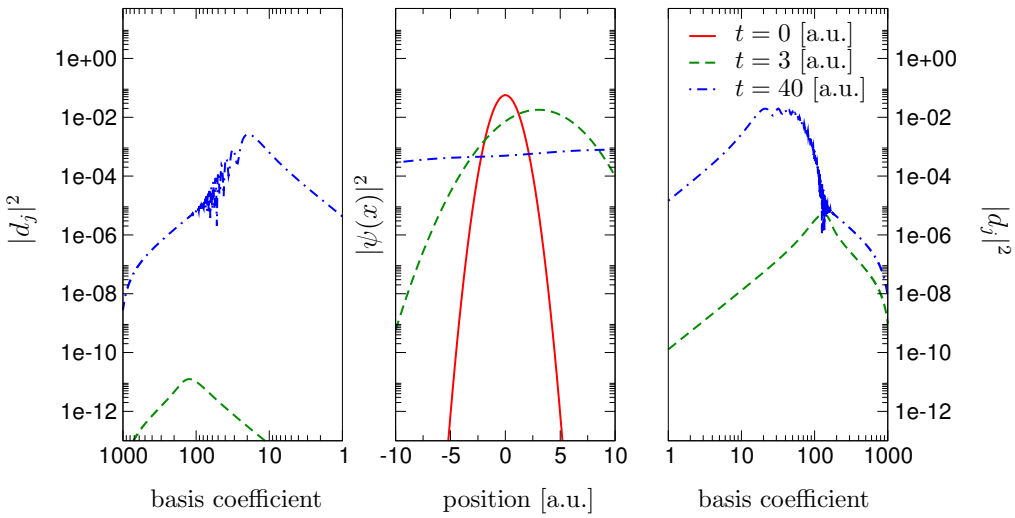

Figure 7.12: Same as Fig. 7.11, but here the Gaussian wave packet has an initial momentum of 1 a.u. pointing to the right.

In the first example (Fig. 7.11) we consider a Gaussian wave packet which is initially localized in the central region. As time passes the packet spreads and leaves the grid in the center. At the same time the expansion coefficients d_j of the basis functions in the left and right lead start to gain amplitude. We emphasize that the wave packet in the central region is not suffering artificial reflections from the grid boundaries at ± 10 a.u.. Instead the wave passes the boundary seamlessly. This nicely illustrates the transparent boundary conditions which are ensured by the phases and amplitudes of the expansion coefficients d_j. Their time evolution guarantees that the correct boundary values are provided at the boundaries of the central region for any given time.

From different calculations with various sizes for the basis sets we found that the propagation can only be trusted up to a maximum time $t_{\max}$ which is linearly related to the basis size N_B, i.e. $t_{\max} = \alpha N_B + \beta$. If the propagation is extended beyond $t_{\max}$ the wavefunction starts to become wiggly and the time evolution is spoiled[4]. The parameters α and β can be determined empirically from a simple interpolation by performing two successive time propagations with different but small basis sizes and finding the corresponding values for $t_{\max}$. Once α and β are known for a given situation the minimal basis size for a maximum propagation time can be estimated.

In Fig. 7.12 we consider the same initial conditions as in Fig. 7.11, except that we give the Gaussian an initial momentum of 1 a.u. pointing to the right. As before, the amplitude of the coefficients d_j builds up as soon as the wave packet is leaving the central grid. Due to the right moving wave packet here the coefficients of the right lead grow faster.

Finally, we investigate, in Fig. 7.13, a single lead mode in the left lead as initial state. This corresponds to an expansion coefficient $d_j = 1$ for one particular basis function j ($j = 10$ in our example), zero occupation of other basis functions and no initial wave amplitude in the central device. Since the lead mode is not an eigenstate of the overall system the initial

[4] This observation originates from the fact that we propagate, due to the finite size of the basis, within a truncated Hilbert space.

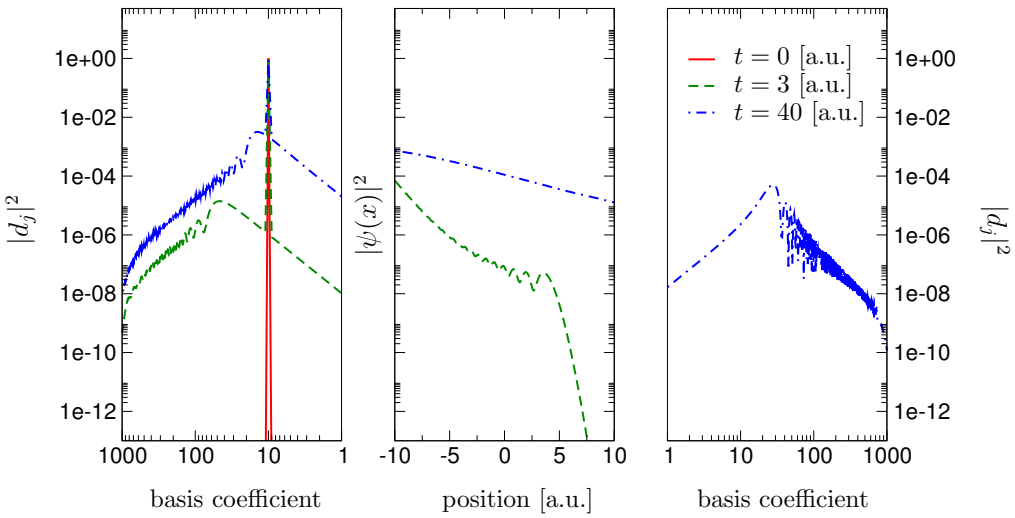

Figure 7.13: Same as Fig. 7.11, but here only a single lead mode of the left lead is occupied initially at $t = 0$. No wave amplitude is contained in the central device and in the right lead. Due to the wave-packet dispersion the initial state starts to propagate into the center and the right lead.

state starts to show dispersion for $t > 0$ and spreads into the central region. After about $t = 3.5$ a.u. the right boundary of the central regions is reached and the coefficients of the right lead start to grow in magnitude. Similar to the previous cases no artificial reflections are observed at the grid boundaries of the central device[5].

In summary, we have presented an approach which is suitable for the description of electronic transport within TDDFT. Initially we started out to find a scheme which avoids memory terms like in Eqs. (7.1) and (7.9). This has been accomplished with the present algorithm. However, the method still shows a quadratic scaling behavior in the maximum propagation time since more basis coefficients are required for larger propagation intervals. The benefits of the present algorithm lie in its simple structure. The approach is not limited to a Crank-Nicholson propagation scheme and can be easily implemented in real-space TDDFT codes like e.g. the OCTOPUS package. In addition, we emphasize that the idea of a mixed basis is not restricted to transport calculations as considered in the present chapter. Other physical situations which involve a central scattering region can be treated in a similar fashion. For example, replacing the Bloch basis with Volkov states allows to compute photo-electron spectra for atomic and molecular systems directly from the expansion coefficients d_j. Also, superconducting systems can be treated by performing a unitary transformation of the Bogoliubov-de-Gennes Hamiltonian in analogy to (7.32).

[5] Movies of all time propagations which have been presented in this chapter can be found on the homepage of the thesis [App07].

7.4 Summary and Outlook

At present, the theoretical *ab-initio* description of electron transport through single molecules is still at an early stage. Approaches based on the Landauer formula, or on non-equilibrium Green's function theory, combined with electronic structure calculations within static DFT are often found to deviate from experimental studies by several orders of magnitude. This discrepancy can be attributed to the low degree of reproducibility in experiments and to the often uncontrolled approximations in the employed theoretical formalisms. Several shortcomings are inherent in a combination of static DFT and Landauer's formula. Due to the scattering from the static Kohn-Sham potential resonant tunneling appears at the wrong energies, even if the exact static exchange-correlation potential was available. Inelastic effects due to the dynamical coupling to the nuclei as, e.g., current induced forces or the rearrangement of atoms in the junction, are not accounted for in approaches based on static DFT. Similar problems plague the combination of static DFT with non-equilibrium Green's function theory.

A promising method to overcome these limitations is time-dependent DFT. A time-dependent description allows naturally for the treatment of non-equilibrium situations. The influence of time-dependent electromagnetic fields, e.g. laser fields, the motion of the nuclei, e.g. in form of Ehrenfest dynamics, or time-dependent switching processes in the applied bias are all naturally incorporated in a TDDFT formalism. In addition, TDDFT suffers no fundamental limitations like the approaches which (ab)use ground-state DFT for non-equilibrium situations. Since the exact time-dependent exchange-correlation potential yields the exact interacting particle density also the exact longitudinal current density, and hence the correct current-voltage characteristics is recovered. The price to pay for this flexibility is a higher computational cost for the required time propagations. To date all TDDFT transport calculations consider either finite systems, periodic boundary conditions, or the propagation of master equations. We have demonstrated that modelling in terms of finite systems has to be done with great care to avoid artefacts due to artificial reflections at the boundaries of the finite system. Even with steadily increasing computational power these limitations remain so that a need for alternative approaches emerges. Instead of treating finite models it is more appropriate to describe electronic transport in terms of extended systems. For time propagations this requires so-called open or transparent boundary conditions. Recently, some first steps towards the description of open boundary conditions have been performed for non-interacting particles.

Since many technical issues still have to be solved before a propagation of the TDKS equations with open boundary conditions in three spatial dimensions can be achieved, we have focussed mainly on the development of algorithms. We have developed numerical techniques which are particularly tailored to a real-space finite-difference representation of the time-dependent Kohn-Sham equations as implemented in software packages like Octopus. We have presented an algorithm to calculate extended eigenstates which arise in the ground-state problem for the unbiased molecular junction. The approach allows one to compute scattering states without constructing the Green's function or solving the Lippmann-Schwinger equation. Only the solution of a complex-valued and state-dependent linear system is required to find the scattering states.

To overcome the limitations encountered in the propagation of finite systems we have introduced a propagation scheme which relies on a mixed basis and allows to propagate the central device region with open boundary conditions. First tests of the technique

show that wave packets can leave or enter the simulation area without suffering artificial reflections. Due to the simple structure of the propagation method an extension to three spatial dimensions is straightforward and will be the next step towards realistic TDDFT calculations in time-dependent transport.
Looking ahead we agree with Alan Turing, *we can see plenty there that needs to be done.*

Part IV

Appendix

A Matrix Formulation of the TDDFT Response Equations

Science is a way of trying not to fool yourself. The first principle is that you must not fool yourself, and you are the easiest person to fool.

— R. P. Feynman, (1918-1988).

The aim of this appendix is to provide a short derivation of the matrix formulation of the TDDFT response equations. These equations became known as Casida's equations [Cas95] in the literature.
As detailed in section 2.3, the frequency-dependent density-response $\rho_1(\mathbf{r},\omega)$ in first order in the perturbing potential $v_1(\mathbf{r},\omega)$ can be formulated according to

$$\rho_1(\mathbf{r},\omega) = \int \chi_{\mathrm{KS}}(\mathbf{r},\mathbf{r}',\omega)\, v_{\mathrm{KS},1}(\mathbf{r}',\omega)\; d^3r' \,, \tag{A.1}$$

where $v_{\mathrm{KS},1}(\mathbf{r},\omega)$ denotes the effective perturbation

$$v_{\mathrm{KS},1}(\mathbf{r},\omega) = v_1(\mathbf{r},\omega) + \int \frac{\rho_1(\mathbf{r}',t)}{|\mathbf{r}-\mathbf{r}'|}\, d^3r' + \int f_{\mathrm{xc}}[\rho_0](\mathbf{r},\mathbf{r}',\omega)\, \rho_1(\mathbf{r}',\omega)\; d^3r' \,. \tag{A.2}$$

In terms of the static KS orbitals, the Kohn-Sham response function χ_{KS} reads

$$\begin{aligned}
\chi_{\mathrm{KS}}(\mathbf{r},\mathbf{r}',\omega) &= \sum_{j,k} (f_k - f_j) \frac{\psi_j(\mathbf{r})\psi_k(\mathbf{r}')\psi_k^*(\mathbf{r})\psi_j^*(\mathbf{r}')}{\omega - (\epsilon_j - \epsilon_k)} \\
&= \sum_{k=1}^{N}\sum_{j=1}^{\infty} \frac{\psi_j(\mathbf{r})\psi_k(\mathbf{r}')\psi_k^*(\mathbf{r})\psi_j^*(\mathbf{r}')}{\omega - (\epsilon_j - \epsilon_k)} - \sum_{k=1}^{N}\sum_{j=1}^{\infty} \frac{\psi_k(\mathbf{r})\psi_j(\mathbf{r}')\psi_j^*(\mathbf{r})\psi_k^*(\mathbf{r}')}{\omega + (\epsilon_j - \epsilon_k)} \\
&= \sum_{i,a} \left(\frac{\psi_a(\mathbf{r})\psi_i(\mathbf{r}')\psi_i^*(\mathbf{r})\psi_a^*(\mathbf{r}')}{\omega - (\epsilon_a - \epsilon_i)} - \frac{\psi_i(\mathbf{r})\psi_a(\mathbf{r}')\psi_a^*(\mathbf{r})\psi_i^*(\mathbf{r}')}{\omega + (\epsilon_a - \epsilon_i)} \right),
\end{aligned} \tag{A.3}$$

where here and in the following the summations are performed according to $\sum_i \equiv \sum_{i=1}^{N}$ and $\sum_a \equiv \sum_{a=N+1}^{\infty}$.
If we define

$$P_{ai}(\omega) := \frac{\int \psi_i(\mathbf{r}')\psi_a^*(\mathbf{r}')v_{\mathrm{KS},1}(\mathbf{r}',\omega)d^3r'}{\omega - (\epsilon_a - \epsilon_i)} \tag{A.4}$$

and

$$P_{ia}(\omega) := \frac{\int \psi_a(\mathbf{r}')\psi_i^*(\mathbf{r}')v_{\mathrm{KS},1}(\mathbf{r}',\omega)d^3r'}{-(\omega + (\epsilon_a - \epsilon_i))} \,, \tag{A.5}$$

the linear density response can be written in the form

$$\rho_1(\mathbf{r},\omega) = \sum_{i,a} \psi_a(\mathbf{r})\psi_i^*(\mathbf{r})P_{ai}(\omega) + \psi_i(\mathbf{r})\psi_a^*(\mathbf{r})P_{ia}(\omega). \tag{A.6}$$

Next, we rewrite Eqs. (A.4) and (A.5) as

$$(\omega - (\epsilon_a - \epsilon_i))\, P_{ai}(\omega) = \int \psi_i(\mathbf{r})\psi_a^*(\mathbf{r})v_{\mathrm{KS},1}(\mathbf{r},\omega)\, d^3r, \tag{A.7}$$

$$(\omega + (\epsilon_a - \epsilon_i))\, P_{ia}(\omega) = -\int \psi_a(\mathbf{r})\psi_i^*(\mathbf{r})v_{\mathrm{KS},1}(\mathbf{r},\omega)\, d^3r, \tag{A.8}$$

abbreviate the Hartree and exchange-correlation contributions with

$$f_{\mathrm{Hxc}}(\mathbf{r},\mathbf{r}',\omega) = \frac{1}{|\mathbf{r}-\mathbf{r}'|} + f_{\mathrm{xc}}(\mathbf{r},\mathbf{r}',\omega), \tag{A.9}$$

and define the matrix elements

$$v_{ai}(\omega) := \int \psi_i(\mathbf{r})v_1(\mathbf{r},\omega)\psi_a^*(\mathbf{r})\, d^3r, \tag{A.10}$$

$$K_{kl,mn}(\omega) := \int\int \psi_l(\mathbf{r})\psi_k^*(\mathbf{r})f_{\mathrm{Hxc}}(\mathbf{r},\mathbf{r}',\omega)\psi_m(\mathbf{r}')\psi_n^*(\mathbf{r}')d^3r\, d^3r'. \tag{A.11}$$

Together with Eq. (A.6) we then arrive at the matrix form

$$(\omega - (\epsilon_a - \epsilon_i))\, P_{ai}(\omega) = v_{ai}(\omega) + \sum_{j,b} \left(P_{bj}(\omega)K_{ai,bj}(\omega) + P_{jb}(\omega)K_{ai,jb}(\omega)\right), \tag{A.12}$$

which can be rearranged according to

$$\sum_{j,b} \Big\{ \left[\delta_{ij}\delta_{ab}(\epsilon_a - \epsilon_i - \omega) + K_{ai,bj}(\omega)\right] P_{bj}(\omega) + K_{ai,bj}(\omega)P_{jb}(\omega) \Big\} = -v_{ai}(\omega). \tag{A.13}$$

Analogous steps lead to

$$\sum_{j,b} \Big\{ \left[\delta_{ij}\delta_{ab}(\epsilon_a - \epsilon_i + \omega) + K_{ai,jb}(\omega)\right] P_{jb}(\omega) + K_{ai,bj}(\omega)P_{bj}(\omega) \Big\} = -v_{ia}(\omega). \tag{A.14}$$

Defining

$$X_{jb}(\omega) := P_{jb}(\omega), \qquad Y_{jb}(\omega) := P_{bj}(\omega), \tag{A.15}$$

$$L_{ia,jb}(\omega) := \delta_{ij}\delta_{ab}(\epsilon_a - \epsilon_i) + K_{ai,jb}(\omega), \tag{A.16}$$

$$M_{ia,jb}(\omega) := K_{ia,bj}(\omega), \qquad V_{ia}(\omega) = -v_{ai}(\omega), \tag{A.17}$$

allows to cast equations (A.13) and (A.14) in the following matrix form

$$\left[\begin{pmatrix} \hat{L}(\omega) & \hat{M}(\omega) \\ \hat{M}^*(\omega) & \hat{L}^*(\omega) \end{pmatrix} - \omega \begin{pmatrix} -1 & 0 \\ 0 & 1 \end{pmatrix}\right] \begin{pmatrix} X(\omega) \\ Y(\omega) \end{pmatrix} = \begin{pmatrix} V(\omega) \\ V^*(\omega) \end{pmatrix}. \tag{A.18}$$

At this point we can argue with the same reasoning as in section 2.3: The right hand side of Eq. (A.18) remains finite if the frequency ω approaches the exact excitation energies $\omega \to \Omega_q$ of the interacting system. On the other hand, the density response on the left hand side of the equation has poles at the true excitation energies Ω_q. Hence, the matrix in the left square bracket cannot be invertible at $\omega = \Omega_q$ which is equivalent to the condition

$$\begin{pmatrix} \hat{L}(\Omega_q) & \hat{M}(\Omega_q) \\ \hat{M}^*(\Omega_q) & \hat{L}^*(\Omega_q) \end{pmatrix} \begin{pmatrix} X(\Omega_q) \\ Y(\Omega_q) \end{pmatrix} = \Omega_q \begin{pmatrix} -1 & 0 \\ 0 & 1 \end{pmatrix} \begin{pmatrix} X(\Omega_q) \\ Y(\Omega_q) \end{pmatrix}. \tag{A.19}$$

For real-valued orbitals and a frequency-independent kernel f_{xc} the condition (A.19) can be written in the form

$$(\hat{L} + \hat{M})(Y + X)_q = \Omega_q (Y - X)_q, \tag{A.20}$$
$$(\hat{L} - \hat{M})(Y - X)_q = \Omega_q (Y + X)_q, \tag{A.21}$$

where we attach q to the brackets to indicate the index of the eigenvectors. Solving Eq. (A.21) for $(Y - X)_q$

$$(Y - X)_q = \Omega_q (\hat{L} - \hat{M})^{-1} (Y + X)_q \tag{A.22}$$

and inserting the result into Eq. (A.20), we arrive at

$$(\hat{L} - \hat{M})(\hat{L} + \hat{M})(X + Y)_q = \Omega_q^2 (X + Y)_q. \tag{A.23}$$

The matrix $(\hat{L} - \hat{M})$ is positive definite, since it contains only positive entries on the diagonal. This allows us to cast (A.23) in the form

$$(\hat{L} - \hat{M})^{1/2}(\hat{L} + \hat{M})(\hat{L} - \hat{M})^{1/2}(\hat{L} - \hat{M})^{-1/2}(X + Y)_q = \Omega_q^2 (\hat{L} - \hat{M})^{-1/2}(X + Y)_q \tag{A.24}$$

which is typically written as

$$\hat{W} F_q = \Omega_q^2 F_q, \tag{A.25}$$

where

$$F_q = (\hat{L} - \hat{M})^{-1/2}(X + Y)_q \tag{A.26}$$

and

$$\hat{W} = (\hat{L} - \hat{M})^{1/2}(\hat{L} + \hat{M})(\hat{L} - \hat{M})^{1/2} \tag{A.27}$$

or more explicitely

$$W_{qq'} = \delta_{qq'}(\epsilon_a - \epsilon_i)^2 + 2\sqrt{(\epsilon_a - \epsilon_i)}\, K_{qq'}(\Omega_q) \sqrt{(\epsilon_{a'} - \epsilon_{i'})}, \qquad q = (a, i). \tag{A.28}$$

The pseudo-eigenvalue problem in Eq. (A.25) is the final form of the TDDFT matrix equation and was originally derived by Casida [Cas95]. The result shows, that the eigenvalues of the

matrix $\hat{W}$ are equivalent to the squares of the true excitation energies. It can also be shown that the interacting oscillator strengths can be obtained directly from the eigenvectors F_q [Cas95].
At this point we emphasize that Casida, in his original derivation of the pseudo-eigenvalue problem, used the ALDA as approximation for the exchange-correlation kernel f_{xc}. Within this approximation the matrix $\hat{W}$ is *frequency independent* so that Eq. (A.25) reduces to a standard eigenvalue problem. Consequently, only shifts of the Kohn-Sham excitation energies towards the true excitation energies are possible and the number of reachable true excitations is equivalent to the number of Kohn-Sham excitations. On the contrary, in the exact response formalism, the matrix $\hat{W}$ carrys a genuine frequency dependence which enters through the frequency dependence of the exchange-correlation kernel f_{xc}. Hence, the pseudo-eigenvalue problem has to be regarded as a *non-linear equation*. Depending on the form of the matrix $\hat{W}$ and the frequency dependence of the kernel the number of solutions of the non-linear equation can differ from the number of Kohn-Sham excitations. This is how true excitation energies emerge as solutions even if they have no direct correspondence in the non-interacting Kohn-Sham system.

B Domain Parallelization

Given enough eyeballs, all bugs are shallow.

— Eric Steven Raymond [Ray99].

The current trend in hardware technology follows a steep increase in the number of processors in each computing machine or facility, as opposed to the trend towards an increase in the clock speed or number of operations that each processing unit may perform per unit time. To use modern computing facilities efficiently, we have to ensure that our codes are able to benefit from such parallel-computing architectures.

B.1 Parallelization Strategies

Recently, we have incorporated into OCTOPUS a multiple-way parallelization scheme that may divide the work among a given number of processors, splitting the tasks either in **k**-points, in Kohn-Sham states, in regions of real-space, or in a combination of all of them. Each single form of the contemplated parallelizations may scale by its very nature only to a certain maximum number of processors. Only combined schemes allow to overcome such limitations.

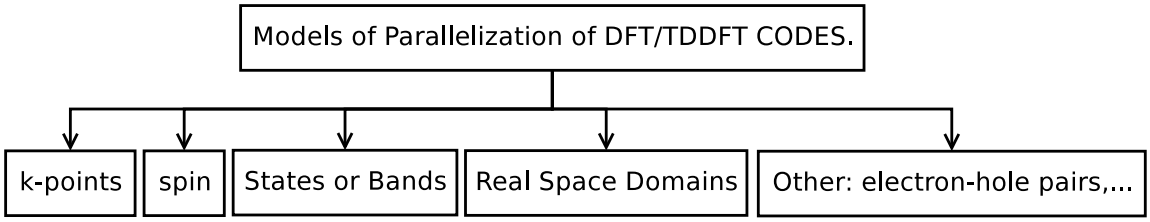

Figure B.1: Parallelization modes for DFT/TDDFT codes.

In Fig. B.1 we have represented the various possible modes for which a task division within a DFT/TDDFT calculation may be obtained:

- **k**-points: In a ground-state DFT calculation each processor solves the KS equation

$$\hat{H}^{\mathrm{KS}}_{\mathbf{k}}\,\varphi_{n\mathbf{k}}(\vec{r}) = \varepsilon_{n\mathbf{k}}\varphi_{n\mathbf{k}}(\vec{r}) \tag{B.1}$$

  for a given but fixed **k**-point. Communication among the nodes is only required for the calculation of the (common) density or other Brillouin-zone integrations. This is the parallelization mode that most ground-state solid-state DFT codes offer. The implementation is straightforward and scales very nicely with the number of processors. However, limitations arise for systems with very large unit cells.

- spin: The different spin subspaces may be treated by different processors. In practice this is rather similar to the **k**-point parallelization, so that both spin and **k**-points are represented as common quantum numbers and are treated on the same footing.

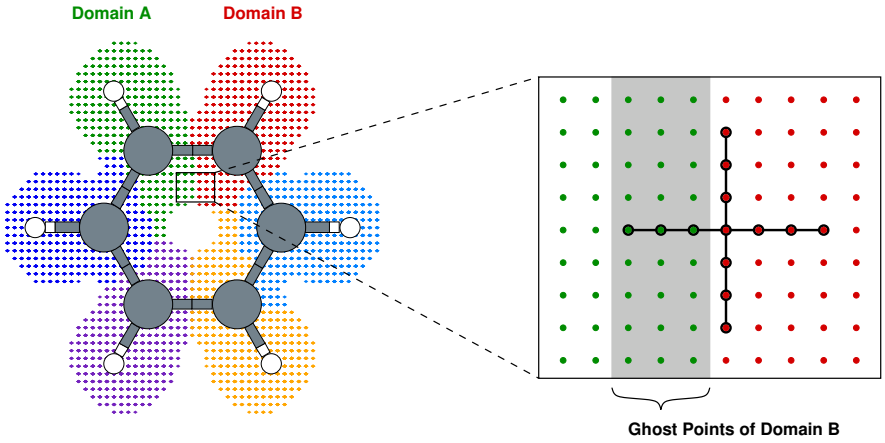

Figure B.2: Ghost points in a domain parallelization.

- Kohn-Sham states: For the ground state a parallelization in state indices or bands is more involved than the **k**-point parallelization. Essentially, the state indices have to be divided into different state-groups. The eigenproblem is then solved for each group and a subsequent orthonormalization of the states is performed among the states of different groups. Special block-diagonalization algorithms are used for this task.

  On the other hand, in time-dependent DFT the parallelization in state indices is straightforward. Since the time-dependent Kohn-Sham equations constitute an N-fold initial value problem, each orbital/state index may be propagated on a different processor. Communication is only required for the calculation of the density and, in some cases, for the calculation of the current.

- real-space regions: The real-space mesh is divided into different domains, so that each processor can treat a different portion of the total mesh. This is illustrated in the left of Fig. B.2, where we show a six-fold domain decomposition of a benzene molecule in the x-y plane. Apart from the distribution of the computational burden over the different nodes, this parallelization strategy has the distinct advantage that the total memory requirement for the storage of the grid points is distributed over the nodes. Much larger systems can be treated if domain parallelization is used.

  The price one has to pay for this flexibility is the rather involved implementation which requires non-trivial communication among the nodes. On the right hand side of Fig. B.2 we show the application of a finite-difference stencil of the Laplacian to a boundary point of Domain B. Due to the non-local character of the stencil this requires points of Domain A (grey shaded area) which are held in memory by a neighboring processor. These points are termed ghost points and need to be commu-

nicated among neighboring nodes every time the function values on the grid change. Low-latency high-bandwidth networks are therefore the preferred interconnects for such an implementation.

- other: electron-hole pairs, scattering states, etc: Depending on the given problem several other parallelization schemes are possible. For example, the basis set in a linear response calculation within time-dependent DFT consists of electron-hole pairs: products of occupied and unoccupied Kohn-Sham states. Typically a large number of matrix elements is required. Since the different matrix elements are independent of each other, a parallelization can obtained by simply distributing their calculation over the different nodes.

  Quantum mechanical transport calculations are naturally described in terms of scattering states at given energies. Similar in spirit to the parallel treatment of Kohn-Sham states, the propagation of these scattering states can be distributed over different nodes.

B.2 Technical Aspects

For the implementation of the multiple-way parallelization in Octopus we have employed version 1 of the message passing standard MPI [SO+95, GHL+98, GLDS96, Ano94]. The choice was mainly motivated by the availability of this MPI variant for virtually any computer architecture, and by the fact that MPI is the de facto standard on large-scale parallel architectures. We did not make use of version 2 or newer developments in the MPI standard since these features are still not available on many platforms. Parallelization techniques like OpenMP have been ruled out from the start, since they are limited to shared memory architectures with many processors in a single machine. The current Top500 list [TOP] contains only a few machines of this kind.

Within Octopus we allow for various different box shapes like spheres, cylinders or parallelepipeds in 3D, or disks and rectangles in 2D. With a recent addition to the code even arbitrary user-defined shapes can be chosen. To treat the segmentation of the real space mesh for all possible geometries and spatial dimensions on the same footing, we convert the sequence of mesh points into a structured graph. The problem of decomposing the real-space mesh into different domains is then translated into a graph-partitioning problem. Several graph algorithms are available for such tasks and we have chosen for our implementation in Octopus a "multilevel k-way partitioning" algorithm as provided by the Metis library [KK98]. The library functions try to minimize the edge cuts while the graph partitioning is performed. Translated back to the real-space mesh this means that the intersection area of neighboring domains is minimized which in turn implies that fewer ghost points have to be communicated between the different nodes. This effect can be seen nicely in the example of the benzene molecule (Fig. B.2) where the domain boundaries computed by Metis always lie between two carbon atoms, the optimal situation in this case.

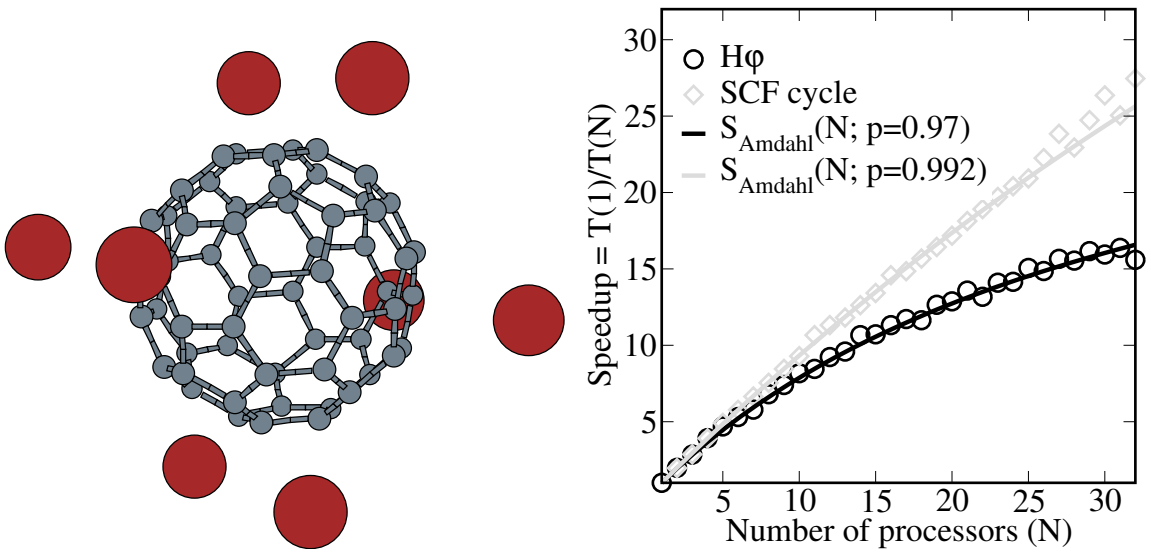

Figure B.3: Measured speedups for a domain-parallel calculation of $Cs_8@C_{60}$.

B.3 Application to $Cs_8@C_{60}$

In Fig. B.3 we show a sample calculation for 8 Cs atoms attached to C_{60}. Due to the size of the Cs atoms a rather large sphere with 26 Å diameter was used as enclosing computational domain. By choosing a grid spacing of Δ=0.20Å a total number of 1.177.863 grid points were contained in the calculation box.
To asses the performance of the domain parallelization we have repeated the ground-state DFT calculation of this system with a varying number of processors ranging from one to 32. On the right hand side of Fig. B.3 we plot the measured speedup as function of the number of processors. The circles correspond to the timings obtained for the application of the Hamiltonian to the wavefunction and the diamonds represent the measured timings for a full SCF cycle. Both curves follow Amdahl's law [Amd67]: Suppose that p is the fraction of a calculation that can be performed in parallel. Then $1-p$ is the percentage which is intrinsically serial. If we define the speedup $S(N,p)$ of a parallel calculation as the ratio $T(1,p)/T(N,p)$, where $T(N,p)$ is the execution time using N processors, we find

$$S(N,p) = \frac{1}{1-p+p/N}. \tag{B.2}$$

Note that the speedup always saturates at $1/(1-p)$ as function of the number of processors, if $p < 1$. In Fig. B.3 we have fitted our measured data to Amdahl's law (solid lines) and obtain parallel fractions $p = 0.97$ for the application of $\hat{H}$ to the wavefunction and $p = 0.992$ for the execution of a full SCF cycle. Both fractions indicate that a high degree of parallelization has been achieved for the domain parallelization in Octopus. Nevertheless, since the saturation is very sensitive to the value of p there is still room for improvement in the future.

Bibliography

[ABD06] X. Antoine, C. Besse, and S. Descombes, *Artificial Boundary Conditions for One-Dimensional Cubic Nonlinear Schrodinger Equations*, SIAM J. Numer. Anal **43**, 2272 (2006). 100

[ABM04] X. Antoine, C. Besse, and V. Mouysset, *Numerical schemes for the simulation of the two-dimensional Schrödinger equation using non-reflecting boundary conditions*, Math. Comp. **73**, 1779 (2004). 100

[AES03] A. Arnold, M. Ehrhardt, and I. Sofronov, *Approximation, stability and fast calculation of non-local boundary conditions for the Schrödinger equation*, Commun. Math. Sci. **1**, 501 (2003). 100

[AGB03] H. Appel, E. K. U. Gross, and K. Burke, *Excitations in Time-Dependent Density-Functional Theory*, Phys. Rev. Lett. **90**, 043005 (2003). 18

[AM76] N. W. Ashcroft and N. D. Mermin, *Solid State Physics*, Holt, Rinehart, and Winston, New York, 1976. 15

[Amd67] G. Amdahl, *Validity of the single processor approach to achieving large scale computer capabilities*, (Atlantic City, NJ), Proc. AFIPS Spring Joint Comp. Conf., vol. 30, AFIPS, 1967, p. 483. 130

[AMGGB02] C. Attaccalite, S. Moroni, P. Gori-Giorgi, and G. B. Bachelet, *Correlation Energy and Spin Polarization in the 2D Electron Gas*, Phys. Rev. Lett. **88**, 256601 (2002). 105

[And77a] T. Ando, *Inter-subband optical absorption in space-charge layers on semiconductor surfaces*, Z. Phys. B **26**, 263 (1977). 7

[And77b] T. Ando, *Inter-subband optical transitions in a surface space-charge layer*, Solid State Commun. **21**, 133 (1977). 7

[Ano94] Anonymous, *MPI: A Message-Passing Interface Standard*, The International Journal of Supercomputer Applications and High Performance Computing **8**, 159 (1994). 129

[App07] H. Appel, *Homepage of the present dissertation*, `http://www.physik.fu-berlin.de/~appel/PhDThesis/`, 1 (2007). 78, 110, 117

[AR74] A. Aviram and M. A. Ratner, *Molecular rectifiers*, 277 (1974). 87

[Arn01] A. Arnold, *Mathematical concepts of open quantum boundary conditions*, Transp. Theory Stat. Phys. **30/4-6**, 561 (2001). 99, 100

[Ayi80] S. Ayik, *Mean-Field Theory and Statistical Treatment of Residual Interactions*, Z. Phys. A **298**, 83 (1980). 43

[Ayi84] S. Ayik, *Extended time-dependent Hartree-Fock Theory in the adiabatic limit*, Nucl. Phys. A **422**, 331 (1984). 43

[Ayr58] R. U. Ayres, *Variational Approach to the Many-Body Problem*, Phys. Rev. **111**, 1453 (1958). 35

[Bal60] R. Balescu, *Irreversible Processes in Ionized Gases*, Phys. Fluids **3**, 52 (1960). 48

[Bar81] L. J. Bartolotti, *Time-dependent extension of the Hohenberg-Kohn-Levy energy-density functional*, Phys. Rev. A **24**, 1661 (1981). 7

[Bau97] D. Bauer, *Two-dimensional, two-electron model atom in a laser pulse: Exact treatment, single-active-electron analysis, time-dependent density-functional theory, classical calculations, and nonsequential ionization*, Phys. Rev. A **56**, 3028 (1997). 65

[BB02] M. A. Buijse and E. J. Baerends, *An approximate exchange-correlation hole density as a functional of the natural orbitals*, Mol. Phys. **100**, 401 (2002). 37, 39

[BBK97] M. Bonitz, R. Binder, and H. S. Köhler, *Quantum Kinetic Equations: Correlation Dynamics and Selfenergy*, Contr. Plasma Phys. **37**, 101 (1997). 47

[BCG05] K. Burke, R. Car, and R. Gebauer, *Density Functional Theory of the Electrical Conductivity of Molecular Devices*, Phys. Rev. Lett. **94**, 146803 (2005). 98, 99

[BF04] H. Bruus and K. Flensberg, *Many-Body Quantum Theory in Condensed Matter Physics*, Oxford University Press, Oxford, 2004. 88

[BILP85] M. Büttiker, Y. Imry, R. Landauer, and S. Pinhas, *Generalized many-channel conductance formula with application to small rings*, Phys. Rev. B **31**, 6207 (1985). 88

[BKV93] G. G. Balint-Kurti and Á. Vibók, *Complex Absorbing Potentials in Time Dependent Quantum Dynamics*, Numerical Grid Methods and their Application to Schrödinger's Equation (C. Cerjan, ed.), vol. 412, NATO ASI series, Series C: Mathematical and Physical Sciences, Kluwer Academic Publishers, 1993, p. 195. 103

[BMO+02] M. Brandbyge, J.-L. Mozos, P. Ordejón, J. Taylor, and K. Stokbro, *Density-functional method for nonequilibrium electron transport*, Phys. Rev. B **65**, 165401 (2002). 88

[Bon98] M. Bonitz, *Quantum kinetic theory*, Teubner, Stuttgart, 1998. 43, 45, 47

[Bop59] F. Bopp, *Ableitung der Bindungsenergie von N-Teilchen Systemen aus* 2*-Teilchen Dichtematrizen*, Z. Phys. **156**, 348 (1959). 35

[BP94] V. A. Baskakov and A. V. Popov, *Implementation of transparent boundaries for numerical solution of the Schrödinger equation*, Wave Motion **14**, 123 (1994). 99

[BPL95] K. Burke, J. P. Perdew, and M. Levy, *Nonlocal density functionals for exchange and correlation: Theory and applications*, Modern Density Functional Theory: A Tool for Chemistry (J. M. Seminario and P. Politzer, eds.), Elsevier, Amsterdam, 1995. 15

[Bre73] R. P. Brent, *Algorithms for Minimization Without Derivatives*, Prentice Hall, Englewood Cliffs, NJ, 1973. 39

[CA00] G. Csányi and T. A. Arias, *Tensor product expansions for correlation in quantum many-body systems*, Phys. Rev. B **61**, 7348 (2000). 39, 57

[CAL+06] Z. Chen, J. Appenzeller, Y.-M. Lin, J. Sippel-Oakley, A. G. Rinzler, J. Tang, S. J. Wind, P. M. Solomon, and P. Avouris, *An Integrated Logic Circuit Assembled on a Single Carbon Nanotube*, Science **311**, 1735 (2006). 86

[Cas95] M. E. Casida, *Time-dependent density functional response theory for molecules*, Recent Advances in Density Functional Methods (D. E. Chong, ed.), World Scientific, Singapore, 1995. 18, 20, 123, 125, 126

[CF76] L. Cohen and C. Frishberg, *Hierarchy equations for reduced density matrices*, Phys. Rev. A **13**, 927 (1976). 35

[CGA02] G. Csányi, S. Goedecker, and T. A. Arias, *Improved tensor-product expansions for the two-particle density matrix*, Phys. Rev. A **65**, 032510 (2002). 39

[CH92] J. Du Croz and N. Higham, *Stability of methods of matrix inversion*, IMA J. Num. Analysis **13**, 1 (1992). 94

[CK61] B. C. Carlson and J. M. Keller, *Eigenvalues of Density Matrices*, Phys. Rev. **121**, 659 (1961). 35

[CKG02] S. Y. Chou, C. Keimel, and J. Gu, *Ultrafast and direct imprint of nanostructures in silicon*, Nature **417**, 835 (2002). 86

[CNW88] W. Cassing, K. Niita, and S. J. Wang, *Dynamical aspects of intermediate-energy nucleus-nucleus collisions*, Z. Phys A. **331**, 439 (1988). 43

[Col63] A. J. Coleman, *Structure of Fermion Density Matrices*, Rev. Mod. Phys. **35**, 668 (1963). 35, 37

[Col93] D. Collins, *Entropy maximizations on electron density*, Z. Naturforsch. A **48 (1/2)**, 68 (1993). 62

[CPdVV93] F. Colmenero, C. Pérez del Valle, and C. Valdemoro, *Approximating q-order reduced density matrices in terms of the lower-order ones. I. General relations*, Phys. Rev. A **47**, 971 (1993). 36

[CR93] D. Calvetti and L. Reichel, *Fast inversion of Vandermonde-like matrices involving orthogonal polynomials*, BIT Num. Math. **33**, 473 (1993). 94

[CRRT99] J. Chen, M. A. Reed, A. M. Rawlett, and J. M. Tour, *Large On-Off Ratios and Negative Differential Resistance in a Molecular Electronic Device*, Science **286**, 1550 (1999). 87

[CV93] F. Colmenero and C. Valdemoro, *Approximating q-order reduced density matrices in terms of the lower-order ones. II. Applications*, Phys. Rev. A **47**, 979 (1993). 36

[CYW+02] H. Cao, Z. Yu, J. Wang, J. O. Tegenfeldt, R. H. Austin, E. Chen, W. Wu, and S. Y. Chou, *Fabrication of 10 nm enclosed nanofluidic channels*, Appl. Phys. Lett. **81**, 174 (2002). 86

[Dan84] P. Danielewicz, *Quantum theory of nonequilibrium processes, I*, Ann. of Phys. **152**, 239 (1984). 42

[Dat95] S. Datta, *Electronic Transport in Mesoscopic Systems*, Cambridge University Press, Cambridge, 1995. 88

[DG82] B. M. Deb and S. K. Ghosh, *Schrödinger fluid dynamics of many-electron systems in a time-dependent density-functional framework*, J. Chem. Phys. **77**, 342–348 (1982). 7

[DGSB93] D. D. Dunlap, R. Garcia, E. Schabtach, and C. Bustamante, *Masking Generates Contiguous Segments of Metal-Coated and Bare DNA for Scanning Tunneling Microscope Imaging*, PNAS **90**, 7652 (1993). 87

[Dir29] P. A. M. Dirac, *Quantum Mechanics of Many-Electron Systems*, Proceedings of the Royal Society of London. Series A, Containing Papers of a Mathematical and Physical Character **123**, 714–733 (1929). 1

[DLS06] N. E. Dahlen, R. van Leeuwen, and A. Stan, *Propagating the Kadanoff-Baym equations for atoms and molecules*, J. Phys. Conf. Ser. **35**, 340 (2006). 42

[DVPL00] M. Di Ventra, S. T. Pantelides, and N. D. Lang, *First-Principles Calculation of Transport Properties of a Molecular Device*, Phys. Rev. Lett. **84**, 979 (2000). 88

[EA01] M. Ehrhardt and A. Arnold, *Discrete Transparent Boundary Conditions for the Schrödinger Equation*, Revista di Matematica della Universita di Parma **6/4**, 57 (2001). 100

[Erd78] R. M. Erdahl, *Representability*, Int. J. of Quant. Chem. **13**, 697 (1978). 35

[ESJ89] J. H. Eberly, Q. Su, and J. Javanainen, *Nonlinear Light Scattering Accompanying Multiphoton Ionization*, Phys. Rev. Lett. **62**, 881 (1989). 65

[Fey59] R. P. Feynman, *Plenty of Room at the Bottom*, http://www.its.caltech.edu/~feynman/plenty.html, 1 (1959). 85

[FFS82] M. D. Feit, J. A. Fleck, and A. Steiger, *Solution of the Schrödinger equation by a spectral method*, J. Comput. Phys. **47**, 412 (1982). 115

[FKW78] H. Flocard, S. E. Koonin, and M. S. Weiss, *Three-dimensional time-dependent Hartree-Fock calculations: Application to ^{16}O + ^{16}O collisions*, Phys. Rev. C **17**, 1682 (1978). 115

[FR05] F. Furche and D. Rappoport, *Density functional methods for excited states: equilibrium structure and excited spectra*, Computational Photochemistry (M. Olivucci, ed.), vol. 16, Elsevier, Amsterdam, 2005. 18

[FS99] H. W. Fink and C. Schonenberger, *Electrical conduction through molecules*, Nature **398**, 407 (1999). 87

[Fuj64] S. Fujita, *Partial self-energy parts of Kadanoff-Baym*, Physica **30**, 848 (1964). 42

[GB06] O. Gritsenko and E. J. Baerends, *A simple natural orbital mechanism of pure van der Waals interaction in the lowest excited triplet state of the hydrogen molecule*, J. Chem. Phys. **124**, 054115 (2006). 40

[GBC06] R. Gebauer, K. Burke, and R. Car, *Kohn-Sham Master Equation Approach to Transport Through Single Molecules*, in: Time-Dependent Density Functional Theory (M. A. L.Marques et. al., ed.), vol. 706, Springer Lecture Notes in Physics, 2006, p. 463. 98

[GBSN00] D. I. Gittins, D. Bethell, D. J. Schiffrin, and R. J. Nichols, *Nanometre-scale electronic switch consisting of a metal cluster and redox-addressable groups*, Nature **408**, 67 (2000). 87

[GD82] S. K. Ghosh and B. M. Deb, *Dynamic polarizability of many-electron systems within a time-dependent density-functional theory*, Chem. Phys. **71**, 295 (1982). 7

[GD83a] S. K. Ghosh and B. M. Deb, *A density-functional calculation of dynamic dipole polarizabilities of noble gas atoms*, Theoret. Chim. Acta **62**, 209 (1983). 7

[GD83b] S. K. Ghosh and B. M. Deb, *A simple density-functional calculation of frequency-dependent multipole polarizabilities of noble gas atoms*, J. Mol. Struct. (Theochem) **103**, 163 (1983). 7

[GD88] S. K. Ghosh and A. K. Dhara, *Density-functional theory of many-electron systems subjected to time-dependent electric and magnetic fields*, Phys. Rev. A **38**, 1149 (1988). 9, 11

[GDM96] E. K. U. Gross, J. F. Dobson, and Petersilka M., *Density Functional Theory of Time-Dependent Phenomena*, Topics in Current Chemisty **181**, 81 (1996). 12, 14

[GE92] R. Grobe and J. H. Eberly, *Photoelectron spectra for a two-electron system in a strong laser field*, Phys. Rev. Lett. **68**, 2905 (1992). 65

[GE93] R. Grobe and J. H. Eberly, *One-dimensional model of a negative ion and its interaction with laser fields*, Phys. Rev. A **48**, 4664 (1993). 65

[GFB+06] J. Gabelli, G. Feve, J.-M. Berroir, B. Placais, A. Cavanna, B. Etienne, Y. Jin, and D. C. Glattli, *Violation of Kirchhoff's Laws for a Coherent RC Circuit*, Science **313**, 499 (2006). 87

[GHL+98] W. Gropp, S. Huss-Lederman, et al., *MPI: The Complete Reference, Volume 2 - The MPI-2 Extensions*, MIT Press, Cambridge MA, 1998. 129

[Gil75] T. L. Gilbert, *Hohenberg-Kohn theorem for nonlocal external potentials*, Phys. Rev. B **12**, 2111 (1975). 33

[GJPZ97] P. Gersdorf, W. John, J. P. Perdew, and P. Ziesche, *Correlation entropy of the H_2 molecule*, Int. J. Quant. Chem. **61**, 935 (1997). 62

[GL76] O. Gunnarsson and B. I. Lundqvist, *Exchange and correlation in atoms, molecules, and solids by the spin-density-functional formalism*, Phys. Rev. B **13**, 4274 (1976). 15, 58

[GLDS96] W. Gropp, E. Lusk, N. Doss, and A. Skjellum, *A high-performance, portable implementation of the MPI message passing interface standard*, Parallel Computing **22**, 789 (1996). 129

[GN07] A. K. Geim and K. S. Novoselov, *The rise of graphene*, Nature Materials **6**, 183 (2007). 86

[GO97] I. Gohberg and V. Olshevsky, *The fast generalized Parker-Traub algorithm for inversion of Vandermonde and related matrices*, J. of Complexity **13(2)**, 208 (1997). 94

[GOK88a] E. K. U. Gross, L. N. Oliveira, and W. Kohn, *Density-functional theory for ensembles of fractionally occupied states. I. Basic formalism*, Phys. Rev. A **37**, 2809 (1988). 15

[GOK88b] E. K. U. Gross, L. N. Oliveira, and W. Kohn, *Rayleigh-Ritz variational principle for ensembles of fractionally occupied states*, Phys. Rev. A **37**, 2805 (1988). 15

[GP64] C. Garrod and J. K. Percus, *Reduction of the N-Particle Variational Problem*, J. Math. Phys. **5**, 1756 (1964). 35

[GPB05] O. Gritsenko, K. Pernal, and E. J. Baerends, *An improved density matrix functional by physically motivated repulsive corrections*, J. Chem. Phy. **122**, 204102 (2005). 39, 40, 57

[GU98] S. Goedecker and C. J. Umrigar, *Natural Orbital Functional for the Many-Electron Problem*, Phys. Rev. Lett. **81**, 866 (1998). 37, 39, 56

[GWW81] P. Grange, H. A. Weidenmüller, and G. Wolschin, *Beyond the TDHF: A Collison Term from a Random-Matrix Model*, Ann. Phys. **136**, 190 (1981). 43

[Har78] J. E. Harriman, *Geometry of density matrices. I. Definitions, N matrices and 1 matrices*, Phys. Rev. A **17**, 1249 (1978). 35

[Har79] J. E. Harriman, *Limitation on the density-equation approach to many-electron problems*, Phys. Rev. A **19**, 1893 (1979). 36

[Hel07] E. J. Heller, *Resonance Fine Art - Quasi Classical Correspondence, Quantum Scars*, http://www.ericjhellergallery.com/index.pl?page=category;catid=4 (2007). 107

[HF94] J. R. Hellums and W. R. Frensley, *Non-Markovian open-system boundary conditions for the time-dependent Schrödinger equation*, Phys. Rev. B **49**, 2904 (1994). 100

[HK64] P. Hohenberg and W. Kohn, *Inhomogeneous Electron Gas*, Phys. Rev. **136**, B864 (1964). 1, 11

[HL03] M. Hochbruck and C. Lubich, *On Magnus Integrators for Time-Dependent Schrödinger Equations*, SIAM J. Numer. Anal **41**, 945 (2003). 115

[HLAG07] N. Helbig, N. N. Lathiotakis, M. Albrecht, and E. K. U. Gross, *Discontinuity of the chemical potential in reduced-density-matrix-functional theory*, Europhys. Lett. **77**, 67003 (2007). 40

[HTC83] G. M Huang, T. J. Tarn, and J. W. Clark, *On the controllability of quantum-mechanical systems*, J. Math. Phys. **24**, 2608 (1983). 64

[II93] S. Iijima and T. Ichihashi, *Single-shell carbon nanotubes of 1-nm diameter*, Nature **363**, 603 (1993). 86

[IS06] M. V. Ivanov and P. Schmelcher, *Electronic transmission through a coupled quantum dot and ring*, Journal of Physics: Condensed Matter **18**, 2963 (2006). 103

[JR05] C. Joachim and M. A. Ratner, *Molecular Electronics Special Feature: Molecular electronics: Some views on transport junctions and beyond*, PNAS **102**, 8801 (2005). 87

[KB76] L. P. Kadanoff and G. Baym, *Quantum Statistical Mechanics*, Benjamin, New York, 1976. 42, 48

[KBKS97] D. Kremp, M. Bonitz, W. D. Kraeft, and M. Schlanges, *Non-Markovian Boltzmann Equation*, Ann. of Phys. **258**, 320 (1997). 47

[Kel65] L. V. Keldysh, *Diagram technique for non-equilibrium processes*, Sov. Phys. JETP-USSR **20**, 1018 (1965). 42

[KF98] K. Kladko and P. Fulde, *On the properties of cumulant expansions*, Int. J. Quant. Chem. **66**, 377 (1998). 53

[KK98] G. Karypis and V. Kumar, *A Fast and High Quality Multilevel Scheme for Partitioning Irregular Graphs*, SIAM J. on Scientific Computing **20**, 359 (1998). 129

[KKER86] W. D. Kraeft, D. Kremp, W. Ebeling, and G. Röpke, *Quantum Statistics of Charged Particle Systems*, Akademie Verlag, Berlin, 1986. 47, 48

[KM99] W. Kutzelnigg and D. Mukherjee, *Cumulant expansion of the reduced density matrices*, J. Chem. Phys. **110**, 2800 (1999). 53

[Koh86] W. Kohn, *Density-functional theory for excited states in a quasi-local-density approximation*, Phys. Rev. A **34**, 737 (1986). 15

[Kor97] A. N. Korotkov, *Coulomb Blockade and Digital Single-Electron Devices*, 157 (1997). 87

[KP98] W. Kohn and J. A. Pople, *Nobel Price in Chemistry 1998*, http://nobelprize.org/nobel_prizes/chemistry/laureates/1998/, 1 (1998). 1

[KS65] W. Kohn and L. J. Sham, *Self-consistent equations including exchange and correlation effects*, Phys. Rev. **140**, A1133 (1965). 1

[KSA+05] S. Kurth, G. Stefanucci, C.-O. Almbladh, A. Rubio, and E. K. U. Gross, *Time-dependent quantum transport: A practical scheme using density functional theory*, Phys. Rev. B **72**, 035308 (2005). 100

[Kum67] H. Kummer, *n-Representability Problem for Reduced Density Matrices*, J. Math. Phys. **8**, 2063 (1967). 35

[LA00] N. D. Lang and Ph. Avouris, *Carbon-Atom Wires: Charge-Transfer Doping, Voltage Drop, and the Effect of Distortions*, Phys. Rev. Lett. **84**, 358 (2000). 87, 88

[Lan57] R. Landauer, *Spatial Variation of Currents and Fields Due to Localized Scatterers in Metallic Conduction*, IBM J. Res. Develop. **1**, 233 (1957). 87

[Lan95] N. D. Lang, *Resistance of atomic wires*, Phys. Rev. B **52**, 5335 (1995). 88

[LCA99] D. Lacroix, P. Chomaz, and S. Ayik, *On the simulation of extended TDHF theory*, Nucl. Phys. A **651**, 369 (1999). 43

[Len60] A. Lenard, *On Bogoliubov's kinetic equation for a spatially homogeneous plasma*, Ann. of Phys. **10**, 390 (1960). 48

[LG06] M. Lein and E. K. U. Gross, *Back to the ground-state: Electron gas*, in: Time-Dependent Density Functional Theory (M. A. L. Marques et. al., ed.), vol. 706, Springer Lecture Notes in Physics, 2006, p. 423. 58

[LGE00] M. Lein, E. K. U. Gross, and V. Engel, *On the mechanism of strong-field double photoionization in the helium atom*, J. Phys. B: At. Mol. Opt. Phys. **33**, 433 (2000). 65

[LHG07] N. N. Lathiotakis, N. Helbig, and E. K. U. Gross, *Performance of one-body reduced density matrix functionals for the homogeneous electron gas*, Phys. Rev. B **(accepted)** (2007). 39

[Löw55] P. O. Löwdin, *Quantum Theory of Many-Particle Systems. I. Physical Interpretations by Means of Density Matrices, Natural Spin-Orbitals, and Convergence Problems in the Method of Configurational Interaction*, Phys. Rev. **97**, 1474 (1955). 35

[LP75] D. C. Langreth and J. P. Perdew, *The exchange-correlation energy of a metallic surface*, Solid State Comm. **17**, 1425 (1975). 58

[LSB+02] W. Liang, M. P. Shores, M. Bockrath, J. R. Long, and H. Park, *Kondo resonance in a single-molecule transistor*, Nature **417**, 725 (2002). 87

[LSW+96] D. G. Lappas, A. Sanpera, J. B. Watson, K. Burnett, P. L. Knight, R. Grobe, and J. H. Eberly, *Two-electron effects in harmonic generation and ionization from a model He atom*, J. Phys. B: At. Mol. Opt. Phys. **29**, L619 (1996). 65

[Lub86] C. Lubich, *Discretized fractional calculus*, SIAM J. Math. Anal. **17**, 704 (1986). 99

[LvL98] D. G. Lappas and R. van Leeuwen, *Electron correlation effects in the double ionization of He*, J. Phys. B: At. Mol. Opt. Phys. **31**, L249 (1998). 65

[May55] J. E. Mayer, *Electron Correlation*, Phys. Rev. **100**, 1579 (1955). 35

[Maz98a] D. A. Mazziotti, *3,5-contracted Schrödinger equation: Determining quantum energies and reduced density matrices without wave functions*, Int. J. Quant. Chem. **70**, 557 (1998). 36

[Maz98b] D. A. Mazziotti, *Contracted Schrödinger equation: Determining quantum energies and two-particle density matrices without wave functions*, Phys. Rev. A **57**, 4219 (1998). 36

[Maz99] D. A. Mazziotti, *Comparison of contracted Schrödinger and coupled-cluster theories*, Phys. Rev. A **60**, 4396 (1999). 36

[Maz02a] D. A. Mazziotti, *Purification of correlated reduced density matrices*, Phys. Rev. E **65**, 026704 (2002). 36

[Maz02b] D. A. Mazziotti, *Solution of the 1,3-contracted Schrödinger equation through positivity conditions on the two-particle reduced density matrix*, Phys. Rev. A **66**, 062503 (2002). 36

[Maz02c] D. A. Mazziotti, *Variational minimization of atomic and molecular ground-state energies via the two-particle reduced density matrix*, Phys. Rev. A **65**, 062511 (2002). 36

[Maz04] D. A. Mazziotti, *Realization of Quantum Chemistry without Wave Functions through First-Order Semidefinite Programming*, Phys. Rev. Lett. **93**, 213001 (2004). 36

[MB01] N. T. Maitra and K. Burke, *Demonstration of initial-state dependence in time-dependent density-functional theory*, Phys. Rev. A **63**, 042501 (2001). 11

[MBA+02] N. T. Maitra, K. Burke, H. Appel, E. K. U. Gross, and R. van Leeuwen, *Ten topical questions in time-dependent density functional theory*, Reviews in Modern Quantum Chemistry: A Celebration of the Contributions of R.G. Parr (K.D. Sen, ed.), World Scientific, 2002, pp. 1186–1225. 11, 18

[MCBR03] M. A. L. Marques, Alberto Castro, George F. Bertsch, and Angel Rubio, *octopus: a first-principles tool for excited electron-ion dynamics*, Comput. Phys. Commun. **151**, 60 (2003). 90, 103, 115

[MI57] Y. Mizuno and T. Izuyama, *Remarks on Mayer's Reduced Density Matrix Method*, Prog. Theor. Phys. **18**, 33 (1957). 35

[Moo65] G. E. Moore, *Cramming More Components Onto Integrated Circuits*, Electronics **38** (1965). 85

[Moo07a] G. E. Moore, *Meet the World's First 45nm Processor*, http://www.intel.com/technology/silicon/45nm_technology.htm, 1 (2007). 85, 86

[Moo07b] G. E. Moore, *Moore's Law*, http://www.intel.com/technology/mooreslaw/, 1 (2007). 85

[Mor72] K. Morris, *Mathematical Thought from Ancient to Modern Times*, Oxford University Press, New York, NY, USA, 1972. 61

[MS59] P. C. Martin and J. Schwinger, *Theory of Many-Particle Systems. I*, Phys. Rev. **115**, 1342 (1959). 42

[Mül84] A. M. K. Müller, *Explicit approximate relation between reduced two- and one-particle density matrices*, Phys. Lett. **105A**, 446 (1984). 37, 39, 56

[MUN+06] M. A. L. Marques, C. A. Ullrich, F. Nogueira, A. Rubio, K. Burke, and E. K. U. Gross, *Time-Dependent Density Functional Theory (Lecture Notes in Physics)*, Springer-Verlag, Berlin, 2006. 42

[MW92] Y. Meir and N. S. Wingreen, *Landauer formula for the current through an interacting electron region*, Phys. Rev. Lett. **68**, 2512 (1992). 88

[Nak76] H. Nakatsuji, *Equation for the direct determination of the density matrix*, Phys. Rev. A **14**, 41 (1976). 35

[NGM+04] K. S. Novoselov, A. K. Geim, S. V. Morozov, D. Jiang, Y. Zhang, S. V. Dubonos, I. V. Grigorieva, and A. A. Firsov, *Electric Field Effect in Atomically Thin Carbon Films*, Science **306**, 666–669 (2004). 86

[NR03] A. Nitzan and M. A. Ratner, *Electron Transport in Molecular Wire Junctions*, Science **300**, 1384 (2003). 87

[OGK88] L. N. Oliveira, E. K. U. Gross, and W. Kohn, *Density-functional theory for ensembles of fractionally occupied states. II. Application to the He atom*, Phys. Rev. A **37**, 2821 (1988). 15

[Pap81] J. S. Papadakis, *Impedance formulation of the bottom boundary condition for the parabolic equation model in underwater acoustics*, in J.A. Davis, D. White and R.C. Cavanagh, "NORDA parabolic equation workshop, 31 march - 3 April 1981", Tech. Note 143, Naval Ocean Research and Development Activity, NSTL Station, MS, 1982, available from NTIS **No.. AD-121 932**, 83 (1981). 99

[Par64] F. Parker, *Inverses of Vandermonde matrices*, Amer. Math. Monthly **71**, 410 (1964). 94

[PBdVD00] D. Porath, A. Bezryadin, S. de Vries, and C. Dekker, *Direct measurement of electrical transport through molecules*, Nature **403**, 635 (2000). 87

[PDR88] A. P. Peirce, M. A. Dahleh, and H. Rabitz, *Optimal control of quantum-mechanical systems: Existence, numerical approximation, and applications*, Phys. Rev. A **37**, 4950 (1988). 64

[Per05] K. Pernal, *Effective Potential for Natural Spin Orbitals*, Phys. Rev. Lett. **94**, 233002 (2005). 52

[PGB91] M. S. Pindzola, D. C. Griffin, and C. Bottcher, *Validity of time-dependent Hartree-Fock theory for the multiphoton ionization of atoms*, Phys. Rev. Lett. **66**, 2305 (1991). 65

[PGG96] M. Petersilka, U. J. Gossmann, and E. K. U. Gross, *Excitation energies from time-dependent density-functional theory*, Phys. Rev. Lett. **76**, 1212 (1996). 15, 17

[PLA+99] H. Park, A. K. L. Lim, A. P. Alivisatos, J. Park, and P. L. McEuen, *Fabrication of metallic electrodes with nanometer separation by electromigration*, Appl. Phys. Lett. **75**, 301 (1999). 87

[PN66] D. Pines and P. Nozieres, *The Theory of Quantum Liquids*, Benjamin, New York, 1966. 58

[PPG+02] J. Park, A. N. Pasupathy, J. I. Goldsmith, C. Chang, Y. Yaish, J. R. Petta, M. Rinkoski, J. P. Sethna, H. D. Abruna, P. L. McEuen, and D. C. Ralph, *Coulomb blockade and the kondo effect in single-atom transistors*, Nature **417**, 722 (2002). 87

[PTY+01] H. W. Ch. Postma, T. Teepen, Z. Yao, M. Grifoni, and C. Dekker, *Carbon Nanotube Single-Electron Transistors at Room Temperature*, Science **293**, 76 (2001). 86

[Ray99] E. S. Raymond, *The Cathedral and the Bazaar: Musings on Linux and Open Source by an Accidental Revolutionary*, O'Reilly Media, 1999. 127

[RG84] E. Runge and E. K. U. Gross, *Density-functional theory for time-dependent systems*, Phys. Rev. Lett. **52**, 997 (1984). 1, 7, 8, 9, 42

[ROB+02] J. Reichert, R. Ochs, D. Beckmann, H. B. Weber, M. Mayor, and H. v. Löhneysen, *Driving Current through Single Organic Molecules*, Phys. Rev. Lett. **88**, 176804 (2002). 87

[Ros68] M. Rosina, *in: Reduced Density Operators with Application to Physical and Chemical Systems*, Queens Papers in Pure and Applied Mathematics, no. 11, Queens University, 1968. 33

[RSD+95] V. Ramakrishna, M. V. Salapaka, M. A. Dahleh, H. Rabitz, and A. Peirce, *Controllability of molecular systems*, Phys. Rev. A **51**, 960 (1995). 64

[RZM+97] M. A. Reed, C. Zhou, C. J. Muller, T. P. Burgin, and J. M. Tour, *Conductance of a Molecular Junction*, Science **278**, 252 (1997). 87

[Sch26] E. Schrödinger, *Quantisierung als Eigenwertproblem*, Ann. Phys. **384**, 361 (1926). 1

[SD95] F. Schmidt and P. Deuflhard, *Discrete transparent boundary conditions for the numerical solution of Fresnel's equation*, Comput. Math. Appl **29**, 53 (1995). 99

[SE91] Q. Su and J. H. Eberly, *Model atom for multiphoton physics*, Phys. Rev. A **44**, 5997 (1991). 65

[SF94] U. Schwengelbeck and F. H. M. Faisal, *Ionization of the one-dimensional Coulomb atom in an intense laser field*, Phys. Rev. A **50**, 632 (1994). 65

[SFS01] S. G. Schirmer, H. Fu, and A. I. Solomon, *Complete controllability of quantum systems*, Phys. Rev. A **63**, 063410 (2001). 64

[SGA+05] A. Scherz, E. K. U. Gross, H. Appel, C. Sorg, K. Baberschke, H. Wende, and K. Burke, *Measuring the kernel of time-dependent density functional theory with X-ray absorption spectroscopy of 3d transition metals*, Phys. Rev. Lett **95**, 253006 (2005). 26

[SJC85] W. Shun-Jin and W. Cassing, *Explicit Treatment of N-Body Correlations within a Density-Matrix Formalism*, Ann. Phys. **159**, 328 (1985). 43, 44, 45, 46, 47

[SO+95] M. Snir, S. W. Otto, et al., *MPI: The Complete Reference, Volume 1 - The MPI Core*, MIT Press, Cambridge MA, 1995. 129

[SSC+96] Y. Saad, A. Stathopoulos, J. Chelikowsky, K. Wu, and S. Ögüt, *Solution of large eigenvalue problems in electronic structure calculations*, BIT **36**, 563 (1996). 66

[Stu99] J. F. Sturm, *Using SeDuMi 1.02, a Matlab Toolbox for Optimization over Symmetric Cones*, Opt. Meth. Soft. **11**, 625 (1999). 36

[Suz93] M. Suzuki, *General Nonsymmetric Higher-Order Decomposition of Exponential Operators and Symplectic Integrators*, J. Phys. Soc. Jpn. **61**, L3015 (1993). 115

[SW07] G. S. Snider and R. S. Williams, *Nano/CMOS architectures using a field-programmable nanowire interconnect*, Nanotechnology **18**, 035204 (2007). 90

[SY92] M. Suzuki and T. Yamauchi, *Convergence of unitary and complex decompositions of exponential operators*, J. Math. Phys. **34**, 4892 (1992). 115

[SY97] F. Schmidt and D. Yevick, *Discrete Transparent Boundary Conditions for Schrödinger-Type Equations*, J. Comput. Phys. **134**, 96 (1997). 99

[The79] A. K. Theophilou, *The energy density functional formalism for excited states*, J. Phys. C **12**, 5419 (1979). 15

[Toh85] M. Tohyama, *One-dimensional Solution of an extended time-dependent Hartree-Fock theory*, Phys. Lett. B **163**, 14 (1985). 43

[Toh87] M. Tohyama, *Application of quantum theory of particle collisions to* ^{16}O + ^{16}O *reactions*, Phys. Rev. C **36**, 187 (1987). 43

[TOP] TOP500, *TOP 500 list*, http://www.top500.org. 129

[Tra66] J. Traub, *Associated polynomials and uniform methods for the solution of linear problems*, SIAM Review **8, No. 3**, 277 (1966). 94

[Tre57] R. H. Tredgold, *Density Matrix and the Many-Body Problem*, Phys. Rev. **105**, 1421 (1957). 35

[Tur50] A. M. Turing, *I.–Computing Machinery and Intelligence*, Mind **LIX**, 433 (1950). 97

[Val85] C. Valdemoro, *Density Matrices and Density Functionals*, Proc. of the A. J. Coleman Symposium, Reidel, Dordrecht, 1985. 36

[vB79] U. von Barth, *Local-density theory of multiplet structure*, Phys. Rev. A **20**, 1693 (1979). 15

[VB96] L. Vandenberghe and S. Boyd, *Semidefinite Programming*, SIAM Review **38**, 49 (1996). 36

[Vig04] G. Vignale, *Mapping from current densities to vector potentials in time-dependent current density functional theory*, Phys. Rev. B **70**, 201102 (2004). 9, 11

[vL99] R. van Leeuwen, *Mapping from Densities to Potentials in Time-Dependent Density-Functional Theory*, Phys. Rev. Lett. **82**, 3863 (1999). 7, 10

[VT04] M. Di Ventra and T. N. Todorov, *Transport in nanoscale systems: the microcanonical versus grand-canonical picture*, J. Phys. Cond. Matt. **16**, 8025 (2004). 97

[WT78] C. Y. Wong and H. K. Tang, *Extended Time-Dependent Hartree-Fock Approximation with Particle Collisions*, Phys. Rev. Lett. **40**, 1070 (1978). 43

[WT79] C. Y. Wong and H. K. Tang, *Dynamics of nuclear fluid. V. Extended time-dependent Hartree-Fock approximation illuminates the approach to thermal equilibrium*, Phys. Rev. C **20**, 1419 (1979). 43

[XDR02] Y. Xue, S. Datta, and M. A. Ratner, *First-principles based matrix Green's function approach to molecular electronic devices: general formalism*, Chem. Phys. **281**, 151 (2002). 88

[XT03] B. Xu and N. J. Tao, *Measurement of Single-Molecule Resistance by Repeated Formation of Molecular Junctions*, Science **301**, 1221–1223 (2003). 87

[YFS01] D. Yevick, T. Friese, and F. Schmidt, *A Comparison of Transparent Boundary Conditions for the Fresnel Equation*, J. Comput. Phys. **168**, 433 (2001). 99

[ZBR98] W. Zhu, J. Botina, and H. Rabitz, *Rapidly convergent iteration methods for quantum optimal control of population*, J. Chem. Phys. **108**, 1953 (1998). 64

[Zie95] P. Ziesche, *Correlation strength and information entropy*, Int. J. Quant. Chem. **56**, 363 (1995). 62

[Zie00] P. Ziesche, *On relations between correlation, fluctuation and localization*, J. Mol. Structure (Theochem) **527**, 35 (2000). 62

[ZRB77] T. Ziegler, A. Rauk, and E. J. Baerends, *On the calculation of multiplet energies by the Hartree-Fock-Slater method*, Theoret. Chim. Acta **43**, 261 (1977). 15

[ZS80] A. Zangwill and Paul Soven, *Density-functional approach to local-field effects in finite systems: Photoabsorption in the rare gases*, Phys. Rev. A **21**, 1561 (1980). 7

Deutsche Kurzfassung

Zeitabhängige Dichtefunktionaltheorie (TDDFT) wird als erfolgreiches Werkzeug zur Berechnung von Anregungsenergien in atomaren und molekularen Systemen eingesetzt. Im ersten Teil dieser Arbeit leiten wir eine Doppelpol-Näherung für die TDDFT-Gleichungen der linearen Antwortfunktion her. Diese Näherung erlaubt die exakte Beschreibung von Systemen mit zwei stark gekoppelten Anregungsenergien, die vom Rest des Spektrums klar getrennt sind. Im Gegensatz zur klassischen Einpol-Näherung liefert die Doppelpol-Näherung Korrekturterme für die Kohn-Sham Oszillator-Stärken. In der vorliegenden Arbeit konnten mehrere kritische Polabstände identifiziert werden. Es stellt sich z.B. heraus, dass die Kopplung zwischen Anregungsenergien das Verschwinden von Übergängen im optischen Spektrum bewirken kann. Weiterhin zeigen wir wie sich die Gleichungen der Doppelpol-Näherung invertieren lassen, was dazu genutzt werden kann, Matrix-Elemente des Austausch-Korrelations-Kernels f_{xc} mit Hilfe von experimentellen Daten zu bestimmen. In Zukunft kann dies als Grundlage für die Konstruktion von Funktionalen dienen.
Die Theorie der reduzierten Dichtematrizen (RDMFT) gilt als vielversprechender Zugang, der eine über DFT hinausgehende Beschreibung von stark korrelierten Vielteilchensystemen ermöglicht. Bisherige Forschungsarbeiten auf dem Gebiet der RDMFT beschränken sich hauptsächlich auf die Beschreibung von stationären Systemen. In der vorliegenden Arbeit versuchen wir erste Schritte im Hinblick auf eine zeitabhängige Erweiterung von RDMFT zu unternehmen. Wir leiten Bewegungsgleichungen für die natürlichen Orbitale und deren Besetzungszahlen ab und zeigen mit Hilfe der Bewegungsgleichung für die Besetzungszahlen, dass eine adiabatische Erweiterung bestehender Funktionale der statischen RDMFT zu zeitlich konstanten Besetzungszahlen führt. Aus den stationären Bedingungen für die Bewegungsgleichungen der N-Teilchen Korrelationen (korrelierte Anteile der N-Teilchen Dichtematrizen) leiten wir eine Klasse von Grundzustands-Funktionalen ab, die für Rechnungen innerhalb der statischen RDMFT verwendet werden können. Als Anwendung betrachen wir Zeitpropagationen der Vielteilchen-Schrödinger Gleichung für eindimensionale Modellsysteme. Mit Hilfe der Theorie der optimalen Kontrolle berechnen wir optimierte Laserpulse für atomare Übergänge in einem Modell für das Helium-Atom. Wir ermitteln mit Hilfe der korrelierten und - zumindest numerisch - exakten Wellenfunktion die exakte Zeitentwicklung der natürlichen Orbitale und Besetzungszahlen für (i) Helium im starken Laserfeldern und (ii) Elektron-Ionen Streuung.
Teil III der vorliegenden Arbeit beschäftigt sich mit zeitabhängigem elektronischen Transport im Rahmen der TDDFT. Wir stellen einen Algorithmus vor, mit dessen Hilfe sich ausgedehnte Eigenzustände von Einteilchen-Hamiltonoperatoren berechnen lassen. Die Methode ist speziell auf eine Finite-Differenzen Diskretisierung der Schrödinger Gleichung zugeschnitten. Wir untersuchen die Zeitpropagation von mesoskopischen Systemen mit Hilfe von endlichen Gittern und diskutieren die Einschränkungen eines solchen Zugangs. Um die Limitierungen von endlichen Simulationsgebieten zu überwinden, entwickeln wir ein Propagations-Schema welches auf einer Darstellung mit gemischter Basis beruht. In

unserem Verfahren werden Zuleitungen und zentrales Streugebiet gleichermaßen behandelt, so dass Artefakte durch Reflexionen an den Gitterrändern vermieden werden.

Publications

1. *Ten topical questions in time-dependent density functional theory*
   N.T. Maitra, K. Burke, H. Appel, E.K.U. Gross, and R. van Leeuwen, in: Reviews in Modern Quantum Chemistry: A Celebration of the Contributions of R.G. Parr, K.D. Sen, ed(s), (World Scientific, 2002), p. 1186-1225.

2. *Static and Time-Dependent Many-Body Effects via Density-Functional Theory*
   H. Appel and E.K.U. Gross, Quantum Simulations of Complex Many-Body Systems: From Theory to Algorithms, J. Grotendorst, D. Marx, A Muramatsu, ed(s), (John von Neumann Institute for Computing, NIC Series, Volume 10, 2002), p. 255-268.

3. *Excitations in Time-Dependent Density-Functional Theory*
   H. Appel, E. K. U. Gross, and K. Burke, Physical Review Letters **90**, 043005 (2003).

4. *Measuring the Kernel of Time-Dependent Density Functional Theory with X-ray Absorption Spectroscopy of 3d Transition Metals*
   A. Scherz, E.K.U. Gross, H. Appel, C. Sorg, K. Baberschke, H. Wende, and K. Burke, Physical Review Letters **95**, 253006 (2005).

5. *Double-Pole Approximation in Time-Dependent Density Functional Theory*
   H. Appel, E.K.U. Gross, and K. Burke, International Journal of Quantum Chemistry **106**, 2840-2847 (2006).

6. *octopus: a tool for the application of time-dependent density functional theory*
   A. Castro, M. A. L. Marques, H. Appel, M. Oliveira, C. A. Rozzi, X. Andrade, F. Lorenzen, E. K. U. Gross and A. Rubio, Physica Status Solidi (b), **243**, 2465-2488 (2006).

7. *XMCD Analysis Beyond Standard Procedures*
   H. Wende, A. Scherz, C. Sorg, K. Baberschke, E.K.U. Gross, H. Appel, K. Burke, J. Minár, H. Ebert, A.L. Ankudinov and J.J. Rehr, Proceedings of the 13th International Conference on X-Ray Absorption Fine Structure-XAFS13 **882**, 78-82 (AIP Conference Proceedings, 2007).

8. *Time-dependent reduced density matrix functional theory*
   H. Appel, E. K. U. Gross, (in preparation).

Acknowledgements

Completing a piece of work, like the present thesis, is not possible without the support of many people. It is therefore a pleasant task to express my sincere gratitude to all who contributed in many ways to the outcome of the present work.

First and foremost I would like to thank Prof. E.K.U. Gross. I have profited enormously from his encouragement, guidance and support, from the freedom he provided to find own pathways, and I have enjoyed our many discussions on physics and unrelated matters. It has been a great privilege to work with him over the past years.

It is a great pleasure to thank Prof. K. D. Schotte for accepting the role as second referee and for taking the time to read the thesis. Similarly, I would like to thank all other members of the committee for the time they have invested.

I would like to thank Prof. K. Burke for the continuous support and the fruitful collaborations during the past years.

The early roots of this work date back to my time in Würzburg. I would like to thank my office mates Robert van Leeuwen and Thomas Kreibich who introduced me to many aspects of time-dependent many-body systems.

I am very grateful to Nicole Helbig, Nektarios Lathiotakis, Sangeeta Sharma, and Kay Dewhurst for the vivid and constructive discussions on density matrices.

My sincere thanks go to Prof. A. Rubio, Stefan Kurth, Gianluca Stefanucci and Esa Räsänen. Many ideas of the present work were inspired by our innumerable discussions on the transport project.

It has been a great pleasure to work with the octopus development team over the last years. I would like to thank Miguel Marques, Alberto Castro, Carlo Rozzi, Micael Oliveira, Xavier Andrade and Florian Lorenzen for the warm hospitality in the project and the many discussions on scientific and non-scientific topics.

Gabriele Herrmann also deserves a great deal of thanks for her help on bureaucratic matters and I wish to thank all other group members for the stimulating atmosphere.

I would like to thank several people for proofreading parts of the thesis and especially Nicole I have to thank for carefully proofreading *all* draft chapters.

I wish to express my sincere thanks to the ZEDV team, especially Wolf-Dieter Woidt, Jens Dreger, Axel Thimm, Henning Glawe and Tobias Burnus. Without their expertise and support the acquisition, installation and maintenance of the group workplaces and the Linux HPC cluster would not have been possible for me.

My deepest gratitude goes to Christiane and my family for their love, support, encouragement and understanding. Without them, none of this would have been possible.

Heiko

Index

W

X

Z

Colophon

This thesis was typeset with LaTeX 2$_\varepsilon$ using Computer modern fonts. Two-dimensional plots have been created using Grace. Contour plots and three-dimensional graphics have been generated using the OpenDX, Matlab, and IDL software packages. The technical drawings in this work have been created with Xfig and Inkscape.